Author:
Schumacker, Nick W

Title:
Development of a tri-layered electrospun scaffold for potential use in small diameter tissue engineered vascular grafting

University of
BRISTOL

DEVELOPMENT OF A TRI-LAYERED ELECTROSPUN SCAFFOLD FOR POTENTIAL USE IN SMALL DIAMETER TISSUE ENGINEERED VASCULAR GRAFTING

NICHOLAS WILLIAM SCHUMACKER

Primary Supervisor: Professor Raimondo Ascione

Co-Supervisor: Professor Sarah George

A dissertation submitted to the University of Bristol in accordance with the requirements for award of the degree of Doctor of Philosophy in the Faculty of Health Sciences, School of Clinical Sciences.

September 2019

Word Count: 51,173

ABSTRACT

Tissue engineered vascular grafts (TEVGs) may have the potential to replace saphenous vein for multiple small diameter (<6mm) coronary artery bypass grafts, which exhibit poor long-term patency, often leading to repeat surgeries. Currently, there are no clinically used TEVGs due to inferior short-term patency rates when compared with autologous saphenous vein. One of main reasons for early TEVG failure is thrombus formation, which is attributed to a sparse or absent luminal endothelial monolayer. Inadequate host cell infiltration and angiogenesis are also thought to contribute to short and long term TEVG failure. The aims of this PhD project were to: (i) determine the feasibility to create a tri-layered electrospun scaffold, combining aligned and random topographies of nano- and macro-size fibres where necessary to: (i) enhance endothelial cell attachment and promote a luminal endothelial morphology (ii) promote a physiologically representative vascular smooth muscle cell (VSMC) morphology (iii) promote cellular infiltration and host remodelling.

This work demonstrated that electrospinning is a versatile technique, which can be used to create seamless multi-layered tubes with layer specific topographies. Endothelial cell attachment was improved for nano-scaled fibre diameters, and endothelial cell orientation was found to be affected by the underlying cell culture substrate topography. The phenomenon of cell orientation in relation to the underlying substrate topography was also observed for smooth muscle cells. Furthermore, this work presented evidence that it is possible for macrophages to transdifferentiate into smooth muscle cells.

In conclusion, this thesis presents an investigation into the optimisation and creation of a tri-layered tube for use a TEGV by using specific electrospun topographies to enhance cellular attachment and promote an aligned morphology. It also demonstrates the potential for TEVGs to be populated with autologous blood from patients

DEDICATIONS AND ACKNOWLEDGEMENTS

Firstly, I would like to thank my parents for their unwavering support throughout my PhD. It would not have been possible to complete this work without their help and support.

I would like to offer great thanks to my primary supervisor, Professor Raimondo Ascione, for providing me with the flexibility to explore my scientific interests during this project and for always listening to my ideas in a respectful manner. I am also thankful for his belief in me and for always being available to support me throughout the process. I am grateful to Professor Ascione for obtaining the PhD funding specifically for me, as this project would not have been possible without his belief in the project and trust in my ability to complete the work.

I would like to thank my co-supervisor, Professor Sarah George, for sharing her wealth of scientific expertise and wisdom that have been invaluable throughout my time in Bristol. I am truly grateful for all of your support throughout this process and helping me at a moment's notice on a continual basis. It certainly would not have been possible without Professor George's help, guidance, patience and compassion.

There are too many people to mention that have played an instrumental part in my research journey and all have contributed to the completion of my PhD. Hopefully you know who you are and I am grateful to have met such wonderfully talented individuals throughout my time on this project. In particular, I would like to thank Dr Helen Spencer for her initial support with helping me find my feet and giving me another northern friend in Bristol. I would like to give special thanks to Laura Walker for the constant reassurance and guidance during the initial period of my PhD, and for providing a pleasant working environment every day. I would also like to thank Sandro Satta for tightening everything so much that there are still items to this day trapped shut in the lab. Thank you to Daniel Lopez for being great fun and suffering through some painful experiments just to help me

out. Thank you to Nadiah Sulaiman for listening to my rants on various topics and keeping me sane in the final phase of my PhD. I would like to give special thanks to Caroline Norris for treading water with me, sipping tea, breaking rules (and equipment), and being the best 'colleague' to work with and someone I now have the pleasure of calling a friend.

I would also like to thank Professor Bo Su for collaborating on this project by providing complete access to his facilities and providing his expert knowledge, which were both essential for the completion of this project. I would further like to thank Paul Chappell and the rest of the UoB workshop team for dealing with my unusual requests and constant tweaks without complaint.

Finally, I would like to thank the University of Bristol Alumni Foundation for providing the continued support for this project and allowing me to have such an incredible experience.

AUTHOR'S DECLARATION

I declare that the work in this dissertation was carried out in accordance with the requirements of the University's Regulations and Code of Practice for Research Degree Programmes and that it has not been submitted for any other academic award. Except where indicated by specific reference in the text, the work is the candidate's own work. Work done in collaboration with, or with the assistance of, others, is indicated as such. Any views expressed in the dissertation are those of the author.

Signed:…… **Date:**

TABLE OF CONTENTS

LIST OF FIGURES

LIST OF TABLES

LIST OF ABBREVIATIONS

A

α-MEM	Alpha Modified Minimum Essential Medium

C

CABG	Coronary Artery Bypass Grafting
CAD	Coronary Artery Disease
CHD	Coronary Heart Disease
CVD	Cardiovascular Disease
CoF	Coefficient of Friction

D

DAPI	4',6-diamidino-2-phenylindole
DMSO	Dimethyl sulfoxide

E

EC	Endothelial Cell
ECM	Extracellular Matrix
EDTA	Ethylenediaminetetraacetic acid
EGM2	Endothelial Growth Media
eNOS	Endothelial nitric oxide synthase

F

FBS	Foetal Bovine Serum

H

hSVF	Human Saphenous Vein Fibroblast
HUVEC	Human Umbilical Vein Endothelial Cell
hVSMC	Human Vascular Smooth Muscle Cell

I

IMA	Internal Mammary Artery

L

LMCA	Left Main Coronary Artery

M

MI	Myocardial Infarction

P

PBS	Phosphate Buffered Saline
PCL	Polycaprolactone
PDGF-BB	Platelet-Derived Growth Factor
PGA	Polyglycolic acid
PLA	Polylactic acid
PLGA	Poly(lactic-co-glycolic acid)
pPBMC	Porcine Peripheral Blood Mononuclear Cell

R

RCA	Right Coronary Artery

S

SMC	Smooth Muscle Cell
SmGm	Smooth Muscle Cell Growth Media
SS	Stainless Steel
SSS	Scaffold Sterilising Solution
SV	Saphenous Vein

T

TEVG	Tissue-Engineered Vascular Graft
TGF-β	Transforming Growth Factor Beta

V

VEGF Vascular Endothelial Growth Factor

1

GENERAL INTRODUCTION

1.1 Cardiovascular Disease

Cardiovascular diseases (CVDs) are the leading cause of global mortality (WHO, 2011). Cardiovascular disease is the term that encompasses a number of separate diseases that lead to 30% of all deaths annually worldwide; of these estimated 17.2 million deaths, coronary heart disease (CHD) accounts for the highest proportion at around 42% (Mendis, Puska and Norrving, 2011). Coronary heart disease (CHD) or coronary artery disease (CAD), which is characterised by intimal plaques, ultimately leads to a myocardial infarction (MI), which in severity or accumulation, can cause death. The complex pathogenesis of CVDs means that currently treatment for symptoms is the most effective approach. In the case of CAD, surgical intervention is commonly used to bypass restricted coronary arteries to help prevent fatal myocardial infarctions, with around 800,000 patients treated per year (Goldman *et al.*, 2004). Currently, mortality rates from cardiovascular diseases are set to rise continually for the foreseeable future, which will continue to cause a significant burden on healthcare resources (Mathers and Loncar, 2006). The major contributing process in the pathogenesis of CAD is atherosclerosis.

1.1.1 Atherosclerosis

Atherosclerosis is the process by which plaque formation occurs. Atherosclerosis is defined by lesions formed through a chronic inflammatory process within the arterial wall; the process has a proclivity for regions of high shear stress like that of arterial bifurcations (Yi Wang *et al.*, 2016). Atherosclerosis is a highly complex heterogeneous process; however, the general concepts for its pathogenesis are: the infiltration of monocytes through the accumulation of apolipoprotein B-lipoproteins into the intima; the induction of an inflammatory response resulting in the deposition of cells, lipid and extracellular matrix, and the eventual production of a necrotic core. This chronic narrowing of the artery can lead to plaque rupture or thrombus formation, which can in turn trigger myocardial infarction in severe cases. This process takes decades to develop life threatening arterial aberrations that can ultimately result in death in severe cases of CVD.

1.1.2 Coronary Artery Disease

CAD is a manifestation of atherosclerosis that can eventually lead to death through MI or stroke by sufficiently restricting the blood flow to the heart or brain. It is widely accepted that lifestyle choices are one of the main contributors to the onset of CAD via atherosclerosis. Western diseases and lifestyle habits significantly increase the incidence of CAD, indicating the presence of severe atherosclerotic lesions. Some of the main known risk factors for CAD are obesity, diabetes, smoking, hypertension, stress and a sedentary lifestyle, with many people in the western world having a number of these conditions (Sowers, Epstein and Frohlich, 2001; Choi *et al.*, 2016; Dimitriadis *et al.*, 2016). Despite current understanding of the risk factors and understanding of the underlying pathogenic mechanisms, translational therapies for the prevention of atherosclerosis are lacking. This means that current treatments for CAD, as a consequence of atherosclerosis, consist of therapies to manage symptoms or known risk factors, which include lifestyle changes, medications such as statins, or surgical interventions.

1.1.3 Surgical Intervention

Although preventative measures to reduce the risk of terminal MIs in CAD patients would be desirable from a patient and healthcare economics perspective, detection of atherosclerosis can be challenging as the disease can be asymptomatic for a number of years. Patients and treating physicians may only identify CAD is present after symptoms appear or in conjunction with other co-morbidities (Scognamiglio *et al.*, 2006). Treatment for CAD may involve preventative treatments that are often employed to reduce the risk of fatal MI as this is a more measurable outcome, as opposed to prevention atherosclerosis itself. This has resulted in surgical techniques becoming the standard treatment for severe cases of CAD in order to help prevent fatal MIs.

The gold standard surgical treatment for CAD is coronary artery bypass grafting (CABG). CABG is used for patients with multiple blocked coronary arteries (≥3) (Kolh and Wijns, 2011). CABG surgery has been carried out since 1967 and is a well-established, safe and effective intervention, and it is used to alleviate symptoms of CAD as well as to prevent

MI. CABG surgery uses autologous grafts from accessible locations around the body, mainly from the saphenous vein (SV), which are used to bypass around narrow or blocked coronary arties by providing an alternative route for the blood to flow unrestricted. In instances requiring only a single bypass graft is needed then the internal mammary artery (IMA) also known as the internal thoracic artery can be used unless anatomically incompatible with the blocked artery. The use of IMA is preferred due to its high patency rate of >90% at 10-15 years, in comparison to SV grafts that have a patency rate of only 50% at 5-10 years (FitzGibbon *et al.*, 1996). Structural differences between the IMA, SV and the native coronary artery is attributed to this premature failure rate. The radial artery can also be used, which also offers superior patency when compared to saphenous vein, providing further evidence that the structural differences between arteries and veins has a clinical impact on CABG (Loop *et al.*, 1986; Tatoulis, Buxton and Fuller, 2011; Lopes *et al.*, 2012)

1.1.4 Coronary Artery Bypass Graft Failure

SV is the primary autologous tissue used for CABG, yet it is suboptimal when compared to IMA suggesting the differences between arteries and veins is crucial in the coronary setting. Poor SV patency rates in CABG patients presents a clinical challenge as surgical interventions have a high cost and require a high level of expertise. With the increase in the prevalence of CAD worldwide, this means that there is an associated increase in cost for more surgical procedures. This is particularly prohibitive for developing countries where expertise and facilities may not be adequate for large volumes of CABG procedures. Additionally, the increase in global lifespans may result in the need for more repeat CABG procedures due to the limited patency of SV grafts, which may previously have supported a patient until the end of their natural life, may in the future be required to last for multiple decades. Furthermore, there is only a limited supply of SV available and it is not always possible to obtain the required tissue for coronary bypass grafting due to the presence on unsuitable SV for grafting or the absence of tissue required for the number of desired grafts (Fukui *et al.*, 2010; Sarzaeem *et al.*, 2010). It would therefore be desirable to develop a graft that has a long-term patency similar to that of IMA.

The aetiology of graft failure is complex due to the long time period over which it occurs, which suggests the involvement of multiple pathways and processes (Shukla and Jeremy, 2012). A primary cause of late vein graft failure is intimal and medial hyperplasia within the vessel itself and at the anastomoses (Kulik and Ruel, 2011). This is the process in which vascular smooth muscle cells (VSMCs) proliferate into the luminal space when luminal endothelial damage occurs, which accelerates the process of atherosclerosis (Kijani *et al.*, 2017). This may be caused by damage to the endothelium during the grafting process; however, atherosclerosis is less prominent in arterial conduits when compared to venous grafts (Shelton *et al.*, 1988). The reasoning for this phenomenon is not currently fully understood, although it is associated with the response to endothelial injury due to hydrodynamic forces produced by arterial flow, whereby arteries likely have anatomic properties that are more adapted to these flow conditions (Otsuka *et al.*, 2013). Motwani and Topol, (1998) outline these anatomical and physiological properties clearly in their work from their published work on saphenous vein graft disease. Overcoming these identified pathologies that lead to vein graft failure will help with preventative treatments in the future. This may be possible through the understanding of the structural differences between arteries and veins.

1.1.5 Venous and Arterial Structure

The difference between IMA patency and that of saphenous vein has been a topic of interest for research. Clearly, there are differences that play a vital role in the patency of heart bypass grafts. Many of these differences have been suggested to be a result of structural differences between arteries and veins, which physiologically do have distinct roles (Canham, Finlay and Boughner, 1997; Cuminetti *et al.*, 2017).

1.1.6 Coronary Artery Anatomy and Structure

Coronary arteries supply blood to the myocardium and are essential for homeostasis (Figure 1.1). There are two major coronary arteries, the left main coronary artery (LMCA) and the right coronary artery (RCA), which then bifurcate into smaller arterial branches (Figure 1.1). The human LMCA has an average length of approximately 10 mm with a range of 2-23 mm with an average diameter of approximately 5 mm. Conversely, the RCA length ranges from 12-14 cm and has a diameter ranging from approximately 3-4 mm (Dodge *et al.*, 1992; Waller *et al.*, 1992; Reig and Petit, 2004; Kastellanos *et al.*, 2018).

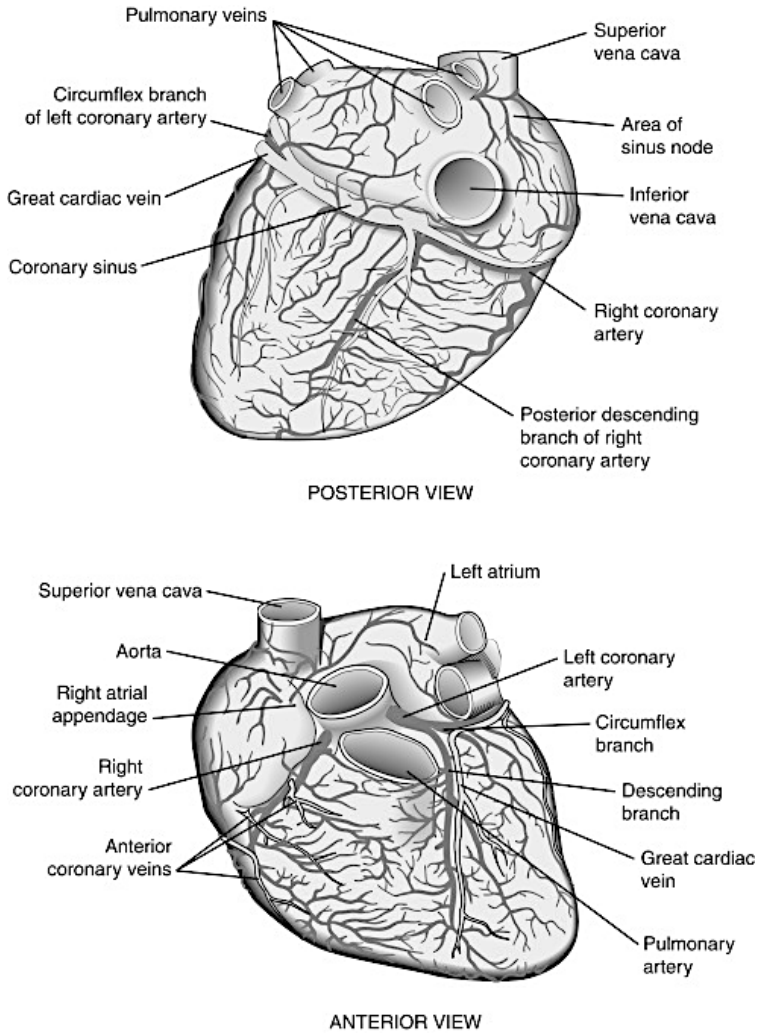

Figure 1.1 - Overview of coronary vasculature. Adapted from Pappano *et al.*, (2013).

Like all arteries, coronary arteries have 3 major layers comprising the intima, media and adventitia (Figure1.2; Table 1.1). The intima is comprised of the luminal endothelium which are attached via connective tissue to the internal elastic lamina. This is adjacent to the medial layer, which is composed of up to six concentric rings of elastic lamellae fenestrated sheets with circumferentially aligned VSMCs. A less well defined external elastic lamina then separates the media and the outer adventitial layer, which contains of fibroelastic connective tissue interspersed with collagen fibres, vascular fibroblasts, tissue macrophages and vascular progenitor cells (Hu *et al.*, 2004; López-Guimet *et al.*, 2017). The total thickness of the left anterior descending coronary artery wall is approximately 1.1 mm in humans (Perry *et al.*, 2013).

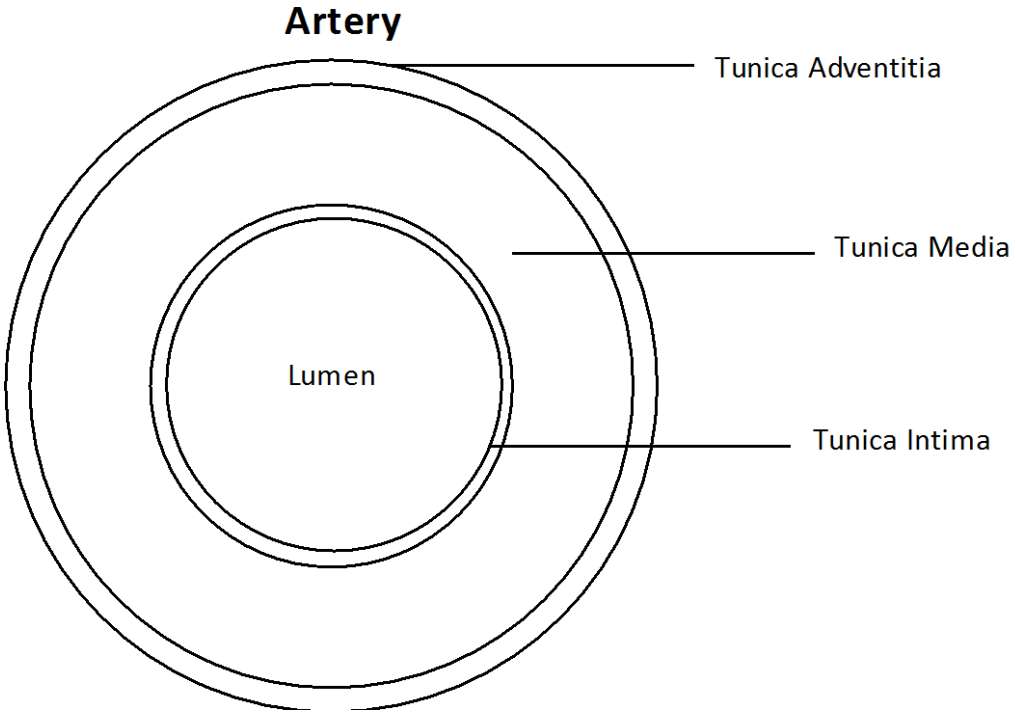

Figure 1.2 – Basic diagrammatic representation of the coronary arterial structure. The ratio between the thickness of the Tunica Intima, Tunica Media and Tunica Adventitia layers is representative only and not to scale.

The semi-permeable endothelial monolayer in the intima play a crucial role in the prevention of clot formation and they may help ensure VSMCs in the media remain quiescent under healthy conditions (Jacot and Wong, 2008). The medial VSMCs have a quiescent and contractile phenotype within healthy coronary arteries and can comprise up to 60 layers of cells. After arterial injury, the VSMCs undergo phenotypic changes that cause proliferation and migration into the intima, which can lead to stenosis. (Bacakova *et al.*, 2018). For the adventitia, fibroblasts are the main cell type and they play an important role in arterial repair (Shi *et al.*, 1996; Li *et al.*, 2000). Arterial fibroblasts are also believed to be a major source of vascular ROS production and it is hypothesised that the adventitial layer has a pivotal role in controlling oxidative stress (Ardanaz and Pagano, 2006; Wang *et al.*, 2010).

The structure of the IMA is similar to that of the coronary artery, which may help to explain its superior patency when compared to SV. The role of grafted IMA is closely related to its primary function of facilitating the transport of blood from the heart; therefore, it is already conditioned to receive high hemodynamic forces. On the other hand, the saphenous vein has a different structure reflecting its related but distinct role. The IMA luminal diameter ranges from around 1.9 mm to 2.6 mm and has an approximate wall thickness ranging from 180 μm to 430 μm (Canham, Finlay and Boughner, 1997).

1.1.8 Saphenous Vein Structure

Saphenous vein structure exhibits the typical venous structure comprising the same major 3 layers found in arteries, the intima, media and adventitia (Figure 1.3; Table 1.1). Contrastingly, the SV wall structure does not contain an internal and external elastic lamina, and the media does not contain elastic fibres or VSMC layers in quantities comparable to that of arteries. Additionally, the ratio between the thickness of each layer relative to the other differs (Figure 1.3). In arteries, the media normally constitutes the largest portion of the thickness of the vessel wall. In contrast, venous walls such as SV have a much smaller medial thickness in proportion to the total wall thickness, which is normally smaller than the adventitia(Ratcliffe, 2000). The overall wall thickness of SV is

approximately 400 μm and the luminal diameter range from around 3.1 mm to 8.5 mm (Canham, Finlay and Boughner, 1997; Perek *et al.*, 2012).

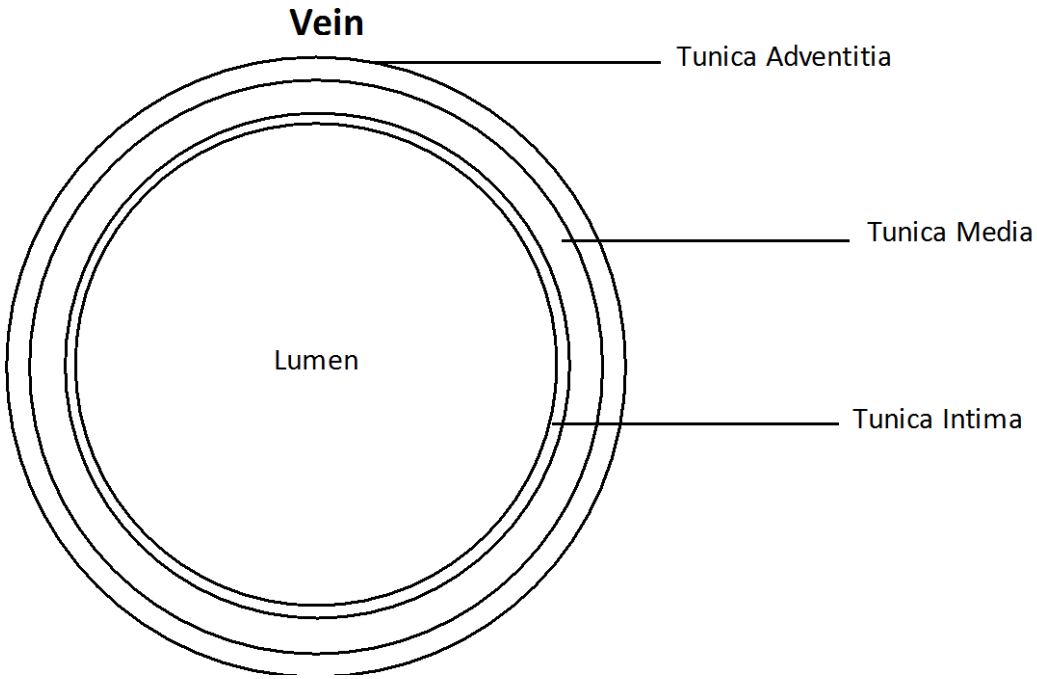

Figure 1.3 - Basic diagrammatic representation of the saphenous vein. The ratio between the thickness of the Tunica Intima, Tunica Media and Tunica Adventitia layers is representative only and not to scale.

Owens *et al.*, (2008) have shown that saphenous veins undergo remodelling when they are repositioned to the heart, which causes structural and cellular changes showing the effect of flow conditions on cellular behaviour. These changes reflect the adaptation of SV to such a drastic change in environmental conditions, which are much more prominent than the minor environmental changes experienced by the IMA. Therefore, the structural differences between IMA and SV are likely a major contributor to the resulting long-term patency rates in CABG.

As saphenous vein has a comparatively poor patency rate when compared to arterial grafts, and availability of useable arterial tissue is limited, it would be desirable to find alternative sources of tissue for CABG. Initially therefore, any future conduit would need to act more like a native artery as this would improve overall patency. Therefore, developing a structure representative to that of a coronary artery may provide a suitable graft replacement for saphenous vein with long-term patency.

Table 1.1 - General structural differences between arteries and veins. Adapted from BCcampus, (2012).

	Arteries	**Veins**
General Structure	Thick walls with small lumens	Thin walls with large lumens
	Generally appear rounded	Generally appear flattened
Tunica intima	Endothelium usually appears wavy due to constriction of smooth muscle	Endothelium appears smooth
	Internal elastic membrane present in larger vessels	Internal elastic membrane absent
Tunica media	Normally the thickest layer in arteries	Normally thinner than the tunica adventitia
	Smooth muscle cells and elastic fibres predominate (the proportions of these vary with distance from the heart)	Smooth muscle cells and collagenous fibres predominate

	External elastic membrane present in larger vessels	External elastic membrane absent
		Nervi vasorum and vasa vasorum present
Tunica adventitia	Normally thinner than the tunica media in all but the largest arteries	Normally the thickest layer in veins
	Collagenous and elastic fibres	Collagenous and smooth fibres predominate, with some smooth muscle fibres
	Nervi vasorum and vasa vasorum present	Nervi vasorum and vasa vasorum present

1.2 Regenerative Medicine

Regenerative medicine has been increasingly researched in recent years due to its potential to revolutionise many areas of medicine that involve the development of *de novo* tissues without the need to grow whole organisms. This emerging field could hold the potential to producing a tissue engineered vascular graft (TEVG) that supersedes the patency of SV. However, this field is highly complex and requires cross disciplinary expertise in order to generate clinically relevant findings. Although often used interchangeably, one critical subset of regenerative medicine is called tissue engineering, which is the creation of tissues using scaffolds and cells, which is encompassed y the term regenerative medicine.

1.2.1 Tissue Engineering

Tissue engineering has been extensively explored in the past decade as a method to develop a TEVG. The basic concept of which involves the combination of a tubular scaffold, adherent cells and biologically active molecules to produce a tissue-like structure for use as a graft. Alternatively, many experiments have also taken place with acellular scaffold structures that are used as tubes to potentially bypass a blocked vessel. Many of this work has provided limited success in producing a clinically applicable TEVG; however, the use of scaffolds and cells to develop an artificial TEVG still holds significant promise.

1.2.2 Cellular and Matrix Remodelling

Scaffolds can be comprised of biological materials, synthetic materials or a mixture of both. In the development of TEVGs, biodegradable polymers or decellularised tissue are primarily used for their availability and relative strength. The constituents of the scaffold have an effect on the host immune response, which in the case of TEVGs often leads to graft occlusion in small-diameter grafts *in vivo* due to the absence or incomplete coverage of luminal endothelium as previously described (Deutsch *et al.*, 2009). Previous work has demonstrated that implanted grafts are remodelled due to the host immune response, which acts to breakdown the foreign scaffold material or in chronic immune responses becomes calcified (Chemla and Morsy, 2009; Cummings *et al.*, 2012; de Valence *et al.*, 2012).

For biological scaffolds such as previous animal tissues that have been decellularised, the implanted material initially elicits an acute immune response, whereby cell surface antigens and DNA that are not fully removed by the decellularisation process may be detected by circulating neutrophils and mononuclear cells (MNCs), which attempt to breakdown the material through phagocytosis and proteolytic enzymes (Zheng *et al.*, 2005; Valentin *et al.*, 2006). Despite this initial response to decellularised tissues, there is little evidence to suggest that the level of immune response at this stage has a significant adverse effect on remodelling (Ratner and Hoffman, 2004; Valentin *et al.*,

2006). After the initial innate immune response and if the tissue does begin to breakdown sufficiently, then fibroblasts will secrete ECM thus resulting in remodelling of the tissue from foreign material to predominantly host material (Zhou, Jin and Willing, 2016). However, this resulting tissue may not have the same desired characteristics of an artery, which can lead to a suboptimal outcome and ultimately occlusion of any existing lumen. Furthermore, if the implanted material does not breakdown sufficiently then this chronic inflammation can result in calcification, which can also end with impaired vessel function or occlusion.

It is unlikely that we can develop TEVGs that completely evade the host immune system altogether in the coming years so development of TEVGs with the ability to direct their own host remodelling will be crucial. It is important to ensure that any implanted TEVG is infiltrated with host cells, that the graft material is safely broken down, that host ECM is deposited and that the resulting tissue is able to perform similarly to a native mammalian blood vessel. Therefore, some inflammation is required for wound healing and remodelling of the TEVG; however, severe immune responses are likely to result in graft failure and rejection (Hibino *et al.*, 2015).

Further research into the host response to both synthetic and biological TEVG materials is crucial towards defining the most appropriate materials and structures for a controlled remodelling of future TEVGs, although this would require longitudinal studies spanning years to determine the exact process involved in acute inflammation and remodelling compared to chronic inflammation and remodelling.

1.2.3 Biological Scaffolds in tissue Engineering

Decellularised scaffolds offer potential for the development of TEVGs as they already contain a matrix structure and component that can support cell attachment and growth. It is logical to propose that removal of cells from existing tissues to remove non-host cells will derive a scaffold that is suitable for implantation. There have been a number of decellularised matrices tested for use as vascular graft conduits, usually from animal products. A list of some of the studies using decellularised tissues is below in Table 1.2:

Table 1.2 - Overview of studies using decellularised tissues as TEVGs. Adapted from Pashneh-Tala, MacNeil and Claeyssens, (2016)

Scaffold Material	Study Type	Group
Decellularised Bovine Carotid Artery	*In vivo* (clinical experience)	(Butler, Baker and Johnson, 1977; Hurt *et al.*, 1983)
Decellularised Bovine Mesenteric Vein	*In vivo* (clinical experience)	(Kovalic, Beattie and Davies, 2002; Katzman *et al.*, 2005)
Decellularised Bovine Ureter	*In vivo* (clinical experience)	(Chemla and Morsy, 2009)
Decellularised Human Vein	*In vivo* (clinical experience)	(Madden *et al.*, 2004)
Decellularised Human Iliac Vein	*In vivo* (human trial)	(Olausson *et al.*, 2012)
Decellularised Porcine Artery	*In vivo* (ovine model)	(Tillman *et al.*, 2012)
Decellularised Canine Carotid Artery	*In vivo* (canine model)	(Cho *et al.*, 2005)
Decellularised Human Umbilical Vein	*In vitro*	(Tosun and Mcfetridge, 2013)
Decellularised Porcine SIS	*In vivo* (canine model)	(Sandusky, Lantz and Badylak, 1995; Roeder, Lantz and Geddes, 2001)

Decellularised tissue is well known for being highly biocompatible, having high strength and being relatively easy to obtain (Helmus, Gibbons and Cebon, 2008). Decellularisation removes the cellular components from tissues in order to leave an intact ECM with little or no remaining cells or DNA. This allows for allo- and xeno-grafts that are highly biocompatible and that biodegrade successfully *in vivo.* Decellularised patches are currently used clinically for cardiac reparative surgeries (Lofland *et al.*, 2012; Dohmen *et al.*, 2014; Hopkins *et al.*, 2014). Utilising animal tissues as TEVGs allows for an easily accessible source and decellularised mammalian veins and arteries are a logical choice for CABG TEVGs. A number of studies have investigated the use of mammalian blood vessels as TEVGs and they do possess the necessary mechanical characteristics of their former living tissues (Schaner *et al.*, 2004; Quint *et al.*, 2011). Further to the ability of decellularised vasculature to withstand haemodynamic forces, the ECM will be very similar in constituents to that of human arterial or venous ECM. Indeed, decellularised cadaver blood vessels have been tested for use as TEVGs in the literature (Madden *et al.*, 2004; Olausson *et al.*, 2012).

However, decellularised grafts still show early signs of graft failure such as thrombosis, stenosis and occlusion (Chemla and Morsy, 2009; Wystrychowski *et al.*, 2014). This could be attributed to the lack of a luminal endothelium, host immune response to foreign proteins and DNA not fully removed from the tissue as well as inadequate host cell infiltration (Sheridan, Duffy and Murphy, 2012; Bruyneel and Carr, 2017). The major drawbacks to decellularised tissue are that its degradation is not tuneable, may contain residual genetic material, and the commonly available tissue sheets require suturing into a blood vessel shape (Rathore *et al.*, 2012)

In addition to decellularised tissue, other biological materials can be used to develop TEVGs, which may be able to overcome some of the limitations currently facing decellularised tissues that are scaffold free and use self-assembly to enable cells to grow and develop into tissues. L'Heureux *et al.*, (1998) developed a TEVG from sheets of cells that were peeled and shaped into a tube. This tube was then conditioned within a bioreactor, which resulted in a TEVG with a burst strength of 2600 mmHg, which is superior even to SV, although this graft failed shortly after implantation. However, the

group have further explored this technique to produce grafts patent up to 8 weeks(L'Heureux *et al.*, 2006). The major limitation with this technique is the intensive *in vitro* preparation of the graft through the growth of cells to the extensive condition step within the bioreactor. Despite this limitation, L'Heureux patented this technique and a clinical trial by McAllister *et al.*, (2009) demonstrated a patency of 60% at 6 months and further work has been conducted on an off-the-shelf version of this type of TEVG producing process (Wystrychowski *et al.*, 2014).

1.2.4 Synthetic Scaffolds in Tissue Engineering

Further to biological scaffolds, TEVG research has also focussed on synthetic materials. Synthetic materials have the advantage of being produced on demand and can be manufactured into the desired shape and size for TEVG purposes, potentially allowing for grafts to be tailored to patients' particular needs. There are numerous synthetic materials that could potentially be used and many man-made materials are used for implantation already such as ceramic and various metals. However, for small diameter TEVGs attention has been focussed on biodegradable materials such as natural ECM components and biodegradable polymers. This is due to the ability of the body to break these materials down so the risk of chronic inflammation is reduced, that the graft can be remodelled, and that there are a number of American Food and Drug administration (FDA) approved materials for implantation. The latter characteristic means that there are fewer barriers to developing a TEVG with a material if it is already approved by the FDA for implantation in humans.

The literature contains evidence of all of the available FDA approved implantable biodegradable materials as all have the potential to be used for TEVGs outlined in a review by (Catto *et al.*, 2014). As with PTFE, these materials on their own have shown limited success due to the risk of thrombosis. Although, a combination of scaffold and antithrombotic drugs could be used, it is neither preferable nor cost effective and produces adverse effects on the body (Sarkar *et al.*, 2007). FDA approved implantable materials differ greatly in their characteristics in relation to producing a TEVG. Idealistic TEGV characteristics would include controllable biodegradability, biocompatibility,

mimicking native arterial structure and strength, being cheaply and easily produced, and be able breakdown into harmless by-products whilst supporting cells and facilitating host repair and remodelling (Bačáková *et al.*, 2004; Bacakova *et al.*, 2007). Unfortunately, none of the FDA approved implantable materials possess all of the key features. Therefore researchers have focused on combinations of scaffolds, different scaffold structures, cells and cytokines in an attempt to produce a patent TEGV (Catto *et al.*, 2014).

1.2.5 Benefits of Cell Seeding and Biomolecules in Tissue Egineering

Cells have been the focus of many papers in the development of a TEVG as it is believed that pre-seeded grafts may help overcome some of the limitations of acellular biological or synthetic scaffolds. Combining cells with scaffolds can provide additional strength as well as immunosuppressive benefits through the use of cells like mesenchymal stem cells and reduced thrombus formation through luminal endothelium (Durand *et al.*, 2004; Miguel, 2012). The added benefit of cells is known to affect the host immune response to the scaffolds and many studies show evidence of pre-seeded cellular scaffolds having increased patency compared to scaffolds alone *in vivo* (He *et al.*, 2009; Quint *et al.*, 2011; Patterson *et al.*, 2012).

The mechanisms by which combined cell and scaffolds methods help the patency of a vessel *in vivo* are still poorly understood. One major drawback of this method is the inability for pre-seeded cells to infiltrate the various scaffolds, despite adequate void volume (Stephen J Eichhorn and Sampson, 2005). Many cell types have been shown to grow on the surface of scaffolds and have limited ability to grow throughout the scaffold despite sufficient void space. This issue has been overcome with the use of pro-migratory cytokines like fibroblast growth factor (FGF) and production of various scaffold structures (Kurane, Simionescu and Vyavahare, 2007). Despite the *in vitro* promise of cell and cytokine combination scaffolds, *in vivo* translation has been difficult due to rapid dispersion of cells and exogenous cytokines by the host (Harrington *et al.*, 2011). Incorporation of cytokines into the electrospun polymers has shown a more controlled release, yet this system still allows exogenous cytokines to contaminate the host blood

stream potentially causing adverse downstream effects (Selcan Gungor-Ozkerim *et al.*, 2013).

1.2.6 Scaffold Fabrication Techniques for TEVGs

To develop a TEVG, fabrication techniques are required to convert biological or synthetic substances into tubular structures supportive of cells. Various techniques can be observed in the literature for the creation of structure that are able to support cells such as three-dimensional (3D) printing. 3D printing has become popular in recent years due to the improvement in 3D printing technologies. 3D printing usually involves the liquification of a polymer through a heated nozzle, which is attached to a roller. Molten material is then printed into specific structures as the roller moves (Kabirian *et al.*, 2018). This allows for the develop of multiple printed levels as new layers can be printed over existing ones to create complex structures such as tubes with macrostructures such as pores (Kabirian *et al.*, 2018). 3D printing can also be used for a range of materials making the technique very versatile. 3D printing has great potential for the development of future TEVGs as, in theory, future 3D imaging of a patient artery could be collected and a synthetic version of the exact specifications could be 3D printed at the benchside. Unfortunately, current extrusion 3D printing technology can only print to a resolution of around 30 microns when using very high-resolution industrial printers. However, light-based 3D printing technologies are showing much more physiologically relevant resolutions of < 100 nm, such as stereolithography that uses light to cross-link photosensitive polymer precursors to develop structures. This has an exciting potential for future TEVGs. Currently, stereolithography can only generally develop small structures (< 1 cm) and it takes considerable time to create the final structure.

In addition to 3D printing, 3D bioprinting has been explored whereby cells can be precisely positioned, which offers great potential for future TEVGs as cells could be printed directly throughout a 3D printed scaffold. Cells are encapsulated with flowable and biocompatible hydrogels to resist damage during the process (Kim, Kim and Jung, 2016). Use of this technology is currently limited as similarly to 3D scaffold printing, the process takes a considerable amount of time, which affects cell viability (Jang *et al.*, 2018).

Another technique using cells for the development of scaffolds for TEVG purposes is the use of cell sheets. Cells grown on flat surfaces can form peel-able monolayers which, as previously described, was a technique used by L'Heureux *et al.*, (2006) to develop a functional TEVG. Interestingly, the TEVGs from L'Heureux *et al.*, (2006) required conditioning within a bioreactor.

Further work using bioreactors has demonstrated the benefits of pre-condition TEVGs containing cells to flow conditions before implantation (Hahn *et al.*, 2007; Yazdani *et al.*, 2009). Bioreactors using pulsatile flow have been shown to improve the development of a muscularised medial layer *in vitro* and improving VSMC proliferation (Yazdani *et al.*, 2009). Therefore, this technique shows promise in providing a model for testing the effectiveness of a TEVG *in vitro*, but also for potentially stimulating and maintaining physiologically relevant vascular cell phenotypes before implantation, which may help improve patency rates.

Electrospinning is an increasingly popular scaffold fabrication technique as it is able to produce micro- and nano-scaled fibres. Resulting fibres have been shown by a number of studies to support cells and allow for the development of tubular structures.

1.3 Electrospinning

Mimicking the structure of the native extracellular matrix (ECM) is the most logical approach to tissue engineered a blood vessel. It is well known that cell behaviour and phenotype are affected by the microenvironment, which is determined by the ECM composition and structure (Stegemann, Hong and Nerem, 2005; Grogan *et al.*, 2014). Despite there being a number of ECM proteins, which would make mimicry difficult with current technologies, the general microarchitecture of native ECM is relatively easily achieved artificially. The mammalian ECM comprises interconnecting fibres ranging from around 50 nm - 500 nm, which allows for high void volume, high porosity, high surface-to-volume ratio and high strength (Smith *et al.*, 2009). One such popular method that is effective at reproducing these key properties is electrospinning. Electrospinning has

been used for decades, yet is being recently explored for its potential versatility in regenerative medicine.

Electrospinning involves forcing a polymer and solvent solution through a needle that has a high voltage applied until it reaches a point of instability, resulting in rapid solvent evaporation, leaving micro and nano scaled fibres on a grounded collector (Figure 1.4). The resulting fibre diameter depends on a variety of factors of which are tuneable for specific needs. This technique allows for the production of strong scaffold material with nano scale fibres mimicking the ECM through a relatively easy and cheap method that can be employed for a number of different materials; appropriately, many of which are FDA approved implantable polymers and proteins making it a viable choice for TEVGs.

Commonly electrospun polymers like poly lactic acid (PLA) and poly glycolic acid (PGA) can be combined to produce copolymers with tuneable ratios, which in turn determine their degradation rate (Makadia and Siegel, 2011). This property makes polymers an enticing choice for researchers trying to produce a TEVGs. Natural ECM components like gelatin can also be electrospun, which are more biocompatible than polymer based scaffolds, but they lack the strength and tuneable degradation rates of polymer based scaffolds (Zhan and Lan, 2012). Hybrid scaffolds have been explored that attempt to combine the strength and reproducibility of polymer scaffolds with the biocompatibility of natural scaffolds with promising results. However, this technique is more difficult and less reproducible than polymer scaffolds alone, which may be key to producing off-the-shelf TEVGs (Zhang *et al.*, 2005; Regis *et al.*, 2014).

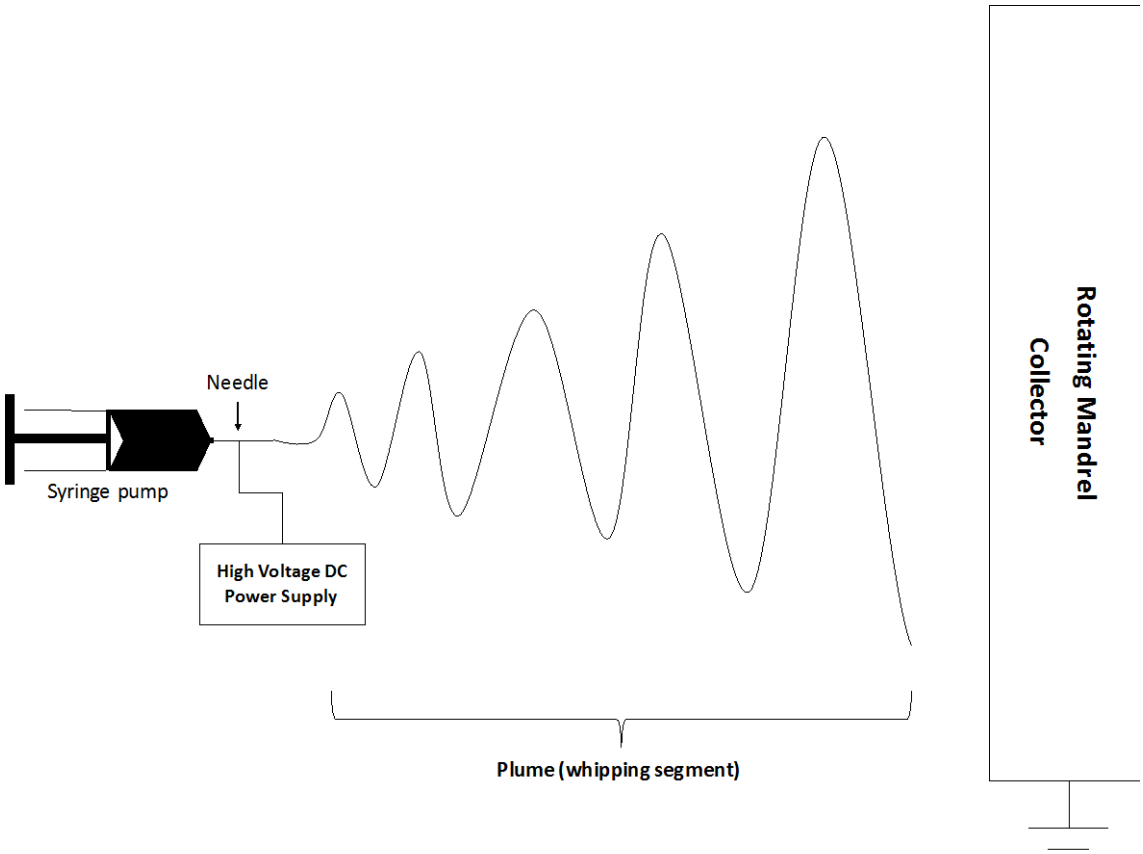

Figure 1.4 - Diagram of a basic electrospinning set up. Briefly, a viscous solution is fed through a needle and a voltage is applied. The increase in charge results in the expulsion of the solution from the apex of a Taylor cone as a jet travelling in the direction of the collector. This jet thins as it travels towards the collector until it becomes unstable and begins to whip. As the remaining solvent evaporates the remaining solute material is revealed as a deposited fibre on the collector.

1.3.1 Electrospinning Materials

Electrospinning can be used to develop fibres for a range of materials that can dissolve in solvents, including water, to form viscous solutions. It is even possible to electrospin metals carbon (Kim *et al.*, 2015; Nar *et al.*, 2016). In tissue engineering applications, natural constituents of the ECM can be electrospun such as gelatin, fibronectin and collagen (Kawelke *et al.*, 2011; No, Jeong and Lee, 2014; Hussein *et al.*, 2016). These materials show high biocompatibility allowing for the support of cells for a range of applications. However, for TEVG purposes the major drawback electrospun constructs from naturally derived materials is their lack of strength (Ramshaw, 2016). In the ECM components are in highly arranged structures to impart the required characteristics such as mechanical strength. For example, collagen is organised into fibrils that constitute larger collagen fibres (Ramshaw, 2016). Furthermore, there are a large number of proteins and macromolecules present within the ECM that combine together to provide its functional characteristics. Therefore, when using individual ECM proteins this organised structure is absent, which results in inferior structural strength when compared with ECM.

However, combining electrospun fibres produced from naturally derived ECM components with stronger materials has been found to improve strength, whilst maintaining high biocompatibility (Heydarkhan-Hagvall *et al.*, 2008; Lobo *et al.*, 2018). This holds promise for future TEVGs as biocompatibility of scaffolds is crucial to ensure cell attachment, growth and survival, especially when considering the need for a functional luminal epithelium to enhance long term patency rates. Despite this promise, there are still limitations to the use of ECM components in TEVGs. Some of these limitations include biological contamination from naturally derived materials, batch-to-batch variation, high purification costs, and concerns with the use of animally derived products for human implantation, which is how most ECM components are obtained. Therefore, exploration of further materials is still warranted and may yield superior results until we are able to more accurately create nano- and micro-structures as intricately as mammalian ECM.

Other natural materials have also been shown interest for their potential use in scaffold fabrication such as spider silk fibroin (Vollrath and Knight, 2001; Dai, Zhang and Ou-Yang, 2003). Spider silk is known to have high mechanical strength for its relative size, which makes it a suitable choice for high strength applications such as the development of TEVGs. Recombinant spider silk protein has been explored for its use in electrospinning and has shown good biocompatibility and high tensile strength (Soffer *et al.*, 2008).

1.3.2 Electrospinning Solvents

Alongside the wide range of materials that can be electrospun, there is a variety of choice for electrospinning solvents to be used. Solvents are required for the electrospinning process to ensure the electrospinning material is dissolved to form a homogenous spinnable solution. The rapid evaporation is also required to consolidate the jet into a fibre. Selection of a solvent for a particular material is fundamental to ensure that smooth fibres can be obtained at the desired fibre diameter range. Whilst many biological polymers can be dissolved in solvents such as and even water, polymers can be electrospun using a variety of solvents that may be more suitable to the electrospinning process. Teas graph is a solubility diagram useful for helping select appropriate solvents for polymer solutions to be electrospun(Teas, 1968). There is also a growing body of published literature that contain methods for the dissolution of TEVG relevant polymers in solvent to form electrospinning solutions (Pattamaprom *et al.*, 2006; Luo, Stride and Edirisinghe, 2012). Solvent choice can have an effect on the resulting fibre morphology and it has also been demonstrated that the mixing of solvents can be utilised to enhance miscibility and improve fibre morphology (Wannatong, Sirivat and Supaphol, 2004; Xu *et al.*, 2017). Therefore, selection of an appropriate solvent can ensure consistently smooth and uniform fibres are obtained.

Solvents used for electrospinning purposes are generally biologically harmful and therefore ensuring all solvent is removed before implantation is essential to prevent adverse effects. The use of solvents is also a limitation of the electrospinning method as the solvents cannot be reused once evaporated. Many solvents also reduce the lifespan of electrospinning equipment due to their corrosive effects during evaporation. Solvent-

free electrospinning such as melt electrospinning, which uses molten solutions to develop the electrospinning jet, can help to overcome this limitation; however, these methods require further exploration and refinement to compete with the low cost solvent electrospinning technique that is more commonly used (Zhang *et al.*, 2017).

1.3.3 Electrospinning Parameters

The electrospinning process requires the development of a Taylor cone or droplet of an electrostatically charged solution to allow for the development of a jet from the apex, which was first identified by Taylor, (1964). It is generally considered that this resulting jet is stretched and becomes thinner in the electric field, and radial charge repulsion results in splitting of the main jet into multiple smaller jets or fibres of relatively equal diameter and charge (Doshi and Reneker, 1995). However, the characterisation of the jet splaying into smaller jets has been rebuked by Hohman *et al.*, (2001) who reported that splaying effect is actually the whipping motion of one continuous jet at an extremely high frequency. It is well established that the various parameters that constitute the electrospinning process can affect the resulting fibre diameter, morphology and alignment. As fibre diameter and morphology can have implications in regard to cell-to-cell interactions, it is important ensure fibres can be consistently generated and reproduced. It is also important to have uniform fibres to ensure consistency in cell-to-scaffold interactions. A common aberration found in electrospun fibre during optimisation of an electrospinning system is the formation of beads along individual fibres. Table 1.3 outlines the major parameters that can have an effect on the electrospinning process and resulting fibre characteristics, which need to be considered when developing fibrous scaffolds using this method.

The main parameter that affects the electrospinning process and fibre formation is the electrospun material. Each material has physical characteristics that can result in the production of fibres with varying morphologies in terms of diameter and surface aberrations. Even once a material is chosen, variations in molecular weight have been demonstrated to have an association between increased molecular mass and increased fibre diameter (Akduman, Kumabasar and Çay, 2014). Furthermore, the percentage of a

given material in solution also has a large determining effect on resulting fibre morphology. There is generally a narrow range in the electrospinning solution concentration in which uniform fibres can be produced in a given system, all other parameters being equal (Shahreen and Chase, 2015). The electrospinning solution spinnability is also largely impacted by the solvent used (Jarusuwannapoom *et al.*, 2005). As the miscibility of a particular material in a solvent varies, the material concentration and resulting solution viscosity may vary drastically between solvents. Solution viscosity is a critical factor in spinnability as solutions that are too thin or too thin cannot be electrospun. The viscosity of a solution can also have a large effect on resulting fibre diameter (Nezarati, Eifert and Cosgriff-Hernandez, 2013). Additionally, electrospinning solvent evaporation rates vary, which can affect the distance of the jet and whipping segment, thus affecting fibre diameter (Eda, Liu and Shivkumar, 2007).

Once an electrospinning system has been developed, it may have a narrow range in which alterations can be made to any of the major parameters before fibres develop beads or stop being produced altogether. The main parameters aside from the electrospin material and solvent, are the processing parameters, which involved the system solution flow rate, needle tip-to-collector distance and the applied voltage. Needle bore size has also been shown to affect resulting fibre diameters, as increased bore sizes correlate with larger fibre diameters (Kuchi, Harish and Reddy, 2018).

The conductivity of a solution is also known to affect fibre diameter, whereby increased solution conductivity is associated with reduced fibre diameters. Solution conductivity can be altered by the additions of miscible salts. Furthermore, humidity, temperature and collector type have also been shown to impact electrospun fibre morphology; however, for effects to be observed these parameters usually have to have deviated significantly from normal ranges (Yalcinkaya, Yalcinkaya and Jirsak, 2015).

Table 1.3 - Effect of parameters on electrospinning. Adapted from Bhattarai *et al.*, (2018)

Parameter	Sub Parameter	Effect on Fibre Morphology	References
Polymer Parameters	Material	Fibre morphology is affected by the specific material used	(Casper *et al.*, 2004; Geng, Kwon and Jang, 2005; Henriques *et al.*, 2009)
	Molecular Weight	Increased molecular weight of polymers can reduce the number of beads. Fibre diameters increase with higher molecular polymer mass	
Solvent Parameters	Solvent Type	Type of solvent used in electrospinning affects solution spinnability	(Jun *et al.*, 2003; Jarusuwannapoom *et al.*, 2005)
	Boiling Point/ Vapour Pressure	Solvent boiling point can affect spinnability and resulting fibre characteristics	
Solution Parameters	Concentration	Increase in concentration of solution increases the fibre diameter	(Deitzel *et al.*, 2001; Jun *et al.*, 2003; Henriques *et al.*, 2009; Shahreen and Chase, 2015)
	Conductivity	An increase in conductivity of solution can decrease fibre diameter	
	Viscosity/Surface Tension	Formation of an unstable jet as a resultant effect of surface tension and viscosity can lead to bead formation	
Processing Parameters	Spinning voltage	An increase in voltage can decrease fibre diameter and can affect bead formation	(Deitzel *et al.*, 2001; Jalili, Hosseini and Morshed, 2005; Adomavičiūtė and
	Tip-to-Collector Distance	The distance between the needle tip and collector can affect evaporation time of the solvent. Too short a distance and too	

		large a distance can increase bead formation. Too short a distance can cause fusing of fibres from inadequate solvent evaporation. Longer distances can decrease fibre diameter.	Milašius, 2007; Henriques *et al.*, 2009)
	Flow Rate	Decreased flow rate can decrease fibre diameter and vice versa. Flow rate can induce bead formation.	
Ambient Parameters	Humidity	High or low humidity can affect solvent evaporation and resulting fibre characteristics.	(Casper *et al.*, 2004; Geng, Kwon and Jang, 2005)
	Temperature	Temperature can affect solvent evaporation and solution viscosity, which in turn can affect fibre characteristics.	
Additives	Salts	Salts can reduce bead formation and reduce fibre diameters	(Cengiz and Jirsak, 2009)

1.3.4 Electrospinning Collectors

The electrospinning collector also has a major role in the process as it can help shape the way fibres are deposited. Collectors are normally conductive materials to ensure they can be grounded so as to attract the incoming charged fibres, although collectors can be added between the incoming charged solution jet and the grounded element to simply intercept the incoming fibres. Commonly, electrospinning set ups use a rotating drum or mandrel, as rotation allows for even distribution of fibres across the surface, which can allow for the development of electrospun sheets of uniform thickness. The collector is usually covered in aluminium foil to assist with the removal of the electrospun fibre sheet from the mandrel as fibres can adhere relatively sufficiently to the collector mandrel preventing damage-free removal.

In principle, any conductive material could be used as a collector and a collector could be as basic as a static metal sheet. However, design advances have allowed for the construction of a range of collectors for the collection of fibres in distinct patterns. For example, a rotating cylindrical collector comprising horizontal bars around the circumference can be used to collect highly aligned fibres (Zhang *et al.*, 2015). The production of aligned fibres is of particular interest for TEVGs as it is known that aligned fibres can stimulate cell alignment, which is relevant to circumferential alignment of medial VSMCs and the alignment of luminal endothelium (Nivison-Smith and Weiss, 2012; Wu *et al.*, 2018). Traditionally, aligned fibres are achieved through the use of high-speed rotating mandrel collectors as this high speed allows for the incoming fibre to wrap around the mandrel and therefore becoming aligned. This works well for aligned fibre sheets, but for the development of 3D tubular structure this is impractical as the resulting flat sheet requires manipulation into a tube, which will require processing to join the outer edges of the sheet together.

Static collectors have also been created with air gaps between two collector electrodes that have allowed for the development of highly aligned fibres without the need for high seed rotating mandrels (Dan Li *et al.*, 2003). Interestingly, Trindade *et al.*, (2013) that incoming fibres would be attracted and attach to one collector then the opposite end

would attract and attach to the opposing collector electrode, thus producing highlight horizontal fibre sheets between the gap. However, Dan Li *et al.*, (2003) demonstrated that the maximum air gap for nanofibres with a diameter of less than 150nm was ≤1 cm, meaning this technique may have limitations in regard to the maximum length of aligned fibre scaffolds it can produce. For TEVG purposes, (Jose *et al.*, 2012) produced seamless electrospin tubes with axially aligned fibres, which holds exciting promise for the development of small-diameter TEVGs containing axially aligned fibres.

Alongside collector material and design, secondary charged plates (electrodes) can be used to affect fibre deposition onto collectors, therefore affecting fibre morphology. Conductive plates have been used to disrupt the electrostatic field of the electrospinning set up to enhance fibre alignment (Acharya, Arumugam and Heiden, 2008). It is hypothesised that by placing secondary charged electros either side of the electrospinning jet the instability of the jet is delayed, providing(Acharya, Arumugam and Heiden, 2008) less time for whipping to occur, which allows for greater alignment of incoming fibres . In addition to this, other collectors such as water baths are also demonstrated in the literature; however, for TEVGs purposes the most prominent collector is that which can produce seamless small diameter tubes (Kostakova *et al.*, 2014).

Despite numerous options being available for fibre collection, the development of multiple layered scaffolds with varying fibre diameters and alignment is yet to be explored. This development of multi-layered seamless electrospun tubes with architecturally distinct layers will allow for more physiologically relevant vasculature-like structures to be investigated for use a TEVGs.

1.3.5 Electrospun Fibre Morphology

Once an electrospinning system has been established, it is important to optimise the system to obtain fibres with desirable characteristics, which may include a suitable fibre diameter, high tensile strength and high degree of alignment. For tissue engineering purposes, fibre diameter, surface roughness, tensile strength and alignment are all

important considerations due to their effects on cell-to-scaffold interactions. Currently, electrospinning is one of the only technologies that can produce consistent, smooth, nano-scaled fibres quickly and cost effectively and that has a fine control over fibre diameter. It is important to understand the effect of fibre characteristics such as diameter on cell-to-scaffold interactions as other techniques for microfibre production may be more suitable if there is no justifiable benefit to using nanosized fibres.

The effect of fibre diameter on cells has been highlighted in the literature. Chen *et al.*, (2007) showed that there was a significance different between cell attachment of 3T3 fibroblasts on 428 nm fibre scaffolds compared to diameters of >1 μm. They also found that 3T3 fibroblast proliferation was also improved on smaller fibre diameters (Chen *et al.*, 2007). Noriega *et al.*, (2012) also found a similar association with chondrocytes on chitosan scaffolds. Additionally, they also identified upregulation in collagen protein expression suggesting fibre diameters stimulate behavioural change beyond cellular adhesion and migration (Noriega *et al.*, 2012). VSMCs have also been demonstrated favouring diameter fibre of <1 μm for proliferation (Han *et al.*, 2019). Furthermore, nanofiber scaffolds have also been shown to enhance stem cell differentiation (Wise *et al.*, 2009).

Another characteristic of nanofibres relevant to TEVG development is the association between smaller fibre diameters, and reduced platelet activation and thrombus formation. Milleret *et al.*, (2012) identified that nanofibres of <1 μm has minimal platelet adhesions when compared to fibre diameters ranging from 2 - 5 μm. Liu *et al.*, (2013) also found that aligned nanofibres had a reduced risk of thrombus formation in a rat model. Further to the anti-thrombogenic properties of randomly orientated and aligned nanofibre scaffolds, fibre orientation has also been shown to affect cell orientation (Jia *et al.*, 2014; Whited and Rylander, 2014).

Pore size is also an important characteristic for an electrospun scaffold that affect cell-to-scaffold interactions. Electrospun scaffolds, as previously stated, are known for small pore sizes, which prevent cellular infiltration. Cells normally require pore sizes that are similar or larger than their own size in order to infiltrate a scaffold, whereas electrospun

non-fibre scaffolds generally have pore size of < 1μm(Cortez Tornello *et al.*, 2018). It is well understood that there is a relationship between fibre diameter and pore size (Stephen J. Eichhorn and Sampson, 2005; Cortez Tornello *et al.*, 2014), which is works in opposition to the observation that nano-scaled fibre diameters are generally associated with improved cellular adhesion as both traits would be desirable within a single scaffold. However, for TEVG purposes, it may be advantageous to have small fibre diameters in the luminal surface to ensure endothelial cells can develop and maintain an impermeable monolayer. Additionally, an outer TEVG layer could be produced to mimic the adventitia that may benefit from larger pores, which may still be suitable for fibroblast growth and infiltration. Therefore, it is of interest to understand the effect of fibre diameter, orientation and pore size on vascular cells to gain a fundamental understanding of vascular cell-to-scaffold interactions to help drive the development of superior next generation TEVGs.

Despite the many advantages offered by the electrospinning technique, there are some disadvantages to the electrospinning technique that require consideration. Although small diameter fibres can be produced with the electrospinning technique, it is currently difficult to develop more complex macrostructures with multiple layers or structures that differ significantly to aligned fibres or a compact lattice. This means that it is difficult to introduce interconnected pores, develop multi-layered structures with differing fibre patterns, shapes and sizes. Some or all of these issues may be overcome with further research but this remains to be determined and it may result in the technique needing to be used in conjunction with other technologies to produce future TEVGs.

1.3.6 The Ideal Characteristics of a Tissue Engineered Vascular Graft

Table 1.4 - Suggested characteristics of an ideal TEVG

Characteristic Type	Desired Characteristic
Biological Characteristics	Biocompatibility
	Resistance to platelet activation and thrombosis
	Ability to support a healthy luminal endothelium
	Ability to promote controlled host degradation and remodelling
	Ability to attract specific host cells or be pre-populated with autologous cell types mimicking those of native vascular
	Produce safe degradation by-products
Mechanical Characteristics	High tensile and burst strength
	Adequate compliance
Fabrication Characteristics	Relatively cheap construction
	Fast to produce
Clinical Characteristics	Tailorable to each patient
	Adequate suturability
	Reduce the risk of aberrant blood flow at anastomoses
	Ensure vascular homeostasis
	Easily sterilised
	Transportable and easy to store

It is clear that a number of materials, cell types and techniques can be utilised in order to development the next generation of TEVGs. An ideal TEVG should possess the following traits identified in Table 1.4.

Many of the previously described characteristics of an ideal TEVG (Table 1.4) are those attributed to the natural ECM. However, TEVGs will likely be produced prior to implantation and not develop *in vivo* like ECM. One of the major current challenges is the lack of understanding of cellular interactions with electrospun fibres as many previous studies utilise electrospun scaffold as cell carriers or as a more physiologically relevant 3D cell culture model. It is important to understand how to enhance electrospun scaffolds to ensure a healthy endothelial layer can be obtained to prevent thrombosis, which may help improve patency rates. Mimicking features of the ECM may help to improve TEVG design and creating TEVGs with tuneable characteristics for specific cellular outcomes may improve graft success. To aid future TEVGs electrospinning fabrication methods and equipment need to be developed to create more complex layered tubular structures that can be tested as possible graft replacements.

1.4 Thesis Rationale

Currently, there are still no small-diameter (<6 mm) electrospun TEVGs being used in the clinic for coronary artery bypass purposes. Electrospinning technology, although having been proposed by a patent in 1902 by John Cooley (Colley, 1902), has more recently begun to show promise for regenerative medicine purposes, particularly in vascular graft scaffold fabrication. This is attributed to the ability of the electrospinning process to produce fibres with nano-scaled diameters, which is a range most other scaffold fabrication technologies are unable to achieve, and a range which is more physiologically representative of mammalian ECM. Despite its promise, there is still a need for academic and practical advancement in the electrospinning field in order to produce more complex 3D structures, such as multi-layered tubes. Therefore, further research is required to establish robust methodologies for the production of small-diameter tubes with specific architectures, and to help elucidate the effect of these micro- and nano-electrospun structures on cellular behaviour and morphology. This would enhance future research by providing fundamental knowledge required to build bottom-up scaffolds that are designed to enhance positive cellular responses, which may in turn help produce tubular scaffolds that have long-term patency for future use in the clinic for CABG.

Further to this, due to the numerous variables affecting resulting electrospun fibre morphology, many biological studies conduct experiments without specifically determining an optimal fibre diameter range to ensure optimal cell adherence, growth and behaviour. This means many studies simply use fibrous scaffolds as a 3D ECM-like cell culture surface when compared to standard two-dimensional plastic cell culture surfaces. However, this change from two-dimensional to 3D cell culture does not consider the effect of the electrospun scaffold material, alignment of the fibres, or diameter upon the experimental cells.

Fibre diameter is known to affect cell attachment and morphology. Although the optimisation of the electrospinning process for each material is time consuming, the ability to select for fibre diameter ranges would help to develop scaffolds that enhance cellular adherence and morphology so cells are more physiologically representative to

those *in vivo*. This may help reduce the occurrence of pathological events in regard to vascular grafts through reducing the occurrence of adverse cellular behaviours. This could allow future scaffolds to more appropriately support specific cell types within distinct regions of a multi-layered scaffold, and help direct cellular behaviour and host remodelling of a TEVG.

This thesis is focussed on investigating the effect of electrospun scaffold fibre diameters on cell attachment and morphology to help provide a further understanding towards why previously produced electrospun TEVGs have not translated into clinical use. It is also focussed on establishing electrospinning fabrication methodologies for the development of a multi-layered electrospun tubular scaffold for TEVG purposes. This understanding may help produce future electrospun TEVGs that provide specific cues to targeted cell types to direct cellular-to-scaffold and host-to-scaffold interactions, and produce and maintain physiologically representative remodelled tissue without the need for growth factors that can have downstream effects *in vivo.* The ultimate aim of this thesis is to create a tri-layered electrospun tubular scaffold with distinct layers for potential use as a small diameter TEVG.

1.4.1 Aims

The aims of this thesis were to:

- Develop and optimise an electrospinning process allowing for the production of fibrous scaffolds with tuneable diameters to determine the effect of fibre diameter on cell attachment and morphology.
- Use the observations of cell-to-scaffold interactions from the fabricated scaffolds to help design and generate a tri-layered TEVG with distinct architectures to enhance cell adherence and to stimulate physiologically representative morphologies when compared to traditional two-dimensional cell culture on relatively flat surfaces.

1.4.2 Hypotheses

The following hypotheses were investigated:

- Nano-scaled beadless PLGA fibres can be electrospun using HFIP as a solvent.
- Nano-scaled electrospun PLGA fibres improve endothelial cell attachment compared to micro-scaled PLGA fibres.
- A seamless tri-layered electrospun tube can be produced containing distinct layers of differing fibre diameters and fibre orientations.
- Aligned electrospun PLGA fibres will enhance endothelial cell alignment compared to randomly orientated PLGA fibres.
- Aligned electrospun PCL fibres will enhance smooth muscle cell alignment compared to randomly oriented PCL fibres.
- Fibroblast scaffold infiltration will be PLGA fibre diameter dependent.
- Monocyte-derived macrophages from porcine blood will adhere to each layer of the tri-layered electrospun scaffold.
- Porcine peripheral blood monocyte-derived macrophages may present endothelial and smooth muscle cell markers after culture and transdifferentiation on electrospun tube layers 1 and 2, respectively.

1.4.3 Experimental Approach

The following experimental approaches were employed to help determine the hypotheses outlined in section 1.4.2.

Chapter 3 investigated the effect of fibre diameter on cell attachment using the following approaches:

- The optimisation of an electrospinning set up using HFIP as a solvent to generate 3 different PLGA fibre diameters was assessed.
- HUVEC attachment on the 3 PLGA fibre diameters was determined.
- A tubular scaffold using the most appropriate fibre diameter, as determined by the previous experimental work in this chapter, was developed.

Chapter 4 investigated whether a tri-layered electrospun tubular scaffold could be fabricated for vascular graft purposes using the following experimental approaches:

- An electrospinning collector was created and optimised to produce longitudinally aligned fibre tubes for Layer 1.
- An electrospinning collector was created and optimised to produce circumferentially aligned fibre tubes for Layer 2.
- The addition of fluorescent dyes to each electrospun tube layer was investigated to help with identification of the separate layers.
- A tri-layered tube fabrication process was established to incorporate the 3 separate layers into 1 seamless tube as a proof of concept.

Chapter 5 investigated the hypothesised effects of each layer's fibre diameter and orientation on cell attachment and morphology using the following experimental approaches:

- Layers 1 and 2 were assessed for their ability to stimulate HUVEC and hVSMC alignment, respectively.
- Layer 3 was investigated for its ability to support hSVF attachment and infiltration.
- The use of porcine blood as an adherent cell source was evaluated.
- The ability of adherent monocyte-derived macrophages to transdifferentiate into endothelial-like and smooth muscle-like cells was initially investigated.

2

MATERIALS AND METHODS

2.1 Materials

Unless otherwise stated, standard manufacturers' protocols were used. All chemicals were purchased from Sigma-Aldrich (Dorset, UK) and all consumable plasticware was purchased from Greiner Bio One (Stonehouse, UK). 1,1,13,3,3-Hexafluoro-2-propanol (HFIP) was purchased from Fisher Scientific (Loughborough, UK). PURASORB PDLG 5010 (50/50 DL-lactide/glycolide copolymer, molecular weight (M_w) ~153, 000 g mol^{-1}; PLGA) was purchased from Corbion (Amsterdam, Netherlands) and is denoted as PLGA throughout this thesis. Polycaprolactone (PCL; M_w ~ 80,000 g mol^{-1}) was purchased from Sigma-Aldrich (Dorset, UK).

2.1.1 Buffers and Solutions

Table 2.1 - Summary of the buffers and solutions used in experiments within this thesis

Buffer/Solution	Composition
Phosphate Buffered Saline (PBS)	10 mM phosphate buffer containing 2.7 mM potassium chloride and 137 mM sodium chloride, pH 7.4
Cell freezing Solution	10% (v/v) Dimethyl Sulfoxide (DMSO) in Foetal Bovine Serum (FBS; Life Technologies, UK)
Peripheral Blood Mononuclear Cell (pPBMC) Isolation Wash Buffer	Dulbecco's PBS (2.67 mM KCl, 1.47 mM KH_2PO_4, 137.93 mM NaCl and 4.29 mM Na_2HPO_4 anhydrous) supplemented with 2% (v/v) FBS
Scaffold Sterilisation Solution (SSS)	9000 international units (IU) mL^{-1} penicillin , 9 mg mL^{-1} streptomycin and 25 µg mL^{-1} amphotericin B
Fixing Solution	4% (w/v) Paraformaldehyde (PFA) in PBS

Table 2.2 - Summary of the chemical reagents used in the experiments within this thesis

Chemicals	Supplier	Catalogue Number
1,1,1,3,3,3-Hexafluoro-2-propanol	Fisher Scientific	10706191
(3-aminopropyl) triethoxysilane	Scientific Laboratory Supplies	A3648
Sodium Acetate	Sigma-Aldrich	S2889
Ammonium Chloride	Alfa Aesar	A15000.30
Sodium Chloride	Sigma-Aldrich	S7653
Osmium Tetroxide	Fisher Scientific	10531641
Sodium Cacodylate Trihydrate	Scientific Laboratory Supplies	20840-25G-F
1,1,1,3,3,3-Hexamethyldisilazane	Fisher Scientific	10568470

Table 2.3 - Summary of the primary antibodies used in the experiments within this thesis

Primary Antibody	Target Species	Host Species	Working Concentration	Supplier	Catalogue Number
Anti-CD144 (VE-Cadherin)	Human	Mouse	5 μg mL^{-1}	Biolegend	348502
Anti-α-Smooth Muscle Actin	Pig	Mouse	14 μg mL^{-1}	Sigma Aldrich	A2547
Anti-CD203a (clone PM18-7)	Pig	Mouse	5 μg mL^{-1}	Bio-Rad	MCA1973GA
Anti-Endothelial Nitric Oxide Synthase	Pig	Rabbit	1 μg mL^{-1}	Abcam	ab5589
Anti-Myosin Heavy Chain	Pig	Rabbit	0.8 μg mL^{-1}	Abcam	ab53219

Table 2.4 - Summary of the secondary antibodies used in the experiments within this thesis

Secondary Antibody	Host Species	Working Concentration	Supplier	Catalogue Number
Biotinylated Anti-Rabbit IgG	Goat	1:200	Vector Labs	BA-1000
Biotinylated Anti-Mouse IgG	Goat	1:200	Vector Labs	BA-9200
Anti-Mouse Alexa Fluor 594 conjugate	Goat	1:200	Life Technologies	A-11005

Table 2.5 - Summary of the fluorophores used in the experiments within this thesis

Fluorophore Conjugate	Working Dilution	Supplier	Catalogue Number
Streptavidin Cy5	1:200	Biolegend	405205
Streptavidin 633	1:200	Life Technologies	10164762

Table 2.6 - Summary of the fluorescent dyes used in the experiments within this thesis

Fluorescent Dye	Working Concentration (w/v)	Supplier	Catalogue Number
DAPI	5 μg mL^{-1}	Biolegend	422801
Rhodamine B	2.5 mg mL^{-1}	Sigma Aldrich	83689
Rhodamine 123	2.5 mg mL^{-1}	Sigma Aldrich	R8004
TO-PRO™-3 Iodide	1 μM	Life Technologies	T3605
Phalloidin-Atto 550	50 μg mL^{-1}	Sigma Aldrich	19083

2.1.2 Tissue Culture Materials

2.1.2.1 HUVEC and hSVF Culture

Endothelial Cell Growth Medium 2 (MV2) PromoCell; catalogue number: C22121) containing 100 IU mL^{-1} (v/v) Penicillin and 0.1 mg mL^{-1} Streptomycin (Sigma-Aldrich; catalogue number: P4333) was used for culturing both Human Umbilical Vein Endothelial Cells (HUVECs) and Human Saphenous Vein Fibroblasts (hSVFs). Other general tissue culture reagents used for HUVECs and hSVFs culture were Accutase (eBioscience; catalogue number: 00-4555-56), Foetal Bovine Serum (FBS; Life Technologies; catalogue number: 10500064), and Phosphate-Buffered Saline (PBS; Sigma-Aldrich; catalogue number: P4417).

2.1.2.2 hVSMC Culture

Smooth Muscle Cell Growth Medium BulletKit (SmBm) Lonza; catalogue number: CC-3181 and CC-4149) containing 100 IU mL^{-1} (v/v) Penicillin and 0.1 mg mL^{-1} Streptomycin (Sigma-Aldrich; catalogue number: P4333) was used for culturing Human Vascular Smooth Muscle Cells (hVSMCs). Other general tissue culture reagents used for hVSMC culture were Accutase (eBioscience; catalogue number: 00-4555-56), Foetal Bovine Serum (FBS; Life Technologies; catalogue number: 10500064), and Phosphate-Buffered Saline (PBS; Sigma-Aldrich; catalogue number: P4417).

2.1.2.3 pPBMC Culture

Roswell Park Memorial Institute-1640 (RPMI-1640) Life Technologies; catalogue number: 31870025) containing 55% (v/v) porcine FBS, 25 µg mL^{-1} amphotericin B, 100 IU mL^{-1} (v/v) Penicillin and 0.1 mg mL^{-1} Streptomycin was used to culture Porcine Peripheral Blood Mononuclear Cells (pPBMCs).

2.1.2.4 Porcine Peripheral Blood Collection

350 mL Citrate Phosphate Dextrose Adenine (CPDA; Vet Direct Holdings Ltd; catalogue number: IMT100/FA) blood bags were used for collecting porcine peripheral blood.

2.1.2.5 pPBMC Isolation

Ficoll-Paque™ PLUS density gradient medium (GE Healthcare Life Sciences, Little Chalfont, UK) was used to isolate pPBMCs.

2.1.2.6 Escherichia coli and Candida albicans Enumeration

Pre-packaged Nutrient Agar 90 mm petri dish (vWR International; catalogue number: 100692ZA) and Sabouraud 4% Dextrose Agar 90 mm petri dish (vWR International; catalogue number: 100884ZA) were used to enumerate E.coli and C.albicans, respectively.

2.1.2.7 Scaffold Sterilisation Solution

25 μg mL^{-1} amphotericin B (Fungizone; Life Technologies; catalogue number: 15290018) and 100 IU mL^{-1} (v/v) Penicillin and 0.1 mg mL^{-1} Streptomycin (Sigma-Aldrich; catalogue number: P4333) were used to sterilise electrospun scaffolds and reffered to as scaffold sterilising solution (SSS)..

2.1.2.8 Slide Coating for PLGA Cryosections

Superfrost Plus glass microscope slides (Thermo Fisher Scientific; catalogue number: 10149870) were coated with (3-aminopropyl) triethoxysilane (APTES; Scientific Laboratory Supplies; catalogue number: A3648).

2.2 Methods

2.2.1 Cell Culture

2.2.1.1 HUVEC Maintenance

Pooled HUVECs used for all experiments were purchased from PromoCell (Heidelberg, Germany). In all experiments HUVECs were cultured in 175 cm2 cell culture flasks at 37°C and 5% CO_2 in endothelial cell medium 2 (MV2; PromoCell, Heidelberg, Germany) supplemented with 5% (v/v) FBS, 5 ng mL^{-1} Epidermal Growth Factor, 10 ng mL^{-1} Basic Fibroblast Growth Factor, 20 ng mL^{-1} Insulin-like Growth Factor, 0.5 ng mL^{-1} Vascular Endothelial Growth Factor 165, 1 µg mL^{-1} Ascorbic Acid, 0.2 µg mL-1 Hydrocortisone (PromoCell, Heidelberg, Germany), 100 IU mL^{-1} (v/v) Penicillin and 0.1 mg mL^{-1} Streptomycin (Sigma-Aldrich, UK). Growth medium was changed every 3 - 4 d.

2.2.1.2 Fibroblast Maintenance

Human Saphenous Vein Fibroblasts (hSVFs) were isolated from patient saphenous vein by Dr Cressida Lyon, University of Bristol, which were extracted from surplus tissue from coronary artery bypass surgeries permitted under the Research and Ethics Committee #14/EE/1097, in accordance with the ethical standards laid down in the 1964 Declaration of Helsinki and its later amendments. The following method was used. Briefly, explanted human saphenous vein pieces were cut longitudinally and opened to expose the luminal surface. The endothelial layer was removed using the inner removable component of a 1 mL sterile plastic syringe. A surgical scalpel and a pair of forceps were used to remove the medial layer, leaving only the adventitia. The remaining adventitia was cut into 1 mm squares and placed into a 25 cm^2 cell culture flask with Roswell Park Memorial Institute-1640 (RPMI-1640; buffered with 25 mM HEPES or sodium bicarbonate) purchased from Gibco (catalogue number: 42401-018). RPMI-1640 was supplemented with FBS (PAA Laboratories; catalogue number: A15-151), L-glutamine (PAA Laboratories; catalogue number: M11-004), penicillin and streptomycin (PAA Laboratories; catalogue number: P11-010), and 0.8 µg mL^{-1} gentamicin (PAA

Laboratories; catalogue number: P11-004). The explants were then incubated at 37°C, 5% CO_2 for 24 h to allow cell outgrowth onto the flask surface.

In all experiments hSVFs were cultured in 175 cm^2 cell culture flasks at 37°C and 5% CO_2 in endothelial cell medium 2 (MV2; PromoCell, Heidelberg, Germany) containing 5% (v/v) Foetal Bovine Serum, 5 ng mL^{-1} Epidermal Growth Factor, 10 ng mL^{-1} Basic Fibroblast Growth Factor, 20 ng mL^{-1} Insulin-like Growth Factor, 0.5 ng mL^{-1} Vascular Endothelial Growth Factor 165, 1 µg mL^{-1} Ascorbic Acid, 0.2 µg mL^{-1} Hydrocortisone (PromoCell, Heidelberg, Germany), 100 U mL^{-1} (v/v) Penicillin and 0.1 mg mL^{-1} Streptomycin (Sigma-Aldrich, UK). Growth medium was changed every 3 – 4 d.

2.2.1.3 Cell Passage

Once cell culture confluence had reached 80%, cells were washed once with PBS (Sigma-Aldrich, Dorset, UK) and incubated at room temperature (RT) for 10 min in Accutase prepared in Dulbecco's PBS, 0.5 nM EDTA and 11 mg L^{-1} Phenol Red (eBioscience, Hatfield, UK). Any remaining adherent cells were dislodged through an abrupt force from the palm of the hand to the side of the flask. The dislodged cells were centrifuged at 110 x g for 5 min, the Accutase solution aspirated and the cell pellet re-suspended in fresh tissue culture medium. Cells were then seeded at a density of 5000 cells per cm^2 in new cell culture flasks. All experiments used HUVECs at passages 2 - 4 and hSVFs at passages 1 – 3, from 5 separate Lot numbers.

2.2.1.4 Cell Counting

Cells were counted on a Countess® Automated Cell Counter (Life Technologies, Paisley, UK). 25 µL of cell suspension was mixed with 25 µL of 0.4% (w/v) Trypan Blue Stain (Life Technologies, UK). 10 µL of this solution was then inserted into each chamber of a Countess Slide (Life Technologies, UK) and analysed by the cell counter. Four counts were performed and the average number of viable cells (non-stained) calculated for subsequent cell seeding.

2.2.1.5 Cell Storage

Cells were dissociated as previously described, re-suspended in 1 mL cell freezing solution, and placed at -80°C in an alcohol-free CoolCell® (Biocision, USA) which stabilises the cooling rate to 1°C min^{-1}. For long term storage cells were transferred to liquid nitrogen and stored under vapour phase. Cells were thawed by submersion in a water bath at 37°C for 3 min, added to 9 mL of culture media, centrifuged at 110 x g for 5 min, and then transferred to flasks containing culture media and incubated at 37°C in 5% CO_2 or used for an experiment accordingly.

2.2.1.6 pPBMC Isolation

pPBMCs were isolated in accordance with the manufacturer's instructions for the SepMate™ tubes (StemCell technologies, Grenoble, France) outlined below.

Porcine peripheral whole blood (pPWB) was drawn from the carotid artery into a sterile, 450 mL whole blood capacity, Citrate Phosphate Dextrose Adenine (CPDA-1) blood bag containing 63 mL CPDA-1 solution (206 mg citric acid monohydrate, 1.66 g sodium citrate dihydrate, 2.01 g glucose monohydrate, 158 mg sodium dihydrogen phosphate dihydrate and 17.3 mg adenine).

The subsequent pPWB solution was diluted with an equal volume of pPBMC isolation wash buffer. 30 mL of the resulting pPWB and pPBMC wash buffer solution was gently added to a 50 mL SepMate™ tube containing 15 mL Ficoll-Paque™ PLUS density gradient medium. The tubes were then centrifuged at 1200 x g for 10 min at RT with the deceleration brake on. The liquid supernatant was poured into a 50 mL falcon tube by fully inverting the SepMate™ tube for no longer than 2 seconds. The resulting enriched mononuclear cell fraction was washed by adding 20 mL of pPBMC isolation wash buffer and centrifuging at 300 x g for 8 min at RT with the deceleration brake on. The supernatant was removed to leave the cell pellet. This step was repeated by centrifuging at 120 x g for 10 min at RT with the brake off to separate the platelets from the PBMC. The resulting platelet-rich supernatant was removed. The enriched PBMC pellet was re-

suspended in cell freezing solution for cryopreservation as described above in section 2.2.1.5 until required.

2.2.1.7 Porcine Serum Isolation

pPWB was drawn into 50 mL falcon tubes. Tubes were left undisturbed at 4°C for 12 h before processing. Tubes were then centrifuged at 2000 x g at 4°C for 10 min. The serum was carefully removed to a fresh 50 mL falcon to minimise red blood cell (RBC) contamination. To remove platelets, the serum containing tubes were re-centrifuged at 2000 x g at 4°C for 10 min and the supernatant carefully transferred to a fresh 50 mL falcon. The resulting serum was then heated at 56°C for 30 min to degrade complement proteins. The serum was then left to cool and subsequently frozen and stored at -20°C. Porcine serum was sterilised using 0.2 μm syringe filters (Sarstedt, Nümbrecht, Germany) before use.

2.2.2 Electrospinning Fabrication Methods

2.2.2.1 Electrospinning Solution Preparation

Solutions were prepared as follows:

11% PLGA Solution ($PLGA^{11}$): PLGA was dissolved in HFIP to obtain an 11% (w/v) solution. The solution was agitated for up to 24 h using a mechanised rocker at RT until a homogenous polymer-solution formed.

11% (w/v) PLGA + 1% (w.v) Sodium Chloride Solution ($PLGA^{11\ NaCl}$): PLGA was dissolved in HFIP to obtain an 11% (w/v) solution containing 1% (w/v) Sodium Chloride (NaCl). The solution was agitated for up to 24 h using a mechanised rocker at RT until a homogenous polymer-solution formed.

25% (w/v) PLGA + 1% (w/v) Sodium Acetate Solution ($PLGA^{25\ NaOAc}$): PLGA was dissolved in HFIP to obtain a 25% (w/v) solution containing 1% (w/v) Sodium Acetate

(NaOAc). The solution was agitated for up to 24 h using a mechanised rocker at RT until a homogenous polymer-solution formed.

13% (w/v) PLGA Solution (PLGA^{13}): PLGA was dissolved in HFIP to obtain an 13% (w/v) solution. The solution was agitated for up to 24 h using a mechanised rocker at RT until a homogenous polymer-solution formed.

15% (w/v) PLGA Solution (PLGA^{15}): PLGA was dissolved in HFIP to obtain an 15% (w/v) solution. The solution was agitated for up to 24 h using a mechanised rocker at RT until a homogenous polymer-solution formed.

11% (w/v) PCL Solution (PCL^{11}): PCL was dissolved in HFIP to obtain an 11% (w/v) solution. The solution was agitated for up to 24 h using a mechanised rocker at RT until a homogenous polymer-solution formed.

2.2.2.2 Flat Sheet Electrospun Scaffold Fabrication

All electrospun scaffold fabrication was carried out at room temperature and humidity. These parameters varied slightly due to UK seasonal conditions, but were assumed to not significantly affect the experimental outcomes; although, this was not scientifically tested. Scaffolds composed of aligned fibres are henceforth denoted with (a); i.e. PLGA^{11} $^{(a)}$. All scaffolds should be assumed to be randomly orientated unless otherwise stated. The initial electrospinning set up is outlined in Figure 2.1.

PLGA^{11}: The polymer solution was drawn into a 10 mL luer lock syringe (Becton-Dickinson Bioscience, UK) connected to a 22 gauge (G) 1 ½ inch blunted needle with a nominal internal diameter of 394 µm (Becton-Dickinson Bioscience, UK). A continuous direct current voltage of 8 kV was applied to the syringe needle. A grounded rotating stainless steel mandrel collector with a diameter of 100 mm was covered in a layer of aluminium foil and placed at a distance 10 cm away from the syringe needle tip. The solution was dispensed at a rate of 2 mL hour^{-1} using a syringe pump (PHD 2000 Infusion Syringe Pump, Harvard Apparatus, Holliston, Massachusetts) set for a syringe diameter

of 15.5 mm. The collecting mandrel drum rotated at 5 x g for randomly orientated fibres. Resulting scaffolds were then dried for 48 h in a fume hood, and stored at 2 - 4°C until required. The scaffold thickness was determined by the spinning time.

PLGA$^{11\ NaCl}$: The set up was identical to the previously described PLGA^{11} method except the applied direct current voltage was increased to 10.5 kV.

PLGA$^{25\ NaOAc}$: The set up was identical to the previously described PLGA^{11} except the applied direct current voltage was increased to 20 kV.

Aligned flat sheets were produced as described above; however, mandrel rotational speed was increased to 2000 x g.

2.2.2.3 Randomly Orientated PLGA Electrospun Tube Fabrication

The electrospinning set up was the same as the previously described flat sheet scaffold method, depending on the particular polymer-solvent solution used, except for the following differences. Solutions were electrospun onto a grounded 4 mm diameter stainless steel mandrel, containing a 100 mm central segment with a diameter of 5 mm. The central segment was covered in an 80 µm diameter copper wire monolayer, ensuring no overlap between the coils (Figure 2.2). The remaining mandrel flanks were insulated with cellophane tape to resist polymer fibre attraction. Solutions were electrospun until the desired tube thickness was achieved. Resulting tubes were air dried for 24 h and then cut to the desired length. The cellophane tape was removed and the copper wire was pulled to release the scaffold from the mandrel. The collecting mandrel drum rotated at 5 x g for randomly orientated fibres. Each tubular scaffold was then sterilised with SSS as described below in and stored in PBS until use.

2.2.2.4 Tri-layered Tube Fabrication

2.2.2.4.1 Layer 1 - Axially Orientated PLGA$^{25\ NaOAc}$ Fibre Layer Fabrication

PLGA$^{25\ NaOAc}$ solution was drawn into a 10 mL luer lock syringe (Becton-Dickinson Bioscience, UK). A 22G 1 ½ inch blunted needle with a nominal internal diameter of 394 μm (Becton-Dickinson Bioscience, UK) was attached to a 125 mm syringe kwill filling tube (GP Supplies, UK), which was in turn attached to the syringe (Figure 2.3). A cardboard support was used to hold the kwill in a horizontal position level with the collector. The needle was pierced through a 60 mm^2 piece of folded aluminium foil that was securely attached to the cardboard support. A continuous direct current voltage of 20 kV was applied to the aluminium foil, which in turn charged the needle. A grounded rotating stainless-steel dual mandrel collector (collector 2) with a diameter of 5 mm was placed at a distance 150 mm away from the syringe needle tip (Figure 2.3). The opposing collector mandrels were separated by an air gap of 40 mm. The solution was dispensed at a rate of 2 mL hour^{-1} using a syringe pump (PHD 2000 Infusion Syringe Pump, Harvard Apparatus, Holliston, Massachusetts) set for a syringe diameter of 15.5 mm. The opposing collector mandrels rotated at 0.00028 x g for randomly aligned fibres.

2.2.2.4.2 Layer 2 - Longitudinally Orientated PCL Fibre Layer Fabrication

PLGA Layer 1 was cut away from collector A and placed onto a 100 mm long, 5 mm diameter, stainless steel rod coated with 25 μm of Polytetrafluoroethylene (PTFE). The scaffold tube was secured into the centre of the rod with cellophane tape at either end leaving 30 mm of the scaffold untouched in the centre (Figure 2.4). This was then fitted to the adapted drill motor collector (collector 3; Figure 2.4).

PCL^{11} solution was drawn into a 10 mL syringe (Becton-Dickinson Bioscience, UK). A 22G 1 ½ inch blunted needle with a nominal internal diameter of 394 μm (Becton-Dickinson Bioscience, UK) was attached to a 125 mm kwill filling tube (GP Supplies, UK), which was

in turn attached to the syringe (Figure 2.4). A cardboard support was used to hold the kwill in a horizontal position level with the collector. The needle was pierced through a 60 mm^2 piece of folded aluminium foil that was securely attached to the cardboard support. The positive charge was applied to the aluminium foil, which in turn charged the needle. A continuous direct current voltage of 10.5 kV was applied to the aluminium foil, which in turn charged the needle. A grounded rotating Teflon coated stainless steel mandrel collector with a diameter of 5 mm was placed at a distance 200 mm away from the syringe needle tip (Figure 2.4). The solution was dispensed at a rate of 2 mL $hour^{-1}$ using a syringe pump (PHD 2000 Infusion Syringe Pump, Harvard Apparatus, Holliston, Massachusetts) set for a syringe diameter of 15.5 mm. The opposing collector mandrels rotated at 2000 x g for randomly aligned fibres.

2.2.2.4.3 Layer 3 - Randomly Orientated PLGA Fibre Layer Fabrication

PLGA[13] solution was drawn into a 10 mL luer lock syringe (Becton-Dickinson Bioscience, UK) connected to a 22G 1 ½ inch blunted needle with a nominal internal diameter of 394 µm (Becton-Dickinson Bioscience, UK). A continuous direct current voltage of 5.5 kV was applied to the syringe needle. Collector 3 containing the dual-layered scaffold was placed at a distance 10 cm away from the syringe needle tip. The solution was dispensed at a rate of 2 mL $hour^{-1}$ using a syringe pump (PHD 2000 Infusion Syringe Pump, Harvard Apparatus, Holliston, Massachusetts) set for a syringe diameter of 15.5 mm. The collecting Teflon coated stainless steel mandrel had a diameter of 5 mm and rotated at 5 x g for randomly orientated fibres. Resulting tri-layered scaffolds were then dried for 48 h in a fume hood, and stored at 2 - 4°C until required.

Table 2.7 - Summary of the standard electrospinning parameters used in the experiments within Chapter 3

Solution Name/ Polymer	Solvent	Polymer Concentration (%)	Additive	Needle Bore Size	Needle Tip-to-Collector Distance (mm)	Needle Voltage (kV)	Flow Rate (mL hour^{-1})	Collector Type	Collector Speed (G-force)
PLGA^{11}	HFIP	11	n/a	22G 1 ½	100	8	2	100 mm Ø or 5 mm Ø rotating mandrel	5
PLGA$^{11\ NaCl}$		11	1% NaCl			10.5			
PLGA$^{25\ NaOAc}$		25	1% NaOAc			20.5			

Table 2.8 - Summary of the electrospinning parameters used in experiments within Chapters 3 and 4 for the fabrication of randomly orientated fibre flat sheets

Solution Name/ Polymer	Solvent	Polymer Concentration (%)	Additive	Needle Bore Size	Needle Tip-to-Collector Distance (mm)	Needle Voltage (kV)	Flow Rate (mL hour^{-1})	Collector Type	Collector Speed (G-force)	Kwill (yes/no)
PLGA^{11}	HFIP	11	n/a	22G 1 ½	100	8	2	100 mm Ø rotating mandrel	5	No
PLGA^{11} NaCl			1% NaCl			10.5				
PLGA^{25} NaOAc		25	1% NaOAc			20.5				
PLGA^{13}		13	n/a			5.5				
PLGA^{15}		15	n/a			5.5				
PCL^{11}		11	n/a		200	10.5				Yes

Table 2.9 - Summary of the electrospinning parameters used in experiments within Chapters 3 and 4 for the fabrication of aligned fibre flat sheets

Solution Name/ Polymer	Solvent	Polymer Concentration (%)	Additive	Needle Bore Size	Needle Tip-to-Collector Distance (mm)	Needle Voltage (kV)	Flow Rate (mL hour^{-1})	Collector Type	Collector Speed (G-force)	Kwill (yes/no)
PLGA^{25} NaOAc (a)	HFIP	25	1% NaOAc	22G 1 ½	150	20.5	2	100 mm Ø rotating mandrel	2000	No
PCL^{11} (a)		11	n/a		200	10.5				Yes

Table 2.10 - Summary of the electrospinning parameters used for the fabrication of the tri-layered tube corresponding to Layers 1, 2 and 3

Layer	Solution Name/ Polymer	Solvent	Polymer Concentration (%)	Additive	Needle Bore Size	Needle Tip-to-Collector Distance (mm)	Needle Voltage (kV)	Flow Rate (mL hour^{-1})	Collector Type	Collector Speed (G-force)	Kwill (yes/no)
1	**PLGA^{25}** NaOAc (a)	HFIP	25	1% NaOAc	22G 1 ½	150	20.5	2	Collector 2	0.00028	Yes
2	**PCL^{11} (a)**		11	n/a		200	10.5		Collector 3	2000	
3	**PLGA^{13}**		13	n/a		150	5.5			5	No

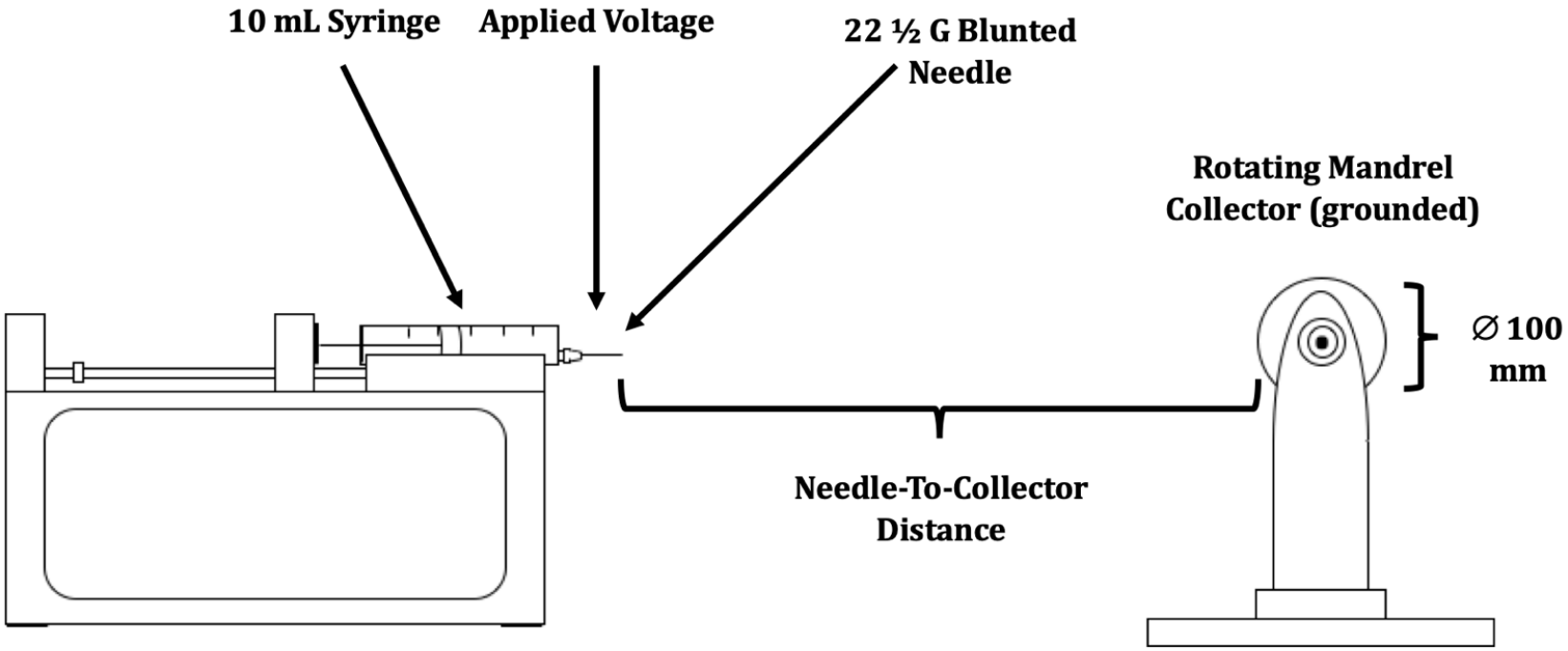

Figure 2.1 - Standard electrospinning set up for fabrication of randomly orientated flat sheets. A 10 mL syringe containing the electrospinning solution was connected to a 22 ½ G blunted needle. The electrospinning process was started by adding an applied voltage to the needle and by applying a flow rate of 4 mL h^{-1}. Fibres were collected onto a 100 mm diameter rotating mandrel at 5 x g.

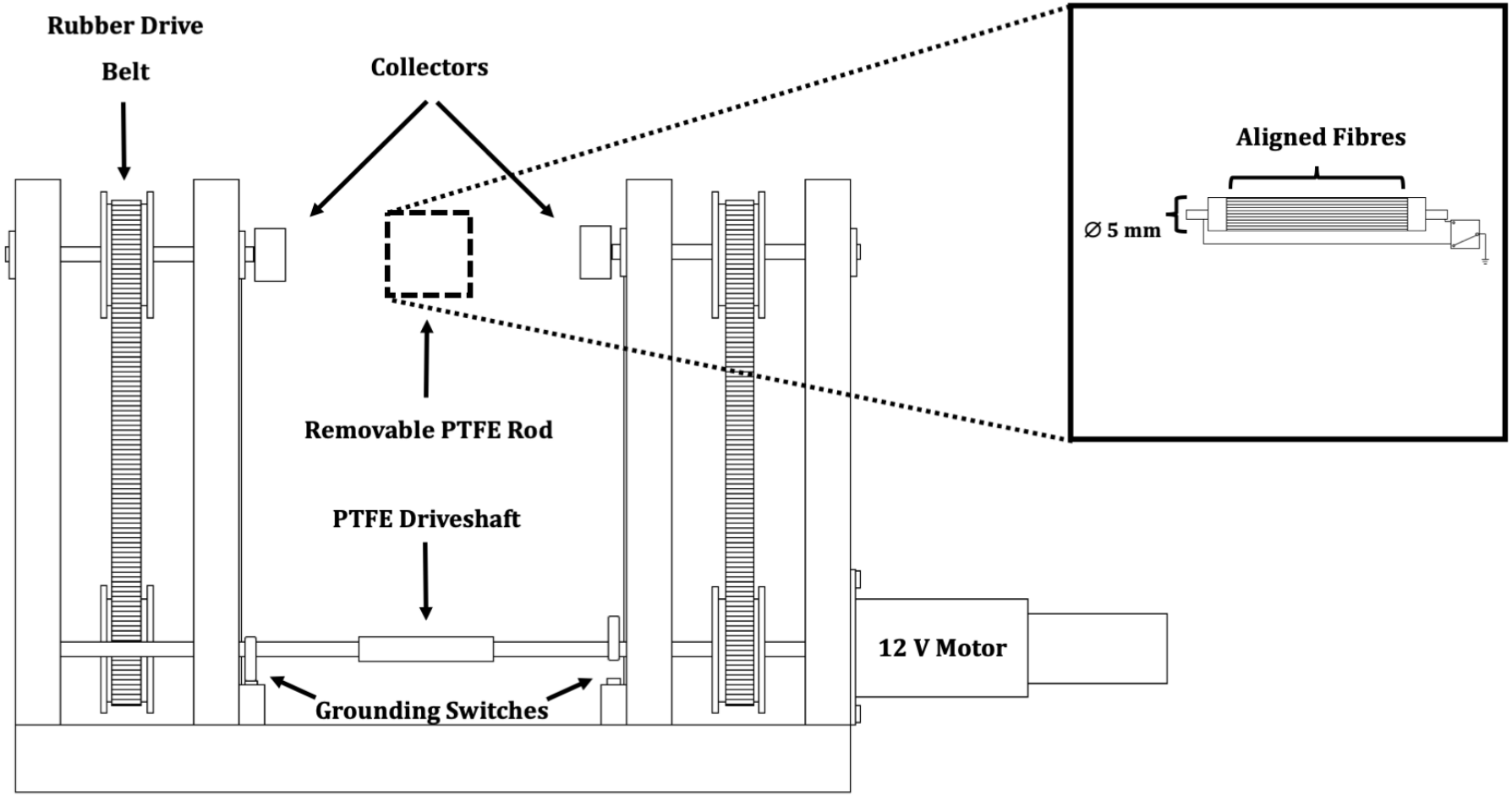

Figure 2.2 - Schematic of axially aligned fibre tube collector 2. Two opposing collector electrodes are separated by a PTFE rod. The motor moves the drive belts, which in turn rotate the collector electrodes and the PTFE rod. The grounding switches ground each collector electrode; as one electrode is grounded and the other is not. Diagram adapted from Jose *et al.,* (2012).

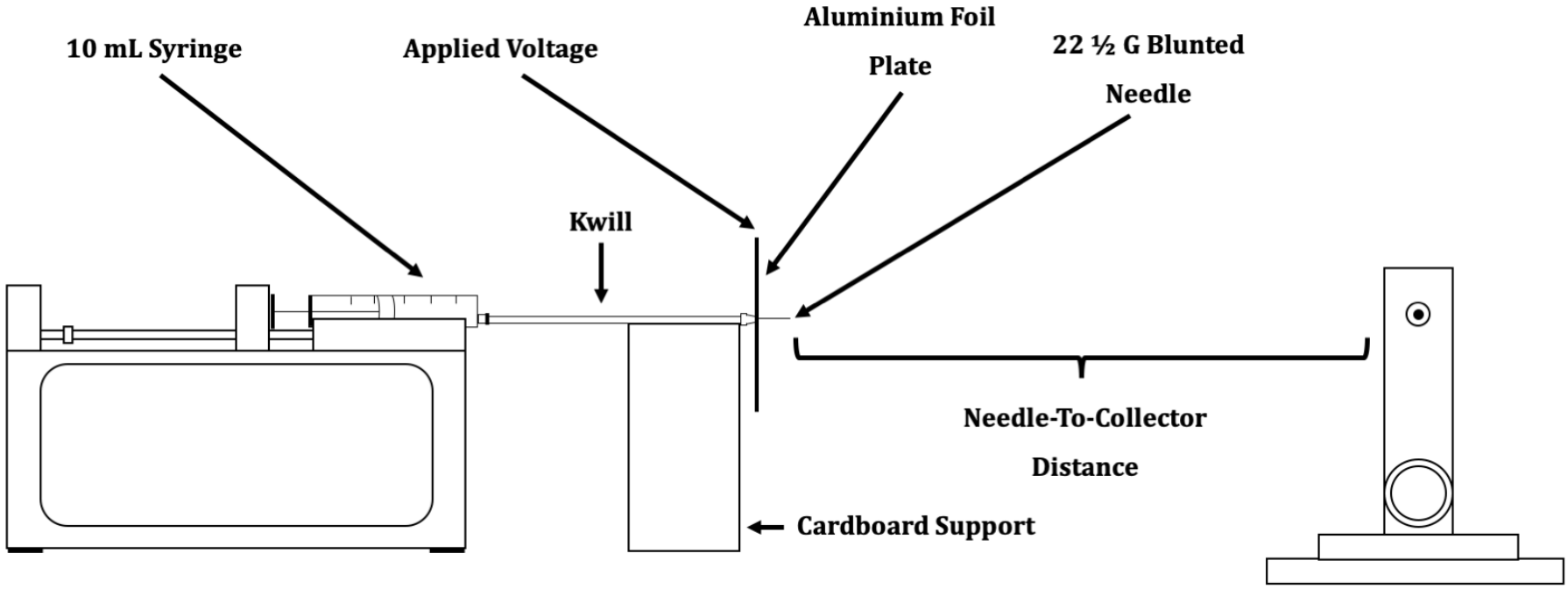

Figure 2.3 - Electrospinning set up of axially aligned fibre tube fabrication. A 10 mL syringe containing the electrospinning solution was connected to syringe kwill, which was then connected to a 22 ½ G blunted needle containing an aluminium foil plate. The electrospinning process was started by adding an applied voltage to the needle and by applying a flow rate of 4 mL h^{-1}. Fibres were collected onto collector 2.

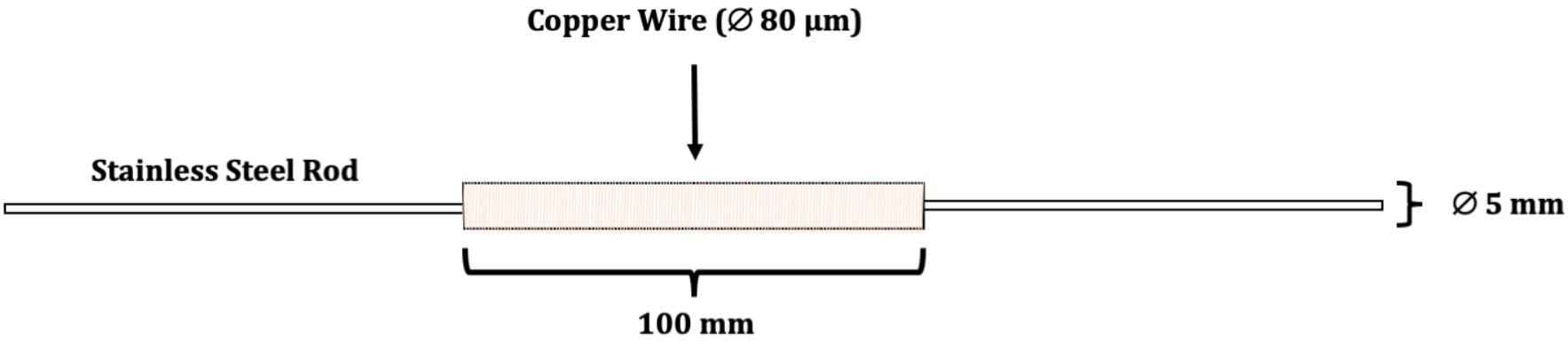

Figure 2.4 - Schematic of a modified collector mandrel containing copper wire monolayer. A stainless-steel rod containing a central segment with an increased diameter of 5 mm was covered In a monolayer of 80 µm copper wire.

2.2.3 Scaffold Sterilisation Testing

Escherichia coli (*E.coli*) and *Candida albicans* (*C.albicans*) were supplied by Dr Cheryl Whittles, Undergraduate Teaching Department, University of Bristol. 8 mm discs were produced from the control PLGA scaffold, using sterile biopsy punches. Discs were placed into 2 mL sterile Dulbecco's modified eagle medium (DMEM; life Technologies, UK) supplemented with 10% (v/v) FBS . They were then inoculated with either *E.coli* or *C.albicans* from the respective stock solution. *C.albicans* or *E.coli* inoculated discs were then incubated at 35°C or 37°C, respectively for 24 h in 5% CO_2 to encourage bacterial or fungal growth and attachment to the discs. Discs were briefly washed once in sterile PBS to remove non-adherent cells. Discs were then added to 2 mL SSS 9000 IU mL^{-1} (v/v) Penicillin, 9 mg mL^{-1} Streptomycin (Sigma-Aldrich, UK) and 25 µg mL^{-1} Amphotericin B (ThermoFisher Scientific, Loughborough, UK). They were then incubated undisturbed at 4°C for 3, 6 and 12 h. Discs were then washed once in sterile PBS and added to 2 mL of sterile DMEM containing 10% FBS and incubated at 35°C or 37°C and 5% CO_2 for 4 d. 100 µL of the incubated DMEM was then plated onto a nutrient agar 90 mm petri dish (vWR International, UK) for *E.coli* enumeration. 100 µL of the inoculated DMEM was also spread onto a Sabouraud 4% Dextrose Agar 90 mm petri dish for *C.albicans* enumeration. Images were taken of each plate and colonies counted. Each colony was assumed to originate from a single cell.

2.2.4 Sterilisation of Electrospun Scaffolds

Scaffolds were air dried for 24 h to allow evaporation of residual HFIP solvent. Scaffolds were mounted onto 70% (v/v) ethanol sterilised 48-well Cell Crowns™ (Scaffdex, UK) and placed into a sterile 48-well plate. The wells were filled with SSS solution and incubated at 4°C for 12 h. SSS solution was then removed and the wells washed with sterile PBS for 5 min. The PBS was then replaced with culture medium for the subsequent experiments to prime the scaffolds. The plates were then incubated at 4°C for at least 12 h.

2.2.5 Cell Crown Cleaning

Cell crowns were cleaned after each use using a solution containing 35% (v/v) ethanol, 49% (v/v) glacial acetic acid (anhydrous), 1% (v/v) household liquid detergent in deionised water. Cell crowns were agitated in the cleaning solution for 12 h via a magnetic stirrer. The cell crowns were then washed 3 times with deionised water before being sterilised in 70% ethanol for 24 h, washed 3 times with PBS and then dried before use.

2.2.6 Scanning Electron Microscopy of Electrospun Fibres

All electrospun polymer samples not used for cell culture were air dried for at least 24 h depending on sample thickness to ensure removal of all residual HFIP solvent. The specimens were coated with gold via a sputtering method using 25 mA and 1.5 kV (EmiTech K575X Sputter Coater, Quorum Technologies Ltd, UK); the thickness of sputtered gold was between 10 and 12 nm. A Jeol JSM-633OF field emission scanning electron microscope (FEG-SEM, UK) was used at an operating voltage of 20 kV, a working distance of 15 mm and spot size 3 to obtain images.

2.2.7 Fluorescent Staining of Fibres for Tri-Layer Identification

Electrospinning scaffold solutions were created as previously described in 2.3.1. Fluorescent dyes were then added at the concentrations outlined in Table 2.6, 1 h before electrospinning.

2.2.8 Scaffold Seeding Methods

2.2.8.1 Seeding Scaffolds with Human Cells

All human cell experiments used freshly thawed cells counted using a CountessTM automated cell counter (Invitrogen, UK), as described previously in 2.2.1.4. 48-well plates were filled with Cell Crowns™ containing the sterilised scaffolds with excess media removed before warming to RT. 200 µL cell suspension in either HUVEC, hSVF or hSVMC culture media was loaded drop-wise onto the centre surface of each scaffold with 1 x10^5

cells. The plates were incubated at 37°C and 5% CO_2 undisturbed for 4 h. 600 µL of cell culture media was then added by pipetting down the side of each well. The plates were then re-incubated at 37°C and 5% CO_2 undisturbed for 24 h. Culture media was refreshed every 24 h for the duration of the experiments, fixed in 4% (w/v) PFA in PBS, or frozen for RT-qPCR.

2.2.8.2 Seeding Scaffolds with Porcine Blood

pPWB was collected in a blood bag as previously described and stored at 4°C until use. Blood was used within 6 h of collection. Cell Crowns™ containing sterilised scaffolds (as previously described) were placed into a 48-well plate and primed for 24 h with priming solution (55% (v/v) porcine serum, 45% (v/v) RPMI-1640), which was supplemented with 100 IU mL^{-1} (v/v) Penicillin, 0.1 mg mL^{-1} Streptomycin and 2.5 µg mL^{-1} Amphotericin B. Excess priming media was removed before warming scaffolds to RT. The blood bag was agitated to evenly distribute the components immediately before pipetting 800 µL drop-wise onto the centre surface of each scaffold. The plates were incubated at 37°C and 5% CO_2 undisturbed for 24 h and then fixed in 4% (w/v) PFA in PBS or washed 3 times with PBS for differentiation experiments.

2.2.8.3 pPBMC Seeding

pPBMCs were thawed and counted as previously described. Cell Crowns™ containing sterilised scaffolds (as previously described) were placed into a 48-well plate and primed for 24 h with priming solution. Excess priming media was removed before warming scaffolds to RT. 200 µL cell suspension in priming media was pipetted drop-wise onto the centre surface of each scaffold with 3 $x10^6$ cells. 600 µL of priming media was then added by pipetting down the side of each well. The plates were incubated in a humidified incubator at 37°C and 5% CO_2 undisturbed for 24 h and then fixed in 4% (w/v) PFA in PBS or washed 3 times with PBS prior to differentiation.

2.2.8.4 SMC Differentiation of pPWB

24 h after seeding pPWB onto PCL[11 (a)], scaffolds were washed 3 times with PBS. 800 µL of smooth muscle cell differentiation media Clonetic™ SmGM-2™ media supplemented with 5% FBS, 0.5 ng/mL human recombinant epidermal growth factor, 2 ng/mL human recombinant fibroblast growth factor, 5 µg mL^{-1} insulin, 50 µg mL^{-1} gentamicin, 100 U mL^{-1} (v/v) Penicillin, 0.1 mg mL^{-1} Streptomycin (Sigma-Aldrich, UK) and 2.5 µg mL^{-1} Amphotericin B (Lonza, Switzerland) was added. The following differentiation medias were compared:

- SmGM-2 and 1 IU mL^{-1} Thrombin
- SmGM-2 and 50 ng mL^{-1} Platelet-derived growth factor (PDGF-BB)
- SmGM-2 and 1 ng mL^{-1} Transforming growth factor beta 1 (TGF-β)

48-well plates were incubated in a humidified incubator at 37°C and 5% CO_2 for 4 d and media was changed after 2 d. Cells cultured in priming media for 4 d were used as negative controls. Scaffolds were then fixed in 4% (w/v) PFA in PBS or stored at -80°C until required for RT-qPCR.

2.2.8.5 Endothelial Cell Differentiation of pWB

24 h after seeding pPWB onto PLGA[25 NaOAc (a)], scaffolds were washed 3 times with PBS. 800 µL of endothelial cell differentiation media; Clonetic™ EGM-2™ (Lonza, Switzerland) supplemented with 5% FBS, 0.5 mL hEGF, 2.0 mL hFGF-B, 0.5 mL VEGF, 0.5 mL ascorbic acid, 0.2 mL hydrocortisone, 0.5 mL Long R3-IGF-1, 0.5 mL heparin and 0.5mL gentamycin/amphotericin. Actual concentrations are not provided by the manufacturer. The following differentiation medias were compared:

- EGM-2 and 10 ng mL^{-1} Pleiotrophin

- EGM-2 and 100 ng mL^{-1} Vascular Endothelial Growth Factor (VEGF)

48-well plates were incubated in a humidified incubator at 37°C and 5% CO_2 for 4 d and media was changed after 2 d. Cells cultured in priming media for 4 d were used as negative controls. Scaffolds were then fixed in 4% (w/v) PFA in PBS or stored at -80°C until required for RT-qPCR.

2.2.8.6 SMC Differentiation of pPBMCs

24 h after the initial seeding period of pPBMCs onto $PCL^{11\ (a)}$, scaffolds were washed 3 times with PBS. 800 µL of smooth muscle cell differentiation SmGM-2™ media or SmGM-2™ media containing 1 IU mL^{-1} Thrombin was added. Seeded scaffolds were incubated in a humidified incubator at 37°C and 5% CO_2 for 4 d and media was changed after 2 d. Cells cultured in priming media for 4 d were used as negative controls.

2.2.8.7 Endothelial Differentiation of PBMCs

24 h after the initial seeding period of pPBMCs onto $PLGA^{25\ NaOAc\ (a)}$, scaffolds were washed 3 times with PBS. 800 µL of smooth muscle cell differentiation EGM-2™ media was added. Seeded scaffolds were incubated in a humidified incubator at 37°C and 5% CO_2 for 4 d and media was changed after 2 d. Cells cultured in priming media for 4 d were used as negative controls.

2.2.9 Scaffold Analyses

2.2.9.1 Scanning Electron Microscopy

Scaffold morphologies of scaffold surfaces containing cells were assessed by scanning electron microscopy. Samples were initially fixed using 4% (w/v) PFA in PBS for 15 min at RT. Samples were then washed 3 times with 0.1 M cacodylate buffer pH 7.4) before post fixation in 2.5% (v/v) glutaraldehyde in 0.1 M cacodylate buffer for 48 h. Samples were then washed 3 times with cacodylate buffer and post-fixed in 1% osmium tetroxide

(O_sO_4) in cacodylate buffer for 1 h. Samples were washed 3 times with cacodylate buffer and dehydrated by exchange with graded ethanol 50%, 70%, 80%, 90%, 95% and three 100% v/v ethanol in cacodylate buffer for 10 min each. The ethanol in the samples was then exchanged with hexamethyldisilazane (HMDS) for 5 min and left to air dry. Finally, the specimens were coated with gold and imaged as previously described. For each sample, 5 images were taken; 1 central image and 4 images evenly spaced around the circumference of the scaffold discs.

2.2.9.2 Fluorescent Microscopy

Scaffolds seeded with cells were washed three times with PBS. Scaffolds were subsequently permeabilised in 0.05% (v/v) Triton™ X-100 for 30 min. To assess cell morphology, scaffolds were stained with 50 μg mL^{-1} Phalloidin-Atto 550 solution in PBS overnight at 4°C, washed three times with PBS and counterstained with 1 μg mL^{-1} 4',6-diamidino-2-phenylindole (DAPI) in PBS for 15 min. Microscopic analysis was performed under an epifluorescence microscope (AxioPlan 2; Imaging System, Carl Zeiss). Images were taken with a connected digital camera (AxioCAM; Carl Zeiss) using AxioVision 4.2 software (Carl Zeiss). For each sample, 5 images were taken; 1 central image and 4 images evenly spaced around the circumference of the scaffold discs. DAPI stained nuclei were quantified using the ImageJ software; images were converted to 8-bit binary to remove image backgrounds. Nuclei were then counted using the particle analyser of the ImageJ software.

2.2.9.3 Confocal Laser Scanning Microscopy

To observe for cell penetration through the scaffolds fluorescent z-stack images were obtained every 5 μm for a total of 300 μm using a Leica SP5-AOBS confocal laser scanning microscope attached to a Leica DM I6000 inverted epifluorescence microscope (Leica, UK) with images being obtained using Velocity® software (Perkin Elmer, UK). Scaffolds were stained and all nuclei were counted using the ImageJ software as previously described. For each sample, 5 images were taken; 1 central image and 4 images evenly spaced around the circumference of the scaffold discs.

2.2.9.4 Analysis of Scaffolds using SEM images

DiameterJ plugin (created by Nathan Hotaling) for Fiji (ImageJ) was used to analyse electrospun fibre diameters, pore areas and porosity from SEM images. Briefly, the software converted SEM micrographs to 8-bit binary images using multiple algorithms. The resulting binary images were manually chosen to best represent the contrast between fibres and background. These images were then used to determine fibre diameter, pore area, porosity and fibre orientation outlined below.

2.2.9.4.1 Fibre Diameter

Binary image fibre diameters were then quantified at multiple points along their lengths. Pore areas were also analysed. DiameterJ data was validated by manual fibre diameter measurements and no statistical difference was found.

2.2.9.4.2 Pore Area

Pore area was automatically quantified as part of the output provided by the DiameterJ plugin, which determined the black pixel area for each unbroken pore; i.e. enclosed by fibres (continuous white pixels) on all sides without interconnecting to any neighbouring pores.

2.2.9.4.3 Porosity

Porosity was automatically quantified as part of the output provided by the DiameterJ plugin. The pore area was calculated for each 2D SEM image by measuring the areas of black pixels (pores) between fibres (white pixels) after SEM images had been converted to binary images. The porosity was then determined from the total percentage area of all black pixels compared to the total scaffold area (all pixels).

2.2.9.4.4 Fibre Orientation

Alignment was confirmed by the OrientationJ (created by Daniel Sage) plugin for Fiji (ImageJ). A 0° reference was manually chosen and all images were orientated so the dominant direction was in line with reference. All fibre orientations were then evaluated against the reference angle and plotted to produce a histogram.

2.2.9.5 Histological Analysis of Electrospun Tubes

Scaffold tubes were snap frozen using liquid nitrogen-cooled 2-Methylbutane (isopentane; Sigma-Aldrich, UK). 2 mm thick sections were then cut across the length of the tube and embedded in optimal cutting temperature compound (OCT). A cryostat was used to cut 10 μm cryosections onto 3-Aminopropyltriethoxysilane (APES)-coated superfrost® Plus (vWR, UK) microscope slides and air dried at RT. Slides were stored at -20°C until staining. Sections were fixed in 4% PFA in PBS for 5 min, washed three times with PBS and stained with 1 μg mL^{-1} TO-PRO®-3 iodide solution in PBS for 30 min to observe nuclei. Epifluorescent microscopy was used to observed TO-PRO®-3 iodide stained nuclei in the far-red spectrum, as previously described.

2.2.9.6 Immunocytochemistry for α-Smooth Muscle Actin

PCL scaffolds were kept secured in the Cell Crowns. Cells were permeabilised in 0.05% triton™ X-100 for 30 min. Cells were then washed three times with PBS for 10 min each. Cells were blocked by incubation in 20% (v/v) goat serum in PBS for 1 h at RT. Cells were washed once with PBS then incubated with 14 μg mL^{-1} mouse anti-α-smooth muscle actin IgG in 1% (w/v) bovine serum albumin (BSA) overnight at 4°C. Non-immune mouse IgG at the same concentration was used as a negative control. Following three washed with PBS, cells were incubated with biotinylated goat anti-mouse IgG diluted 1:200 in 1% (w/v) BSA in PBS for 1 h at RT. Cells were washed three times with PBS then incubated with streptavidin Alexa Fluor 633 diluted 1:200 in 1% (w/v) BSA in PBS for 1 h at RT. Cells were then washed three times with PBS before staining with 1 μg mL^{-1} DAPI for 15 min at RT. Cells were washed three times with PBS and mounted in fluoromount-G™

(Thermo Fisher, UK) aqueous mounting medium onto a glass slide. The percentage of positive cells was quantified by manual counting the number of fluorescent cells (red) and total number of blue nuclei per field using ImageJ. For each sample, 5 images were taken; 1 central image and 4 images evenly spaced around the circumference of the scaffold discs.

2.2.9.7 Immunocytochemistry for Myosin Heavy Chain

PCL scaffolds were kept secured into the Cell Crowns. Cells were permeabilised in 0.05% triton™ X-100 for 30 min. Cells were then washed three times with PBS for 10 min each. Cells were blocked by incubation in 20% (v/v) goat serum in PBS for 1 h at RT. Cells were washed once in PBS then incubated with 0.8 μg mL^{-1} rabbit anti-myosin heavy chain IgG in 1% (w/v) bovine serum albumin (BSA) overnight at 4°C. Non-immune rabbit IgG at the same concentration was used as a negative control. Following three washed with PBS, cells were incubated with biotinylated goat anti-rabbit IgG diluted 1:200 in 1% (w/v) BSA in PBS for 1 h at RT. Cells were washed three times with PBS then incubated with streptavidin 633 diluted 1:200 in 1% (w/v) BSA in PBS for 1 h at RT. Cells were then washed three times with PBS before staining with 1 μg mL^{-1} DAPI for 15 min at RT. Cells were washed three times with PBS and mounted in fluoromount-G™ (Thermo Fisher, UK) aqueous mounting medium onto a glass slide. The percentage of positive cells was quantified by manual counting the number of fluorescent cells per field using imageJ. For each sample, 5 images were taken; 1 central image and 4 images evenly spaced around the circumference of the scaffold discs.

2.2.9.8 Immunocytochemistry for Endothelial Nitric Oxide

PLGA scaffolds were kept secured into the Cell Crowns. Cells were permeabilised in 0.05% triton™ X-100 for 30 min. Cells were then washed three times with PBS for 10 min each. Cells were blocked by incubation in 20% (v/v) goat serum in PBS for 1 h at RT. Cells were washed once in PBS then incubated with 1 μg mL^{-1} rabbit anti-endothelial nitric oxide IgG in 1% (w/v) bovine serum albumin (BSA) overnight at 4°C. Non-immune rabbit IgG at the same concentration was used as a negative control. Following three washed

with PBS, cells were incubated with biotinylated goat anti-rabbit IgG diluted 1:200 in 1% (w/v) BSA in PBS for 1 h at RT. Cells were washed three times with PBS then incubated with streptavidin 633 diluted 1:200 in 1% (w/v) BSA in PBS for 1 h at RT. Cells were then washed three times with PBS before staining with 1 μg mL^{-1} DAPI for 15 min at RT. Cells were washed three times with PBS and mounted in fluoromount-G™ (Thermo Fisher, UK) aqueous mounting medium onto a glass slide. The percentage of positive cells was quantified by manual counting the number of fluorescent cells per field using imageJ. For each sample, 5 images were taken; 1 central image and 4 images evenly spaced around the circumference of the scaffold discs.

2.2.9.9 Immunocytochemistry for CD203a

PLGA and PCL scaffolds were kept secured into the Cell Crowns. Cells were permeabilised in 0.05% triton™ X-100 for 30 min. Cells were then washed three times with PBS for 10 min each. Cells were blocked by incubation in 20% (v/v) goat serum in PBS for 1 h at RT. Cells were washed once in PBS then incubated with 5 μg mL^{-1} mouse anti-CD203a IgG in 1% (w/v) bovine serum albumin (BSA) overnight at 4°C. Non-immune mouse IgG at the same concentration was used as a negative control. Following three washed with PBS, cells were incubated with biotinylated goat anti-mouse IgG diluted 1:200 in 1% (w/v) BSA in PBS for 1 h at RT Cells were washed three times with PBS then incubated with streptavidin 633 diluted 1:200 in 1% (w/v) BSA in PBS for 1 h at RT. Cells were then washed three times with PBS before staining with 1 μg mL^{-1} DAPI for 15 min at RT. Cells were washed three times with PBS and mounted in fluoromount-G™ (Thermo Fisher, UK) aqueous mounting medium onto a glass slide. The percentage of positive cells was quantified by manual counting the number of fluorescent cells per field using imageJ. For each sample, 5 images were taken; 1 central image and 4 images evenly spaced around the circumference of the scaffold discs.

2.2.9.10 Immunocytochemistry for VE-cadherin

PLGA scaffolds were kept secured into the Cell Crowns. Cells were permeabilised in 0.05% triton™ X-100 for 30 min. Cells were then washed three times with PBS for 10 min

each. Cells were blocked by incubation in 20% (v/v) goat serum in PBS for 1 h at RT. Cells were washed once in PBS then incubated with 5 μg mL^{-1} mouse anti-VE-cadhering IgG2a in 1% (w/v) bovine serum albumin (BSA) overnight at 4°C. Non-immune mouse IgG at the same concentration was used as a negative control. Following three washed with PBS, cells were incubated with biotinylated goat anti-mouse IgG2a diluted 1:200 in 1% (w/v) BSA in PBS for 1 h at RT Cells were washed three times with PBS then incubated with streptavidin 594 diluted 1:200 in 1% (w/v) BSA in PBS for 1 h at RT. Cells were then washed three times with PBS before staining with 1 μg mL^{-1} DAPI for 15 min at RT. Cells were washed three times with PBS and mounted in fluoromount-G™ (Thermo Fisher, UK) aqueous mounting medium onto a glass slide. The percentage of positive cells was quantified by manual counting the number of fluorescent cells per field using imageJ. For each sample, 5 images were taken; 1 central image and 4 images evenly spaced around the circumference of the scaffold discs.

2.2.9.11 DBA Lectin Staining

PLGA scaffolds were kept secured into the Cell Crowns. Cells were permeabilised in 0.05% triton™ X-100 for 30 min. Cells were then washed three times with PBS for 10 min each. Cells were blocked by incubation in 20% (v/v) goat serum in PBS for 1 h at RT. Cells were washed once in PBS then incubated with DBA-lectin diluted 1:200 in 1% (w/v) bovine serum albumin (BSA) overnight at 4°C. Following three washed with PBS, cells were incubated with streptavidin 594 diluted 1:200 in 1% (w/v) BSA in PBS for 1 h at RT. Cells were then washed three times with PBS before staining with 1 μg mL^{-1} DAPI for 15 min at RT. Cells were washed three times with PBS and mounted in fluoromount-G™ (Thermo Fisher, UK) aqueous mounting medium onto a glass slide. The percentage of positive cells was quantified by manual counting the number of fluorescent cells per field using imageJ. For each sample, 5 images were taken; 1 central image and 4 images evenly spaced around the circumference of the scaffold discs.

3

OPTIMISATION OF ELECTROSPUN PLGA FIBRE DIAMETERS FOR IMPROVED CELLULAR ADHESION

3.1 Introduction

Electrospinning can be used to create tubular shaped scaffolds, which have the capacity to support mammalian cells for tissue engineering purposes. It has been shown that cellular-to-scaffold interactions can be affected by the scaffold material and scaffold structure (Harley *et al.*, 2007; Corin and Gibson, 2010; Murphy *et al.*, 2012). The electrospinning process can be used to fabricate scaffolds from a variety of materials with different fibre diameters, porosities, and micro- and macro-structures. In particular, fibre diameter is a parameter known to affect cellular adhesion and growth. However, this has not been extensively examined in the literature. Therefore, it is important to understand whether electrospun scaffold fibre diameters can be selected to enhance cellular adhesion to help towards the development of a TEVG that can support and maintain physiologically relevant cellular morphologies.

Mammalian arteries contain distinct layers of cells, each with a distinct role, and these cells maintain a healthy morphology through the use of biological, chemical and mechanical cues (Furchgott and Zawadzki, 1980; Michel, Li and Lacolley, 2012; Rajendran *et al.*, 2013; Wang *et al.*, 2017). Mechanical cues are imparted from the supporting ECM, through the individual biological components of the ECM and its structures(Humphrey, Dufresne and Schwartz, 2014). Arterial tissues from human or animal donors can be decellularised to produce ECM scaffolds that support cell attachment and growth, which is a common method for the development of TEVGs within the literature (Quint *et al.*, 2012). However, during arterial development, cells grow and produce ECM to support the creation of tissue, which is the result of interconnecting cells and their supporting connective tissue (Lluri and Aboulhosn, 2014). Removal of mammalian cells during the decellularisation process can affect the ECM structure and composition (Liao, Joyce and Sacks, 2008). Therefore, simply re-introducing cells to decellularised ECM may not allow cells to fully infiltrate and integrate into biological scaffold in a physiologically representative manner. This may affect the process in which cells interact with the ECM components, which may result in cells not receiving the necessary mechanical cues to remain physiologically healthy.

Despite the effects of biological and chemical cues upon cells in the field of tissue engineering being relatively advanced, few studies explore the influence of mechanical cues from the underlying scaffold upon cellular behaviour. Further understanding of the role of mechanical cues from TEVG scaffolds could help produce next generation scaffolds that facilitate the selection of specific cell types and enhance cell seeding efficiency, which may help develop TEVGs with more physiologically relevant characteristics to native arties.

Electrospun fibres have the capacity to provide adequate mechanical cues to stimulate specific cellular behaviours due to the ability of this technique to produce nano-scaled fibres, which are more physiologically similar in diameter to mammalian ECM than other scaffold fabricating techniques (Mohammadian and Haghi, 2014). To date, no studies have been identified that have assessed the role of electrospun fibre diameter on cellular attachment and growth relating to TEVGs. An understanding of how fibre diameter affects cell behaviour could lead to the development of scaffolds that can enhance physiologically beneficial cellular characteristics, which could ultimately help reduce the incidence of early graft failure of current generation TEVGs. Scaffolds that are able to support and direct the behaviour of cells through mechano-transduction alone would also be highly desirable and remove the need to use biological and chemical agents.

PLGA is a biodegradable material that has been extensively studied and has been deemed safe for mammalian implantation by the FDA. PLGA has been shown to be favourable to cell attachment and growth relative to other biodegradable polymers (Anderson and Shive, 2012). Further to this, the degradation profile of PLGA is dependent on the ratio between PLA and PGA, which allows for tuneable *in vivo* degradation rates. Biodegradable polymers such as PLGA also have comparatively high tensile strength in comparison to biological materials that can be electrospun such as gelatin. Therefore, PLGA is a suitable material for use in an electrospun TEVG.

There is evidence that electrospun fibre diameter may affect the attachment and morphology of a number of cell types, including endothelial cells; a crucial vascular component that reduces the risk of thrombosis, by maintaining a smooth luminal

monolayer (Noriega *et al.*, 2012; Whited and Rylander, 2014b). Thrombosis in TEVGs is one of the major causes of graft failure (Jackson *et al.*, 2000; van Det *et al.*, 2009; Takagi *et al.*, 2010). The overall aim of this chapter is to understand the feasibility of developing a TEVG by understanding the effect of fibre diameter on cell attachment and morphology. I hypothesised that nano-scaled PLGA fibres would improve endothelial cell attachment when compared to micro-scaled fibres.

To test this hypothesis, I initially established a robust electrospinning system that could produce a range of fibre diameters from micrometres to nanometres. I further established methodologies for sterilisation and cellular seeding of these scaffolds. To then determine if there was any effect on cellular adhesion between the different scaffold fibre diameters, I compared the attachment and growth of HUVECs as an endothelial cell model. To understand if the research was translatable for vascular graft purposes, a small diameter electrospun scaffold methodology was established and subsequent electrospun tubes were tested for cellular adhesion using a dynamic seeding system.

3.2 Results

3.2.1 Optimisation of PLGA concentration for beadless fibre fabrication

To fabricate electrospun fibres, various solutions of PLGA in a 1:1 DMF:THF solvent mixture or HFIP were made. Previously published literature was assessed to determine a range of working concentrations and a relevant solvent for electrospinning PLGA (Xin, Hussain and Mao, 2007; Baker *et al.*, 2009; Jean-Gilles *et al.*, 2010a; Bonani *et al.*, 2012; Tseng *et al.*, 2013). The flow rate, needle gauge and collector were kept the same to allow the determination of a concentration range in which fibres could be produced in the electrospinning apparatus using the chosen polymer-solvent system. Due to the large number of combinations and the high reproducibility of this technique, only a single solution concentration was produced and tested. SEM images were visually assessed for any surface defects. The primary goal was to eliminate samples with randomly distributed beads, which could lead to non-reproducible results due to altered cell attachment (Figure 3.1). SEM images were also used to quantify the mean fibre diameters within the resulting fibrous scaffolds (Figure 3.2).

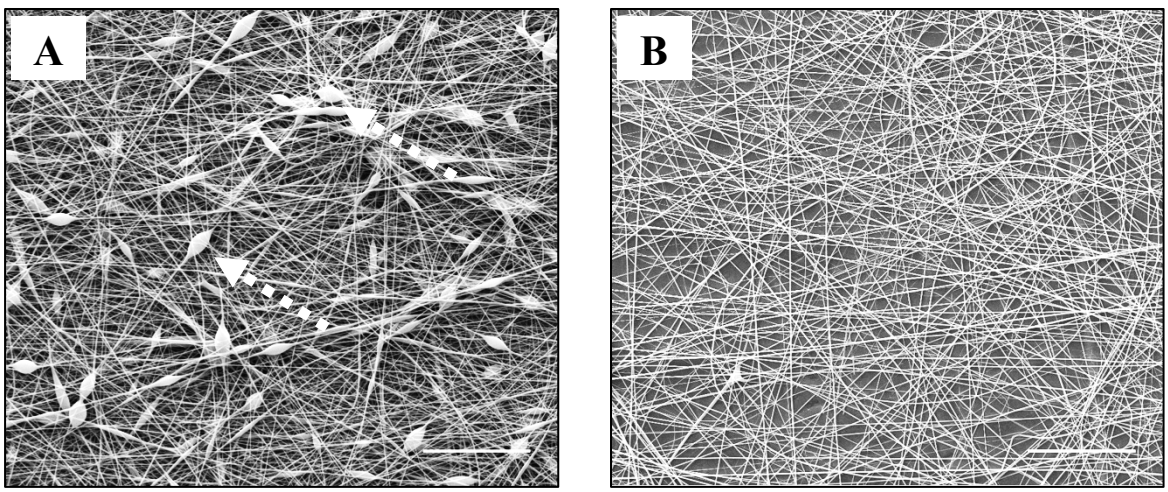

Figure 3.1 - Representative images of electrospun fibre beading. Representative images of PLGA electrospun scaffolds (A) with beading and (B) without beading. White arrows show individual beads. Scale bars represent 100 μm.

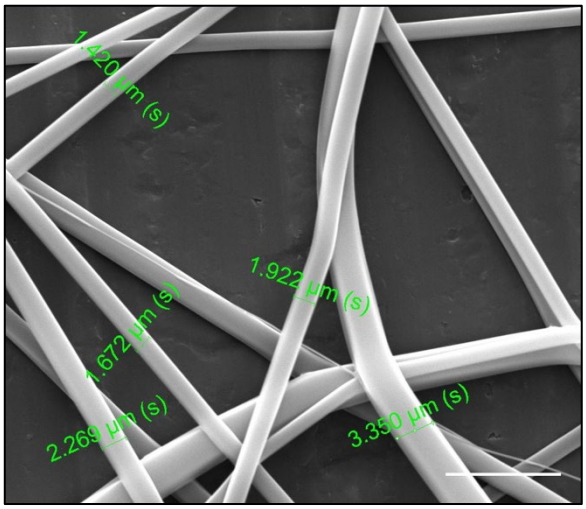

Figure 3.2 - Electrospinning fibre diameter measurement. Representative image of a PLGA electrospun scaffold with individual fibre diameters being manually measured to determine the mean fibre diameter of the resulting scaffold. Scale bar represents 10 µm.

Various fibre diameters could be created using both solvent systems with PLGA concentrations ranging from 7% - 20% (Table 3.1). For both solvent systems, there was a relationship between polymer concentration and the resulting mean fibre diameter (Table 3.1). However, the two solvents produced different mean fibre diameters at the same PLGA concentration, with the DMF:THF solvent system being able to accommodate higher concentrations of PLGA than the HFIP solvent system whilst still producing solutions with viscosities suitable for electrospinning (Table 3.1).

Table 3.1 - Optimisation of PLGA-solvent solutions. Optimisation of PLGA-solvent solutions. Solutions (w/v) of PLGA (molar ratio 50:50) in either HFIP or DMF:THF were electrospun at 2 mL min^{-1} through a blunted 22 ½ G needle with a 100 mm diameter rotating collector at 50 x g. Voltages were set once a visible Taylor cone was present. Fibre diameters were manually counted using Fiji (ImageJ) software. At least 100 fibres were counted from 4 random SEM images. (n=1).

PLGA Concentration (%)	**Needle tip-to-Collector Distance (cm)**	**Needle Voltage (kV)**	**Solvent (s)**	**Mean Fibre Diameter (µm)**	**Fibre Diameter Range (µm)**
11	10.0	5.0	HFIP	1.204	1.587
11	14.0	5.5	HFIP	1.394	2.617
11	17.0	5.5	HFIP	1.141	2.749
12	10.0	5.0	HFIP	1.751	0.373
12	14.0	5.5	HFIP	1.627	0.521
12	17.0	5.0	HFIP	1.341	1.096
12	10.0	9.5	DMF/THF 1:1	0.158	0.196
12	17.0	10.5	DMF/THF 1:1	0.223	0.931
13	9.5	11.0	DMF/THF 1:1	0.110	0.084
15	9.0	8.0	DMF/THF 1:1	0.158	0.246
17	8.0	7.5	DMF/THF 1:1	0.200	0.171
20	15.0	7.5	DMF/THF 1:1	0.768	1.063
22	15.0	8.0	DFM/THF 1:1	0.543	1.356

Beading was observed randomly distributed amongst the fibres from the HFIP and DMF:THF solvent systems at PLGA concentrations below 11% and 22%, respectively. It was noted that to observe visible Taylor cones, the needle-to-collector distance had to be adjusted.

PGLA fibres produced from the HFIP and DMF:THF solvent systems were smooth and contained no observable fibre surface defects such as beading at PLGA concentrations above 10% and 20%, respectively (Figure 3.3). Using 11% PLGA in HFIP, the resulting fibrous scaffolds contained no observable beading and this was therefore determined to be the minimum PLGA concentration in HFIP for no beading (Figure 3.3A). Concentrations below this were considered non-uniform and were therefore disregarded for any further investigation. For the DMF:THF solvent system, beadless fibres were achieved at a minimum concentration of 22% (Figure 3.3B). At the minimum beadless concentrations for both solvent systems, mean fibre diameters were approximately 1.204 μm and 0.543 μm for DMF:THF and HFIP, respectively.

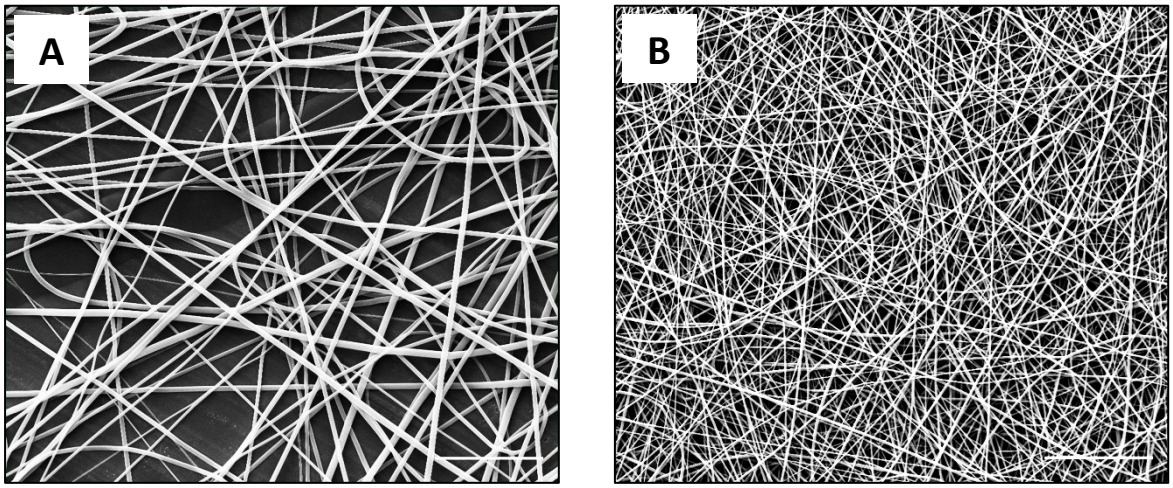

Figure 3.3 - Electrospun PLGA fibre morphology in different solvent systems absent beading. (A) Representative image of an 11% (w/v) solution of PLGA in 1,1,1,3,3,3-Hexafluoro-2-propanol (HFIP) was electrospun through a blunted 22 ½ G needle at 5 kV, with a flow rate of 2 mL hour^{-1}, at a collector distance of 100 mm, with a 100 mm diameter rotating mandrel at 50 x g. (B) Representative image of 22% (w/v) solution of PLGA in DMF:THF 1:1 was electrospun through a blunted 22 ½ G needle at 8 kV, with a flow rate of 2 mL hour^{-1}, at a collector distance of 150 mm, with a 20 mm diameter rotating mandrel at 50 x g. Scale bars represent 20 µm.

3.2.2 Automated electrospun fibre diameter quantification is comparable to manual quantification

Fiji (ImageJ) software was used to measure individual fibre diameters and calculate the mean fibre diameter for each electrospun PLGA solution. To reduce analysis time and to minimise human error, an automated ImageJ plugin was compared against manual measurement. The minimum concentration required for beadless fibres using the HFIP solvent system was electrospun, and subsequently obtained SEM images were assessed using the manual and automated measurement method. 100 fibres were manually measured evenly distributed across four SEM images that were randomly taken across the surface of each scaffold '*n*' number. All fibres were then quantified using the automated software. Measurements were then randomly selected to generate the same number of fibres counts as the manual method; i.e. 100 measurements across 4 SEM images per 'n' number. No statistically significant difference was found between the two quantification methods (Figure 3.4). The automated quantification process is outlined in Figure 3.5.

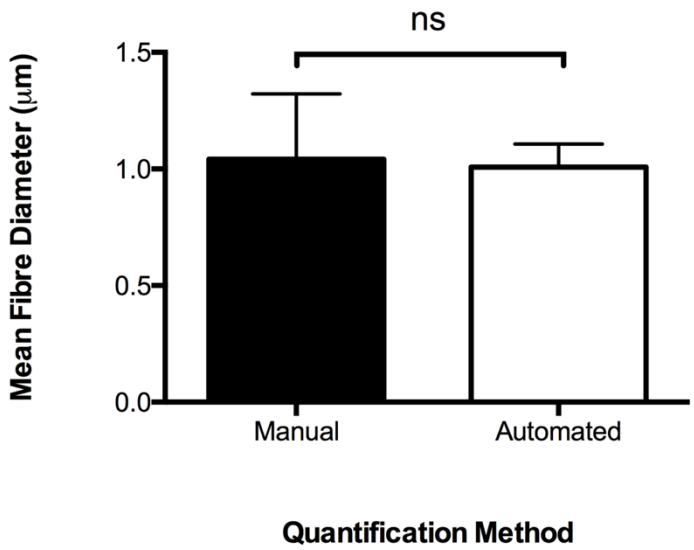

Figure 3.4 - Validation of DiameterJ software for fibre diameter quantification automation. An 11% (w/v) solution of PLGA in 1,1,1,3,3,3-Hexafluoro-2-propanol (HFIP) was electrospun through a blunted 22 ½ G needle at 8 kV, with a flow rate of 2 mL hour^{-1}, at a collector distance of 100 mm, with a 100 mm diameter rotating mandrel at 50 x g. Fibre diameters were manually counted or quantified using the DiameterJ plugin for Fiji (ImageJ) software. Data represent the average results taken from ≥ 12 random microscopic fields per experiment. ≥100 fibres were counted per experiment. Data are mean ± SD, n=3. Statistical analysis: two-tailed, paired t-test. ns denotes no statistical significance.

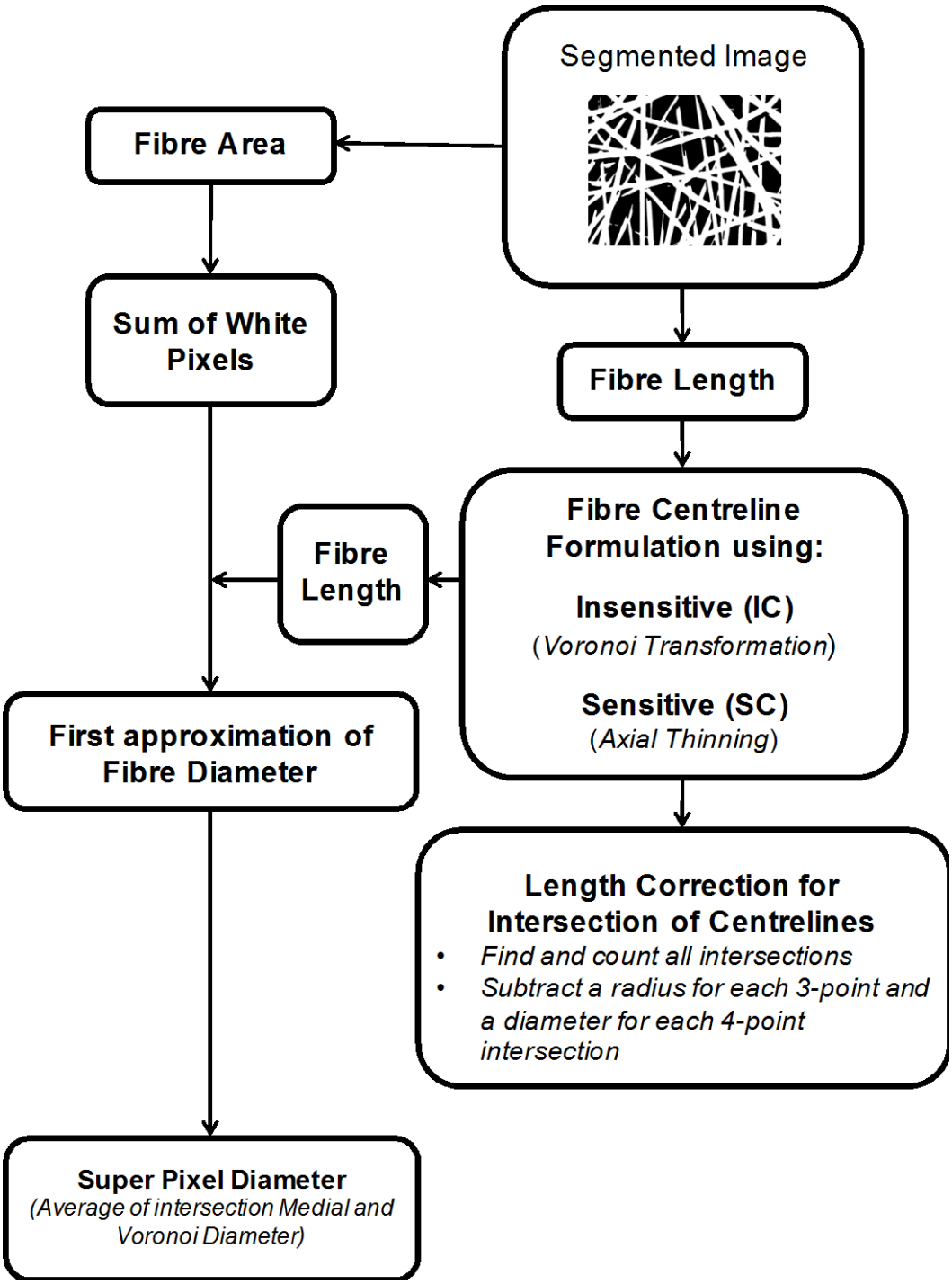

Figure 3.5 – Automated process used by the DiameterJ plugin for Fiji (ImageJ) software for fibre diameter quantification. Images are converted to a binary form and white pixels are classified as fibre area. Centrelines are estimated for each fibre and this is combined with the sum of the white pixels either side of the centreline along each fibre.

3.2.3 Basic parameter changes had no effect on fibre diameter in the PLGA-HFIP solvent system

In order to determine the reproducibility of the electrospinning process using PLGA and HFIP, and to investigate the ability of this system to easily manipulate resulting fibre diameters, the effect of alterations to basic parameter changes upon resulting fibre diameters was investigated. The minimum 'beadless' concentration of PLGA in HFIP was electrospun using the initial parameters: An 11% (w/v) solution of PLGA (molar ratio 50:50) in 1,1,1,3,3,3-Hexafluoro-2-propanol (HFIP) was electrospun through a blunted 22½ G needle at 8 kV, with a flow rate of 2 mL $hour^{-1}$, at a collector distance of 100 mm, and a 20 mm diameter rotating mandrel at 50 x g. The following parameters were chosen for assessment as evidence from previously published literature identified these parameters as having the most significant effects on resulting electrospun fibre diameters in similar systems, without changing the solution concentration: flow rate, distance between the needle tip and the collector, and the collector rotation speed (Beachley and Wen, 2009). However, previous uses of HFIP in the literature suggested that HFIP solutions are resistant to minor parameter changes (Zhang, Zuo and Bai, 2009; Jean-Gilles *et al.*, 2010b; Gu *et al.*, 2014). These parameters were then individually tested within a small range, to determine their effect upon the resulting mean fibre diameters.

An increase or decrease to the flow rate to 1 and 4 mL $hour^{-1}$, respectively did not significantly affect the mean fibre diameter compared to the control (Figure 3.6A). A slight decrease in flow rate also showed no statistically significant change to the mean fibre diameter in comparison to the control (Figure 3.6A). Interestingly, there was also no statistically significant difference between the mean fibre diameters of both the decreased and increased flow rates tested (Figure 3.6A).

An increase and decrease in the needle to collector distance also had no statistically significant effect upon the resulting mean fibre diameter, even when comparing the highest and lowest distances (Figure 3.6B).

A 100 times decrease in the collector rotational speed had no statistically significant effect on the mean fibre diameter (Figure 3.6C). A 10 times increase in the collector rotational speed compared to the control also had no statistically significance effect on the mean fibre diameter (Figure 3.6C).

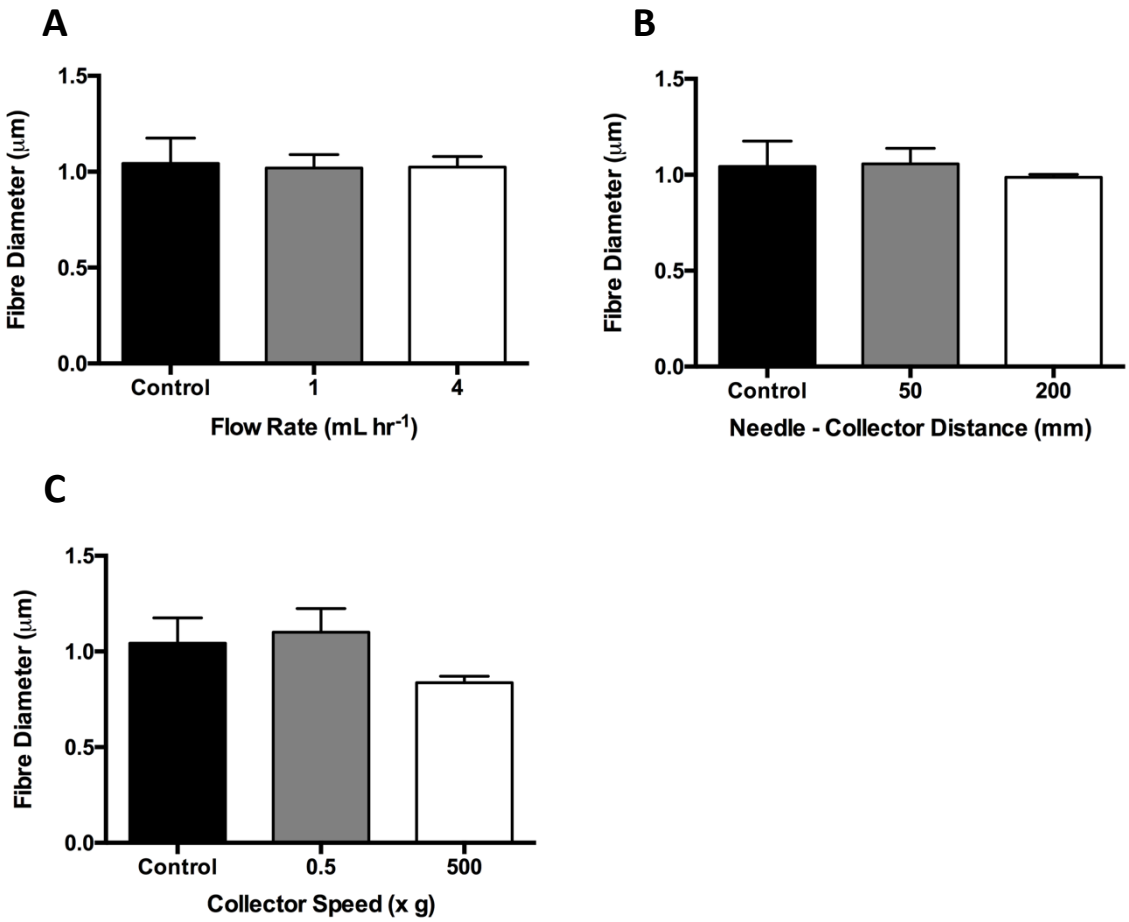

Figure 3.6 - Effect of parameter changes on resulting PLGA[11] fibre diameter. An 11% (w/v) solution of PLGA in 1,1,1,3,3,3-Hexafluoro-2-propanol (HFIP) was electrospun through a blunted 22 ½ G needle at 8 kV, with a flow rate of 2 mL hour-1, at a collector distance of 100 mm, with a 100 mm diameter rotating mandrel at 50 x g. **(A)** Effect of flow rate **(B)** Effect of the distance between the tip of the needle and the collector **(C)** Effect of collector rotation. Data represent the average results taken from ≥ 12 random microscopic fields per experiment. ≥100 fibres were counted per experiment. Data are mean ± SD, n=3. Statistical analysis: ANOVA was used in conjunction with Tukey's *post hoc* test to assess statistical significance; control vs. 500 x g adjusted $P = 0.0515$.

3.2.4 The addition of NaCl reduced PLGA fibre diameters

Once a suitable control fibrous scaffold was achievable in a reproducible electrospinning set up, my aim was to produce nano-sized fibres, which I defined as having a mean fibre diameter of less than 1 μm. I also aimed to fabricate multiple fibre diameters from the electrospinning set up. As previously identified from Table 3.1, a reduction in PLGA concentration showed a trend towards a decreased mean fibre diameter; however, the minimal concentration before the formation of beading was 11% (w/v). Further to this, the parameter changes outlined in Figure 3.6 showed no statistical difference to the mean fibre diameter compared to that of the control. Therefore, significant reductions in the mean fibre diameter was difficult to achieve with minor changes to some of the parameters of the electrospinning set up. To understand if the mean fibre diameter could be significantly reduced using the HFIP solvent, previously published literature was used to elucidate additional changes that could be introduced to the electrospinning set up to achieve this.

A previously published paper identified by Jean-Gilles et al. (2010) that NaCl had a dramatic effect on electrospun PLGA fibre diameters when dissolved in HFIP. Therefore, NaCl was added to the control solution to identify the effect on the resulting mean fibre diameter. A concentration of 1% (w/v) was used as indicated by the previously published piece of literature (Jean-Gilles *et al.*, 2010b). A higher concentration of 5% (w/v) was also tested to determine if any expected effect was enhanced with an increased NaCl concentration.

Resulting fibres were free from beading and had no observable defects, making them morphologically similar to the control fibres (Figure 3.7). The addition of 1% (w/v) NaCl significantly reduced the mean fibre diameter compared to the control (Figure 3.8). The mean fibre diameter was reduced by approximately 50% with the addition of 1% (w/v) NaCl to the electrospinning solution, with no observable adverse effects to fibre morphology (Figures 3.7 and 8). NaCl crystals could be observed undissolved in solution, however this did not produce any observable effects on fibre morphology (Figure 3.7). The further addition of 5% (w/v) NaCl to the electrospinning solution had no statistically

significant effects beyond that observed with 1% (w/v) NaCl. As expected, there was an increased amount of undissolved NaCl in solution after the addition of 5% (w/v) NaCl when compared with the 1% (w/v) NaCl solution.

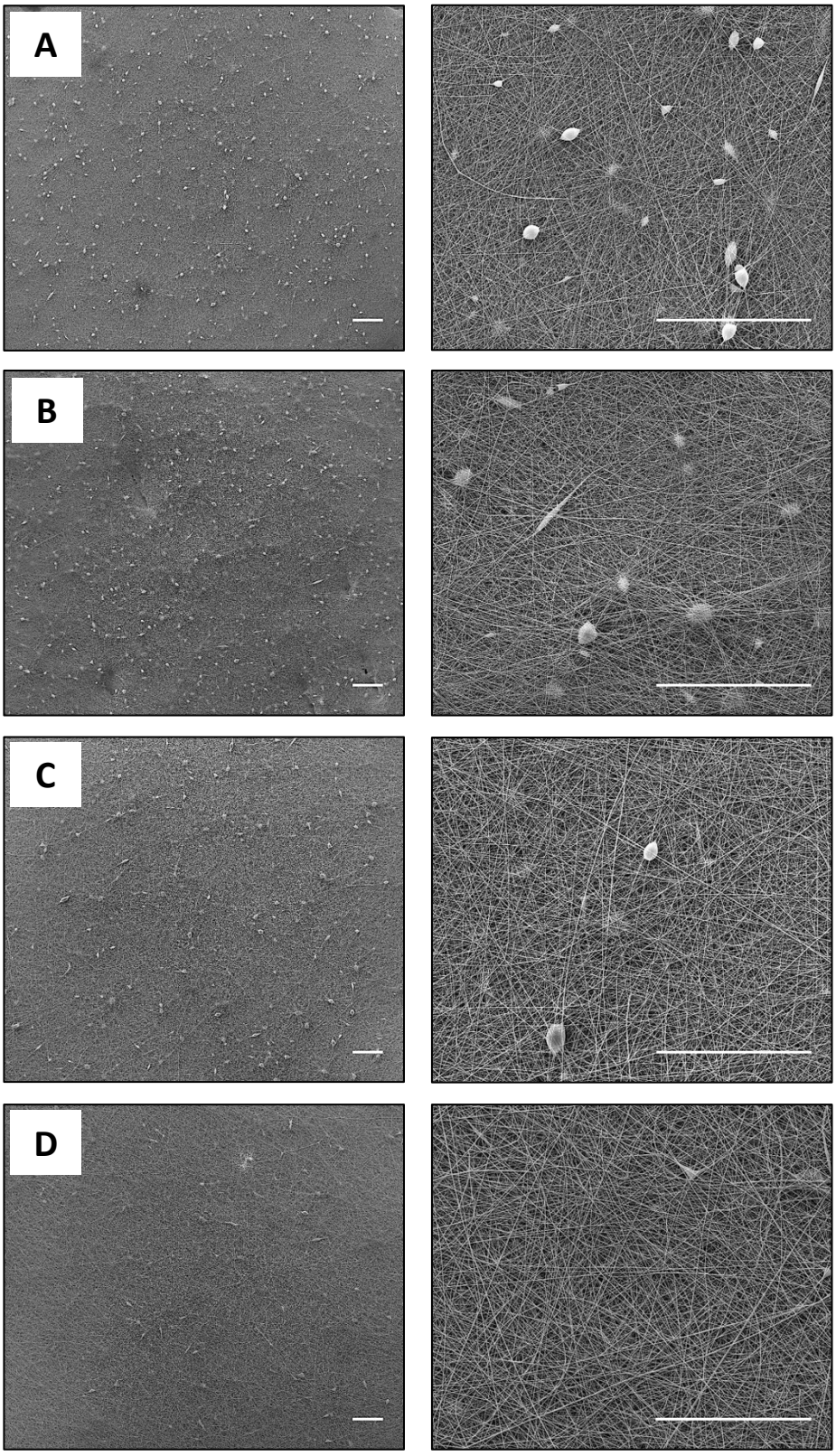
A
B
C
D

Figure 3.7 - Beading in electrospun fibres containing NaCl. Solutions of PLGA in 1,1,1,3,3,3-Hexafluoro-2-propanol (HFIP) **(A)** 7% PLGA, 1% (w/v) NaCl **(B)** 8% PLGA, 1% (w/v) NaCl **(C)** 9% PLGA, 1% (w/v) NaCl and **(D)** 10% PLGA, 1% (w/v) NaCl were electrospun through a blunted 22 ½ G needle, with a flow rate of 2 mL hour-1, at a collector distance of 100 mm, with a 100 mm diameter rotating mandrel at 50 x g. The applied voltages were 9.5 kV, 10 kV and 10.5 kV, respectively, to ensure a visible Taylor cone was present. Scale bars represent 200 μm.

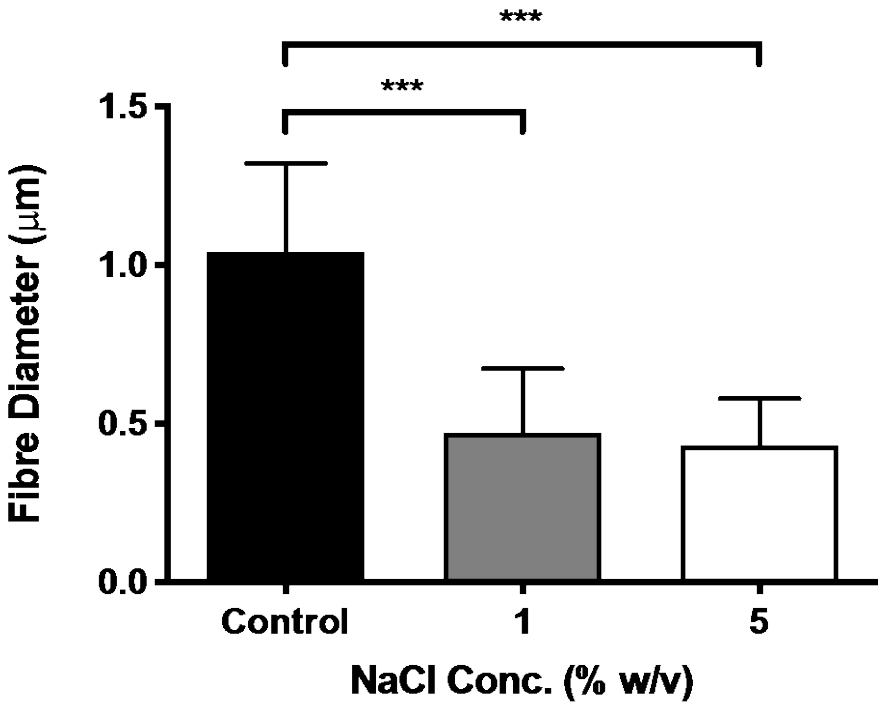

Figure 3.8 - Effect of NaCl concentration on resulting PLGA[11] fibre diameter. 11% (w/v) solutions of PLGA in 1,1,1,3,3,3-Hexafluoro-2-propanol (HFIP) containing no NaCl (control), 1% (w/v) NaCl or 5% (w/v) NaCl. The solutions were electrospun through a blunted 22 ½ G needle with a flow rate of 2 mL hour-1, at a collector distance of 100 mm, with a 100 mm diameter rotating mandrel at 50 x g. The applied voltages were 8 kV, 10.5 kV and 10.5 kV, respectively, to ensure a visible Taylor cone was present. Data represent the average results taken from ≥ 12 random microscopic fields per experiment. ≥100 fibres were counted per experiment. Data are mean ± SD, n=3. Statistical analysis: ANOVA was used in conjunction with a Tukey's *post hoc* test; ***$P < 0.001$.

3.2.5 The addition of NH_4Cl, and NaOAc further reduced fibre diameter

There is limited information about the solubility of compounds in HFIP, and about the miscibility of other solvents in HFIP. Therefore, this was tested empirically. The undissolved precipitate found at a low NaCl concentration of 1% demonstrated a low saturation limit for NaCl in HFIP. Therefore, to determine which element of the NaCl compound was responsible for the reduction in mean fibre diameter, and to determine their saturation limit in HFIP, two further salts were investigated. Ammonium Chloride (NH_4Cl) and Sodium Acetate (NaOAc) were initially chosen to help elucidate the effect of Sodium and Chloride ions separately on the electrospinning solutions. These salts were chosen due to their relative safety, accessibility and low cost.

1% (w/v) NH_4Cl was added to PLGA[11] and electrospun using the control parameters, as with all experiments. The voltage was adjusted to ensure there was a visible Taylor cone present at the edge of the needle, which in the case of the NH_4Cl solution was 17.5 kV. The mean fibre diameter of the resulting electrospun fibrous mats from the NH_4Cl solution was reduced by approximately 75% compared to the control, which was very statistically significant (Figure 3.9). This reduction was also approximately 50% lower than the effect produced from the addition of 1% (w/v) NaCl as shown in Figure 3.8.

Despite this large decrease in fibre diameter for the NH_4Cl solution, macroscopic aberrations were notable from SEM images of the fibrous mats (Figure 3.9B). These aberrations appeared to be formed by a concentration of fibres that were more densely populated than the rest of the fibrous mat (Figure 3.9B). This increased density caused these areas to become raised, not unlike that of the beading phenomenon. However, these raised radial structures were significantly larger in size than those caused by beading, with diameters of approximately 100 μm (Figure 3.9B). These structures were found sparsely and randomly distributed across the mats often with millimetres between them.

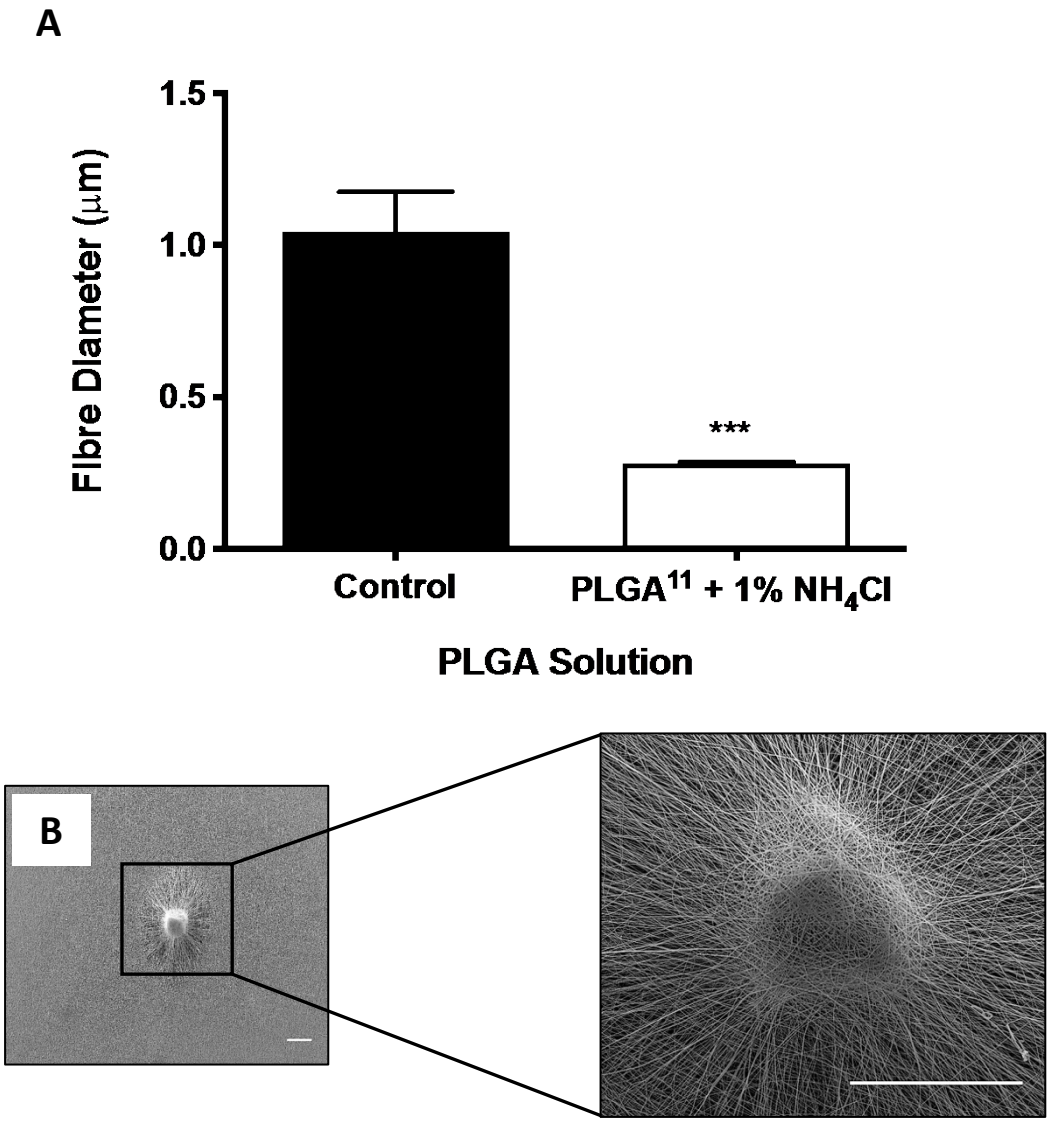

Figure 3.9 - Effect of NH_4Cl on resulting $PLGA^{11}$ fibre diameter. 11% (w/v) solutions of PLGA in 1,1,1,3,3,3-Hexafluoro-2-propanol (HFIP) containing no NH_4Cl (control) or 1% (w/v) NH_4Cl. The solutions were electrospun through a blunted 22 ½ G needle with a flow rate of 2 mL $hour^{-1}$, at a collector distance of 100 mm, with a 100 mm diameter rotating mandrel at 50 x g. The applied voltages were 8 kV and 17.5 kV, respectively, to ensure a visible Taylor cone was present. Data represent the average results taken from ≥ 12 random microscopic fields per experiment. ≥100 fibres were counted per experiment. Data are mean ± SD, n=3. Statistical analysis: two-tailed, unpaired t-test; ***$P < 0.001$. Scale bars represent 200 μm.

1% (w/v) NaOAc was added to PLGA[11] and left overnight to dissolve and form a homogenous solution. It was observed that the NaOAc did dissolve fully unlike NaCl. However, the resulting viscosity of the solution was noticeably reduced. The solution was found to be too liquid to successfully electrospin. Therefore, to increase the viscosity the PLGA concentration of the solutions was increased until a sufficiently viscous sample was achieved. Viscosity was observed visually and samples deemed suitably viscous were further tested via electrospinning. Electrospinning solutions containing at least 22% were found to be adequately suitable for the electrospinning process. A range of solutions containing PLGA at a concentration of 22% (w/v), 24% (w/v), 26% (w/v) and 30% (w/v) were produced to determine whether beadless fibres with no surface defects could still be produced. All solutions also contained 1% (w/v) NaOAc. The voltage was adjusted to ensure there was a visible Taylor cone present at the edge of the needle. The voltages were 9.5 kV, 10 kV, 10.5 and 10.5 kV, respectively. There was no visible precipitate present in the solutions.

Beading was present in the 22% and 24% fibrous mats (Figure 3.10A and B). No beads were present in the 26% and 30% solutions (Figure 3.10C and D). As 26% was the lowest PLGA concentration for beadless scaffolds, a further reduction to a concentration of 25% was then tested to be certain of the minimum beadless concentration. The mean fibre diameter of the fibrous mats produced from the 25% solution were calculated and compared against the PLGA[11] control (Figure 3.11). There was a very statistically significant reduction in the mean fibre diameter when compared to the control, despite a 127.27% increase in PLGA within the solution. Similar to the addition of NH_4Cl, the mean fibre diameter in the NaOAc solution fibres was reduced by approximately 75% to roughly 250 nm when compared to the control. Compared to the NH_4Cl fibrous mats, the NaOAc fibres contained no macro or micro defects.

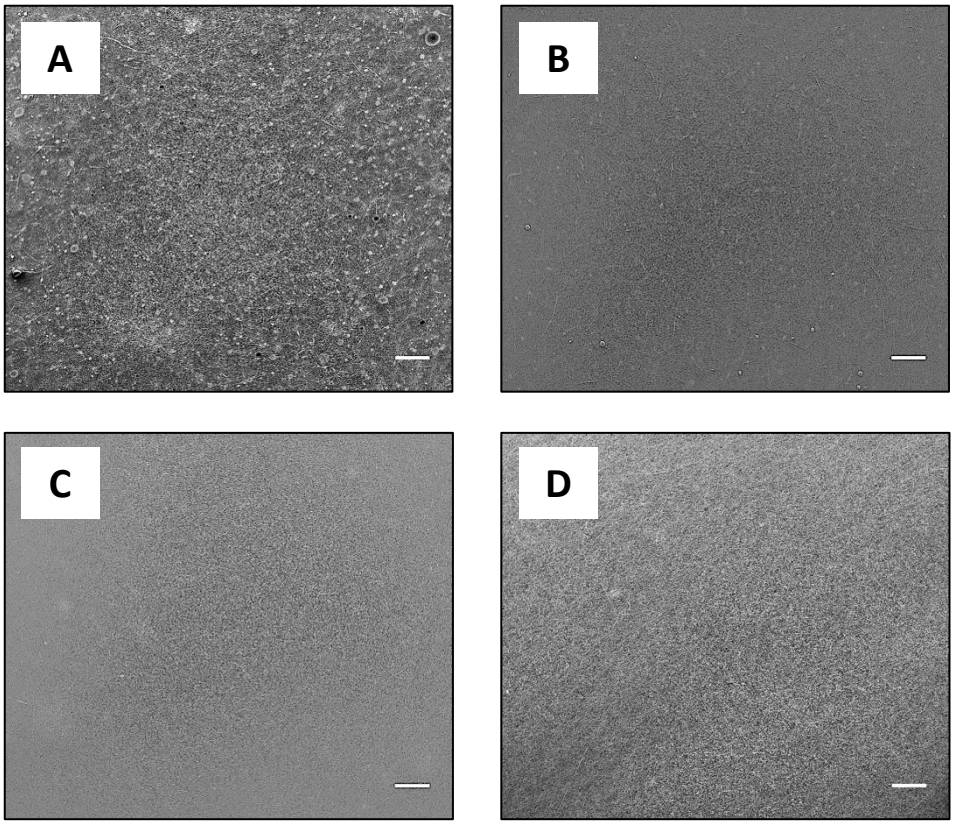

Figure 3.10 - Optimisation of PLGA concentration in a solution containing NaOAc. Solutions of PLGA in 1,1,1,3,3,3-Hexafluoro-2-propanol (HFIP) **(A)** 22% PLGA, 1% (w/v) NaOAc **(B)** 24% PLGA, 1% (w/v) NaOAc **(C)** 26% PLGA, 1% (w/v) NaOAc **(D)** 30% PLGA, 1% (w/v) NaOAc were electrospun through a blunted 22 ½ G needle, with a flow rate of 2 mL $hour^{-1}$, at a collector distance of 100 mm, with a 100 mm diameter rotating mandrel at 50 x g. The applied voltages were 9.5 kV, 10 kV and 10.5 kV, respectively, to ensure a visible Taylor cone was present. Scale bars represent 200 µm.

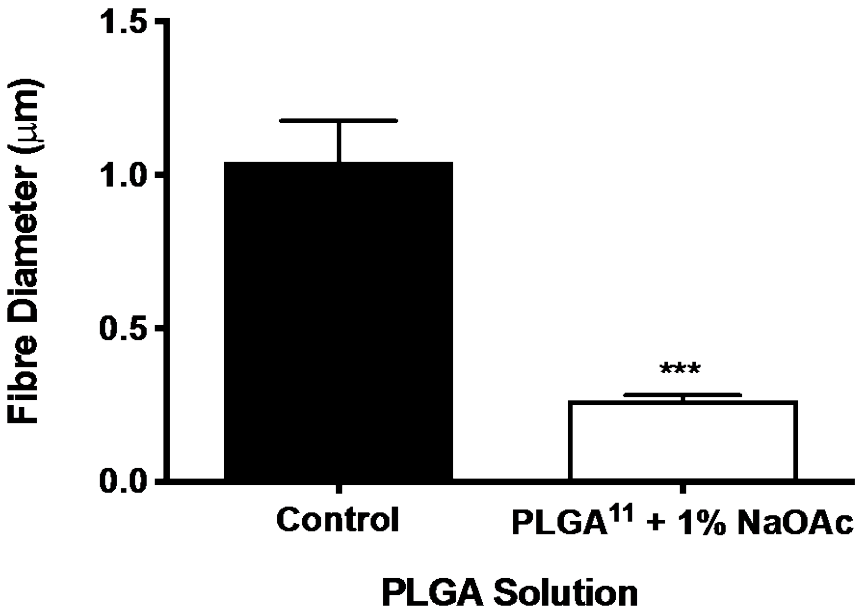

Figure 3.11 - Effect of NaOAc on resulting PLGA^{25} fibre diameter. 11% (w/v) solutions of PLGA in 1,1,1,3,3,3-Hexafluoro-2-propanol (HFIP) containing no NaOAc (control) and a 25% (w/v) PLGA solution containing 1% (w/v) NaOAc. The solutions were electrospun through a blunted 22 ½ G needle with a flow rate of 2 mL hour^{-1}, at a collector distance of 100 mm, with a 100 mm diameter rotating mandrel at 50 x g. The applied voltages were 8 kV and 20.5 kV, respectively, to ensure a visible Taylor cone was present. Data represent the average results taken from ≥ 12 random microscopic fields per experiment. ≥100 fibres were counted per experiment. Data are mean ± SD, n=3.. Statistical analysis: two-tailed, unpaired t-test; *** $P < 0.001$.

3.2.6 Fibre diameter range decreased with a decreasing fibre diameter and the addition of NaCl and NaOAc

As previously shown, 3 electrospinning solutions could be used to produce resulting fibrous scaffolds with approximate mean diameters of 1000 nm, 500 nm and 250 nm, providing a suitable fibre diameter range for cellular testing. The resulting scaffolds are subsequently referred to as $PLGA^{11}$, $PLGA^{11\ NaCl}$ and $PLGA^{25\ NaOAc}$, respectively. It was also important to understand the distribution of fibre diameters within each scaffold, as the mean fibre diameter does not show the frequency of fibres at given diameters, which may affect cell-to-scaffolds interactions. To ascertain the distribution of fibre diameters for the 3 solutions, 100 fibres were randomly selected from 4 images per '*n*' number.

The $PLGA^{11}$ scaffold had the largest range of fibre diameters, followed by $PLGA^{11\ NaCl}$ and then $PLGA^{25\ NaOAc}$ (Figure 3.12). This pattern was inverted for the interquartile range. All median values were similar to the mean (Figure 3.12). The majority of fibre diameters closely distributed around the median values for all scaffolds (Figure 3.12).

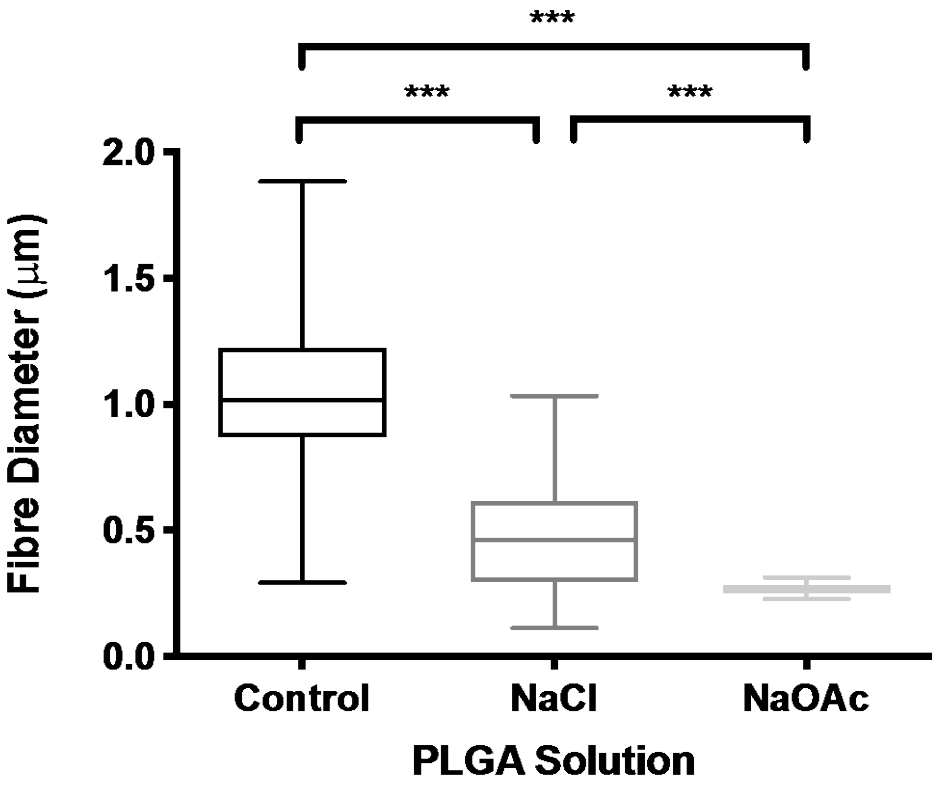

Figure 3.12 - Distribution frequency of 3 standard fibre diameters for PLGA scaffold configurations. Solutions of PLGA in 1,1,1,3,3,3-Hexafluoro-2-propanol (HFIP) at either 11% (w/v) PLGA, 11% PLGA, 1% (w/v) NaCl or 25% (w/v) PLGA, 1% (w/v) NaOAc were electrospun through a blunted 22 ½ G needle, with a flow rate of 2 mL hour^{-1}, at a collector distance of 100 mm, with a 100 mm diameter rotating mandrel at 50 x g. The applied voltages were 8 kV, 10.5 kV and 20.5 kV, respectively, to ensure a visible Taylor cone was present. Data represent the average results taken from ≥ 12 random microscopic fields per experiment. ≥100 fibres were counted per experiment. Data are mean ± maximum and minimum values, n=3. Statistical analysis: ANOVA was used in conjunction with Tukey's *post hoc* test; ***$P < 0.001$.

3.2.7 Fibre diameter had no effect on scaffold porosity

Further to understanding the ability of cells to attach to various fibre diameters, it is useful to understand the porosity of a scaffold, as this could affect gas and nutrient exchange along with affecting how cells interact with the scaffold. The porosities of the 3 PLGA scaffolds; $PLGA^{11}$, $PLGA^{11\ NaCl}$ and $PLGA^{25\ NaOAc}$ were measured using 2D SEM images, which were then assessed using the DiameterJ plugin for ImageJ. The pore area was calculated for each 2D SEM image by measuring the areas of black pixels between fibres after SEM images had been converted to binary images. The porosity was then determined from the total percentage area of all pores compared to the total scaffold area. All of the scaffolds had a median porosity of approximately 50% and there was no statistical difference between the scaffolds, despite the change in fibre composition (Figure 3.13).

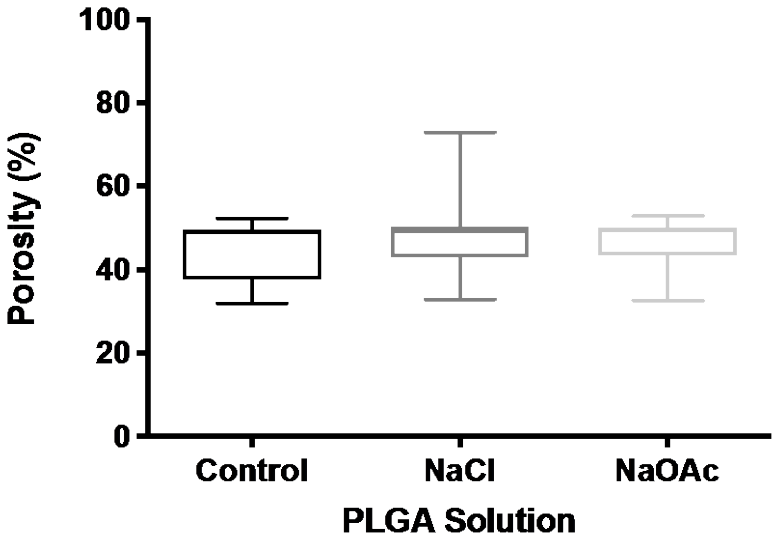

Figure 3.13 - Porosity of 3 standard PLGA scaffold configurations. Solutions of PLGA in 1,1,1,3,3,3-Hexafluoro-2-propanol (HFIP) of either 11% (w/v) PLGA**,** 11% PLGA, 1% (w/v) NaCl or 25% (w/v) PLGA, 1% NaOAc were electrospun through a blunted 22 ½ G needle, with a flow rate of 2 mL $hour^{-1}$, at a collector distance of 100 mm, with a 100 mm diameter rotating mandrel at 50 x g. The applied voltages were 8 kV, 10.5 kV and 20.5 kV, respectively, to ensure a visible Taylor cone was present. Data represent the average results taken from ≥ 12 random microscopic fields per experiment. ≥100 fibres were counted per experiment. Data are mean ± maximum and minimum values, n=3. Statistical analysis: ANOVA was used to assess statistical significance.

3.2.8 Pore area decreased with decreasing fibre diameter

It is also important to understand the mean pore area for each scaffold to help predict how specific cell types might interact with the scaffold, similarly to scaffold fibre diameter data. Additionally, the visualisation of the distribution of these pore areas also helps determine the feasibility of cells being able to enter and migrate through the scaffold. The pore areas of the 3 PLGA scaffolds; $PLGA^{11}$, $PLGA^{11\ NaCl}$ and $PLGA^{25\ NaOAc}$ were measured using 2D SEM images, which were then assessed using the DiameterJ plugin for ImageJ. For the pore area distribution data, all pores were calculated for each SEM image and plotted on box and whisker charts, with the whiskers representing the maximum and minimum values (Figure 3.13).

The differences in mean pore areas from each scaffold to one another were statistically significant (Figure 3.14). The mean pore areas showed a decreasing trend from the control to the $PLGA^{25\ NaOAc}$ scaffold (Figure 3.14). Mean pore area decreased in relation to a decrease in mean fibre diameter (Figure 3.14). This relationship is linear, with a 50% reduction in mean fibre diameter closely correlating to a 50% reduction in mean pore area (Figure 3.14). Interestingly, the range of each scaffold type decreased with decreasing pore areas (Figure 3.14). Furthermore, the interquartile range reduces with decreasing pore area (Figure 3.14).

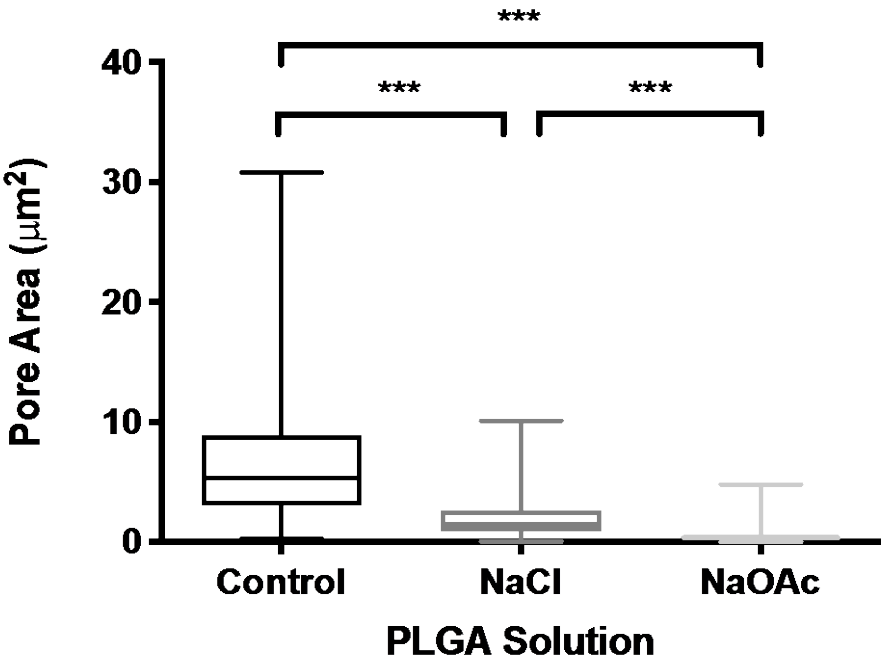

Figure 3.14 - Distribution frequency of pore area of 3 standard PLGA scaffold configurations. Solutions of PLGA in 1,1,1,3,3,3-Hexafluoro-2-propanol (HFIP) **(A)** 11% (w/v) PLGA, **(B)** 11% PLGA, 1% (w/v) NaCl and **(C)** 25% (w/v) PLGA, 1% NaOAc were electrospun through a blunted 22 ½ G needle, with a flow rate of 2 mL $hour^{-1}$, at a collector distance of 100 mm, with a 100 mm diameter rotating mandrel at 50 x g. The applied voltages were 8 kV, 10.5 kV and 20.5 kV, respectively, to ensure a visible Taylor cone was present. Data represent the average results taken from ≥ 12 random microscopic fields per experiment. ≥100 fibres were counted per experiment. Data are mean ± maximum and minimum values, n=3. Statistical analysis: ANOVA was used in conjunction with Tukey's *post hoc* test; ***$P < 0.001$.

3.2.9 Ethanol caused an increase in fibre diameter

PLGA scaffolds were submerged in 70% ethanol as this is a well-established sterilisation method for *in vitro* work. Treatment in 70% ethanol was found to increase overall fibre diameter (Figure 3.15A) and cause visible deformation to the scaffold and individual fibres (Figure 3.15B). This is consistent with results found by Shearer *et al.,* (2006) who observed PLGA 50:50 scaffold deformation from submersion in ethanol; although they were not reporting on PLGA electrospun fibres. Conversely, Braghirolli *et al.*, (2014) had consistent results when testing ethanol on PLGA electrospun fibre scaffolds. However, in contrast to this work, they found that scaffold diameters decreased from this treatment. This may be explained by their scaffolds being produced onto coverslips, which may have kept the scaffolds under tension in comparison to the unfixed scaffold discs used in this thesis. The contraction of the overall scaffold structure in this work may have caused the increase in fibre diameter, which may have been resisted if the scaffolds were kept under tension. This may have obscured any diameter reducing effect exerted by the ethanol, which may have been caused by the removal of water from the PLGA.

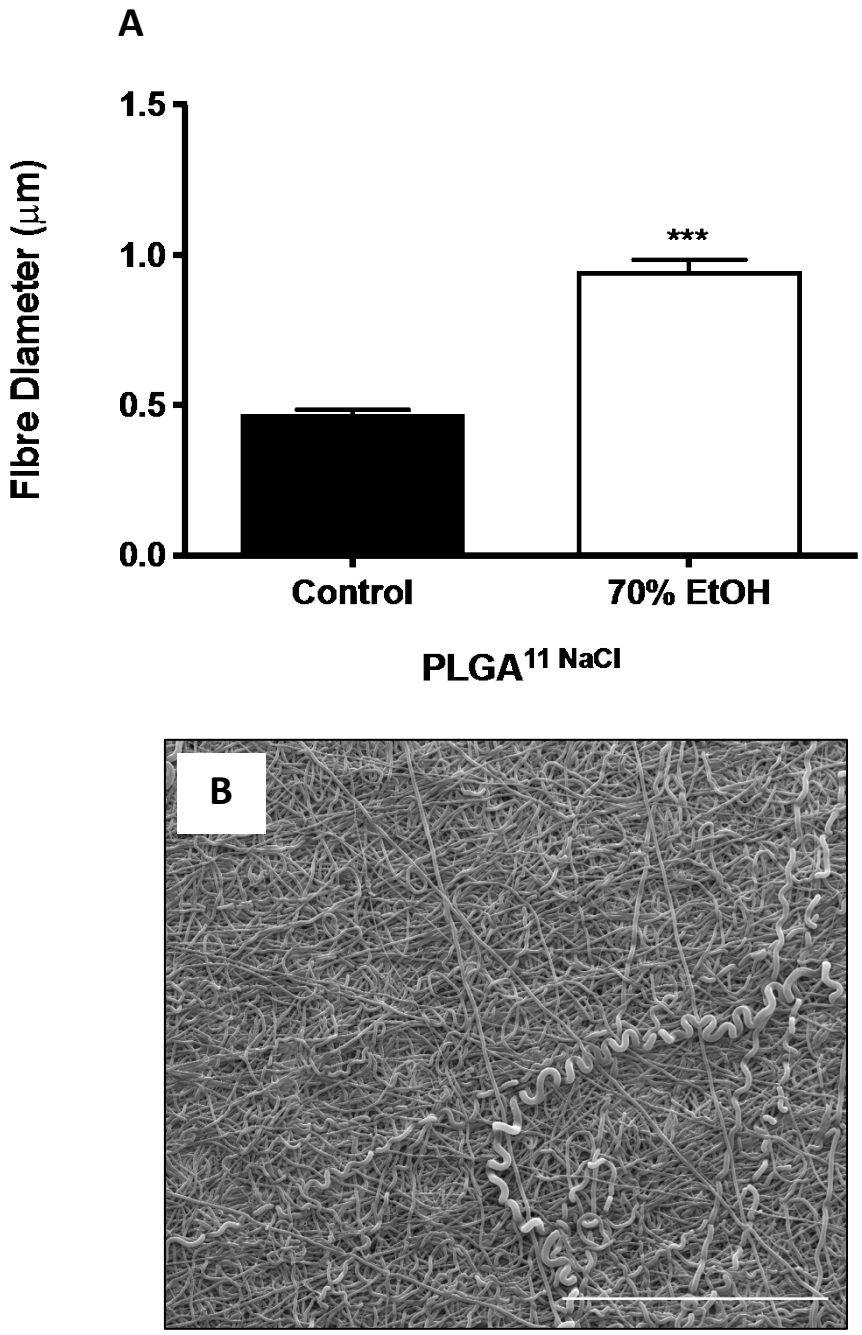

Figure 3.15 - Effect of 70% Ethanol on PLGA^{11} fibres. (A) PLGA^{11} scaffolds were cut into 6 mm discs and placed into 1 mL 70% ethanol for 1 h, air dried and platinum coated. Samples were observed under SEM. **(B)** Representative SEM image. Data represent the average results taken from ≥ 12 random microscopic fields per experiment. ≥100 fibres were counted per experiment. Data are mean ± SEM, n=3. Statistical analysis: paired Wilcoxon test was used; * $P < 0.01$. Scale bar represents 100 μm.

3.2.9 The SSS prevented bacterial and fungal growth on the scaffolds

Additional common sterilisation methods were considered for the PLGA scaffolds such as ethylene oxide and autoclaving; however, these methods were deemed to be too destructive to the scaffolds due to the high temperatures involved. Therefore, an antibiotic and antimycotic solutions was chosen to help reduce the risk of common sources of cell culture infections. This method was chosen as it had previously been shown to cause the least damage to PLGA scaffolds when compared to other common sterilisation techniques (Braghirolli *et al.*, 2014). As the SSS was found to have the least significant adverse effect on the PLGA scaffolds, this was chosen as the sterilisation method for the scaffolds to allow for subsequent *in vitro* testing. Therefore, it was important to understand the efficacy of this solution and determine a suitable minimum sterilisation time. $PLGA^{11}$, $PLGA^{11\ NaCl}$ and $PLGA^{25\ NaOAc}$ scaffolds were inoculated with *E.coli* and *C.albicans* and left for 3, 6 and 12 hours. The resulting *E.coli* and *C.albicans* infected scaffolds were incubated in fresh sterile culture media for 24 h at 37°C to enumerate any microorganisms from the scaffolds into solution. This incubated media was then aliquoted onto nutrient agar and sabouraud dextrose agar, respectively, and incubated for 24 h at 37°C. The resulting quantification of colonies for both *E.coli* and *C.albicans*, were found to be reduced by more than 99.99% for all time points on all scaffolds. The negative control scaffolds that were not inoculated with either *E.coli* or *C.albicans,* or sterilised, produced no observable colonies on the respective plates (Figure 3.16).

PLGA$^{11\ NaCl}$ + *C.albicans*	**PLGA$^{25\ NaOAc}$ + *C.albicans***	**PLGA$^{11\ NaCl}$ + *E.coli***	**PLGA$^{25\ NaOAc}$ + *E.coli***
Positive Control	Positive Control	Positive Control	Positive Control
	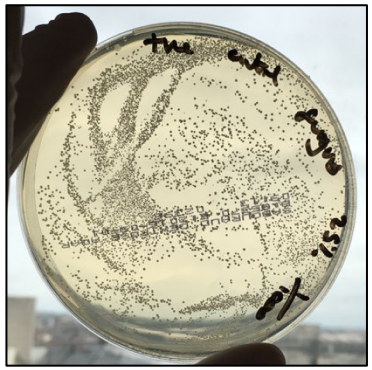		
Sterilised with SSS	Sterilised with SSS	Sterilised with SSS	Sterilised with SSS
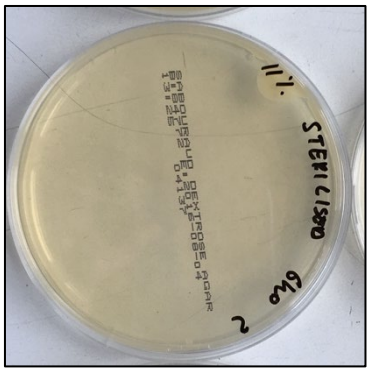	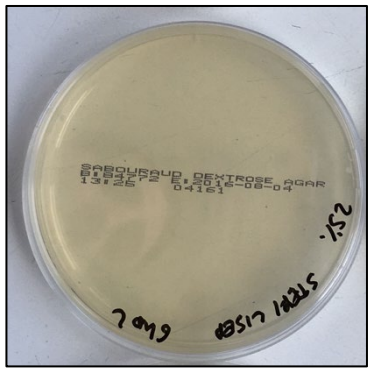		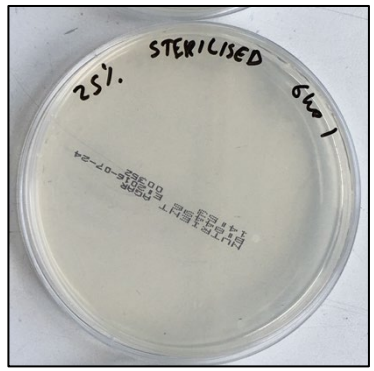

Figure 3.16 - Representative images of electrospun scaffold sterilisation using SSS. Representative images of $PLGA^{11\ NaCl}$ and $PLGA^{25\ NaOAc}$ electrospun discs 6 h post sterilisation with SSS. Discs were inoculated with *E.coli* and *C.albicans.* subsequently submerged in scaffold sterilising solution (SSS) for up to 12 hours, placed in sterile growth media and incubated, before being plated onto fresh Nutrient Agar and Sabouraud Dextrose Agar, respectively.

3.2.10 Nano-sized fibre diameters increase HUVEC attachment

In order to test whether mean fibre diameter affects cell attachment, HUVECs were seeded onto PLGA^{11} (1000 nm), PLGA$^{11\ NaCl}$ (500 nm) and PLGA$^{25\ NaOAc}$ (250 nm) scaffolds and nuclei were quantified using fluorescent microscopy after 4 and 24 h. Scaffold discs (surface area of 350 μm^2) were seeded with $1x10^5$ cells and the resulting DAPI stained nuclei were quantified from randomly selected images. This provided a number of cells per field of view, the area of which was calculated. The number of DAPI stained cells per area was then multiplied to provide an estimated cells number for the whole scaffold disc to allow comparison of the originally seeded cell number. This assumes no cells infiltrated the scaffolds. HUVECs were used as a cell model due to their relation to vascular endothelial cells, and their ability to grow and divide sufficiently quickly in culture.

There was a statistically significant increase in cell number on scaffolds with a mean diameter of 500 (PLGA$^{11\ NaCl}$) and 250 nm (PLGA$^{25\ NaOAc}$) compared to the scaffold with a mean fibre diameter of 1000 nm (PLGA^{11}) for both time points (Figure 3.17). There were approximately 150% more cells attached to the PLGA$^{11\ NaCl}$ scaffold compared to the PLGA^{11} scaffold at 4 h post seeding (Figure 3.17). At 24 h, there were approximately 100% more cells present on the PLGA$^{11\ NaCl}$ scaffold compared to the PLGA^{11} scaffold (Figure 3.17). Approximately 30% of the seeded cells were present on the PLGA^{11} scaffold after 4 h, which increased by around 50% after 24 hours (Figure 3.17).

Approximately 70% and 75% of the seeded cells were present on the PLGA$^{25\ NaOAc}$ and PLGA$^{11\ NaCl}$ scaffolds after 4 h, respectively, in regard to DAPI quantification compared to the number of seeded cells (Figure 3.17). This assumes that 4 h is the minimum time required for HUVEC cell attachment and that no cell division, apoptosis or necrosis had taken place. Cell numbers increased by around 30% and 15% for the PLGA$^{25\ NaOAc}$ and PLGA$^{11\ NaCl}$ scaffolds after 24 h, respectively (Figure 3.17). There was no difference between the number of cells at 4 h and 24 h for the PLGA^{11} and PLGA$^{11\ NaCl}$ scaffolds (Figure 3.17). However, there was a statistically significant increase in cell number at 24 h for the PLGA$^{25\ NaOAc}$ scaffold compared to 4 h (Figure 3.17).

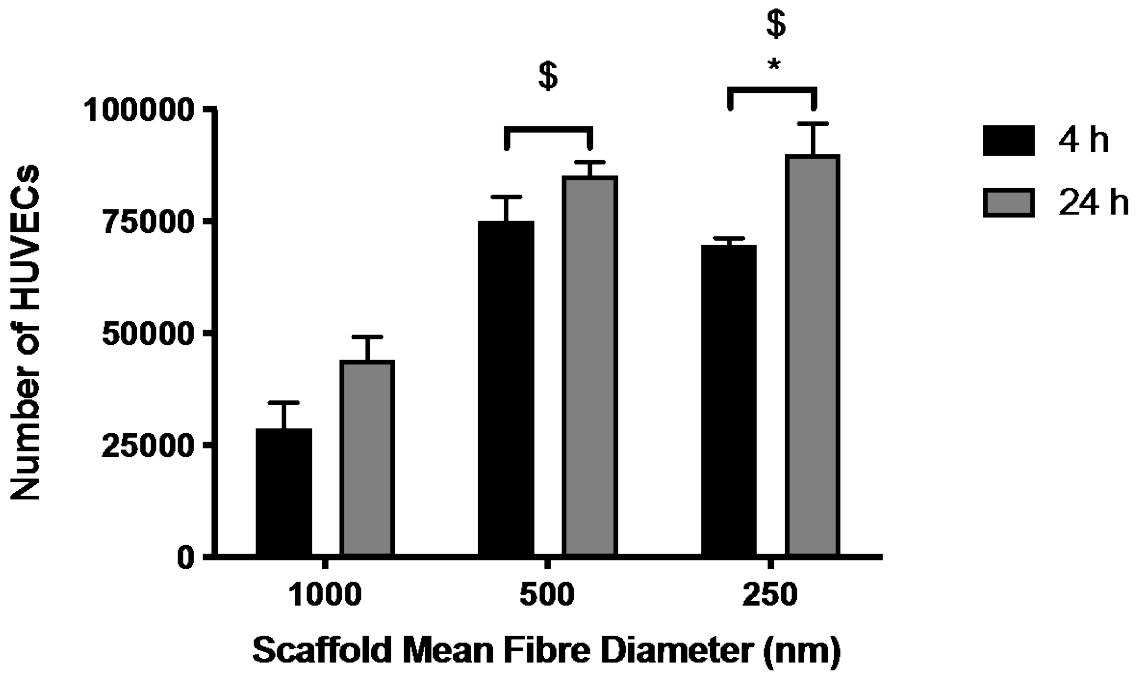

Figure 3.17 - HUVEC attachment and growth on 3 standard PLGA scaffold configurations. HUVECs were seeded onto PLGA fibrous scaffolds with varying mean fibre diameters at a density of $1x10^5$ per 380 μm^2. Scaffolds were fixed in 4% (w/v) PFA at 4 h and 24 h, stained with DAPI and nuclei were quantified. Data represent the average results taken from ≥ 12 random microscopic fields per experiment. Data are mean ± SEM, n=3. Statistical analysis: two way ANOVA was used in conjunction with a Sidak's *post hoc* test; $ indicates $P < 0.001$ vs. 1000 (4 h & 24 h) * $P < 0.01$

3.2.11 Electrospinning collector diameter had no effect on fibre diameter

After establishing a fabrication method for the PLGA electrospun scaffold sheet that was able to support cells, it was important to produce a method allowing for the production of tubular scaffolds in order to test this works suitability for vascular replacement purposes, and to determine if the results from the scaffold sheet investigations would be comparable to a tubular shaped scaffold. As previously identified, the PLGA$^{25\ NaOAc}$ structural characteristics were found to help retain a high percentage of cells from the original inoculum, as well as allow the number of cells to increase.

To initially test the feasibility of producing small diameter tubular scaffolds, it was important to understand if changes to the electrospinning collector diameter would affect the mean fibre diameter of the resulting electrospun scaffold. Therefore, the PLGA$^{25\ NaOAc}$ electrospinning solution was electrospun onto a 5 mm diameter collector and the resulting fibre diameters were quantified. This was compared to the fibre diameters produced from electrospinning the same solution onto a 100 mm diameter collector, which was the collector used for all previous flat sheet work.

There was no statistically significant difference in mean fibre diameters between the two collectors at the given parameters (Figure 3.18). The resulting fibre range increased for scaffolds produced on the 5 mm collector compared to the 100 mm (Figure 3.18).

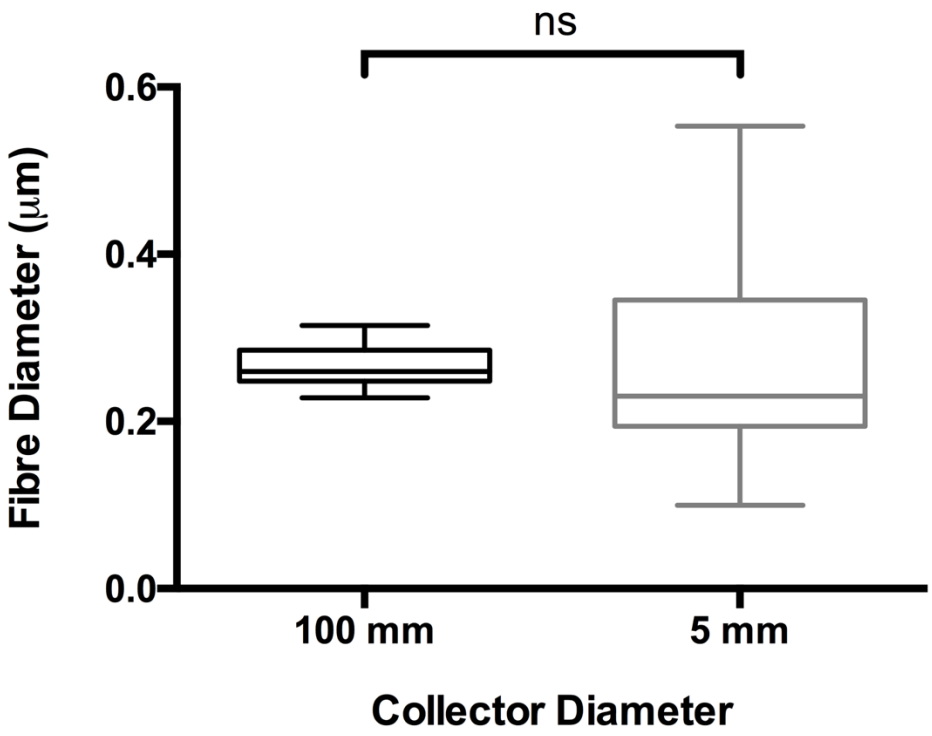

Figure 3.18 - Effect of mandrel size on resulting PLGA$^{25\ NaOAc}$ fibre diameter. A 25% (w/v) solution of PLGA in 1,1,1,3,3,3-Hexafluoro-2-propanol (HFIP) containing 1% (w/v) NaOAc was electrospun through a blunted 22 ½ G needle at 20.5 kV, with a flow rate of 2 mL hour^{-1}, at a collector distance of 100 mm, onto a 100 mm or 5 mm diameter rotating mandrel at 50 x g. Fibre diameters were quantified using the DiameterJ plugin for Fiji (ImageJ) software. Data represent the average results taken from ≥ 12 random microscopic fields per experiment. ≥100 fibres were counted per experiment. Data are mean ± SEM, n=3.Statistical analysis: two-tailed, unpaired, t test

3.2.12 Copper wire allowed for easy removal of electrospun tubes

Further to establishing that there was no statistically significant difference to the mean fibre diameter of the PLGA$^{25\ NaOAc}$ scaffold when electrospun onto a 5 mm collector, a covering material needed to be chosen in order to aid the removal of a tubular scaffold from the collector. Any material placed over the collector is required to be, or contain, a highly conductive element to ensure the electrostatic potential difference (electric tension) between the needle and the collector. Aluminium foil is a cheap and effective choice, and this was used for all previous experiments; however, electrospun scaffolds created onto aluminium foil usually adhere to the foil surface and they subsequently require removal via peeling. This was hypothesised to damage the scaffold due to the potential difficulty of removing aluminium foil from the inside of the 5 mm diameter electrospun tube. Therefore, copper wire was also tested as this is previously identified removal technique for small-dimeter electrospun tubes in the literature (Errico *et al.*, 2011). The copper wire was wound around the collector to create a gapless monolayer (Figure 3.19).

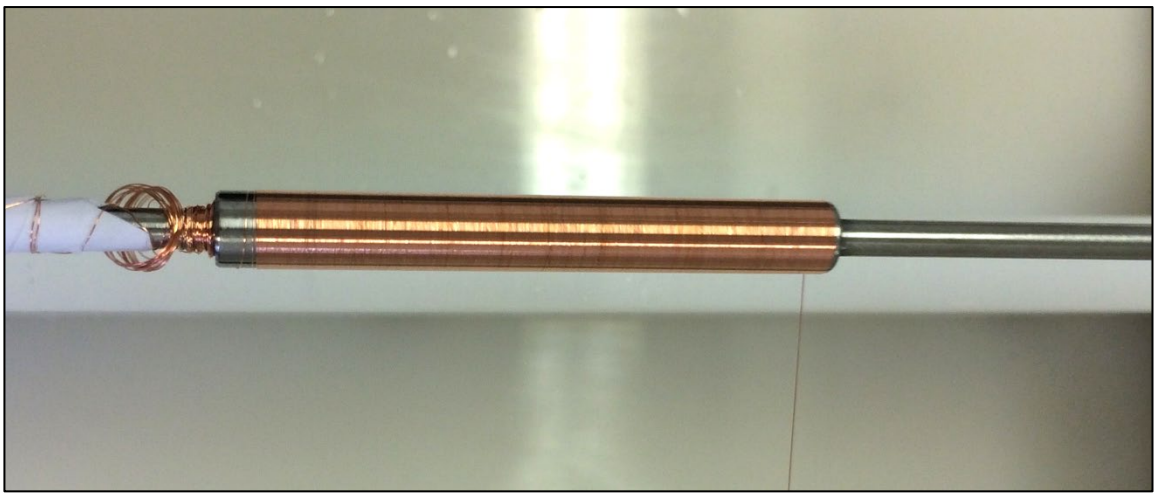

Figure 3.19 - Copper wire coating of collector. Representative image of a single layer of 80 µm copper wire being wound onto the collector before electrospinning tubular scaffolds.

Aluminium foil was used to cover the 5 mm collector and the PLGA$^{25\ NaOAc}$ solution was electrospun using the parameters outlined in Chapter 2, Table 2.8. Separately, a

monolayer of copper wire was wrapped around the 5 mm collector and the PLGA$^{25\ NaOAc}$ solution was electrospun using the parameters stated in Chapter 2, Table 2.8.

Both materials allowed for tubular scaffolds to be removed from the collector, demonstrated by the compressed sections of the tube wall shown in Figure 3.20A where forceps had to tightly hold the structure in order for removal from the aluminium foil (white arrows). Tubes fabricated onto aluminium foil were easily removed from the collector; however, removal of the aluminium foil required moderate force usually resulting in tube deformation (Figure 3.20C). The copper wire was easily removed from the occupied space between the tube lumen and the collector, which created a gap that allowed for the tubular scaffolds to be removed via gravity. However, macro-sized grooves were present across the surface of the lumen after the removal of the copper wire. Both tubes showed a microstructure containing individual fibres (Figures 3.20B and C).

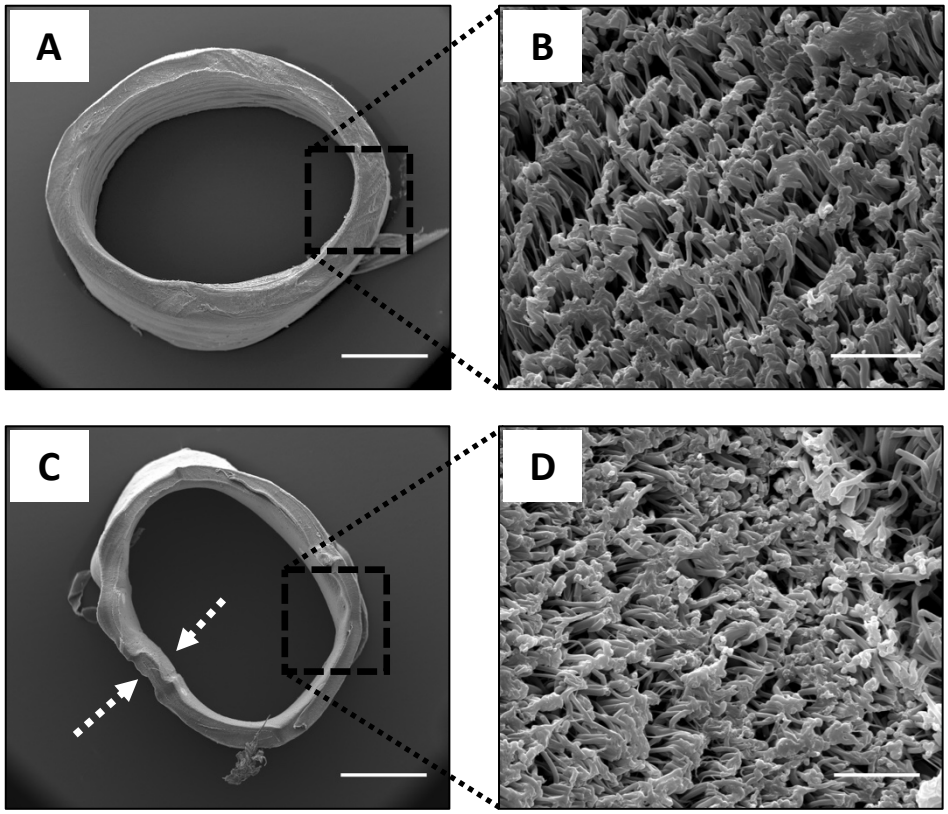

Figure 3.20 - SEM micrographs of PLGA$^{25\ NaOAc}$ tube fabrication. A 25% (w/v) solution of PLGA in 1,1,1,3,3,3-Hexafluoro-2-propanol (HFIP) containing 1% (w/v) NaOAc was electrospun through a blunted 22 ½ G needle at 20.5 kV, with a flow rate of 2 mL hour^{-1}, at a collector distance of 100 mm, onto a rotating 5 mm diameter mandrel at 50 x g covered with a **(A, B)** monolayer of copper wire **(C, D)** aluminium foil. **(B, D)** Representative image of scalpel cut cross section of vessel wall. White arrows show forceps impressions. Solutions were electrospun for 30 mins and resulting tubes were removed from the mandrel. Scale bars represent **(A, C)** 1 mm **(B, D)** 10 μm.

The resulting electrospun tube fibre diameters and wall thicknesses were measured (Figures 3.21A and B). Wall thickness was measured to determine if there was an effect of the different materials on attraction of electrospun material. The mean fibre diameters of scaffolds produced on both collectors were similar to that of the PLGA$^{25\ NaOAc}$ flat sheets, at approximately 250 nm (Figure 3.21). There was no statistically significant difference in the resulting mean fibre diameters between the copper wire and aluminium covered collectors (Figure 3.21A). The tube fabricated onto copper wire had a significantly thicker wall than the tube electrospun onto aluminium foil, with a mean thickness of 323 μm and 262 μm, respectively (Figure 3.21B).

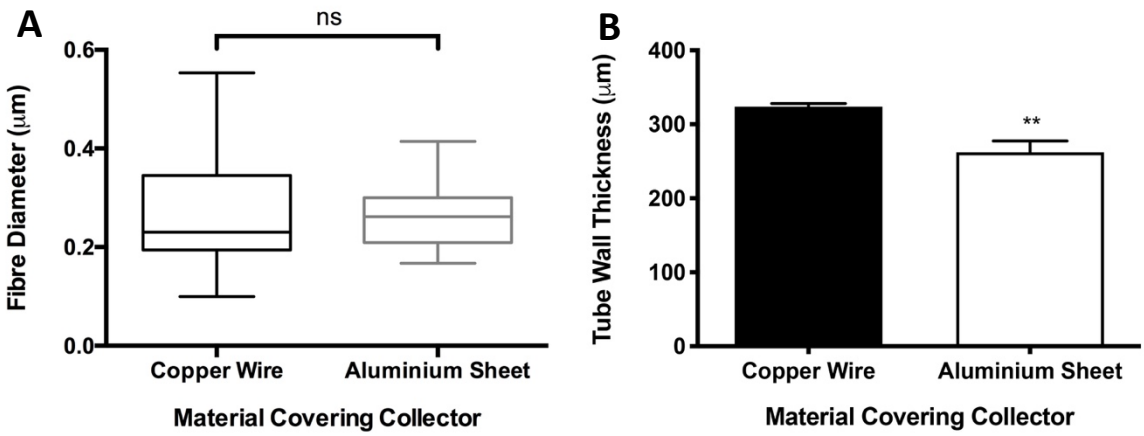

Figure 3.21 - Effect of collector covering material on resulting PLGA$^{25\ NaOAc}$ tube fibre diameter. A 25% (w/v) solution of PLGA in 1,1,1,3,3,3-Hexafluoro-2-propanol (HFIP) containing 1% (w/v) NaOAc was electrospun through a blunted 22 ½ G needle at 20.5 kV, with a flow rate of 2 mL hour^{-1}, at a collector distance of 100 mm, onto a 5 mm diameter rotating collector at 50 x g covered with a monolayer of copper wire or aluminium foil. **(A)** fibre diameter **(B)** tube wall thickness. Solutions were electrospun for 30 mins. Fibre diameters were quantified using the DiameterJ plugin for Fiji (ImageJ) software. Data represent the average results taken from ≥ 12 random microscopic fields per experiment. ≥100 fibres were counted per experiment. Data are mean ± SEM, n=3. Statistical analysis: two-tailed, unpaired t-test was used; ***P < 0.001.

3.3 Discussion

Small diameter tissue engineered-vascular grafts for use in adult coronary artery bypass are an unmet clinical need. Current research has focused on using FDA materials as ECM substitutes, and as cellular or biological carriers in the hope that the host immune system will incorporate and remodel these materials into native tissues with physiologically relevant characteristics. However, this approach has neglected the fundamental process of cell-to-scaffold attachment and the importance of the scaffold architecture and its role upon attachment and growth. The aim of this chapter was to produce a robust electrospinning system that could produce scaffolds varying fibre diameters within the nano- and micro-metre range, and to test how fibre diameter affects cell attachment and growth. The first aim of this chapter was to establish a robust process for electrospinning nano- and micro-sized fibres to help investigate whether specific PLGA scaffold fibre diameters could be selected to improve specific cellular adhesion. The second aim was to determine if a small diameter tissue engineered-vascular could be created using electrospun PLGA.

Electrospun polymer scaffold fibre diameters have been shown to affect cell attachment and proliferation in previous studies (Badami *et al.*, 2006; Bashur, Dahlgren and Goldstein, 2006; Chen *et al.*, 2007b, 2009; Yan *et al.*, 2012; Burton, Corcoran and Callanan, 2017). Scaffold fibre diameter have also been shown to affect blood activation (Milleret *et al.*, 2012b).

PLGA is a copolymer produced by combing PLA and PGA. PLGA with a ratio of 1:1 was initially chosen as the material for the electrospun scaffolds in this study due to the large amount of evidence proving its ability to support cells, and its characteristics that make it particularly favourable to cell adherence in comparison to other available biodegradable polymers (Makadia and Siegel, 2011). The ability of this material to biodegrade, along with its tuneable degradation rate were also advantageous. PLGA is known to dissolve in a number of organic solvents, which allows for the production of homogenous solutions required for the electrospinning process. Therefore, an initial literature review illuminated a number of possible solvents and solvent mixtures

specifically able to dissolve PLGA 50:50 for resulting electrospun fibres. A DMF:THF solvent mixture was chosen due to its relatively cheap cost and for the capability to alter the ratio between the two solvents, adding additional capacity to control the resulting fibre morphology. Contrastingly, a relatively specialist and therefore more expensive solvent, HFIP, was used as published research suggested it was able to help electrospun fibres resist significant morphological changes in response to system parameter changes, which would reduce the system sensitivity (Gu *et al.*, 2014).

The use of HFIP as the solvent for electrospinning polymer systems has also been shown to produce smoother electrospun fibres with significantly fewer fibre defects and generate more consistent fibres in comparison to other solvents (Gu *et al.*, 2014). However, to develop a reproducible scaffold, it was important to determine the minimum concentration of PLGA in order to achieve beadless fibres due to their unpredictable effects on overall scaffold properties (Feng *et al.*, 2015).

It was determined that both DMF:THF and HFIP were able to form a homogenous solution with PLGA at room temperature over an 8 hour period. The ability to produce homogenous solutions that were within an appropriate viscosity (assessed visually) for use in the electrospinning process was consistent with percentage ranges found in the literature. In the electrospinning set up, the increased PLGA concentration resulted in fibres with an increased diameter as expected. It was evident that a difference of 1% was enough to produce either beaded fibres or bead-less fibres. However, due to the specificity of an electrospinning system created from the many specific equipment settings, local environment, solvent and polymer, it was essential to determine the exact lowest PLGA concentration that could be used to produce smooth fibres, as this was hypothesised to have the lowest fibre diameter at the current settings and would therefore provide a starting point to then further reduce the fibre diameter, if necessary. HFIP was found to produce the most consistent and smooth fibres as observed by SEM so this solvent was chosen moving forward over the DMF:THF alternative. A recent study by Aniagyei et al. (2017) supports the observation that HFIP produces greater reproducibility in PLGA electrospun fibres. Aniagyei et al. (2017) also found that HFIP

produced PLGA fibres were also easier to remove from the collector after deposition due to lower adhesion and a higher overall strength of the resulting fibrous mats.

The optimisation process involved in determining fibre diameters within this thesis meant that there would be a large volume of scaffolds produced that would all need fibre diameter measurements. It was therefore important to identify a reliable and rapid fibre diameter measurement process to reduce time consumption. There are a number of different methods can could have been employed to assess fibre diameters within a given scaffold. To reduce human error and bias, I compared the results from the semi-automated (referred to as simply 'automated') DiameterJ plugin for ImageJ against manual measuring of individual fibres using the standard ImageJ software tools. This plugin has since been validated by (Hotaling *et al.*, 2015). The automated method showed no difference to the manual method but did have a considerable time reduction and a more consistent measurement approach across all scaffolds in the experimental work. Additionally, the automated method provide data for the average diameter across the whole length of each fibre instead of a select region in comparison to the manual method. The automated method also quantified 2D pore size data. The automated method was therefore used for the remaining work. The automated method did require additional image processing to convert images into a binary format and the binary formats required manual selection of the most suitable images for quantification. However, the process was still significantly quicker than manual quantification. The automated method also reduces the risk of selection bias from the operator.

There are a number of electrospinning parameters that can affect the resulting fibre diameters. It is therefore essential to identify the degree of effect that these parameters have in order to maintain a stable experimental set up and to help with further optimisations in future experimental work. As the HFIP solvent was chosen for further experimental work, selective parameters were chosen to test for their effect on resulting fibre diameters. Atmospheric parameters such as humidity and temperature were not assessed as no system was available to maintain or control these variables; however, test scaffolds were produced before each experiment and quantified (data not shown) to

ensure there was no significant deviation from the originally determined mean fibre diameters during seasonal temperature and humidity changes.

The main parameter changes known in the previous literature to affect fibre diameter are the solution viscosity and concentration, solvent system, applied voltage, needle bore size or gauge, needle-to-collector distance and flow rate, all of which were assessed in this work except for needle bore size. Bore size was a variable deemed suitable to keep consistent as this would reduce the optimisation process without restricting the ability to reduce the mean fibre diameter. It has also been suggested that this parameter has a minimal effect of fibre diameter (Macossay *et al.*, 2007). It was identified that during some parameter changes a Taylor cone was not visible, although this did not affect fibre deposition meaning that this electrospinning feature may have occurred inside the needle. However, voltage was increased or decreased in order to generate a visible Taylor cone to ensure experiments were consistent. Without a visible Taylor cone, it is difficult to assess if the tip of needle is affecting the resulting fibres. If the Taylor cone forms inside the bore of the needle, the resulting may not be continuous and may be breaking, which would affect resulting fibre formation. There are also a variety of droplets that can form without the presence of a Taylor cone whilst still producing fibres (Yarin, Koombhongse and Reneker, 2001). Therefore, to ensure consistency across experiments a visible Taylor cone was required for each experiment.

The parameter changes in these experiments had no effect on the resulting fibre diameters, which may be due to there not being a great enough change to any one parameter. It may also be due to the resistance of the HFIP solvent system to the effects of minor parameter changes, which has been identified by Jean-Gilles et al. (2010). Within this solvent system and particular PLGA copolymer ratio, and molecular weight, 11% (w/v) was determined to be the lowest whole percentage that produced beadless fibres.

Although there are a large number of published studies that have demonstrated the feasibility of producing PLGA fibre diameters of less than 1000 nm, many have used different solvents and PLGA copolymers. Further to this, in electrospinning setups not using HFIP, the previously discussed parameter changes may also have allowed for a

significant reduction in fibre diameters in comparison to the 1000 nm achieved in this work. A study by Ramos *et al.,* (2015) did use PLGA 50:50 at a relatively high concentration of 25% (w/v) and HFIP, and achieved a mean fibre diameter of 473 nm; however, this study used PLGA with a much lower molecular weight of approximately 17,000 g mol^{-1} compared to the PLGA used in this thesis that had an approximate molecular weight of 153,000 g mol^{-1}. It has been shown that increased molecular weight in poly (vinyl) alcohol increased average electrospun fibre diameter (Akduman, Kumabasar and Çay, 2014). Therefore, it is possible that molecular weight has a significant impact on resulting fibre diameters for the same polymers or co-polymers and that PLGA fibre diameter could have been decreased by using a lower molecular weight polymer. However, changes in molecular weight may also affect other electrospinning characteristics such as viscosity, fibre strength, biocompatibility and degradation so further study would be required to select for the most appropriate molecular weight in each situation (Gupta, Revagade and Hilborn, 2007; Pillai and Sharma, 2010).

The addition of salts is well known to affect fibre morphology by changing the conductivity of the polymer solution (Qin *et al.*, 2007; Yalcinkaya and Jirsak, 2015). Salts have also been shown to improve fibre uniformity and reduce bead formation (Lee, Kim and Kim, 2005). More importantly for this work, some studies have demonstrated a reduction in fibre diameters from the addition of salts through increasing the solution conductivity (Zong *et al.*, 2002; Choi *et al.*, 2004). However, identifying previously published literature that has used a similar polymer and solvent is difficult due to the large variety of possible parameters that affect the electrospinning process, meaning this had to be investigated experimentally. I therefore examined the literature for a suitable salt that could dissolve in HFIP to initially reduce the propose experimental work, in order to test whether there was an effect on fibre diameter. Interestingly, there are relatively few reports on the use of HFIP for electrospinning in the literature (Jean-Gilles et al. 2010; Aviss et al. 2010; You et al. 2006), and only one study was identified to be using NaCl to help reduce the average fibre diameter in PLGA scaffolds using a HFIP as the solvent system (Jean-Gilles *et al.*, 2010b).

Theoretically, it is believed that the addition of salts can increase the conductivity of polymer solutions, which affects the electrospinning process as solutions become, what is referred to as, leaky dielectric because charges are generated on the surface of the forming jet (Taylor, 1964, 1969). Carroll and Joo (2006) found that an increase in solution conductivity prolonged the jet thinning process resulting in thinner fibres.

Following this study, I added 1% (w/v) NaCl to the solution finding a significant decrease in fibre diameter, which was also observed by Ding et al. (2010). However, I noted that salt did not fully dissolve in the PLGA/HFIP solution and most of the added NaCl could be seen undissolved, even after mixing overnight. Jean-Gilles et al. (2010) also too reported [personal communication] that, even at 1% (w/v), NaCl was not found to fully dissolve in a PLGA/HFIP solution. It may therefore be likely that a smaller quantity of NaCl could have been used to generate the fibre diameter reducing effect; however, the excess salt was not observed to have any adverse effects on fibre morphology. Adding further salt was not deemed possible as NaCl was not miscible in HFIP even at 1% (w/v). Furthermore, Arayanarakul et al. (2006) reported that too much salt actually increased fibre diameter due to instabilities caused by the changes in conductivity and charge of the electrospinning solution.

NH_4Cl and NaOAc were added separately at 1% (w/v) to help determine if the effect on fibre diameter could be attributed to sodium or chloride ions within NaCl. I hypothesised that NH_4Cl or NaOAc would be more miscible than NaCl, allowing for a greater reduction in fibre diameter.

NH_4Cl produced a smaller mean fibre diameter than the addition of NaCl, which suggests this exerts an effect similar to NaCl and that the chloride ion contributes significantly to this effect. However, the resulting fibres from solutions containing NH_4Cl presented a phenomenon that could not be found in published literature. In select regions of the depositing fibre sheet, fibres were more densely populated creating surface aberrations. Multiple aberrations in the form of raised bumps could be visibly seen and under SEM they were approximately 100 μm. These structural defects could be the result of charge accumulation within the anode causing a self-reinforcing process whereby fibres are

attracted to a region within the anode with an increased charge, which further increases the charge, further attracting more fibres from the electrospinning jet. Normally, charge is discharged randomly across the scaffold as each new fibre is deposited by the evaporation of the remaining solvent. However, uneven distribution and an increase in discharge time may lead to an accumulation of fibres as shown in this thesis, which is explained in detail by Collins et al. (2012). There are also known issues with uneven deposition from poor fibre attraction in scaffolds thicker than 1 mm, however this was not the case for the NH_4Cl scaffolds as they were less than 50 μm thick (Filatov, Budyka and Kirichenko, 2007).

Adding 1% (w/v) NaOAc significantly reduced the mean fibre diameter. In literature published during this experimental work, Lawson et al. (2016) independently identified that sodium acetate is beneficial to a PCL electrospinning solution for improving control over fibre characteristics when using an alternative needleless electrospinning approach due to improved charge transfer. However, they found that the addition of NaOAc actually increased solution viscosity, which is in contradiction of the decrease in viscosity identified in this experimental work. In support of this work, a study on polyacrylonitrile demonstrated that the addition of chloride salts did decrease the electrospinning solution viscosity; however, this was identified at concentrations above 4% (w/v) (Qin *et al.*, 2007). As previously eluded to, the addition of salts is believed to increase solution charge and prolong the elongation of the polymer jet thereby decreasing fibre diameter (Carroll and Joo, 2006). Although, contrastingly, the addition of lithium chloride to polyethelene oxide solutions was found to increase fibre diameters in a salt concentration-dependent manner (Yalcinkaya, Yalcinkaya and Jirsak, 2015), which was not identified with NaCl in this work. This shows that understanding of the fundamental chemistry behind how salts affect electrospinning solutions is still poor.

The effect of NaCl on fibre diameter in this experimental work was limited due to the miscibility of NaCl in HFIP meaning any concentration dependent associations could not be observed or investigated. However, as shown by the experimental data, NaOAc can overcome this barrier due to being more readily miscible in HFIP. However, the thinning effect NaOAc has on the electrospinning solution prevents further fibre diameter

reductions as solutions become too thin to electrospin. Despite this, increasing the polymer concentration, which is widely known to increase solution viscosity (Koski, Yim and Shivkumar, 2004; Al-Shammari *et al.*, 2011; Nezarati, Eifert and Cosgriff-Hernandez, 2013), helped overcome the thinning whilst still providing a large reduction in fibre diameter compared to the addition of NaCl.

Polymer solution viscosity has been reported to be related to polymer molecule chain entanglement (Hu *et al.*, 2015). Chain entanglement is the phenomenon whereby polymer chains do not simply cross or intermingle, but entangle, which significantly increase adhesion (Porter and Johnson, 1966). It could therefore be hypothesised that in this solvent system, the addition of acetic acid affects the polymer chain entanglement, thereby affecting viscosity. Further chemical experimentation would be required to understand the cause of a decrease in viscosity from the addition of NaOAc as this has not been reported in the published literature for PLGA solutions using HFIP, to my knowledge. However, this observation shows the potential for increasing polymer concentration of electrospinning solutions, which could reduce electrospinning fabrication time and solvent waste.

Further investigation into fibre reductions were halted at this stage due to the process being established for the production of 3 different fibre diameters for PLGA allowing for further hypothesis testing using biological cells. Further diameter decreases may be possible with the optimisation of salt concentration and refinement of the electrospinning system parameters. The salt interaction with the polymer and solvent solution will likely also play a role in the effect on resulting fibre diameter. Identifying salts that increase the electrospinning solution conductivity may be more effective at reducing fibre diameters than increased salt concentrations.

Zong et al. (2002) suggested that salts with smaller ionic radii help to produce smaller diameter fibres due to higher charge densities allowing for increased mobility through the electrospinning solution. The acetate ion has a smaller atomic radius than the chloride ion, which helps support the observations in this work.

The increase in fibre diameter uniformity could be attributed to the increase and more even distribution of charge across the electrospinning solution imparted by the addition of salts. The proposed increased stretching of the electrospinning jet in solutions containing salt as previously described may also account for the increased resistance to beading (Carroll and Joo, 2006) helping to improve individual fibre diameter variances and subsequently improving the relative fibre diameters of a given scaffold. The increased charge density of NaOAc may have magnified this effect accounting for the narrower range of fibre diameters in comparison to no salt and the addition of NaCl (Zong *et al.*, 2002).

No differences were identified between the porosities of the 3 scaffolds, despite the change in mean fibre diameters. Increased porosity should allow for an increased diffusion of molecules, which could enhance the local environment for cellular attachment and growth. However, porosity alone does not allow for the determination of interconnectivity of the pores, which Is essential for gas exchange, fluid and cellular migration through the scaffold.

Furthermore, measuring porosity using 2D images may not be representative of the porosity of a 3D structure and this calculation of surface porosity could have obscured any differences found in actual porosity between the 3 scaffold types. The DiameterJ software may also have lost critical information for porosity calculation when converting SEM images to binary images, as darkened areas containing fibres may have been determined as pore areas depending on the light intensity threshold for determining the presence of fibres. Additionally, variations in the amount of PLGA deposited onto the scaffolds before SEM could have increased or reduced the amount of fibres present on a 2D SEM image due to the deposition of fibres on different planes. Although 2D porosity calculations are an easy and cheap method for estimating scaffold porosity, the limitations may result in values that are unrepresentative of the true 3D porosity preventing the establishment of useful conclusions. A liquid displacement or nitrogen absorption method may be more suitable for future work.

In contrast, the pore areas showed a positive relationship with decreasing fibre diameter. The literature demonstrates methods for increasing pore area using techniques such as salt leaching (Nam *et al.*, 2007). However, pore size of electrospun scaffolds can vary depending on fibre diameter, the deposition of fibres and the degree to which fibres join. Larger fibre diameters would be expected to increase scaffold pore size due to the increased distance between the underlying fibres and the newly deposited ones, which is supported by this work.

Scaffold pore size has been shown to affect cellular interactions with scaffolds (Zeltinger *et al.*, 2001; O'Brien *et al.*, 2005) and affect vascularisation of the scaffold *in vivo* (Klenke *et al.*, 2008; Bai *et al.*, 2011). It would be advantageous for a TEVG to be able to promote endothelial cell attachment and growth to ensure a luminal endothelium could be developed prior to implantation and repair after implantation if any damage were to occur. Narayan and Venkatraman, (2008) found that pore sizes of 20 – 40 μm in PLGA scaffolds enhanced endothelial cells numbers, which suggest pore size may play a role alongside fibre diameter in enhancing specific cell attachment.. Yuzhen Wang *et al.*, (2016) also found that pore sizes that when pore sizes are more varied within a scaffold, and are therefore similar to native ECM, they promote wound healing compared to scaffolds with more uniform pore sizes. In this work, it was found that the larger fibre scaffolds such as PLGA^{11} had a wider range between pore sizes, which may enhance cellular wound healing and be more suited to fibroblast culture. Electrospun scaffolds are also regarded as poor as promoting cellular infiltration due to their compact structures. However, large diameter fibres can increase the void space between layers and increase pore sizes. A mixture of large diameter fibres and smaller diameter fibres within a single electrospun scaffold have been employed and demonstrate improved infiltration (Balguid *et al.*, 2009).

PLGA scaffolds were submerged in 70% ethanol as this is a well-established sterilisation method. This was found to increase overall fibre diameter and caused visible deformation of the scaffold fibres. This is consistent with results found by Shearer et al. (2006) who observed PLGA 50:50 scaffold deformation from submersion in ethanol; although they were not reporting on PLGA electrospun fibres. Conversely, Braghirolli et al. (2014) had

consistent results when testing ethanol on PLGA electrospun fibre scaffolds. However, in contrast to this work, they found that scaffold diameters decreased from this treatment. This may be explained by their scaffolds being produced onto coverslips, which may have kept the scaffolds under tension in comparison to the unfixed scaffold discs used in this thesis. The contraction of the overall scaffold structure in this work may have caused the increase in fibre diameter, which may have been resisted if the scaffolds were kept under tension. This may have obscured any diameter reducing effect exerted by the ethanol, which may have been caused by the removal of water from the PLGA.

Shearer et al. (2006) concluded that antibiotic treatment provides a convenient and effective method for scaffold sterilisation. Further work by Braghirolli et al. (2014) was also found to support this conclusion in the use of electrospun fibre scaffolds. This work utilised this antibiotic and antimycotic solution for scaffold sterilisation due to the low impact a solution would have upon the PLGA scaffolds. This method was also low cost and easy to implement.

To test the effectiveness of this solution on electrospun PLGA scaffolds and determine the minimum time required for effective sterilisation. Newly fabricated unsterilised scaffolds contained no viable *E.coli* or *C.albicans*, which could indicate that these microorganisms were not present in the environment in which the scaffolds were fabricated. This could also suggest that residual HFIP could be present in the scaffolds and during fabrication, which is inhibitory or toxic to these microorganisms. Although this hypothesis could raise the risk of scaffold toxicity from residual HFIP, the positive control scaffolds showed that *E.coli* and *C.albicans* are able to adhere to the scaffolds in significant quantities demonstrating that the removal of HFIP during PBS washing is sufficient.

As expected, due to the well documented effectiveness and routine use of penicillin/streptomycin and amphotericin B, the SSS prevented bacterial and fungal growth after just 3 hours. This result confirmed its use an effective antibacterial and antifungal agent for PLGA electrospun scaffolds. Despite the effectiveness of the solution, it is still possible that scaffolds could have become infected with viruses and other microorganisms unaffected by penicillin/streptomycin or amphotericin B; however, for

the purposes of this work, the SSS was deemed sufficient for further *in vitro* experimentation under standard aseptic laboratory conditions.

HUVECs were used as a vascular endothelial cell model due to their endothelial characteristics and ability to grow sufficiently in culture. Scaffold fibre diameter was assessed by determining the ability of HUVECs to attach to each scaffold under identical conditions to help elucidate whether endothelial attachment could be improved through varying fibre diameter.

Cell seeding efficiency was relatively high in comparison to reported cell efficiency reported for static seeding methods in the literature (Soletti *et al.*, 2006; Thevenot *et al.*, 2008; Fu *et al.*, 2012). This could be due to many studies focussing on cell infiltration and distribution within the scaffolds. Whereas the scope of this work was to determine what effect scaffold fibre diameter had on initial cell attachment and cell numbers were quantified within a short period of time after seeding. These data showed that HUVECs initially attach more successfully to fibres below approximately 500 nm. Interestingly, this is in contrast to findings by Rüder *et al.*, (2013) who identified that HUVECs adhesions was reduced by fibres at the submicron range when using copolyetheresterurethane scaffolds, which suggests this effect may be scaffold material dependent and not solely an effect of fibre diameter. It is possible that rather than attachment, increased proliferation could have attributed to the increase in cell number on smaller fibre diameter scaffolds. It was assumed that 4 hours would be only enough time for initial attachment of the HUVECs to the scaffold, which would reduce the chance of cell division. However, this could not be ruled out and further testing could determine the role proliferation may have attributed to the results seen in this thesis. Contrastingly, there may have been rapid apoptosis on the larger diameter scaffold, which attributed to a lower cell density. This would also require further testing for apoptotic markers to determine the effect this may have had on the experiment in this thesis. It is also possible that HUVECs may have taken longer to adhere to the larger fibres and that this would not affect cell numbers over time and a further time course experiment would be required to understanding the significance of these findings.

Furthermore, the larger fibre diameter scaffold also had larger pore areas, which may have cause cells to infiltrate the scaffold and not be visible to DAPI staining. However, the HUVECs were considerably larger than the average pore sizes in the PLGA[11] scaffold and there was no visible evidence of cell infiltration beyond the surface layer under fluorescent microscopy. Further testing may elucidate some of the questions raised by these findings as to whether HUVECs are cultured more successfully on submicron PLGA electrospun scaffolds over the long term, what effects this may have on cell phenotypes and whether this translates to luminal endothelium.

To initially optimise and test the electrospinning solutions in the previous experimental work, a small diameter rotating mandrel was used as this could produce small electrospun flat sheet scaffolds for testing. To improve efficiency, a larger mandrel was used to allow for the fabrication of scaffold sheets with larger surface areas. This would reduce the time required to electrospin numerous separate scaffold sheets using the smaller mandrel as the set-up time of the equipment would be minimised. Therefore, it was important to determine whether a change in mandrel diameter would affect fibre diameter.

To generate a significant amount of scaffold flat sheet for the initial testing of the electrospinning process in this thesis, a rotating collector with a diameter much larger than that of a mammalian coronary artery was used. To create a small diameter tube, it was important to determine whether fibre diameter was affected by the collector diameter when all other parameters remained constant. Previous work has shown that electrospinning collector can affect fibre diameter (Alfaro De Prá *et al.*, 2017), however this is usually from a change in collector structure, which was not altered in this work, at this stage. Adomavičiute and Stanys (2011) found that collector material did not affect fibre diameter for PVA fibres, which is supported by this work. The resistance of this electrospinning solvent system to parameter changes may also have minimised any effect on fibre diameter from the change in mandrel diameter.

Electrospun fibre tubes were found to partially adhere to the collector preventing their removal without causing significant structural damage. In the previous work of this

chapter, scaffolds were found to adhere to the foil-coated collector; however, gentle peeling allowed for the separation of the scaffold from the foil. Experiments were also carried out on the surface of the scaffolds to prevent any microscopic damage to the peeled side of the scaffolds affecting experimental results. Tubular scaffolds could not be removed in this way. As with previous work in this chapter, foil was tested to allow tubes to be removed from the collector leaving only the foil to be removed from the lumen of the tube. Copper wire was also investigated as this had been previously shown to aid in tube removal from a cylindrical collector (Errico *et al.*, 2011).

The copper wire allowed for a reduction in contact area between the tube lumen and the conductive substrate allowing for easy removal unlike the aluminium foil, which was in contact with the entire luminal surface. The increase in tube wall thickness for the copper wire scaffolds can be attributed to the higher conductivity of copper, which allows for a greater charge potential between the needle and the collector in comparison to aluminium foil.

3.4 Conclusion

To summarise, this chapter demonstrates the need for electrospinning optimisation. This chapter has provided evidence that NaOAc used in conjunction with HFIP can be used to generate nano-scaled PLGA fibres, and that fibre diameters below 1 μm improves HUVEC attachment. Furthermore, this chapter outlines a robust electrospinning method for successfully fabricating small diameter PLGA tubular scaffolds.

4

FABRICATION OF A TRI-LAYERED ELECTROSPUN TUBULAR SCAFFOLD

4.1 Introduction

The electrospinning technique can be used to produce 3D fibrous structures and allows for the optimisation of specific fibre diameters as shown in Chapter 1 of this thesis. Further to the effects on cell-to-scaffold interactions produced from varying electrospun fibre diameter, cell morphology has been shown to be affected by fibre orientation and alignment of electrospun fibres (Shang *et al.*, 2010; Liu *et al.*, 2015). Producing electrospun fibre scaffolds with a high degree of alignment has traditionally been achieved using a mandrel collector rotating at a high RPM (Shang *et al.*, 2010; Gnavi *et al.*, 2015). This is a convenient method for alignment deposited electrospun fibres. The resulting aligned scaffolds have been shown to cause cells to elongate and align with the direction of the fibres (Shang *et al.*, 2010).

There is also evidence that aligned fibre tubular scaffolds can reduce the occurrence of thrombus formation in a rat model (Liu *et al.*, 2013). In addition to this, aligned fibres have been shown to provide increased tensile stress in dominant fibre direction (Jahani *et al.*, 2012). Producing aligned fibres is therefore of increasing importance for studies using cells that would be physiologically aligned such as luminal endothelia and smooth muscle cells of the arterial intima. Aligned fibre scaffolds could be used to improve *in vitro* cell models and, more specifically, could be used to generate more physiologically relevant environments to control cell behaviour for TEVG purposes.

In this chapter, a tri-layered vessel design was investigated to help develop a tissue engineered vascular graft. Figure 4.1 shows the proposed design and the basis for the hypothesises and subsequent experimental work in this chapter.

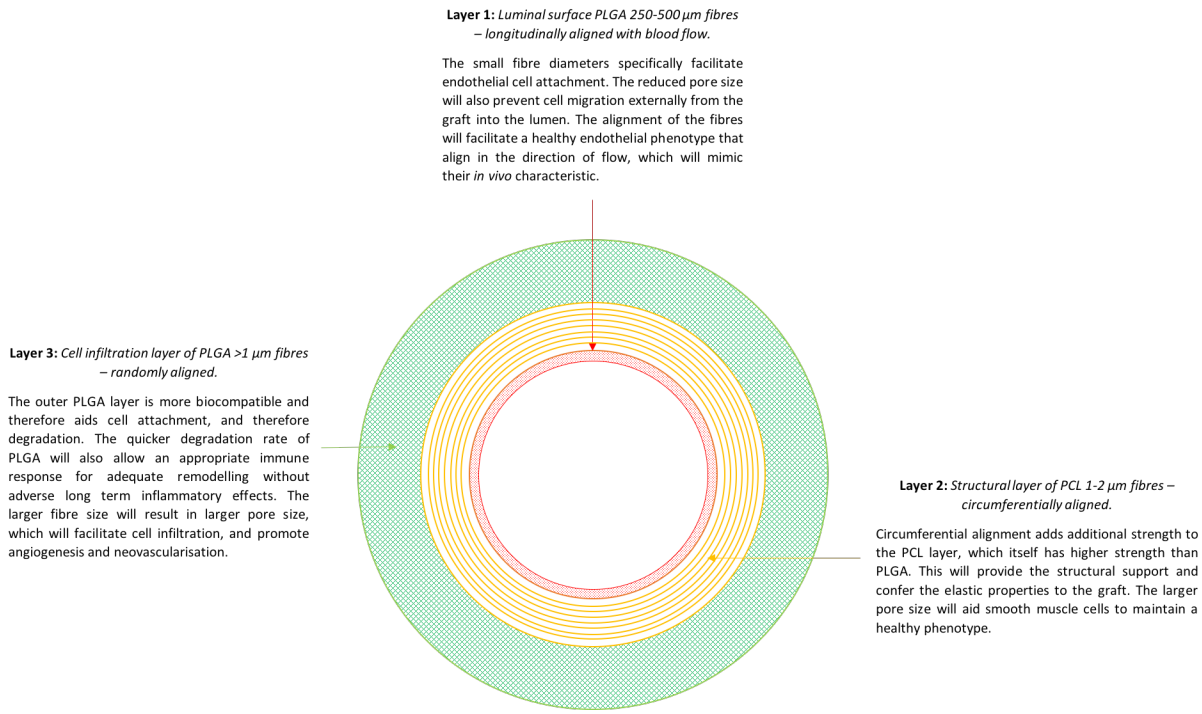

Figure 4.1 - Proposed tri-layered electrospun TEVG design. The tube consists of 3 layers, each consisting of a specific fibre diameter to enhance cell adhesions or infiltration based on previous experimental work and published literature. Layer 1 consists of longitudinally aligned fibres of PLGA, Layer 2 consists of circumferentially aligned PCL fibres and Layer 3 consists of randomly orientated PLGA fibres.

Briefly, it was hypothesised that longitudinally aligned fibres with a mean diameter of approximately 250 nm would be most suitable for endothelial cell attachment, morphology and alignment based on previous literature and experimental work from Chapter 3 (Whited and Rylander, 2014b). Previous work in Chapter 3 suggested that both 250 nm or 500 nm may be suitable for further use in a TEVG. However, 250 nm was chosen as this value was close to ECM sized ranges than 500 nm. Furthermore, the literature suggested that submicron diameter fibres may also reduce platelet adhesion (Milleret *et al.*, 2012b). Therefore, the smallest fibre diameter of 250 nm was chosen for further investigation. Additionally, I hypothesised that a further two layers could be incorporated into the electrospun tube to help select for, and maintain, cell characteristics found in physiological arteries; the second layer was proposed to help improve tubular scaffold strength by a different polymeric material, polycaprolactone (PCL), which has an increased resistance to degradation and tensile strength compared to PLGA (Chou and Woodrow, 2017). Furthermore, the PCL fibres would be orientated in

the circumferential direction providing additional strength to resist the high hydrostatic pressure from blood. Finally, I hypothesised that a third layer of randomly aligned PLGA could be incorporated, which would provide larger pore sizes helping to aid neovascularisation and angiogenesis, as shown by previous literature (Druecke *et al.*, 2004; Yang *et al.*, 2006; Xiao *et al.*, 2015).

In order to create a scaffold with 3 separate layers that had distinct fibre diameters and orientations, a new fabrication process had to be developed. To enable this, I had to design two electrospinning collectors, and have them built and optimised for the experimental work. The collectors were built onsite based on my designs at the University of Bristol by an engineering workshop. Therefore, the optimisation of the collectors during their construction are not presented in this thesis before they were used for experimental work. However, any further adaptations to any single collector that was required as a result of experimental optimisation is reflected in this chapter.

This chapter evaluates the feasibility of developing two new collectors based on previously published literature and the desired outcome, and the optimisation of the electrospinning set up for each layer to obtain the desired fibre diameters and fibre orientation. This chapter also demonstrates the process of bringing each layer together to create a seamless tri-layered electrospun tube.

4.2 Results

4.2.1 Fabrication of aligned PLGA flat sheets using high speed rotation

High-speed rotation of an electrospinning collector is well known to produce aligned electrospun fibres (Gnavi *et al.*, 2015; Baudequin *et al.*, 2017). Therefore, PLGA$^{25\ NaOAc}$ and PLGA^{11} were electrospun at either 50 x g or 500 x g to determine the effect of the mandrel rotation speed on fibre alignment. The effect of high-speed rotation of the collector mandrel was assessed for PLGA$^{25\ NaOAc}$ to determine if this was a suitable method to produce aligned fibres for subsequent cellular experiments. PLGA^{11} was included to assess whether high speed rotation had a comparable effect on different average fibre diameters.

At a rotational speed of 500 x g PLGA$^{25\ NaOAc}$ fibres became visually aligned compared to 50 x g under SEM assessment (Figure 4.2). Additionally, before observing fibres under SEM, the 500 x g produced scaffold had a visibly more reflective surface in comparison to the 50 x g scaffold (images not shown).

At a rotational speed of 500 x g PLGA^{11} fibres became visually aligned compared to 50 x g under SEM assessment (Figure 4.3). A similar increased reflective effect was also visible in the 500 x g produced scaffold in comparison to the 50 x g scaffold (images not shown). However, we did not have adequate facilities to further test this observed effect.

Graphically, PLGA^{11} had a higher proportion of fibres orientated in the same direction in comparison to PLGA$^{25\ NaOAc}$, although this was not tested statistically (Figures 4.2B and 4.3B).

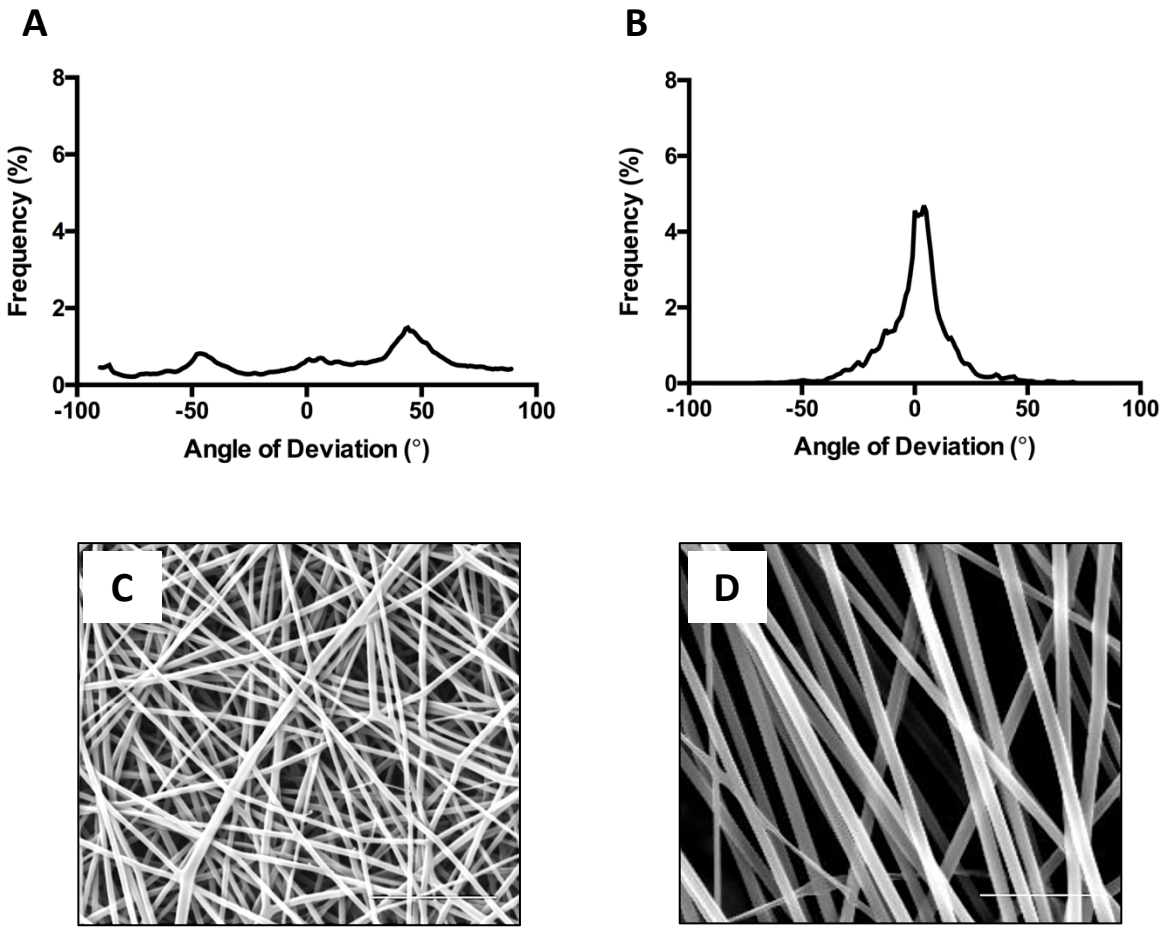

Figure 4.2 - PLGA$^{25\ NaOAc}$ fibre alignment using high speed rotation. A 25% (w/v) solution of PLGA in 1,1,1,3,3,3-Hexafluoro-2-propanol (HFIP) containing 1% (w/v) NaOAc was electrospun through a blunted 22 ½ G needle at 20.5 kV, with a flow rate of 2 mL hour^{-1}, at a collector distance of 100 mm, onto a 100 mm diameter rotating mandrel at **(A)** 50 x g and **(B)** 500 x g. Fibre diameters were quantified using the DiameterJ plugin for Fiji (ImageJ) software. Fibre orientation angles were calculated from SEM images using the OrientationJ plugin for ImageJ using 100 fibres per image. Data represent the average results taken from ≥ 12 random microscopic fields per experiment. ≥100 fibres were counted per experiment. Data n=3. Scale bars represent 5 µm..

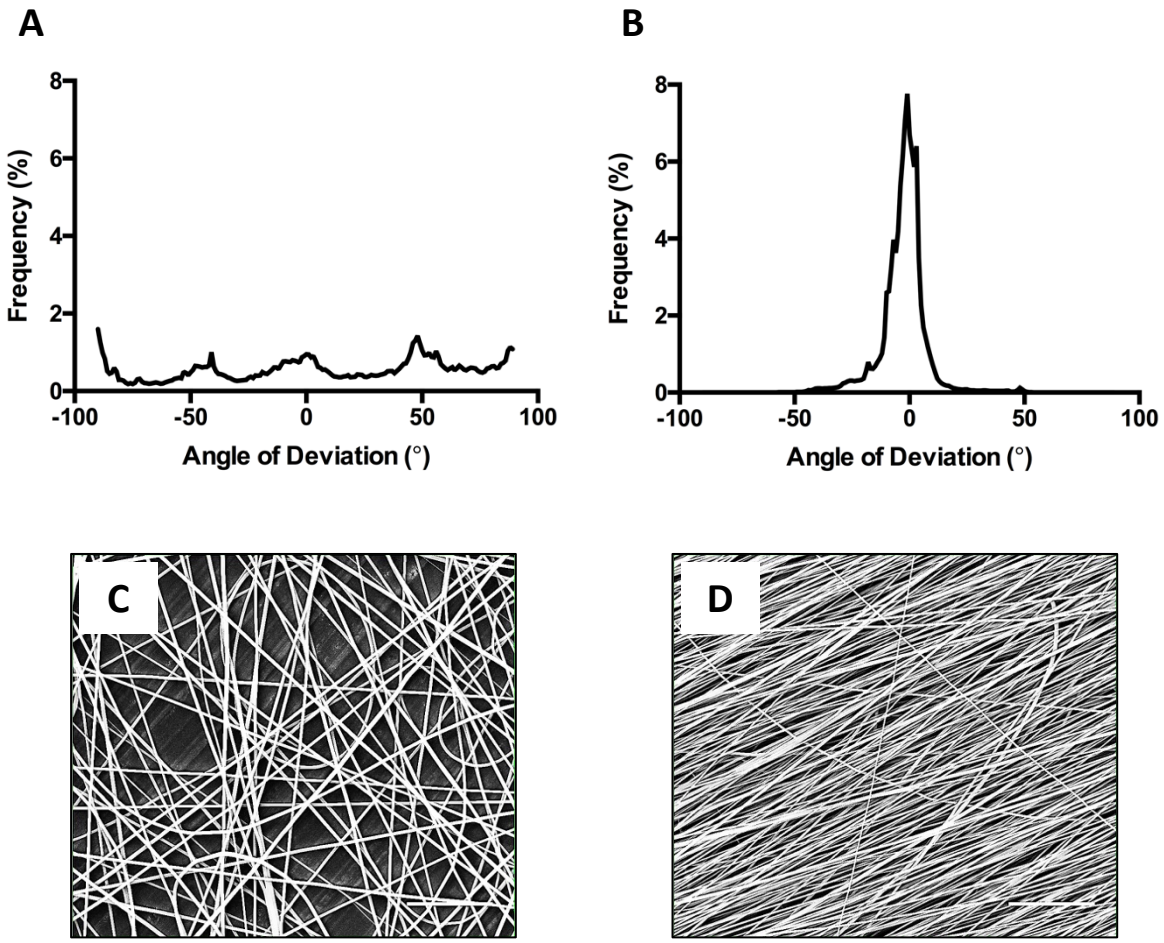

Figure 4.3 - PLGA[11] fibre alignment using high speed rotation. An 11% (w/v) solution of PLGA in 1,1,1,3,3,3-Hexafluoro-2-propanol (HFIP) was electrospun through a blunted 22 ½ G needle at 8 kV, with a flow rate of 2 mL hour^{-1}, at a collector distance of 100 mm, onto a 100 mm diameter rotating mandrel at **(A)** 50 x g and **(B)** 500 x g. Fibre diameters were quantified using the DiameterJ plugin for Fiji (ImageJ) software. Fibre orientation angles were calculated from SEM images using the OrientationJ plugin for ImageJ using 100 fibres per image. Data represent the average results taken from ≥ 12 random microscopic fields per experiment. ≥100 fibres were counted per experiment. Data n=3. Scale bars represent 50 µm.

4.2.2 Highly aligned fibres can be produced using dual collectors and an air gap

After aligned fibrous scaffolds had been created for further *in vitro* work, it was important to create a seamless tube with axially aligned tubes, resulting in the need for a newly developed collector. Previous work has shown that an airgap between two grounded collector electrodes can produce aligned fibres (Dan Li *et al.*, 2003; Secasanu, Giardina and Wang, 2009; Sahay, Thavasi and Ramakrishna, 2011). A previous study used cylindrically pointed collectors and suggested the angle of the point dictated the resulting tube diameter (Jana *et al.*, 2012), which was used to help design the collector used in this experiment (Figure 4.4). Similar observations could be made about electrospun fibres initially forming a curved morphology between the two-pointed collectors, then subsequently compress into a more linear shape (Figure 4.4A and B). SEM images displayed aligned fibres; however, the diameter of the resulting tube was so small that there was no visual lumen (Figure 4.4C).

The relationship between the collector point angle and resulting tube diameter has not been properly defined in the literature making it difficult to adapt this type of collector for the desired 5 mm internal diameter required. Further to this, the static collectors suffered from the force of the incoming electrospinning material causing the newly deposited fibres to be forced against the already formed tubular scaffold. This further depressed any visible lumen.

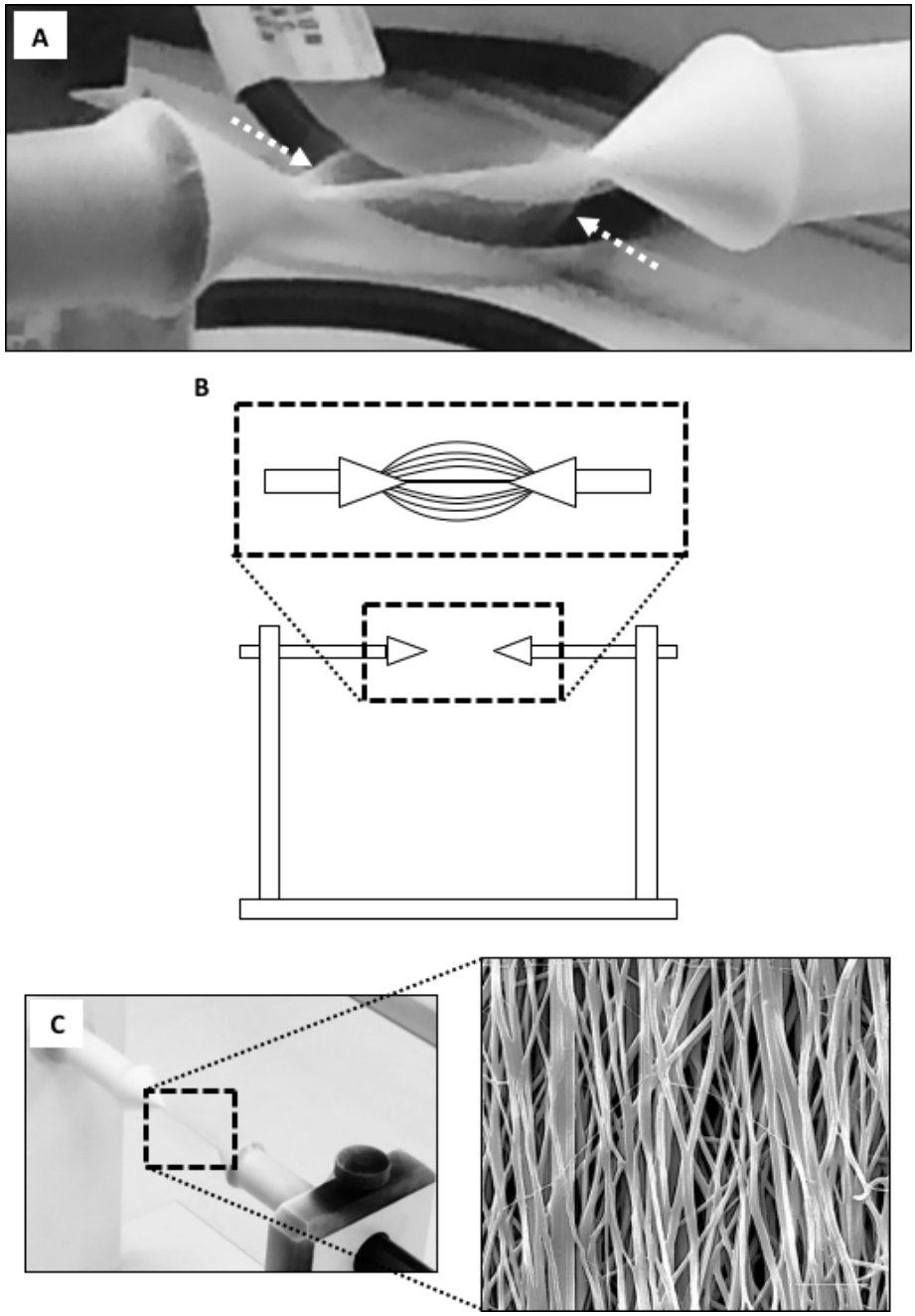

Figure 4.4 - PLGA25 NaOAc fibre alignment using a modified static collector. An 25% (w/v) solution of PLGA in 1,1,1,3,3,3-Hexafluoro-2-propanol (HFIP) containing 1% (w/v) NaOAc was electrospun through a blunted 22 ½ G needle at 20.5 kV, with a flow rate of 2 mL hour^{-1}, at a collector distance of 150 mm, onto a specifically constructed static collector (collector 1) containing an air gap between the grounded collector mandrel elements of 4 cm. **(A)** Electrospun fibres can be seen forming curves around the main fibre bundle (white arrows). **(B)** Diagrammatic representation of the collector and the observed deposition of fibres. **(C)** Representative SEM image of the resulting fibre bundle produced. Scale bar represents 10 μm.

4.2.3 Highly aligned fibrous tubes can be produced using a slowly rotating modified collector

To adapt upon the previously created collector containing an air gap to produce axially aligned fibres, a further collector was designed and produced based on designs used by Jose *et al.*, (2012) and Jana and Zhang, (2013) to produce a larger diameter tube, increasing the lumen to a more representative mammalian coronary arterial diameter. The opposing collector electrodes were stainless steel cylinders with an internal diameter of 5 mm, a wall thickness of 1 mm and a length of 5 mm (Figure 4.5A). The collector electrodes were also controlled via an electronic motor to enable synchronised rotation (Figure 5.5A). Each grounding electrode was connected to a separate cam plate that upon rotation would compress or release a grounding switch (Figure 4.5A). As one switch was compressed, the opposing switch would be released therefore grounding one collector electrode at a time (Figure 4.5A). This created a frequency between the collector electrodes causing them to alter between a grounded and ungrounded state.

A gap of 40 mm was chosen between the collector electrodes to allow enough surplus electrospun tubing to be present for there to be at least 20 mm of tubular scaffold after cutting and attachment to a bioreactor (Figure 4.5B). The needle-to-collector distance, needle height from the ground and voltage were then visually evaluated to ensure a stable Taylor cone was present indicating an attraction of the polymer/solvent solution to the collector.

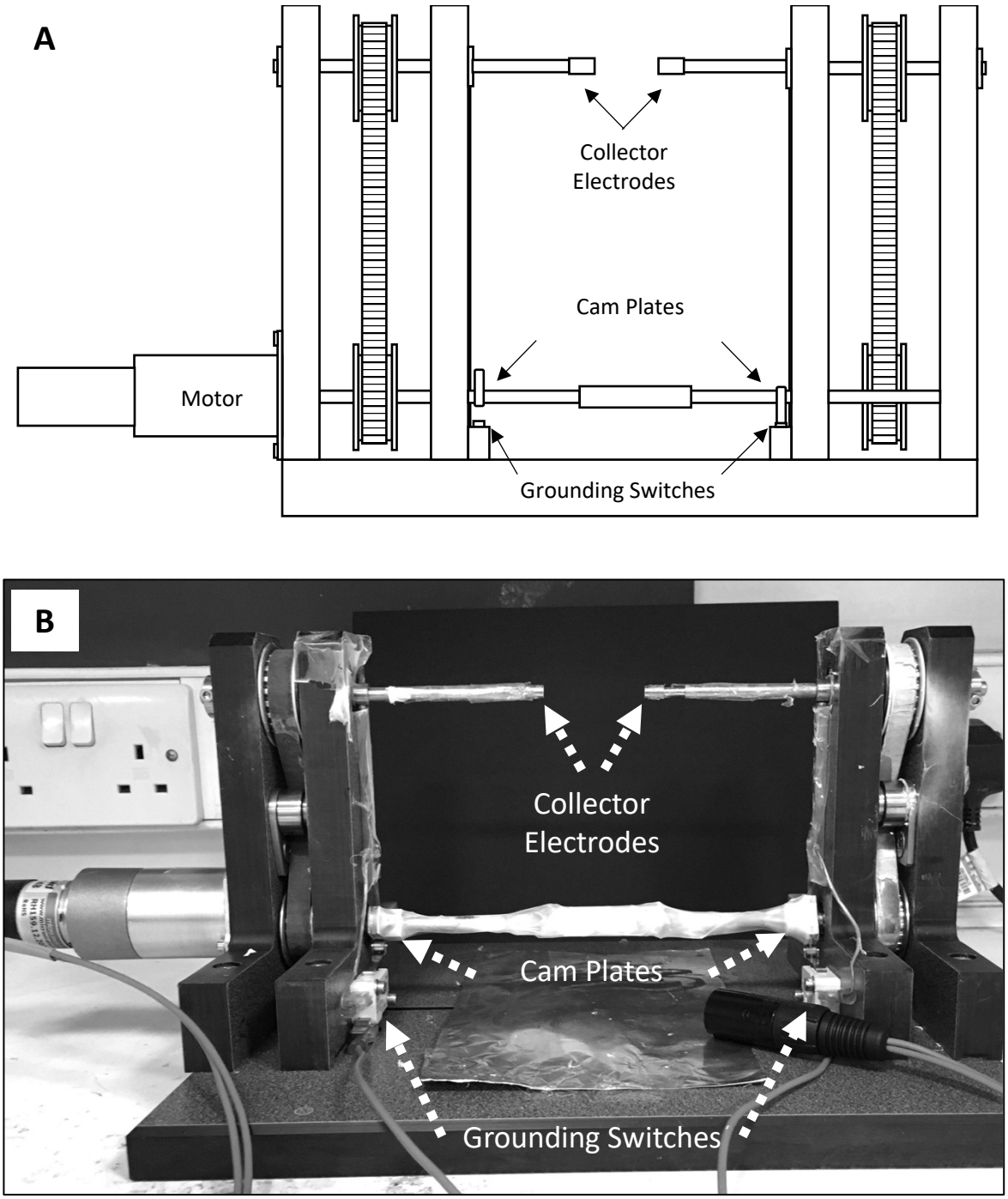

Figure 4.5 - Design and final fabrication of a rotating dual collector for aligned fibre production. A rotating collector containing two opposing collector mandrels with an adjustable air gap (white arrow) was designed and created. **(A)** Diagrammatic representation of the collector and **(B)** Representative image of the final collector (collector 2).

The electrospun material was found to deposit onto the two collector electrodes at the periphery, traversing the gap between them. Freshly deposited material was observed to initially form an ellipse around the central gap between the collector electrodes where the tube formed (Figure 4.6A). This effect was observed until the electrospinning process was stopped whereby the remaining material in the ellipse would contract onto the produced tubular scaffold (Figure 4.6B).

The resulting tubular structure was representative of a hyperbolic cylinder whereby the diameter decreased from the edges of the collector electrodes to the centre of the tube (Figure 4.6B). This occurred regardless of the air gap distance between the two collector electrodes. Under SEM observation, resulting tubular scaffolds did visually contain aligned fibres (Figure 4.6C). It was also observed that the force of incoming fibres would exert pressure onto the forming electrospun tube, which on one occasion occurred in the tube collapsing as the lumen adhered to itself whilst still wet.

Significant amounts of electrospun material were found deposited on all conductive surfaces of the collector. Although not reported, an increase in electrospinning time did not appear to proportionally increase the resulting tubular wall thickness. Furthermore, in results not presented in this thesis, the alternating grounding of the individual collector electrodes was found to have no effect upon the resulting tube fabrication. Alternating current was used by Jose *et al.*, (2012) to provide a frequency of grounding between the collector mandrels. This was suggested to attract the incoming end of electrospun fibres to the grounded collector mandrel, then as the grounded collector mandrel swapped, this would draw the opposing end of the fibre to the opposing mandrel collector. However, in this electrospinning set up and collector, no effect was observed by the alternating of a grounded collector mandrel. This was not tested further due to time constraints, but may have had a modest effect on fibre alignment. However, to reduce any variability that this could have introduced from frequency changes caused by changes in the electrode rotation speed, both collector electrodes were connected using copper wire to ensure both were grounded at all time during the electrospinning process.

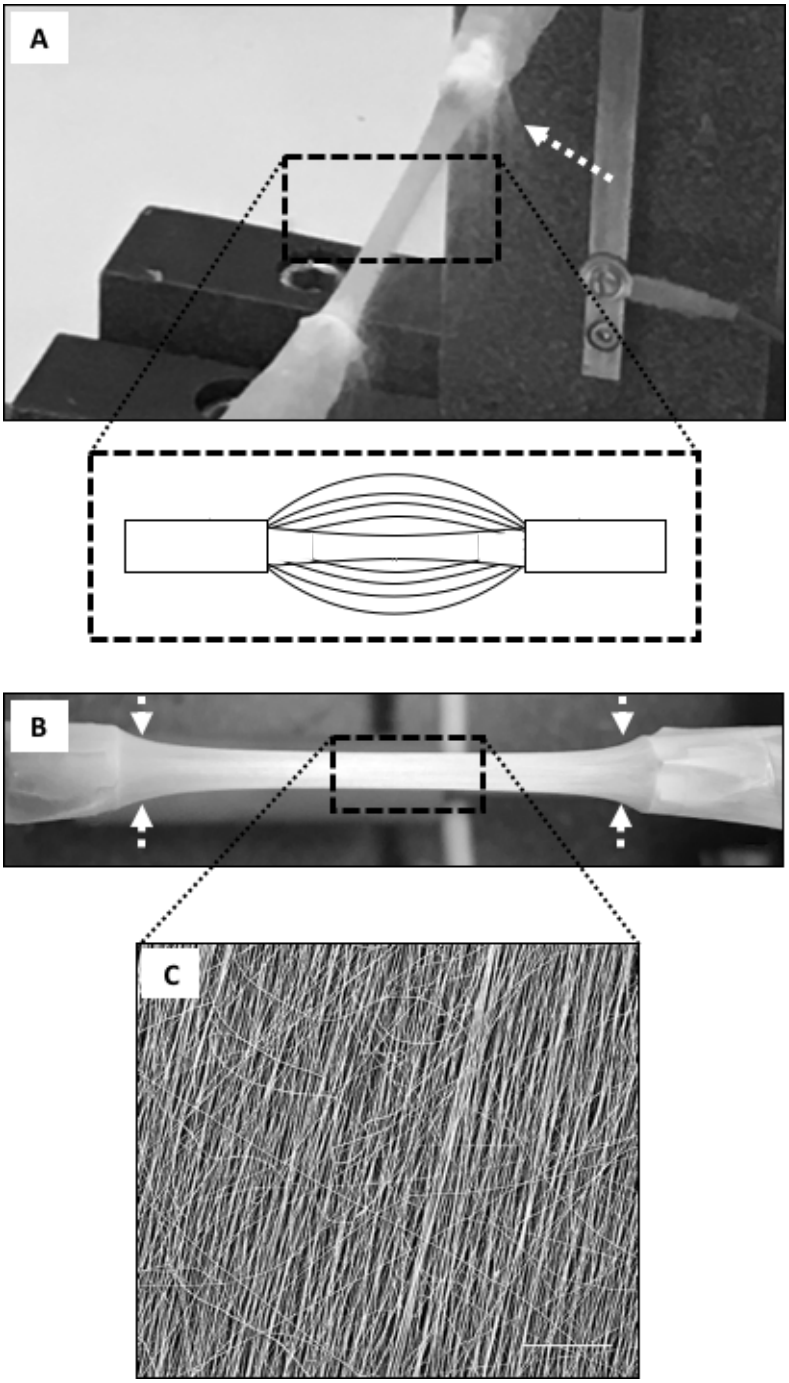

Figure 4.6 - PLGA25 NaOAc fibre alignment using a fabricated rotating dual collector. A 25% (w/v) solution of PLGA in 1,1,1,3,3,3-Hexafluoro-2-propanol (HFIP) containing 1% (w/v) NaOAc was electrospun through a blunted 22 ½ G needle at 20.5 kV, with a flow rate of 2 mL hour^{-1}, at a collector distance of 150 mm, onto rotating dual collector mandrels between an air gap of 4 cm. **(A)** Representative image of an electrospun tube using the rotating dual collector and a fibre curving phenomenon of newly depositing fibres (white arrows). **(B)** Representative image of an electrospun tube with a narrowing central diameter (white arrows). **(C)** Representative SEM image of electrospun tube fibres. Scale bars represent 200 µm.

4.2.4 Elimination of collector air gap maintains uniform luminal diameter

Although an air gap was shown to enable fibres to connect between the two collector electrodes whilst maintaining an unobstructed lumen, the previous experimental work (4.2.3) produced tubes with suboptimal diameters due to a hyperbolic effect causing a gradual decrease in lumen diameter to the centre of the tube. It was hypothesised that filling the air gap between the two collector electrodes could prevent structural contraction of the tubular scaffolds as they formed, to maintain a consistent 5 mm diameter. This was also hypothesised to prevent any adverse effects to the tubular structure associated with the force produced by the oncoming electrospinning jet.

In order to minimise the risk of fibres adhering to the material used to fill the air gap between the collector electrodes, PTFE was chosen due to its adherent-resistant and non-conductive properties. A PTFE rod was loosely placed between the two collector electrodes so that it did not rotate with the collector mandrels during the electrospinning process (Figure 4.7A). It was found that the PTFE rod did physically prevent the restriction of the tube lumen as it formed. The resulting tubes were also easily separated from the PTFE rod with no adherence between the two on any of the produced scaffolds. Upon SEM examination of the fabricated tubes, the fibres were visibly random in orientation (Figure 4.7B).

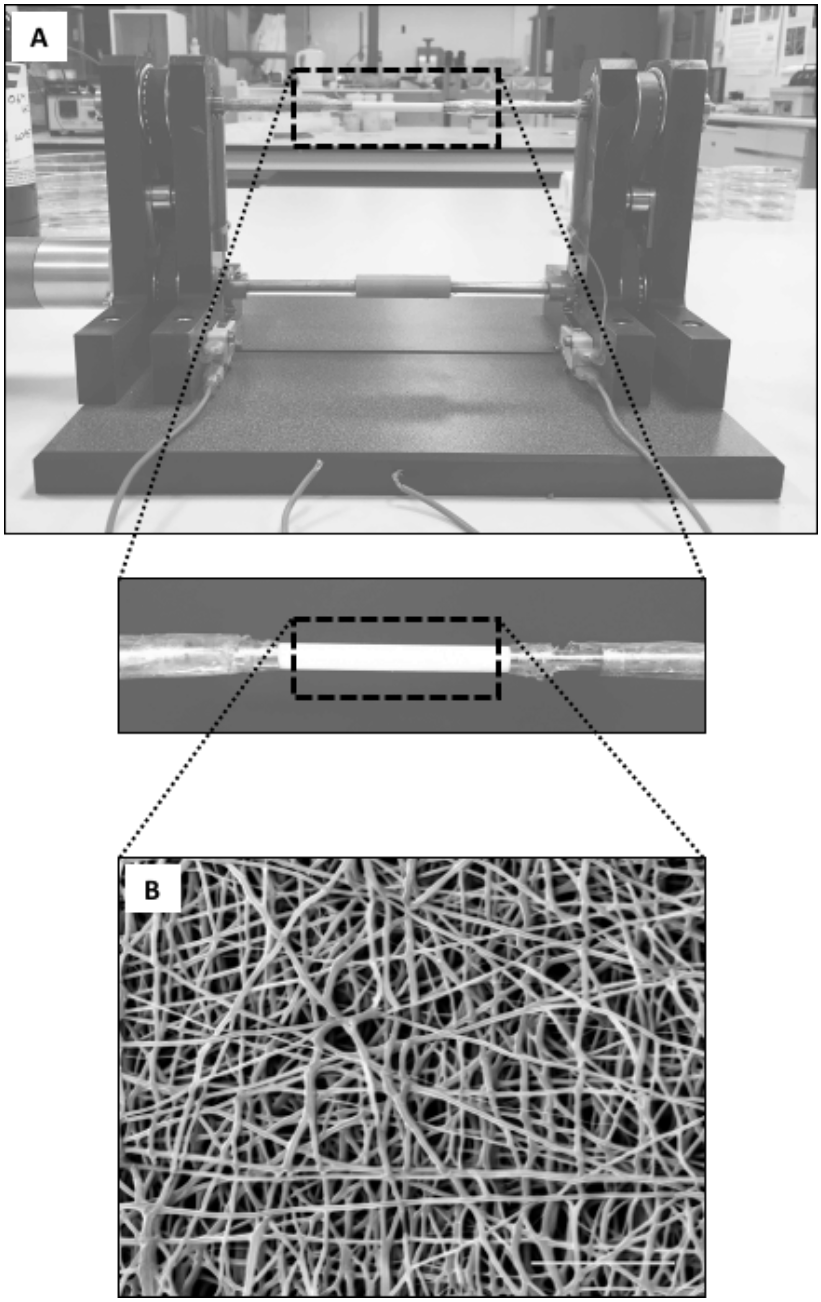

Figure 4.7 - PLGA$^{25\ NaOAc}$ fibre deposition using a fabricated rotating dual collector with a static PTFE rod. A 25% (w/v) solution of PLGA in 1,1,1,3,3,3-Hexafluoro-2-propanol (HFIP) containing 1% (w/v) NaOAc was electrospun through a blunted 22 ½ G needle at 20.5 kV, with a flow rate of 2 mL hour^{-1}, at a collector distance of 150 mm, onto a rotating dual collector with a 4 cm gap containing **(A)** a PTFE rod that did not rotate with the collector. Image of an electrospun tube using the rotating dual mandrel collector. **(B)** Representative SEM image of electrospun tube fibres. Scale bar represents 20 μm.

As there was significantly visible off-target accumulation of electrospun material across the collector, which may have disrupted fibre deposition, it was hypothesised that further optimisation of the electrospinning set up would enable uniform longitudinally aligned fibre tubes to be produced using the PTFE rod. A syringe kwill was used to extend the electrospinning needle away from the syringe pump to reduce the risk of interference from conductive materials. The kwill was also fitted to allow the direction and height of the needle to be more easily manipulated so it could be aligned more closely in the direction of the two collector electrodes (Figure 4.8A and B). Furthermore, an aluminium foil sheet was created (100 mm by 100 mm) and place over the needle to reduce the risk of electrospinning material travelling backwards (Figure 4.8A and B). Thin plastic adhesive tape was used to insulate areas of exposed metal on the collector unless it would affect mechanical movements; 2 mm of metal on the end of each collector electrode was left exposed to enable fibre attraction. Finally, the PTFE rod was also fixed into place via pressure exerted onto each end by the respective collector electrode. This enabled the PTFE rod to rotate in unison with the collector electrodes due to friction.

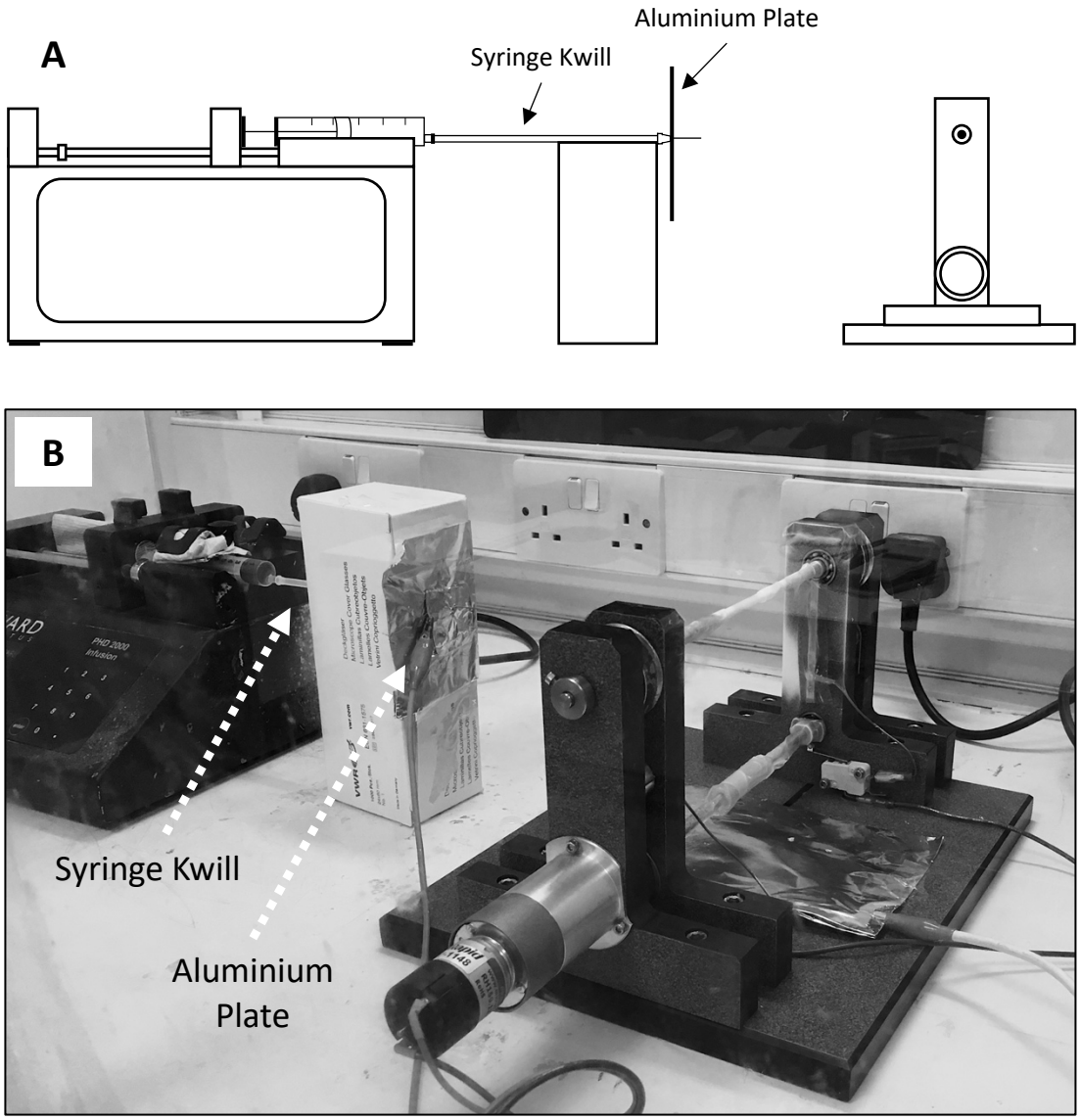

Figure 4.8 - Optimisation of the electrospinning set up for the rotating dual collector. A 25% (w/v) solution of PLGA in 1,1,1,3,3,3-Hexafluoro-2-propanol (HFIP) containing 1% (w/v) NaOAc was electrospun through a 100 mm kwill containing a blunted 22 ½ G needle with a voltage of 20.5 kV, a flow rate of 2 mL hour^{-1}, at a collector distance of 150 mm, onto a rotating dual collector with a 4 cm gap containing a PTFE rod rotated in unison with the collector mandrels. **(A)** Diagrammatic representation of the optimised electrospinning set up for highly aligned fibre tubes. **(B)** Representative image of optimised electrospinning set up for highly aligned fibre tubes.

After the optimisation steps, the resulting electrospinning material on the collector was visibly reduce, although this was not quantified. Importantly, material was deposited more quickly between the collector electrodes. The change in PTFE rod movement did not affect the advantageous ability to easily remove the resulting electrospun tubes. Additionally, no other previously identified observations were affected as a result of the optimisation steps.

Under SEM observations, the resulting electrospun tubes had visibly aligned fibres (Figure 4.9D). Electrospun material was found to deposit heavily on both exposed arms of the collector electrodes (Figure 4.9B) and a thinner layer would form over the insulated areas closely surrounding the electrospun tube (Figure 4.9A). The disproportionally high accumulation of electrospun material at each end of the tube enabled the tube to be cut away from the collector electrodes with ease and helped to prevent structural damage to the thin tubes (Figure 4.9B). They also provided structural support for removal of the tube from the PTFE rod (Figure 4.9C).

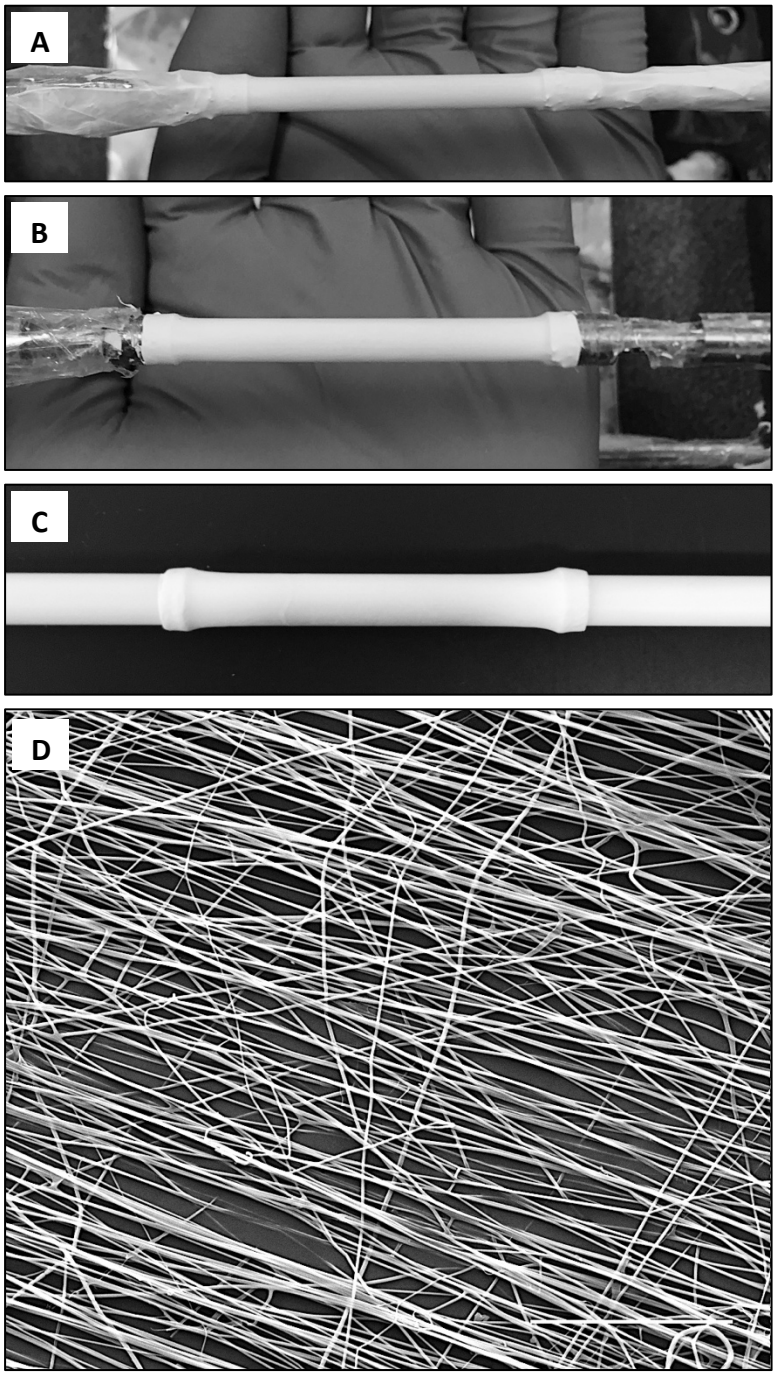

Figure 4.9 - PLGA$^{25\ NaOAc}$ fibre deposition using a fabricated rotating dual collector with an dependently rotating PTFE rod. A 25% (w/v) solution of PLGA in 1,1,1,3,3,3-Hexafluoro-2-propanol (HFIP) was electrospun through a 100 mm kwill containing a blunted 22 ½ G needle with a voltage of 20.5 kV, a flow rate of 2 mL hour^{-1}, at a collector distance of 150 mm, onto a rotating dual collector with a 4 cm gap containing a PTFE rod that rotated in unison with the collector mandrels. **(A)** Representative image of fibre deposition on the collectors. **(B)** Representative image of electrospun tube once excess fibrous material is removed. **(C)** Representative image of removed electrospun tube on a PTFE rod. **(D)** Representative SEM image of electrospun tube fibres. Scale bar represents 50 μm.

To quantify the resulting fibre alignment of the tubes, SEM imaged fibres were compared against a predetermined orientation labelled as 0°. Fibres were assessed for their deviation from 0° and the relative frequency distribution of fibre angles in relation to 0° were graphically presented (Figure 4.10A). The optimised electrospinning was used to operate the dual electrode collector at two rotational speeds, 0.00007 and 0.00028 x g, to determine if this had an effect on fibre alignment. Both RCF values produced highly aligned fibres (Figure 4.10). There was no statistical difference between the relative frequency of alignment between the two speeds (Figure 4.10A).

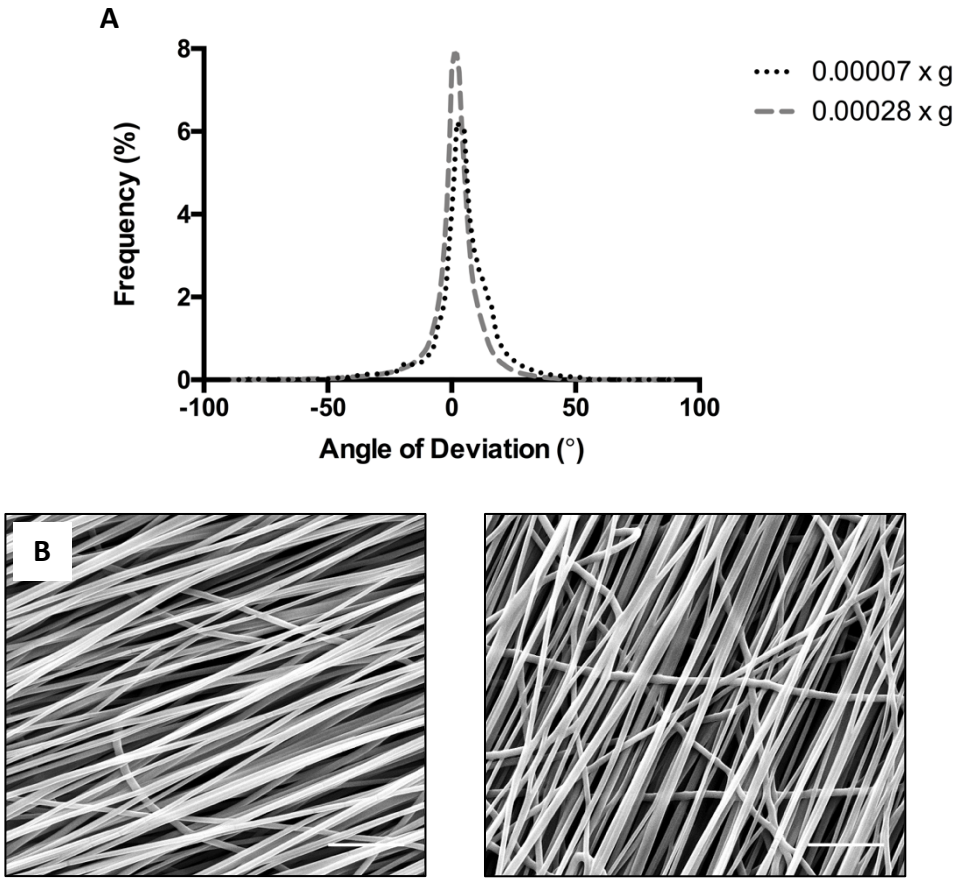

Figure 4.10 - The effect of relative centrifugal force on fibre orientation angle for electrospun PLGA$^{25\ NaOAc}$ A 25% (w/v) solution of PLGA in 1,1,1,3,3,3-Hexafluoro-2-propanol (HFIP) containing 1% (w/v) NaOAc was electrospun through a 100 mm kwill containing a blunted 22 ½ G needle with a voltage of 20.5 kV, a flow rate of 2 mL hour^{-1}, at a collector distance of 150 mm, onto a rotating dual collector (collector 2) with a 4 cm gap containing a PTFE rod that rotated in unison with the collector mandrels at a rotational speed of **(A, B)** 0.00007 x g and **(A, C)** 0.00028 x g. Fibre orientation angles were calculated from SEM images using the OrientationJ plugin for ImageJ using 100 fibres per image. n=3. Scale bars represent 10 μm.

4.2.6 Secondary charged aluminium plates can affect fibre deposition

To create the secondary layer of the theorised tri-layered tube, PCL was used for its increased strength, degradation time and elasticity. A rotating collector using a 5 mm stainless steel bar was used and spun at a high rpm matching the speed of the rotating collector used in 4.2.1, as it was hypothesised that the PCL fibres would align similarly to the PLGA fibres in 4.2.1.

After optimisation of the electrospinning set up and polymer solvent solution, it was found that the use of a syringe kwill and aluminium sheet was also advantageous to reduce non-specific material deposition (data not shown; Figure 4.11A). Electrospun PCL collected on a 5 mm rotating mandrel at 6000 rpm did not produce visually aligned fibres detectable under SEM (Figure 4.11B).

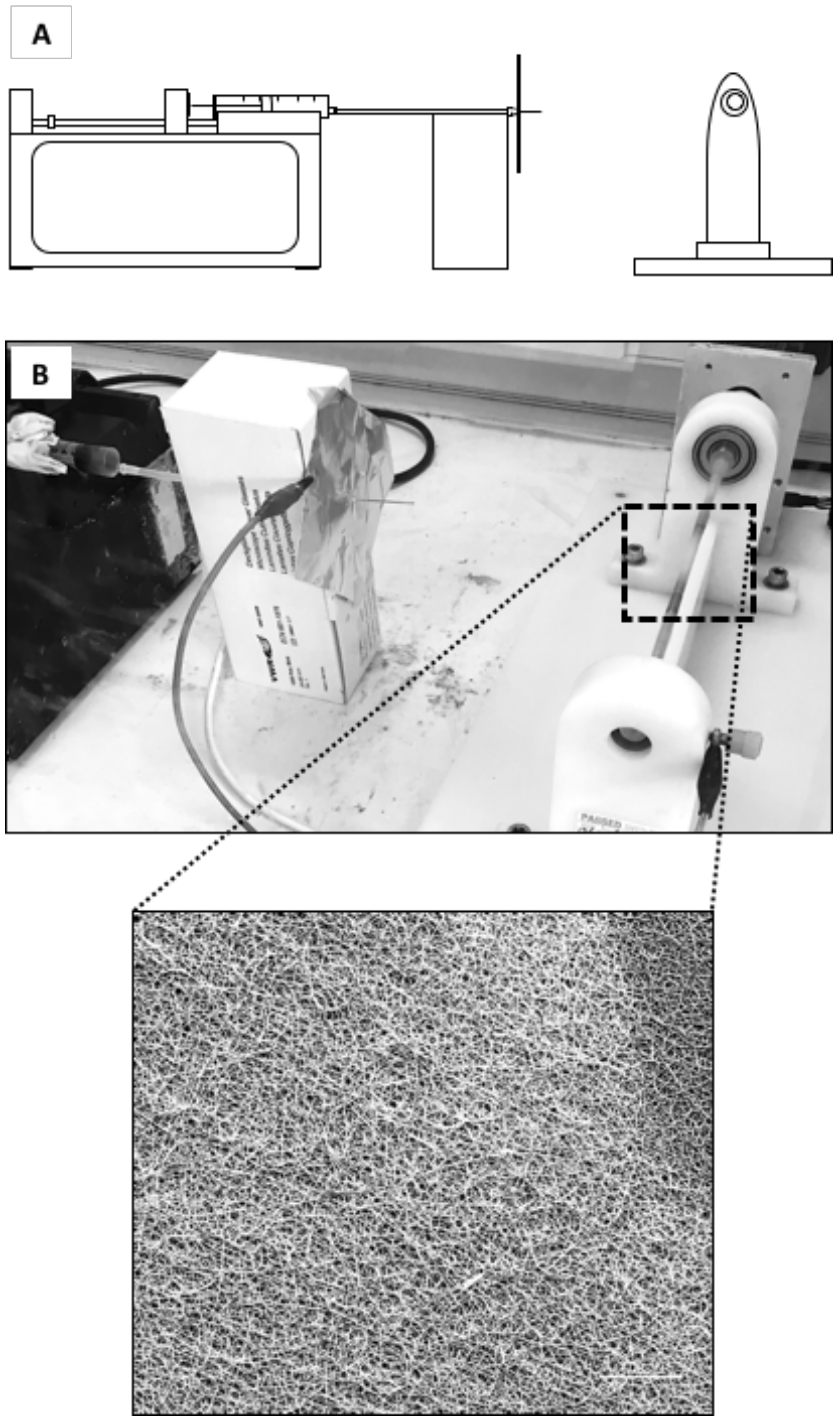

Figure 4.11 - Testing of a high-speed electrospinning set up for aligned PCL fibrous tubes. An 11% (w/v) solution of PCL in 1,1,1,3,3,3-Hexafluoro-2-propanol (HFIP) was electrospun through a 100 mm kwill containing a blunted 22 ½ G needle with a voltage of 10.5 kV, a flow rate of 2 mL hour^{-1}, at a collector distance of 200 mm, onto a 5 mm diameter rotating stainless steel at 100 x g **(A)** Diagrammatic representation of the optimised electrospinning set up for highly aligned fibre tubes. **(B)** Representative **i**mage of optimised electrospinning set up for PCL fibre tubes and an SEM image of the resulting fibres. n=3. Scale bar represents 200 μm.

As the use of high rotation was not able to align the PCL fibres, further adaptations to the electrospinning set up were introduced to encourage fibre alignment. Aluminium plates (15 mm by 150 mm) were added above and below the rotating mandrel and a voltage of 2.5kV was applied (Figure 4.12A and B). Under SEM assessment, the fibres were visually aligned; however, the fibres had an undulating pattern in their distinctive direction (Figure 4.12B).

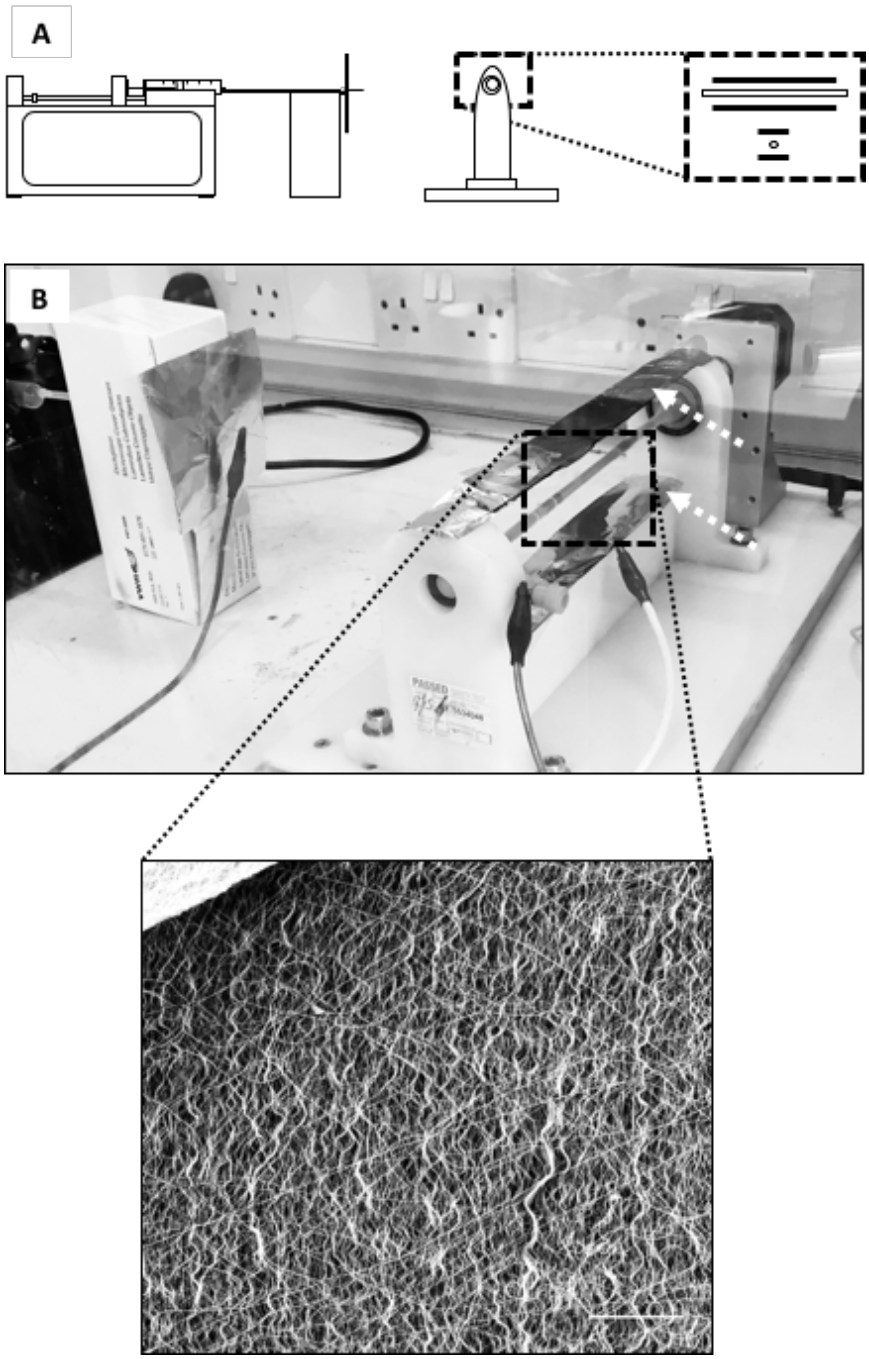

Figure 4.12 - The effect of charged parallel plates on PCL tube fibre alignment. An 11% (w/v) solution of PCL in 1,1,1,3,3,3-Hexafluoro-2-propanol (HFIP) was electrospun through a 100 mm kwill containing a blunted 22 ½ G needle with a voltage of 10.5 kV, a flow rate of 2 mL hour^{-1}, at a collector distance of 200 mm, onto a 5 mm diameter rotating stainless steel at 100 x g. A voltage of 2.5 kV was applied to charged plates (white arrows) were placed above and below the collector. **(A)** Diagrammatic representation of the optimised electrospinning set up for highly aligned fibre tubes**. (B)** Representative image of optimised electrospinning set up for PCL fibre tubes and an SEM image of the resulting fibres. n=3. Scale bar represents 200 μm.

To further assess how the addition of secondary charged aluminium plates affected fibre alignment, a 180 mm by 60 mm plate was used charged at a voltage of 2.5 kV between the needle and the collector (Figure 4.13A). It was hypothesised that this would delay the point at which the incoming electrospun jet would destabilise. The resulting fibres did not visually align when observed under SEM in comparison to the fibres generated in section 4.2.1 (Figure 4.13B). Further aluminium sheet sizes and voltages were tested, but none of the combinations improved fibre alignment (data not shown). Increased voltages prevented the formation of the electrospinning jet (data not shown). Changes to the size of the aluminium sheet had no striking visual effects on the fibre orientation and therefore was not investigated any further (data not shown).

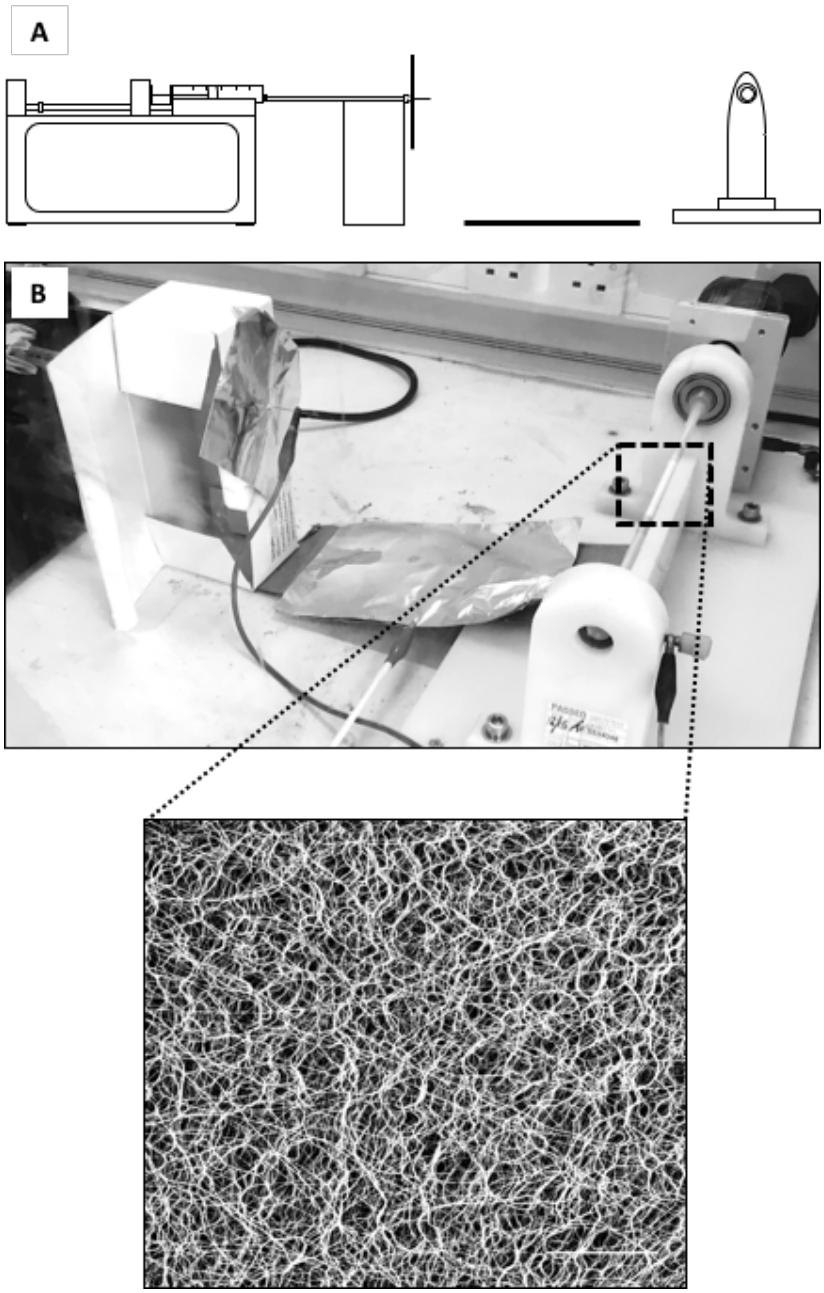

Figure 4.13 - The effect of a charged aluminium sheet on PCL tube fibre alignment. An 11% (w/v) solution of PCL in 1,1,1,3,3,3-Hexafluoro-2-propanol (HFIP) was electrospun through a 100 mm kwill containing a blunted 22 ½ G needle with a voltage of 10.5 kV, a flow rate of 2 mL hour^{-1}, at a collector distance of 200 mm, onto a 5 mm diameter rotating stainless steel at 100 x g. A voltage of 2.5 kV was applied to a 120 mm x 90 mm charged aluminium sheet placed between the needle and collector. **(A)** Diagrammatic representation of the optimised electrospinning set up for highly aligned fibre tubes. **(B)** Representative **i**mage of optimised electrospinning set up for PCL fibre tubes and an SEM image of the resulting fibres. n=3. Scale bar represents 200 µm.

Separately, an aluminium sheet (15 mm by 150 mm) was placed under the rotation mandrel and shaped into a vertical curve (Figure 4.14A and B). This curved plate was charged at 2.5 kV and the electrospinning parameters were kept the same. The resulting fibres displayed some visual alignment but a large proportion of fibres were still visibly overlapping in comparison to previously generated aligned fibres (Section 4.2.1).

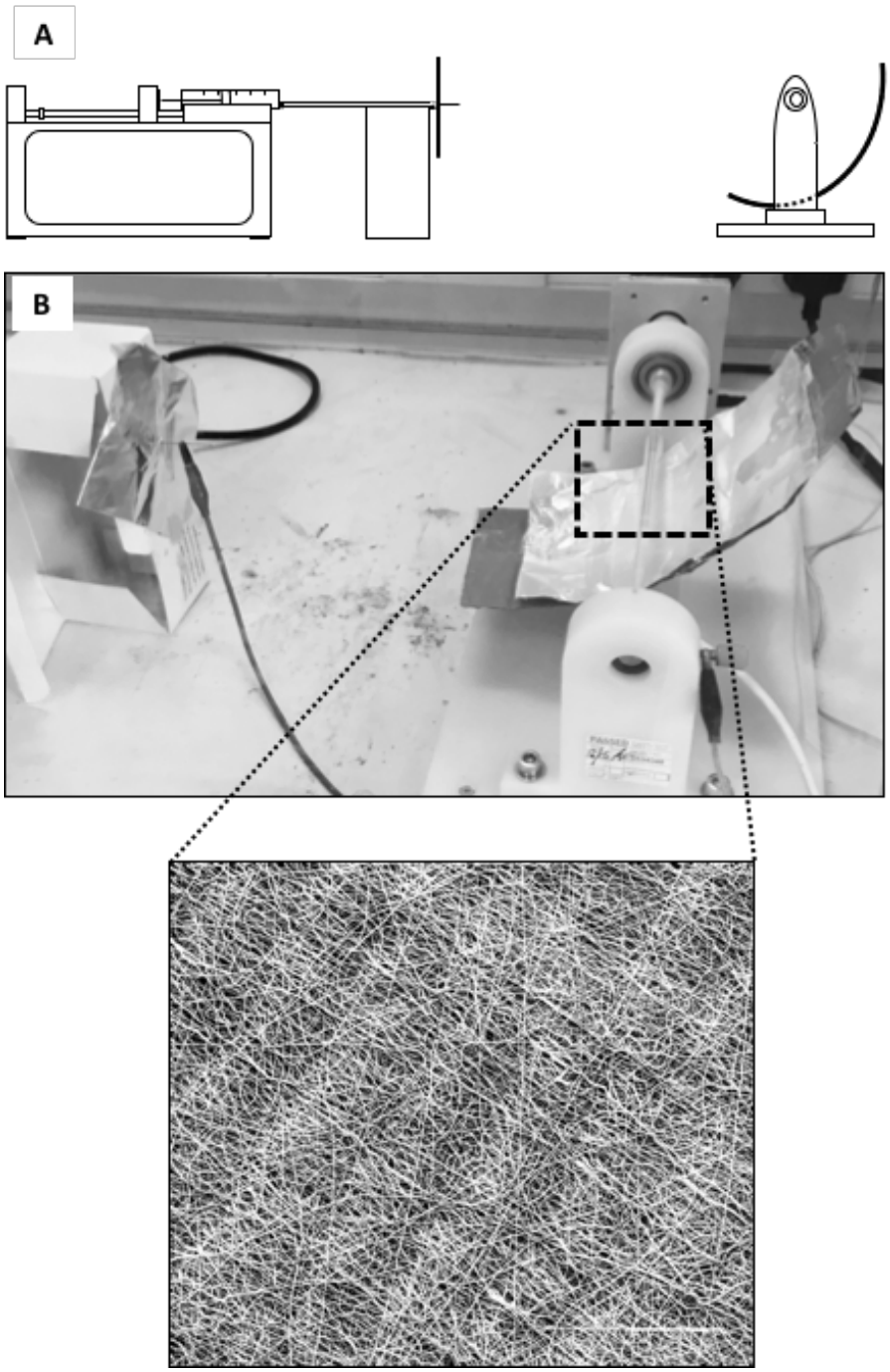

Figure 4.14 - The effect of a curved charged aluminium sheet on PCL tube fibre alignment. An 11% (w/v) solution of PCL in 1,1,1,3,3,3-Hexafluoro-2-propanol (HFIP) was electrospun through a 100 mm kwill containing a blunted 22 ½ G needle with a voltage of 10.5 kV, a flow rate of 2 mL hour^{-1}, at a collector distance of 200 mm, onto a 5 mm diameter rotating stainless steel at 100 x g. A voltage of 2.5 kV was applied to a curved 120 mm x 90 mm charged aluminium sheet placed underneath the collector. **(A)** Diagrammatic representation of the optimised electrospinning set up for highly aligned fibre tubes. **(B)** Representative **i**mage of optimised electrospinning set up for PCL fibre tubes and an SEM image of the resulting fibres. n=3. Scale bar represents 200 µm.

4.2.7 High RCF and not high RPM determines fibre orientation in PCL[11]

As the additional changes to the electrospinning set up were unable to help produce highly aligned fibres comparable to section 4.2.1, it was proposed that RCF (G-force) and linear velocity determined fibre alignment as opposed to RPM. RCF considers the diameter of the rotating object meaning that the smaller 5 mm diameter collecting mandrel would require much higher RPM to achieve a similar RCF to the previously tested mandrel used in section 4.2.1. To assess this a new device had to be fabricated to achieve an RPM of over 25,000 (RCF = 1.12 x Radius x $(RPM/1000)^2$). A drill motor was used, which could achieve a laser calculated RPM of 30,000. This was built into a custom machine, which was designed myself to minimise the exposure of conductive surfaces and to allow smooth rotation of the mandrel without significant vibrations or friction (Figure 4.15A). The machine was tested and operated at maximum speed (30,000 RPM) to account for a slight inconsistency in the measured RPM over time. The machine was run for 4 hours to test its durability and consistency to maintain its RPM. The RPM was measured every 10 minutes to check for consistency. The RPM was not observed to fall or increase by more than 10% meaning that an RPM above the required 25,000 was maintained. The RPM was measured at the beginning of each experiment using the collector to ensure a stable starting RPM of 30,000 was achieved.

To determine if RCF adjusted RPM would align fibres, PCL was electrospun onto the collector 3 mandrel. Fibres were observed to visibly align using the collector (data not shown) under the SEM; however, no direct processing or calculations were made using the SEM images, as the proof of concept had been achieved. To determine if fibres would consistently align under the set conditions, further specific experiments were conducted.

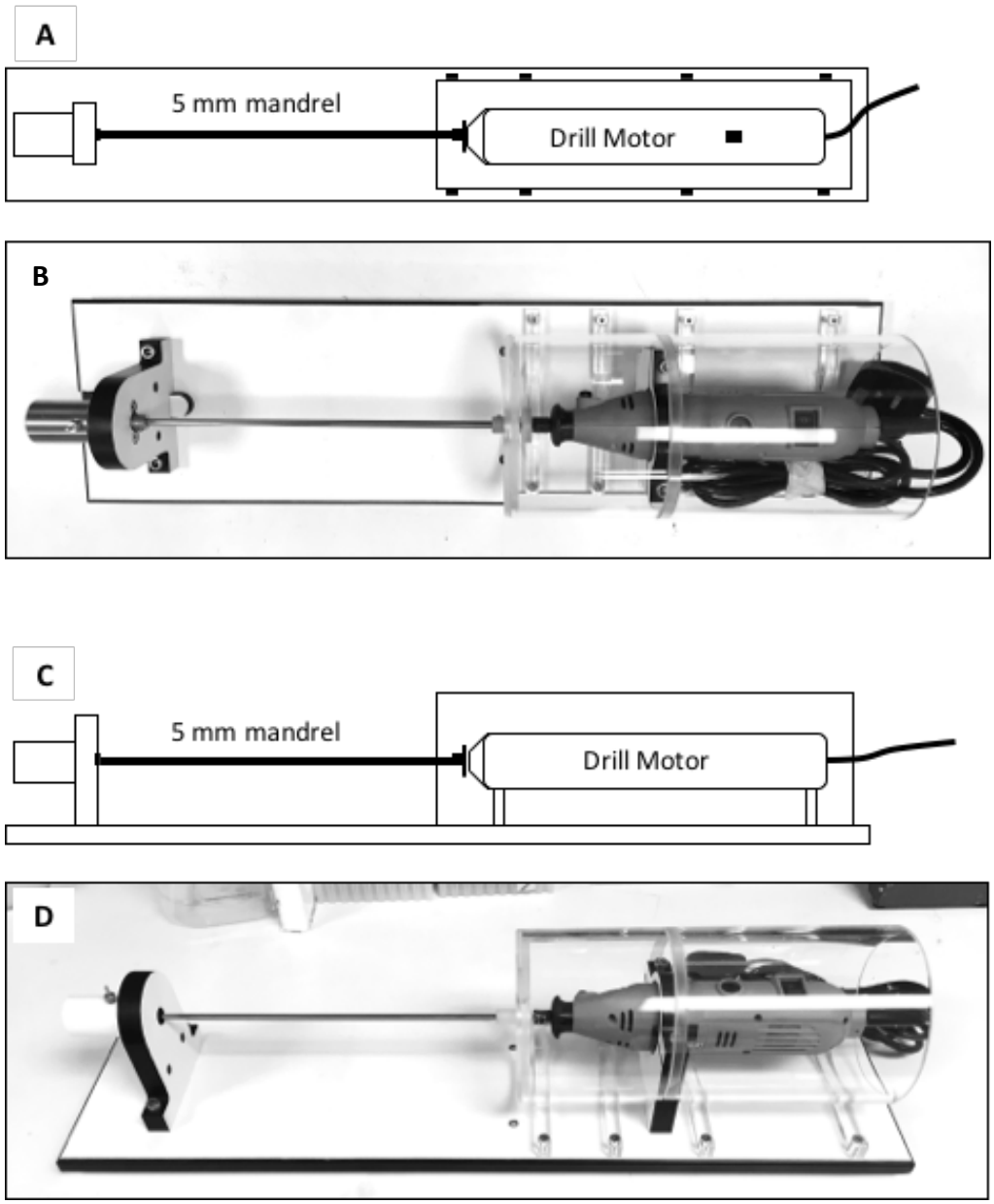

Figure 4.15 - Fabrication of an ultra-high-speed small diameter rotating collector. An ultra-high-speed rotating collector containing a 5 mm diameter removal mandrel was designed and created**. (A, C)** show a diagrammatic representation of the collector and **(B, D)** show images of the final device.

4.2.8 Needle-to-collector distance has no effect on fibre alignment and diameter

After being unable to attain highly aligned fibres using RPM ranges previously ascribed to align fibres on collectors with large diameters, even with the addition of charged plates; high speed rotation was still hypothesised to enable fibre alignment. The previously calculated rpm required of 25,000 for the 5 mm mandrel was achieved by designing and creating an additional collector (collector 3) that used a high-speed motor outlined in Figure 4.15. This motor could achieve speeds of up to 30,000 rpm, which was an equivalent G-force to lower RPM values for larger diameter mandrels shown to align fibres in the published literature (J. I. Kim *et al.*, 2016; Yu *et al.*, 2017). Using standard parameters outlined in Table 2.10 PCL electrospun fibres were produced that were highly aligned (Figure 4.16)

Fibre diameter has been shown to be affected by the needle-to-collector distance (Hekmati *et al.*, 2013). It was hypothesised that the needle-to-collector may have an effect on fibre alignment. Therefore, to confirm that fibres were reproducibly aligned using this new collector, and to assess the effect of changes to the needle-to-collector distance on fibre alignment and diameter, PCL was spun onto the collector mandrel at a distance of 150 mm and 200 mm. Fibre alignment was not significantly affected between a needle-to-collector distance of 150 mm and 200 mm (Figure 4.16). Fibres were highly aligned but displayed a similar undulating pattern observed in section 4.16 (Figure 4.16B and C). To determine if distance affected fibre diameter, the resulting aligned fibres from the SEM images were analysed. Mean fibre diameter was 925 nm and there was no significant difference between a needle-to-collector distance of 150 mm compared to 200 mm (Figure 4.17).

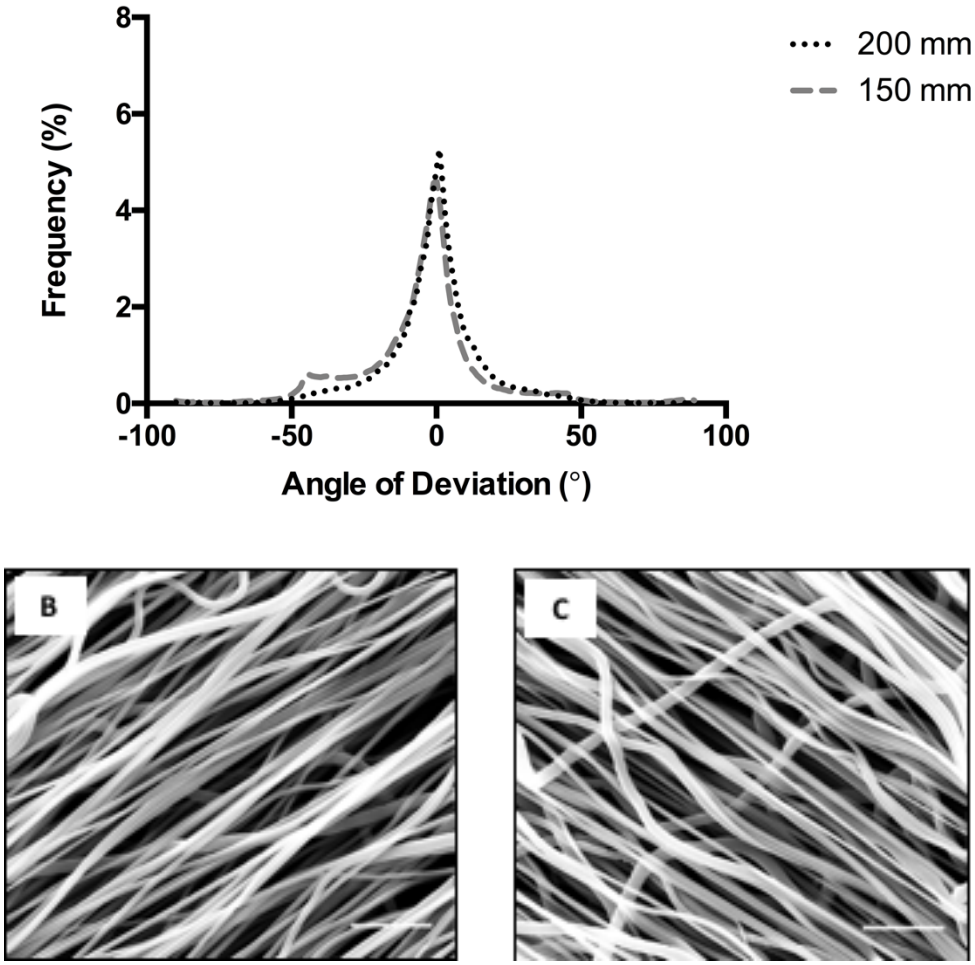

Figure 4.16 - The effect of needle-to-collector distance on PCL fibre alignment. An 11% (w/v) solution of PCL in 1,1,1,3,3,3-Hexafluoro-2-propanol (HFIP) was electrospun through a 100 mm kwill containing a blunted 22 ½ G needle with a voltage of 10.5 kV, a flow rate of 2 mL hour^{-1}, at a collector distance of **(A, B)** 150 mm or **(A, C)** 200 mm, onto a 5 mm diameter rotating stainless steel collector at 2000 x g. Fibre orientation angles were calculated from SEM images using the OrientationJ plugin for ImageJ from ≥ 100 fibres. . Data represent the average results taken from ≥ 12 random microscopic fields per experiment. ≥100 fibres were analysed per experiment. n=3. Scale bars represent 10 µm.

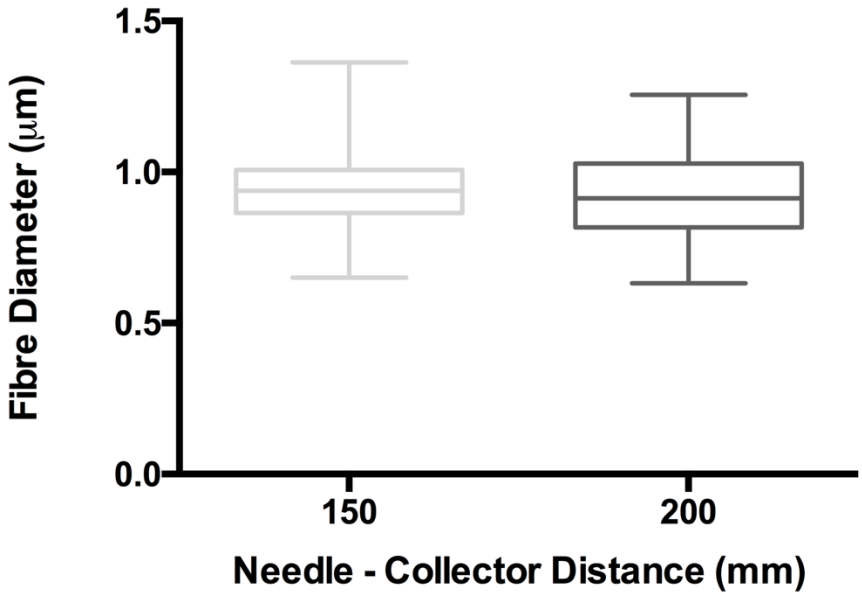

Figure 4.17 - The effect of the needle-to-collector distance on PCL fibre diameter. An 11% (w/v) solution of PCL in 1,1,1,3,3,3-Hexafluoro-2-propanol (HFIP) was electrospun through a 100 mm kwill containing a blunted 22 ½ G needle with a voltage of 10.5 kV, a flow rate of 2 mL hour^{-1}, at a collector distance of 250 mm and 200 mm onto a 5 mm diameter rotating collector at 2000 x g. Fibre diameters were quantified using the DiameterJ plugin for Fiji (ImageJ) software. Data represent the average results taken from ≥ 12 random microscopic fields per experiment. ≥100 fibres were counted per experiment. Data are mean ± SEM, n=3. Statistical analysis: unpaired t-test was used; ***P < 0.001.

4.2.9 Collector material and surface structure improves scaffold removal and affects resulting fibre diameter

It was found that the electrospun PCL fibres were strongly adhering to the collector mandrel preventing the removal of an undamaged circumferentially aligned fibre tube. The copper wire method from chapter 3.3.3 was not used as the minimum rotation speed for the drill motor was too high for a copper wire monolayer to be produced consistently. Therefore, it was hypothesised that if the mandrel were constructed of a conductive rod (stainless steel; SS) thinly coated with a material that had a low coefficient of friction (CoF) then this would reduce the ability of fibres to adhere to the mandrel, whilst still attracting fibre deposition. Additionally, it was hypothesised that a toothed rod may be even more effective due to a reduction in surface contact with any circumferentially aligned deposited fibres. Therefore, a 5 mm diameter SS rod was coated in approximately 20 μm Teflon (PTFE; Impreglon, Tamworth, UK). A 5 mm diameter carbon alloy (SAE 52100; Table 4.1) toothed rod (pinion wire; Wint Wire, Sheffield, UK) was also coated in 20 μm Teflon for comparison. The resulting rods were then machined down to 100 mm in length and the collector was adapted to accommodate a smaller length of mandrel to help reduce the risk of damage to electrospun tubes during removal.

The pinion wire and SS rod both produced aligned fibres under SEM observation (Figure 4.18B and C). The SS rod produced a significantly smaller mean fibre diameter compared to the pinion wire (Figure 4.18A). The uniformity between fibre diameter across each fibre deposited on both mandrel types was also relatively consistent (Figure 4.18A).

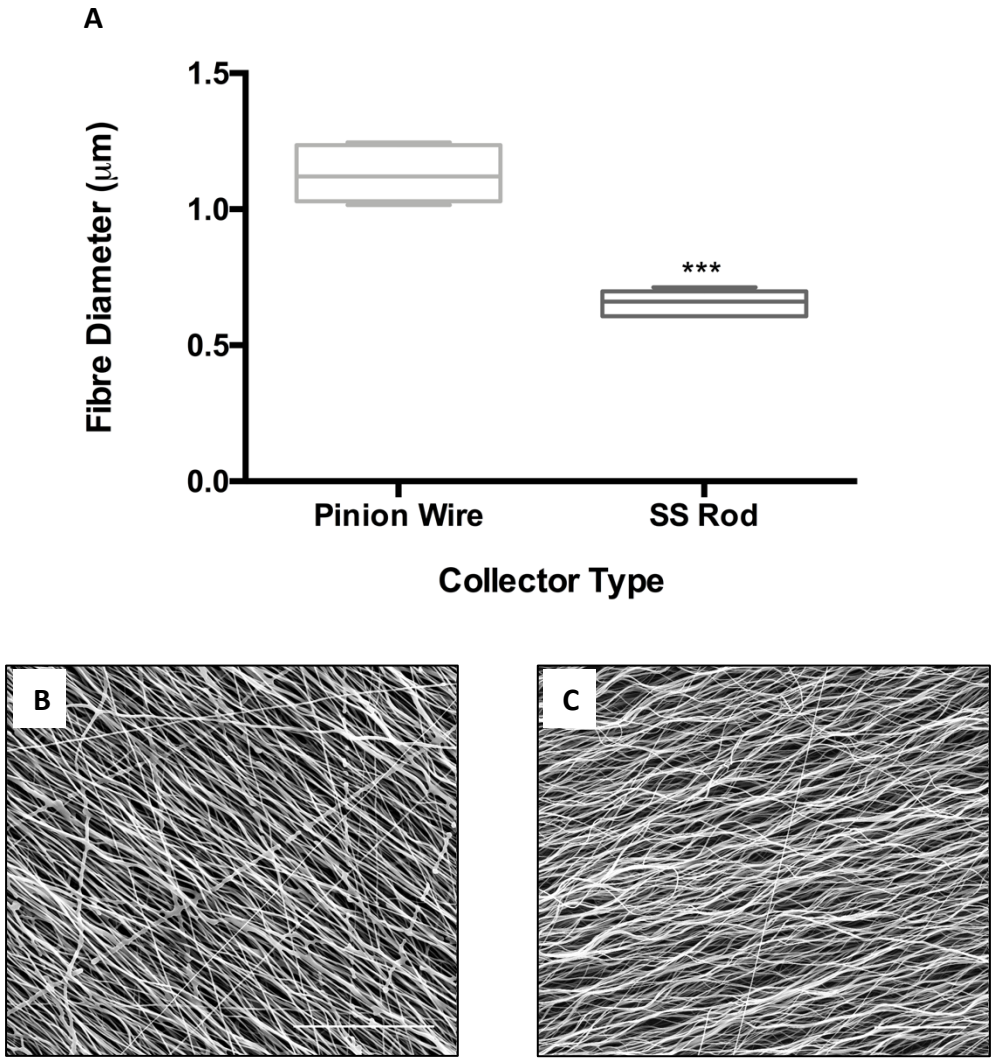

Figure 4.18 - The effect of PTFE-coated collector material type and surface structure on PCL fibre diameter. An 11% (w/v) solution of PCL in 1,1,1,3,3,3-Hexafluoro-2-propanol (HFIP) was electrospun through a 100 mm kwill containing a blunted 22 ½ G needle with a voltage of 10.5 kV, a flow rate of 2 mL hour^{-1}, at a collector distance of 200 mm onto a 5 mm diameter rotating **(A, B)** Teflon-coated pinion wire **(A, C)** Teflon-coated stainless steel (SS) rod. stainless steel collector at 2000 x g. Fibre diameters were quantified using the DiameterJ plugin for Fiji (ImageJ) software. Data represent the average results taken from ≥ 12 random microscopic fields per experiment. ≥100 fibres were counted per experiment. Data are mean ± SEM, n=3. Statistical analysis: unpaired t-test was used; ***P < 0.001. Scale bars represent 100 µm.

Table 4.1 - Pinion wire stainless steel alloy SAE 52100 composition.

Element	Content (%)
Iron, Fe	96.5 – 97.32
Chromium, Cr	1.30 – 1.60
Carbon, C	0.980 – 1.10
Manganese, Mn	0.250 – 0.450
Silicon, Si	0.150 – 0.300
Sulphur	≤ 0.0250
Phosphorous	≤ 0.0250

4.2.10 Optimisation of outer layer

PLGA was proposed for the final outer layer of the tri-layered tube due to its desirable degradation rate and biocompatibility. Pore size has been shown to increase with increased fibre diameter, which can enhance cellular infiltration and neovascularisation (Stephen J Eichhorn and Sampson, 2005; Wu and Hong, 2016). Two electrospinning solutions, a 13% (w/v) and 15% (w/v) solution of PLGA in HFIP, were electrospun onto the created collector, which was run at its lowest rotational speed (5 x g). The parameters were adjusted to create a stable jet and visible Taylor cone and the optimised final parameters are shown in Table 2.8.

The PLGA^{13} and PLGA^{15} solutions were successfully electrospun into tubular structures onto the pinion wire mandrel, producing mean fibre diameters of approximately 2.3 μm and 3.8 μm, respectively (Figure 4.19).

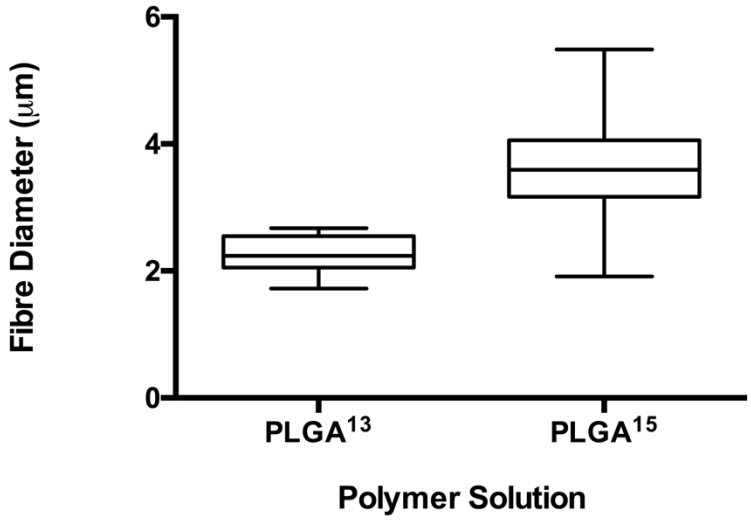

Figure 4.19 - PLGA^{13} fibre diameter. A 13% (w/v) and 15% (w/v) solution of PLGA in 1,1,1,3,3,3-Hexafluoro-2-propanol (HFIP) was electrospun through a blunted 22 ½ G needle with a voltage of 5.5 kV, a flow rate of 2 mL hour^{-1}, at a collector distance of 150 mm, onto a 5 mm diameter rotating stainless steel collector at 5 x g. Fibre diameters were quantified using the DiameterJ plugin for Fiji (ImageJ) software. Data represent the average results taken from ≥ 12 random microscopic fields per experiment. ≥100 fibres were counted per experiment. Data are mean ± SEM, n=3. Statistical analysis: unpaired t-test was used to asses statistical significance.

4.2.11 Fluorescent dyes can be added to HFIP solution to produce fluorescent electrospun fibres

In order to observe the position of each fibre type within a multi-layered structure, fluorescent dyes were added to a PCL solution made in HFIP. Fluorescent dyes were referenced in the literature for those observed to dissolve in HFIP. Some additional dyes were visually tested for their ability to dissolve forming a homogenous coloured solution. After initial testing DAPI, Rhodamine B and Rhodamine 123 and TO-PRO™-3 Iodide presented a strong ability to dissolve readily in HFIP after 30 mins of mixing, and provided strong fluorescent signals under a fluorescent microscope. Solutions were optimised to obtain similar levels of fluorescence (Table 4.1). Fibres were not seen to be visually affected by the addition of the dyes and individual fibres could be observed under fluorescent microscopy (Figure 4.20.1A-D).

Table 4.2 - Final fluorescent dye concentrations for identification of electrospun fibres

Fluorescent Molecule	Concentration (w/v)
DAPI	5 μg mL^{-1}
Rhodamine B	2.5 mg mL^{-1}
Rhodamine 123	2.5 mg mL^{-1}
TO-PRO™-3 Iodide	1 μM

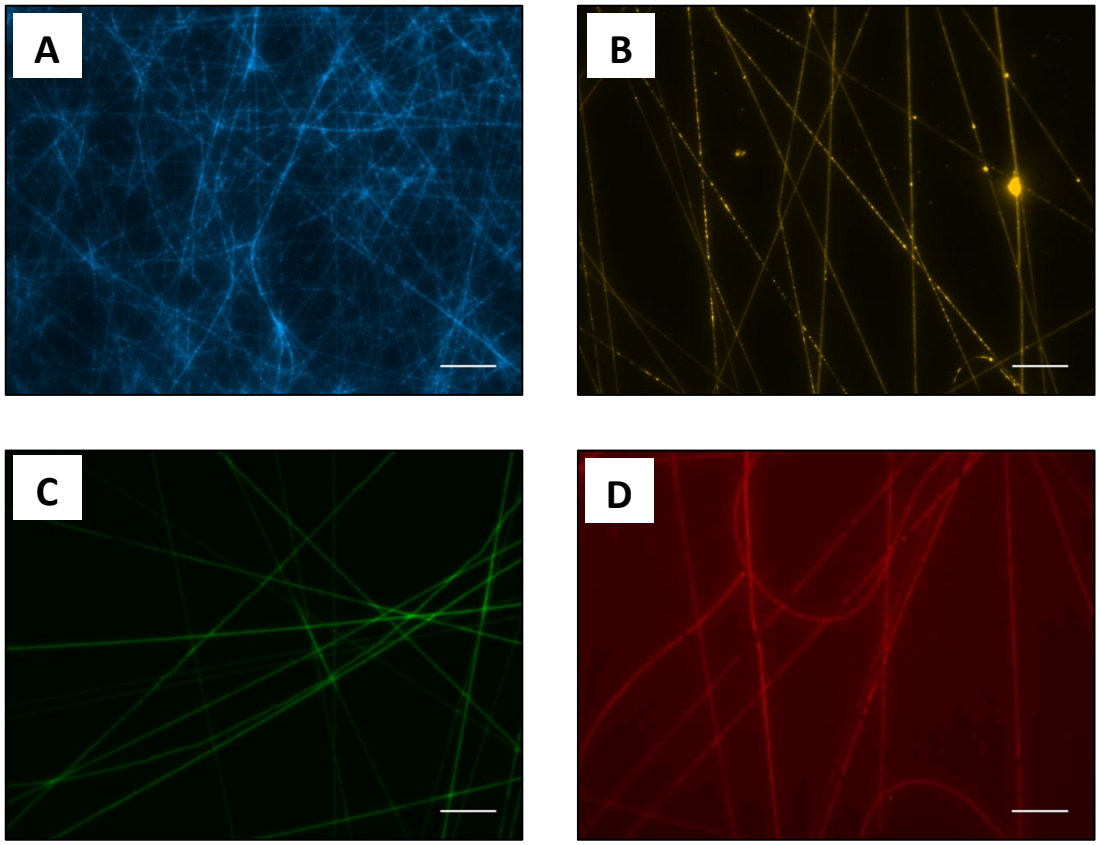

Figure 4.20 - Optimisation of fluorescent dyes for identification of electrospun fibres. An 11% (w/v) solution of PCL containing either **(A)** 5 µg mL^{-1} DAPI **(B)** 2.5 mg mL^{-1} Rhodamine B **(C)** 2.5 mg mL^{-1} Rhodamine 123 **(D)** 1 µM TO-PRO™-3 Iodide in 1,1,1,3,3,3-Hexafluoro-2-propanol (HFIP) was electrospun through a 100 mm kwill containing a blunted 22 ½ G needle with a voltage of 10.5 kV, a flow rate of 2 mL hour^{-1}, at a collector distance of 150 mm, onto a 100 mm diameter rotating stainless steel collector at 5 x g. Representative fluorescent and phase contrast images are shown. n=3. Scale bars represent 50 µm.

4.2.12 A seamless tri layered tube can be produced

To determine the feasibility of producing a multi-layered electrospun tube with distinct layers, the inner PLGA$^{25(a)}$ layer was produced on its respective mandrel (collector 2) (Figure 4.21A). This layer was then cut away and placed onto the coated pinion wire in collector 2 (Figure 4.21B). The middle PCL$^{11(a)}$ layer was then electrospun over the inner PLGA$^{25(a)}$ layer at maximum rotational speed. The final PLGA^{13} layer was then electrospun at the lowest rotational speed onto the dual layer of PLGA$^{25(a)}$ and PCL$^{11(a)}$ (Figure 4.21C). The parameters for each layer are outlined in Table 2.10. One of the fluorescent dyes identified in Table 2.6 was added to an individual electrospinning solution so each layer so each layer could be identified under fluorescent microscopy (Figure 4.21E).

The produced tubes were relatively easy to cut away from the pinion wire, although this could cause visible blade marks on the pinion wire (data not shown). Visually, the tubes looked seamless and no distinction between the layers could be observed (data not shown). The tubes were flexible and did not show irreparable deformation at approximately 250 μm in total wall thickness, although this was not experimentally determined at this proof-of-concept stage. Distinct layers could be seen through the cross-section of the tubular wall under phase contract microscopy with the inner layer being darker than the middle and outer layers (Figure 4.21D). An aligning of fibrous structures could be seen in the middle PCL$^{11(a)}$ layer under phase contrast (Figure 4.21D). Under fluorescent excitation, each layer was highly visible and showed distinct borders between them (Figure 4.21E).

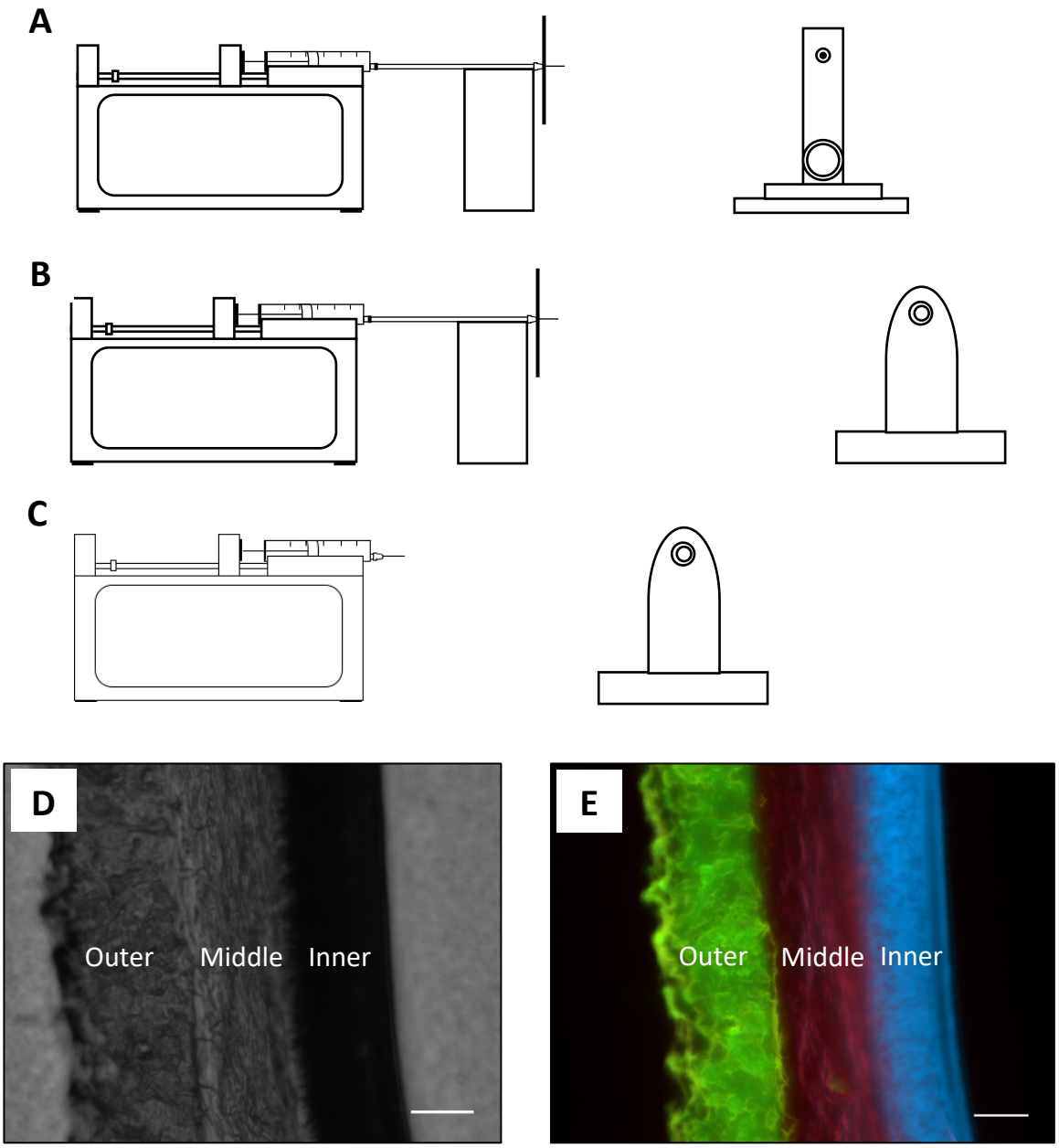

Figure 4.21 - Visualisation of an electrospun tri-layered scaffold using fluorescent dyes. An electrospun tri-layered tube was fabricated by electrospinning 3 separate solutions sequentially. The tri-layered tube was snap frozen in liquid nitrogen-cooled isopropanol, set in OCT and cryosectioned.at -70°C.

(A, D, E) – Layer 1: The Inner layer was fabricated using electrospinning set up A using collector 2. A 25% (w/v) solution of PLGA containing 1% (w/v) NaOAc and 5 µg mL^{-1} DAPI in 1,1,1,3,3,3-Hexafluoro-2-propanol (HFIP) was electrospun through a 100 mm kwill containing a blunted 22 ½ G needle with a voltage of 20.5 kV, a flow rate of 2 mL $hour^{-1}$, at a collector distance of 150 mm, onto collector 2 at 0.00028 x g.

(B, D, E) – Layer 2: The Middle layer was fabricated using electrospinning set up B using collector 3. An 11% (w/v) solution of PCL containing 2.5 mg mL^{-1} Rhodamine B in 1,1,1,3,3,3-Hexafluoro-2-propanol (HFIP) was electrospun through a 100 mm kwill containing a blunted 22 ½ G needle with a voltage of 10.5 kV, a flow rate of 2 mL $hour^{-1}$, at a collector distance of 200 mm, onto collector 3 at 2000 x g.

(C, D, E) – Layer 3: The Outer layer was fabricated using electrospinning set up C using collector 3. A 13% (w/v) solution of PLGA containing 2.5 mg mL^{-1} Rhodamine 123 in 1,1,1,3,3,3-Hexafluoro-2-propanol (HFIP) was electrospun through a blunted 22 ½ G needle with a voltage of 5.5 kV, a flow rate of 2 mL $hour^{-1}$, at a collector distance of 150 mm, onto collector 3 at 5 x g.

Representative fluorescent and phase contrast images are shown. Scale bars represent 50 μm.

4.3 Discussion

Physiologically, endothelial cells in the lumen of a mammalian blood vessel are orientated in the direction of blood flow. There is strong evidence that cells can become highly aligned due to mechanical cues from the substrate they are cultured on (Nestor-Bergmann, Goddard and Woolner, 2014; Tondon and Kaunas, 2014; J. H. Kim *et al.*, 2016). There is evidence that aligned electrospun fibres can stimulate this cellular alignment. Highly aligned cells may be more physiologically representative of luminal endothelial cells.

It is widely accepted that high speed rotational collectors can be used to produce highly aligned electrospun fibres using different materials and solvent systems. However, to my knowledge, there has been no examination of the effectiveness of this rotation on different fibre diameters and there is an assumption that rotational speeds of approximately 1500 RPM and upwards are sufficient to produce highly aligned fibres.

These data demonstrate that high speed rotation is able to align PLGA fibres of different average fibre diameters. Increased rotational speeds have been shown to improve the degree of fibre alignment (Nguyen and Anderson, 2015). Interestingly, these data suggest that smaller fibre diameters may require higher rotational speeds to achieve the same degree of alignment for larger diameter fibres.

Highly aligned fibres using high rotation are useful for generating sheets of scaffold material or tubes with circumferentially aligned fibres. However, to produce small diameter tubes they would need to be shaped and fused together using methods such as suturing. This would result in an uneven line of material through the length of the tube, which would likely increase the risk of thrombus formation and affect fluid flow dynamics. Opposing collectors have been used to also produce highly aligned fibres (Dan Li *et al.*, 2003), which allow incoming electrospun fibres to fill the airspace between the collectors with each opposing end of the fibres adhering to the opposing collectors.

These data demonstrated the feasibility of this technique; however, the relationship between the collector point angle to the internal diameter of the resulting electrospun tube was not determined. It was also unpredictable as to whether fibres would be able to adhere close to, or on, the tip of the collector element. This could have resulted in electrospun fibres occupying the luminal space, although this not an observation detailed by studies using similar collectors such as work by Jana and Zhang, (2013). Interestingly, Jana and Zhang, (2013) also noted the distinct curved morphology of the tube during the electrospinning process, which was identified in this thesis. They postulate that the charge if the underlying electrospun layer causes the newly deposited layer to be repulsed, resulting in a convex shape. This repulsive force is then counterbalanced by the repulsion between the layer depositing above forcing the middle layer down to the underlying layer. Jana and Zhang, (2013) also highlight that their resulting vessel has a slight concave shape once complete, which was not observed in this thesis. This may be due to the small size of the vessel or the difference in polymer used compared to their work.

To overcome the inadequacies of the this first dual static collector (collector 1), I designed a second collector based on a more complex design adapted from Jose *et al.*, (2012) (collector 2). The addition of rotation capabilities was added to ensure even distribution of fibres. The collector electrodes were fabricated without apical points and they were created hollow to ensure fibres were only deposited onto the walls of the electrodes thus preventing fibres from developing in the luminal space of a fabricated tube. Fibres did not appear to adhere to the entirety of the electrode's cylindrical walls; they were situated on the outer edge. This is likely due to fibres being attracted and adhering to the first conductive surface they reach. Then any further fibres adhere over the initially deposited layer. Although not fully tested, tube wall thickness did not visibly increase from increased electrospinning time meaning there was a limitation to the number of layers that would successfully form before the attractive force of the grounded electrodes could not overcome the repulsive forces of the underlying fibres. It was therefore established that 30 minutes electrospinning time was sufficient to create the axially aligned tubes with no benefit conferred by increasing the electrospinning time. This is a limitation to the method that would need to be overcome for axially aligned fibre tubes

that require thicker tube wall thicknesses. It may be possible that increasing the thickness of the collector mandrel walls would help alleviate this issue. Another possible solution may be to use a more conductive material for the electrodes such as copper may help to increase the number of deposited fibre layers and thus increase the tube wall thickness.

To remove prevent the central constriction of the fabricated electrospun tubes, a PTFE rode was placed between the two electrodes to fill the void space. The PTFE had no adverse effects upon the electrospinning process as expected due to its non-conductive and inert properties. Fibres did not adhere to the surface of the PTFE presumably due to there being no electric potential created and the non-adherent property of the material. The resulting tubes no longer contracted centrally and their uniform shape remained after removal from the electrospinning collector. This supports the previous explanation proposed for this phenomenon originally postulated by Jana and Zhang, (2013) and suggests that contraction caused by further solvent evaporation is unlikely or at least not the primary cause.

Unexpectedly, aligned fibre tubes could only be fabricated when the PTFE rod was fixed in place and moved in tandem with the rotating collector electrodes. Randomly orientated tubes formed when the PTFE rod was unfixed may have been due to triboelectric charge being produced by the PTFE rubbing against the stainless steel electrodes as they moved independently of each other (Liu, Seyam and Oxenham, 2013). This charge may have affected the electric potential between the needle and collector electrodes, resulting in fibres landing on the developing tube due to the velocity of the oncoming jet as opposed to the attraction to the opposing electrodes. Therefore, this work suggests that small changes in charge dynamics may have an impact on electrospinning systems. This work also provides a possible solution to helping prevent contraction of aligned scaffold tubes generated using dual collectors across an air gap.

Collector electrode rotation speed had no effect on fibre alignment, which is likely due to them being too low. A study by Zhu *et al.*, (2016) showed that when high rotation speeds are used on collectors with a similar opposing electrode design, similar to the one presented in this thesis, fibres start to deposit on uniform angles related to the rotation

speed. However, this was not a feature that would be advantageous for this work as the goal was to create fibres aligned in the direction of potential blood flow. These data demonstrate the feasibility of fabricating highly axially aligned PLGA tubes with tuneable internal diameters.

After successfully producing an axially aligned luminal layer (Layer 1), the second layer of the tri-layered tube needed to be created with circumferentially aligned fibres. PCL was used for this circumferentially aligned layer (Layer 2) as PCL is known to have more favourable properties for a potential TEVG in regard to flexibility, resistance to permanent deformation and relative strength compared to other polymers such as PLGA (Chou and Woodrow, 2017). This was therefore deemed a more suitable material for the central layer of the TEVG to confer strength, and it would also create the ability for the vessel to expand and return to its original shape depending on internal pressure. These features would allow the macrostructure of the vessel to more physiologically relevant to a mammalian artery. It is possible that PCL would also have been suitable for the Layer 1. This was not explored further due to PCL being described in the literature as less biocompatible than PLGA. Enhanced biocompatibility was desired for layer 1 to improve the adherent, growth and support of endothelial cells to prevent graft thrombosis in a future TEVG.

General optimisation experiments were carried out to establish a method for generating consistent PCL fibres (data not shown). The most suitable fibre diameter for PCL to enhance SMC attachment or the ability to maintain a healthy morphology has not been directly tested in the available literature. SMCs have been shown to adhere to electrospun fibre scaffolds with a wide range of fibre diameters (Xu *et al.*, 2004; Venugopal *et al.*, 2005; Zhou *et al.*, 2015). Additionally, a study using PLGA fibres with varying diameters within the micron range identified that decreasing fibre diameters enhanced cellular alignment in mouse fibroblasts (Hwang *et al.*, 2009). Furthermore, work by Liu *et al.*, (2009) found that alignment of fibroblasts was not affected in poly(methyl methacrylate) scaffolds with fibre diameters less than 1 μm. Therefore, I optimised the electrospinning system to produce fibres with an average diameter of approximately 1 μm to enhance alignment whilst also trying to maximise cellular attachment.

High RPM was used to help align PCL fibres on the 5 mm mandrel as this had been shown to align PLGA fibres. However, this was found not to align the PCL fibres and had no visible effect on fibre deposition. Further to high speed, secondary electric fields created from electrically charged plates have also been shown to help align fibres by delaying the point at which the electrospinning jet destabilises causing a whipping of the jet (Wang *et al.*, 2014; Walser and Ferguson, 2016). This is proposed to reduce the size of the whipping segment of the jet meaning that the electrospun jet stays straighter before landing on the collector. Therefore, allowing aligned fibres to be produced without using high speed rotation.

Positively charged aluminium plates were used in this study to help direct the electrospinning jet, to help improve alignment on the high-speed rotating collector. This method did slightly improve fibre alignment but the results were intermittent, meaning greater understanding of the fundamental physics of electrospinning and electric fields would need to be investigated. Interestingly, secondary charged plates reduced the visible amount of fibre deposition in off-target regions, which may be explained by the reduction of the whopping segment thereby reducing the region in which fibres could deposit. The use of a kwill also reduced off-target deposition, which is likely due to the reduction of the attractive effect of the conductive casing of the syringe pump. It is possible that shielding of electromagnetic forces could be reduce any off-target deposition, which may be suggestable for future electrospinning work.

The undulating pattern seen from some of the resulting scaffolds may have been caused by micro vibrations in the 5 mm rod from the high-speed rotation. A similar fibre pattern was identified by Liu *et al.*, (2010). Interestingly, they found that a wavy pattern was formed when the flow rate increased to 3 mL h^{-1}. However, they did not use a rotating collector and they attribute this phenomenon to forces generated by the use of magnets in their experimental method, which may suggest this fibre pattern is not generated from vibrations in the rod and is instead due to disruptions caused by additional electric fields within the electrospinning set up.

The literature contains numerous reports of the use of high speed rotating mandrels to align electrospun fibres, using a multitude of materials (Ayres *et al.*, 2006; McClure *et al.*, 2009; Wang *et al.*, 2009; Kai *et al.*, 2011; Koepsell *et al.*, 2011). Most papers reviewed for this thesis used RPM as the unit of measurement for collector rotational speed, although Arras *et al.*, (2012) and Nerurkar *et al.*, (2011) were found to report collector rotation speed in ms^{-1}. The literature reports that speeds of approximately 1000 rpm or above can start to produce aligned fibres (Motamedi *et al.*, 2017), with many studies choosing to align fibres using a speed of approximately 2000 rpm (Chew *et al.*, 2007; Xie *et al.*, 2010; Sakamoto *et al.*, 2014; Song *et al.*, 2018). The reported rotation speeds do vary showing a trend towards increased alignment with higher rotational speeds (Choi *et al.*, 2008).

The results from this thesis showed that a rotation speed of 2000 rpm was insufficient to produce highly aligned fibres for a 5 mm diameter mandrel. As all parameters for the electrospinning system were kept constant except for the electrospun material; therefore, this observation is likely due to the change in collector size. RPM does not consider the diameter of the rotating mandrel, which this work has shown is essential for aligning electrospun fibres. Therefore, Relative Centrifugal Force (RCF) was used in this study to consider the 5 mm diameter of the collector, with a calculated equivalent rpm speed of approximately 25,000 rpm to attain the same RCF as the previously tested alignment on the larger mandrel used for the flat sheets at the beginning of this chapter. This work has highlighted the need for published literature to ensure that either the rotating mandrel diameter is stated or that the rotation speed is denoted in RCF or ms^{-1}.

The use of the collector 3 allowed for aligned fibres to be achieved, further reinforcing the hypothesis that tangential speed determines fibre alignment and not rotational speed. The resulting fibres displayed the same undulating pattern as section 4.2.6, which may be due to vibrations of the mandrel as previously described.

After successfully fabricating circumferentially aligned fibres using the high-speed collector, it was important to create tubes that could be cut and removed from the mandrel for further testing. The fibre tubes could not be removed from the mandrel without detrimental damage. It was believed that the evaporation of residual solvent

could have caused fibres to constrict around the mandrel, preventing removal. Residual solvent could have caused fibres to fuse to the mandrel, which would not be a problem during the fabrication of a tri-layered tube as this PCL layer would be fabricated over Layer 1. To reduce friction between the mandrel and the electrospun tubes, 5 mm stainless steel rods were coated in Teflon. Additionally, pinion wire was also coated in Teflon as it was hypothesised that the reduced surface contact of the toothed rod would also aid in tube removal. This may be the first use of a Teflon coated mandrel for use in electrospinning small diameter TEVGs and this offers considerable benefits for damage free removal of thin electrospun tubular scaffolds from mandrels. These data suggest that this technique may be useable employable across various mandrel designs and materials without significantly affecting performance. Further research would be required to understand if the Teflon coating had any adverse effects in regard to fibre attraction to the mandrel. For instance, the Teflon layer may reduce the force that attracts fibres to the mandrel and this may result in more weakly compacted electrospun structures compared to uncoated mandrels.

The mean fibre diameter of PCL electrospun onto the pinion wire was similar to that of the mandrel used in section 4.2.9 and the fabricated electrospun tubes could be easily removed. Comparatively, the stainless-steel rod produced fibres with a significantly lower mean fibre diameter. The Teflon coating may have reduced the attractive force between the oncoming electrospinning jet and the mandrel thus reducing the speed of the oncoming jet. This reduction in speed may have provided additional time for solvent evaporation, resulting in the formation of smaller fibres (Semnani, 2016). The higher conductivity of the carbon alloy pinion wire may have maintained a higher attractive force to the previously used uncoated mandrel in section 4.2.9, resulting in a similar mean fibre diameter. To my knowledge, this was the first reported use of pinion wire as a collector structure. I hypothesised that pinion wire may be able to produce aligned fibres without the need for high tangential speed as cylindrical collector mandrels with evenly spaced bars do not require high speed rotation to achieve highly aligned circumferential fibres. Unfortunately, for small diameter TEVG purposes such collector mandrels are not produced in small enough diameters. However, pinion wire was considered due to its shape having similarities to these large collectors. Due to time constraints and the

requirement of further custom-made equipment, this hypothesis was not investigated further

To develop the final outer layer of the proposed tri-layered tube (Layer 3), PLGA was electrospun to produce a randomly aligned scaffold. Previous studies have shown that large pore sizes enhance angiogenesis (Artel *et al.*, 2011), which is needed to support vascular grafts as they require a substantial blood supply (Rouwkema *et al.*, 2009). Therefore, a higher concentration of PLGA was used to increase the mean fibre diameter, which in turn would increase mean pore size. Two concentrations of PLGA were electrospun using the parameters outlined in Table 2.10 onto collector 3. The electrospinning method was similar to the method for Layer 1; however, to produce a sable Taylor cone, the applied voltage was amended. Two concentrations within a narrow range were chosen to electrospin to determine if there was a significant difference in fibre size, which these data show is true.

After determining that each layer could be individually created to the desired specification, a two-layer tube was created (data not shown). Observations under SEM demonstrated that distinct layers were difficult to identify. Therefore, it was hypothesised that fluorescent molecules could be used to label the fibres in each distinct layer, thus allowing for observation of a tri-layered tubes using fluorescence microscopy. To test this hypothesis, fluorescent dyes were selected from the available literature based on their separate fluorescent excitation spectra and their limited toxicity to reduce any cellular toxicity if used during *in vitro* experiments. All dyes were then optimised using a standard electrospinning solution of PCL where the fibre diameters would be large enough to be observed using fluorescent microscopy.

All of the dyes tested were fortunately miscible in HFIP, which is of interest for future work requiring fluorescently identifiable fibres in electrospinning systems that use HFIP as a solvent. The concentration of each dye was increased until they could be viewed using an epifluorescent microscope, with the minimum effective centration being used to reduce any potential for cellular toxicity. All dyes were distributed evenly throughout the fibres using practice concentrations thus providing a group of dyes for future work using

electrospun materials using HFIP as a solvent. It is possible that fluorescent dyes could have affected the electrospinning solutions and this should be tested further. However, the fluorescent labelling of fibres was conducted to determine if distinct layers of a tri-layered tube could be verified so their impact on resulting fibres would have had a limited affect.

After identifying a suitable system for detecting each layer, the final experiment was carried out to determine if all 3 layers could be produced in sequence, resulting in a tri-layered tube. A fluorescent dye was added to each separate electrospinning solution. The first layer was then fabricated as previously outline. This layer was then removed from the collector and placed onto collector 2. This layer was fixed in place with adhesive tape at each end to keep the structure under tension. The second layer was then immediately electrospun over the top. The final PLGA solution was then immediately electrospun over the current two layers. Once complete, this structure was then cut into small rings and removed from the mandrel. Tri-layered rings were then cooled to 4°C to increase the stiffness and placed onto a slide for examination under fluorescent excitation.

After cutting and observation under SEM, no distinction could be made between the layers as seen previously (data not shown). This suggests that the use of the same solvent and immediate electrospinning of the subsequent layer allows for the merging of the incoming fibres, creating a seamless tube with no separation between the layers; although this was not investigated further and layers may separate when introduced to cell culture liquids. Examination using fluorescent microscopy showed that there were 3 distinct layers, which was also supported by the phase contrast images. The darkest region was the inner layer, which was expected to be a bundle of highly aligned fibres whose ends would be directly facing the light source, reducing the amount of light that entered the view finder lens. Individual fibres in the middle layer could be observed as orientated in the circumferential direction, although individual fibres could not be seen effectively for scientific assessment on the fluorescent images of the rings. This may have been due to fibres being so closely bundled that the fluorescent signal of each fibre could not be assessed and the maximum resolution of the epifluorescent microscope, which

may have been overcome with the use of more technology advanced imaging techniques such as multiphoton imaging.

4.4 Conclusion

These data presented in this chapter show the feasibility of producing a multi-layered electrospun tube with alternating aligned and randomly orientated fibres in opposing directions, which to my knowledge has not been shown in the available literature. Furthermore, this work has highlighted that rpm is not responsible for fibre alignment from rotation collectors. This chapter provides a proof of concept for the fabrication of a multi-layered tube with specific micro- and nano-scaled architecture, which may help enhance and direct cellular responses.

5

ALIGNED ELECTROSPUN FIBRES PROMOTE VASCULAR CELL ALIGNMENT

5.1 Introduction

After demonstrating the feasibility of producing a tri-layered electrospun tube that adhered to the original design, the hypothesised effects of each layer on specific cell attachment and morphology needed to be investigated. Each layer was hypothesised to affect a specific cell type that would be found in the respective layer of a mammalian artery. It is important to create second generation scaffolds that can direct and maintain physiologically healthy cells.

It is known that a luminal endothelium is required for reducing the occurrence of thrombus formation, which is a common cause of TEVG failure (Yau, Teoh and Verma, 2015). Additionally, luminal endothelial cells are known to help maintain medial smooth muscles cells by preventing infiltration into the vessel lumen, which can lead to neointima formation, resulting in an increased risk of vessel occlusion (Ruusalepp, Vaage and Valen, 2003). Therefore, the production of a physiologically suitable layer of endothelial cells across the lumen of a TEVG is a clinical challenge. Changes to the behaviour of vascular smooth muscle cells is also known to increase the risk of bypass graft failure (Allaire and Clowes, 1997). Therefore, creating scaffold structures that can help to maintain a healthy morphology would be advantageous to a TEVG.

Implanted TEVGs have also been shown to lack an adequate blood supply and therefore nutrient exchange (Rouwkema *et al.*, 2009). Larger pore sizes have been shown to enhance angiogenesis and neovascularisation of implanted scaffolds, and enhance the quality of new blood vessels. These processes are essential to supply the TEVG with oxygen to increase the ability of the vessel to function like native tissue. Larger pore sizes are also known to increase cell infiltration through scaffolds, helping aid remodelling (Rnjak-Kovacina *et al.*, 2011).

This chapter investigates each layer separately to determine the effect each scaffold layer on basic cell behaviour. Fibre orientation on cell alignment and morphology is assessed and cell attachment and infiltration is assessed for the outer third layer. These investigations were carried out to determine if a multi-layered scaffold could enhance the

behaviour of cell types to be more representative of the physiological cells found in a mammalian artery. Each layer was produced separately for *in vitro* testing.

In addition to the separate layer testing with human cell models, each layer was also seeded with porcine blood as a model for the *in vivo* human environment. The seeding of specific cell types onto the respective layers in the tri-layered tube was not deemed feasible as cells could not be added to each layer before the subsequent layer was electrospun. Therefore, cells seeded onto the scaffold may be unable to reach the central second layer generating challenges for the translation aspect of this work as the ability of each layer to affect cell behaviour may only occur on mature cells.

Previous literature has shown that nonadherent monocytes from the blood can differentiate into macrophages during inflammation (Dal-Secco *et al.*, 2015). Furthermore, blood monocyte-derived macrophages have been shown to transdifferentiate into endothelial-like and smooth muscle cell-like cells (Ninomiya *et al.*, 2006; Yan *et al.*, 2011). There is also evidence that endothelial and smooth muscle progenitor cells exist in blood that have the capacity to differentiate in endothelial-like and smooth muscle cell-like cells, respectively (Simper *et al.*, 2002; Sabry, Noh and Samir, 2016). Therefore, in this chapter, I test the hypothesis that blood can be used to seed the electrospun scaffold layers with macrophage-derived monocytes that can be transdifferentiated into endothelial-like and smooth muscle cell-like cells *in vitro*.

5.2 Results

5.2.1 HUVECS align in the direction of orientated PLGA^{25} fibres in vitro

Each layer of the tri-layered tubular scaffold was produced separately as a sheet for *in vitro* experimentation to determine the effect of each layer on cells.

Physiologically, luminal endothelial cells align in the direction of blood flow (Dewey *et al.*, 1981). Previous evidence in the literature has shown that endothelial cells can orientate in response to the scaffold structure without the need for hydrostatic flow. It was therefore hypothesised that the luminal axially aligned fibre layer would enhance endothelial cell alignment in the longitudinal direction in static cell culture conditions.

To determine whether PLGA aligned fibres could help endothelial cell alignment, HUVECs were seeded onto both random and aligned PLGA$^{25\ NaOAc\ (a)}$ and stained with VE-cadherin to help visualize cell boundaries and morphology. Nuclei orientation was then quantified.

The PLGA scaffolds were highly autofluorescent and the 3D structure resulted in many cells being situated over multiple z-planes, resulting in difficulty capturing highly contrasting images (data not shown). Sudan black was assessed for its ability to reduce autofluorescence, but the results were inconsistent so its use was not continued for work presented in this thesis (data not shown). However, 24 hours post-seeding HUVECs on the aligned scaffolds were more visibly orientated together in a given direction compared to HUVECs seeded onto randomly orientated scaffolds (Figure 5.1A and B). This effect was also observed under SEM observation (Figure 5.1C and D). Nuclei orientation showed that a large proportion of HUVEC nuclei on the aligned scaffolds were orientated within a similar narrow range (Figure 5.1E). This is contrasted by the HUVEC nuclei orientations on the randomly aligned scaffolds, whereby the frequency of nuclei orientation shows no distinct pattern (Figure 5.1F).

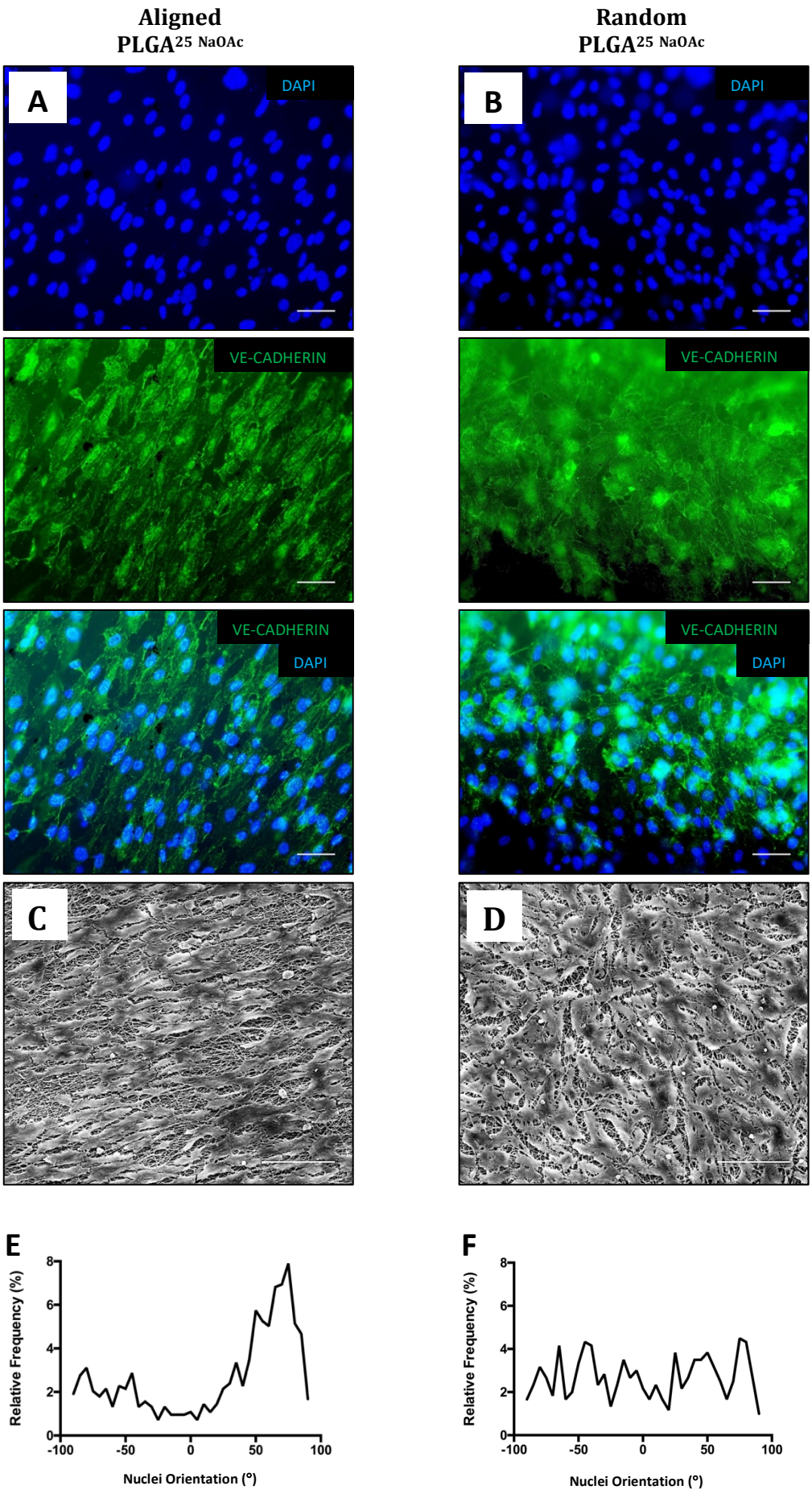
Aligned
PLGA25 NaOAc
Random
PLGA25 NaOAc
A
DAPI
B
DAPI
VE-CADHERIN
VE-CADHERIN
VE-CADHERIN
DAPI
VE-CADHERIN
DAPI
C
D
E
Relative Frequency (%)
Nuclei Orientation (°)
F
Relative Frequency (%)
Nuclei Orientation (°)

Figure 5.1 - The effect of PLGA$^{25\ NaOAc}$ orientation on HUVEC alignment. . HUVECs were seeded onto PLGA$^{25\ NaOAc}$ scaffolds with random and aligned fibres at a density of 1x10^5 per 380 μm^2. Scaffolds were fixed in 4% (w/v) PFA at 24 h, stained with **(A, B)** DAPI and VE-cadherin, and **(E, F)** nuclei orientation was quantified using CellProfiler software based on width to length ratio. **(C, D)** SEM images were also taken. Data represent the average results taken from ≥ 36 random microscopic fields per experiment. Data are mean ± SEM, n=3. Scale bars represent 100 μm.

5.2.2 hVSMCs align in the direction of orientated PCL^{11} fibres in vitro

It has been previously shown that human smooth muscle cells can align in the direction of electrospun fibres (Nivison-Smith and Weiss, 2012). This is a characteristic that is physiologically similar to smooth muscle cells situated within the medial layer of human vasculature, whereby the smooth muscle cells align circumferentially. To determine if the specific fibre diameter, material and direction could support and stimulate human smooth muscle cells to align, aligned PCL$^{11\ (a)}$ was used to mimic the middle layer of the electrospun tri-layered vascular graft and a randomly orientated PCL$^{11\ (r)}$ scaffold was used a comparative negative control. Human vascular smooth muscle cells extracted from patient saphenous vein were seeded onto PCL$^{11\ (a)}$ and PCL$^{11\ (r)}$ scaffolds to provide a physiologically relevant cell source.

Cytoskeletal staining using phalloidin showed that VSMCs on the PCL$^{11\ (a)}$ scaffolds were highly aligned in the orientation of the scaffold fibres and consistently aligned in the same direction, relative to each other (Figure 5.2A). Contrastingly, VSMCs were randomly orientated on the PCL$^{11\ (r)}$ scaffolds (Figure 5.2A). The VSMCs on the aligned fibres showed an elongated and thin morphology, spreading along the length of the fibres (Figure 5.2A). In comparison, the VSMCs on the PCL$^{11\ (r)}$ displayed a rounder morphology; however, they did also show spreading along fibres in all directions (Figure 5.2A). Nuclei orientation supported the fluorescent and SEM observations with the VSMC on the PCL$^{11\ (r)}$ nuclei showing no consistent directionality (Figure 5.2B) and the VSMC on the PCL$^{11\ (a)}$ nuclei showing a higher relative frequency at approximately -50° (Figure 5.2C).

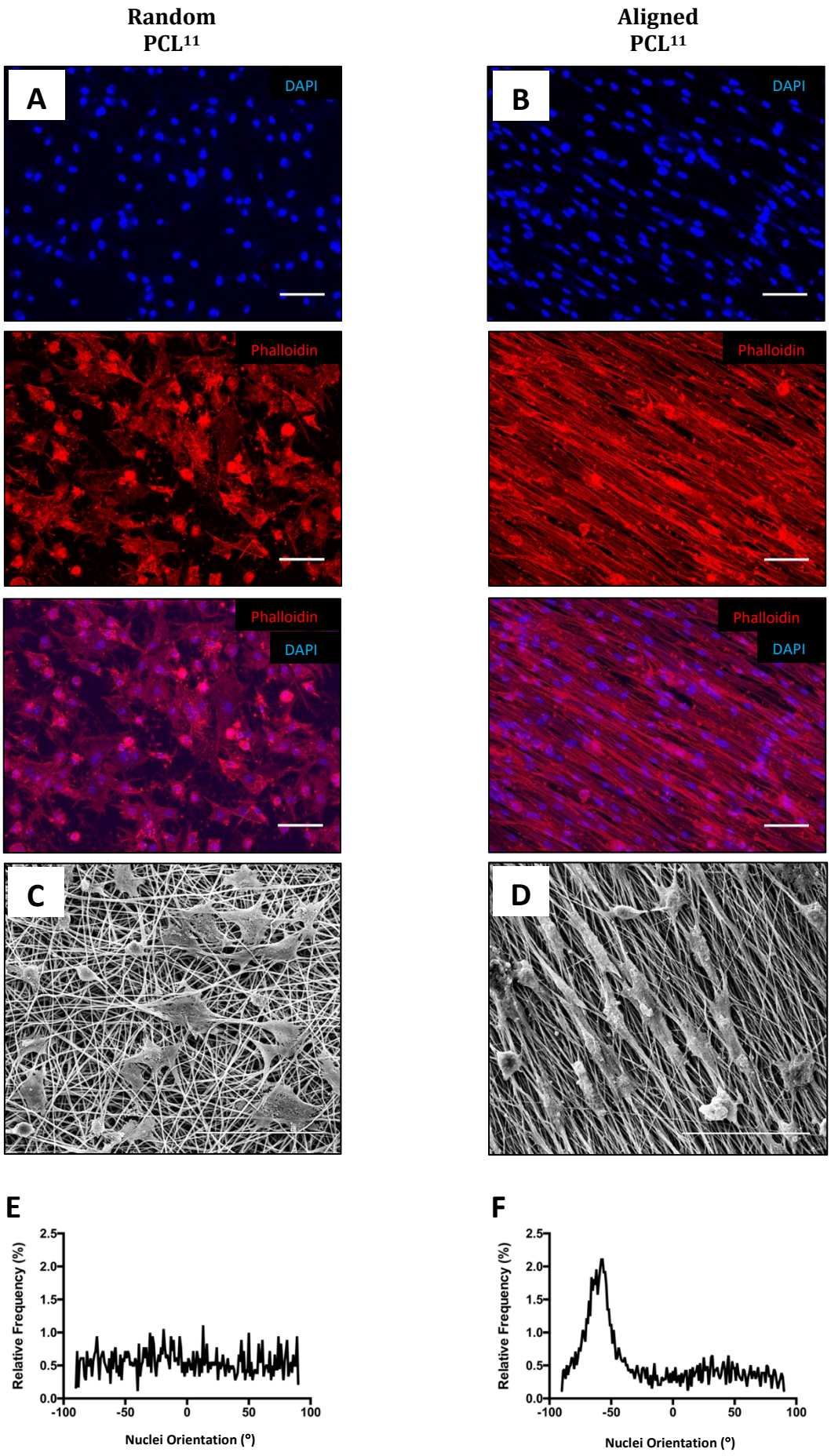
Random
PCL11
Aligned
PCL11
A
B
DAPI
DAPI
Phalloidin
Phalloidin
Phalloidin
DAPI
Phalloidin
DAPI
C
D
E
F
Relative Frequency (%)
2.5
2.0
1.5
1.0
0.5
0.0
-100
-50
0
50
100
Nuclei Orientation (°)
Relative Frequency (%)
2.5
2.0
1.5
1.0
0.5
0.0
-100
-50
0
50
100
Nuclei Orientation (°)

Figure 5.2 - The effect of PCL^{11} orientation on hVSMC alignment. hVSMCs were seeded onto PCL^{11} scaffolds with random and aligned fibres at a density of 1x10^5 per 380 μm^2. Scaffolds were fixed in 4% (w/v) PFA at 24 h, stained with **(A, B)** DAPI and Phalloidin, and **(E, F)** nuclei orientation was quantified using CellProfiler software based on width to length ratio. **(C, D)** SEM images were also taken. Data represent the average results taken from ≥ 36 random microscopic fields per experiment. Data are mean ± SEM, n=3. Scale bars represent 100 μm.

To understand whether aligned fibres had an effect on cell adherence, VSMCs were seeded on random and aligned PCL^{11} scaffolds. VSMCs were then quantified after nuclei staining with DAPI 24 hours post seeding. There was no significant difference between the total adherent VSMCs on the PCL$^{11\ (r)}$ scaffold compared to the PCL$^{11\ (a)}$ scaffold (Figure 5.3).

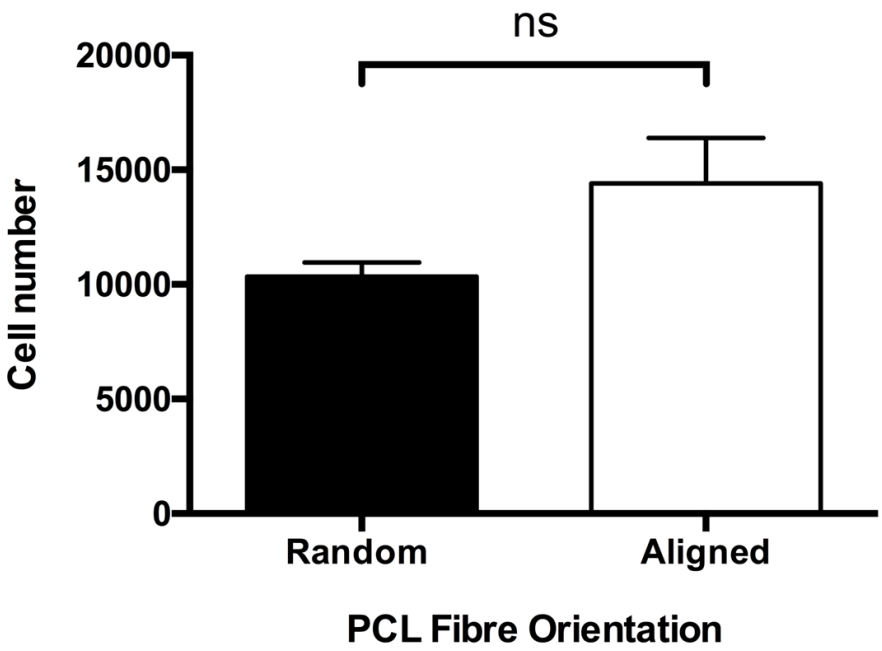

Figure 5.3 - Effect of PCL11 orientation on hVSMC attachment. Smooth muscle cells were seeded onto PCL^{11} scaffolds with random and aligned fibres at a density of 1x10^5. Scaffolds were fixed in 4% (w/v) PFA at 24 h, stained with DAPI and quantified. Data represent the average results taken from ≥ 36 random microscopic fields per experiment. Data are mean ± SEM, n=3. Statistical analysis: unpaired t-test was used to assess statistical significance.

5.2.3 Fibroblast attachment increases with a decreased PLGA fibre diameter

The outer layer of the tri-layered electrospun tube was designed to allow cell infiltration to aid remodelling and integration of a tubular graft into the host tissue. It was important to understand whether hSVF could adhere to this outer layer and to understand the relationship between fibre diameter and cell attachment to ensure the correct diameter was used to enhance cell attachment. It was also important to determine if hSVFs could proliferate on the scaffolds. Electrospun flat sheets of 13 (w/v) and 15% (w/v) were electrospun using the same parameters for the tri-layered tubular scaffold. hSVFs were used as a model cell type due to their abundance in the mammalian adventitia of vascular tissue, ability to migrate, resist contact inhibition, and proliferate quickly. To assess the effect of PLGA fibre diameter on cell attachment and cell numbers over a short time period in static culture, hSVFs were seeded onto $PLGA^{13(r)}$ and $PLGA^{15(r)}$ scaffolds and quantified at 3 time points (4 h, 24 h and 4 d).

$PLGA^{13(r)}$ achieved a seeding efficiency of approximately 30% compared to approximately 15% for $PLGA^{15(r)}$, which was statistically significant (Figure 5.4). After 4 d the number of hSVFs on the $PLGA^{13(r)}$ was similar to the initial seeding number and statistically higher than the number of hSVFs on the $PLGA^{15(r)}$ scaffold (Figure 5.4). The number of hSVFs on the $PLGA^{13(r)}$ scaffold significantly increased from 24 h to 4 d (Figure 5.4).

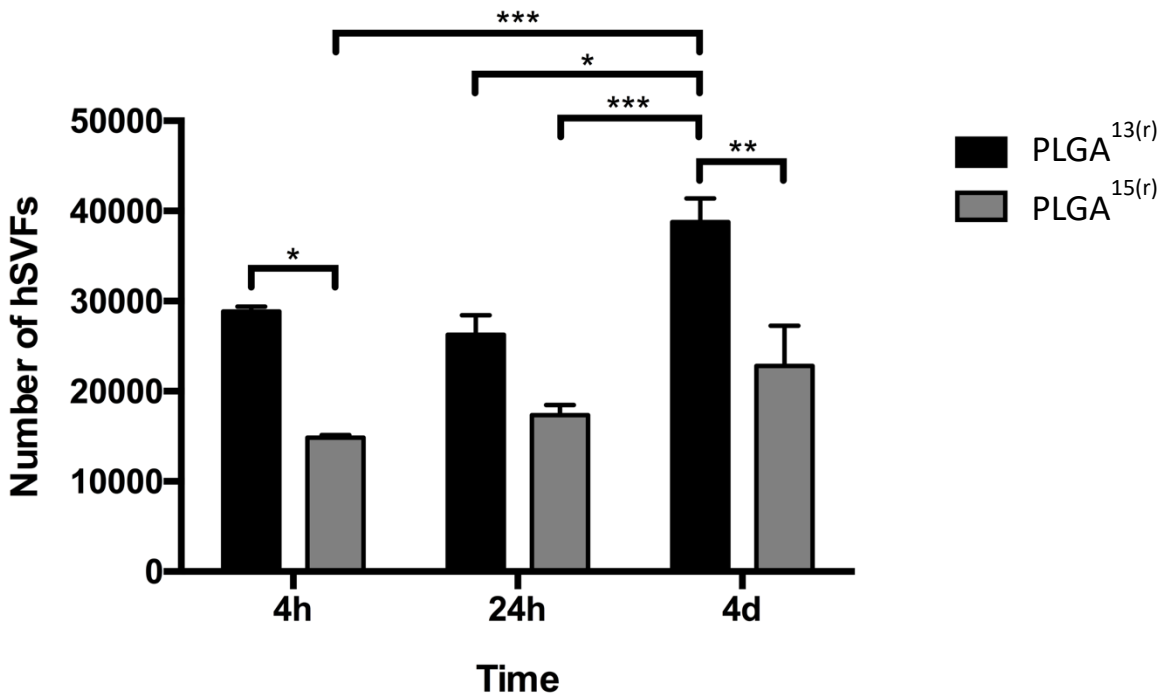

Figure 5.4 - Effect of PLGA fibre diameter on hSVF attachment. hSVFs were seeded onto PLGA^{13} and PLGA^{15} scaffolds with randomly orientated fibres at a density of 1x10^5 per 380 μm^2. Scaffolds were fixed in 4% (w/v) PFA at 24 h, stained with DAPI and quantified. Data represent the average results taken from ≥ 36 random microscopic fields per experiment. Data are mean ± SEM, n=3. Statistical analysis: two way ANOVA was used in conjunction with a Sidak's *post hoc* test; *P < 0.05, **P < 0.01, ***P < 0.001.

Further to the ability of the scaffolds to support cell attachment and growth, cell infiltration was also a consideration. hSVF morphology differed between PLGA$^{13(r)}$ and PLGA$^{15(r)}$. Cells on the PLGA$^{15(r)}$ scaffold were more spread out and infiltrated more than one plane of the scaffold compared to cells on PLGA$^{13(r)}$ at 4h post seeding (Figure 5.5A and 5.6A). After 24h cells, cells on the PLGA$^{13(r)}$ scaffold had begun to elongate and spread across the surface of the scaffold (Figure 5.5B). On the other hand, cells on PLGA$^{15(r)}$ showed infiltration into the scaffold without forming a layer across the surface (Figure 5.5B). After 4d, cells were covering the surface of the PLGA$^{13(r)}$ scaffold (Figure 5.5C). Cells on PLGA$^{15(r)}$ showed a high density similar to PLGA$^{13(r)}$, however, cells were distributed amongst the upper layers of the scaffold and were not covering only the surface (Figure 5.6C).

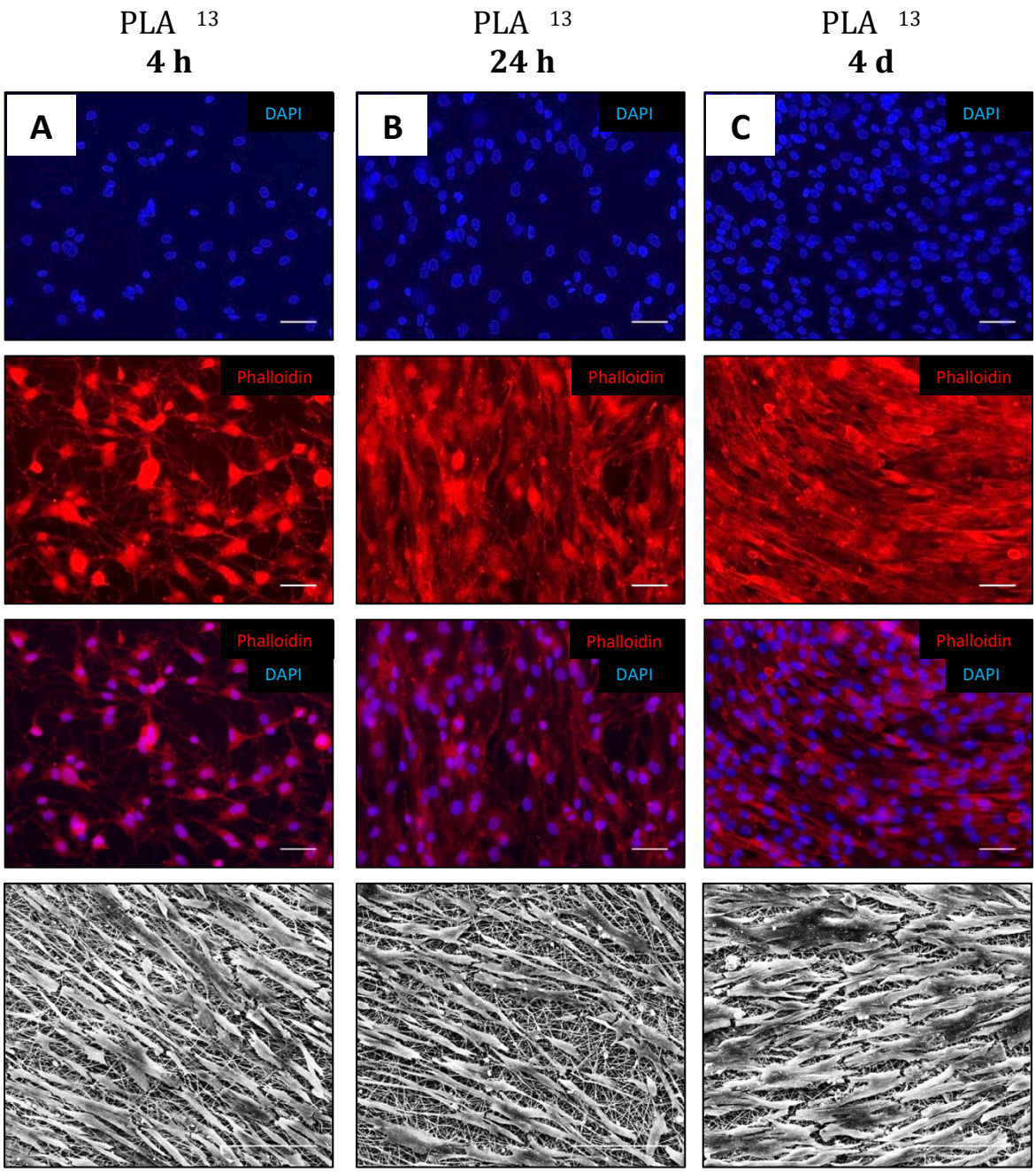

Figure 5.5 - Effect of PLGA[13] fibre diameter on hSVF attachment. hSVFs were seeded onto PLGA[13] scaffolds with randomly orientated fibres at a density of $1x10^5$ per 380 μm^2 and cultured for **(A)** 4 h **(B)** 24 h and **(C)** 4 d. Scaffolds were fixed in 4% (w/v) PFA at 24 h, then stained with DAPI and Phalloidin. Representative fluorescent and SEM images are shown. Scale bars represent 100 μm.

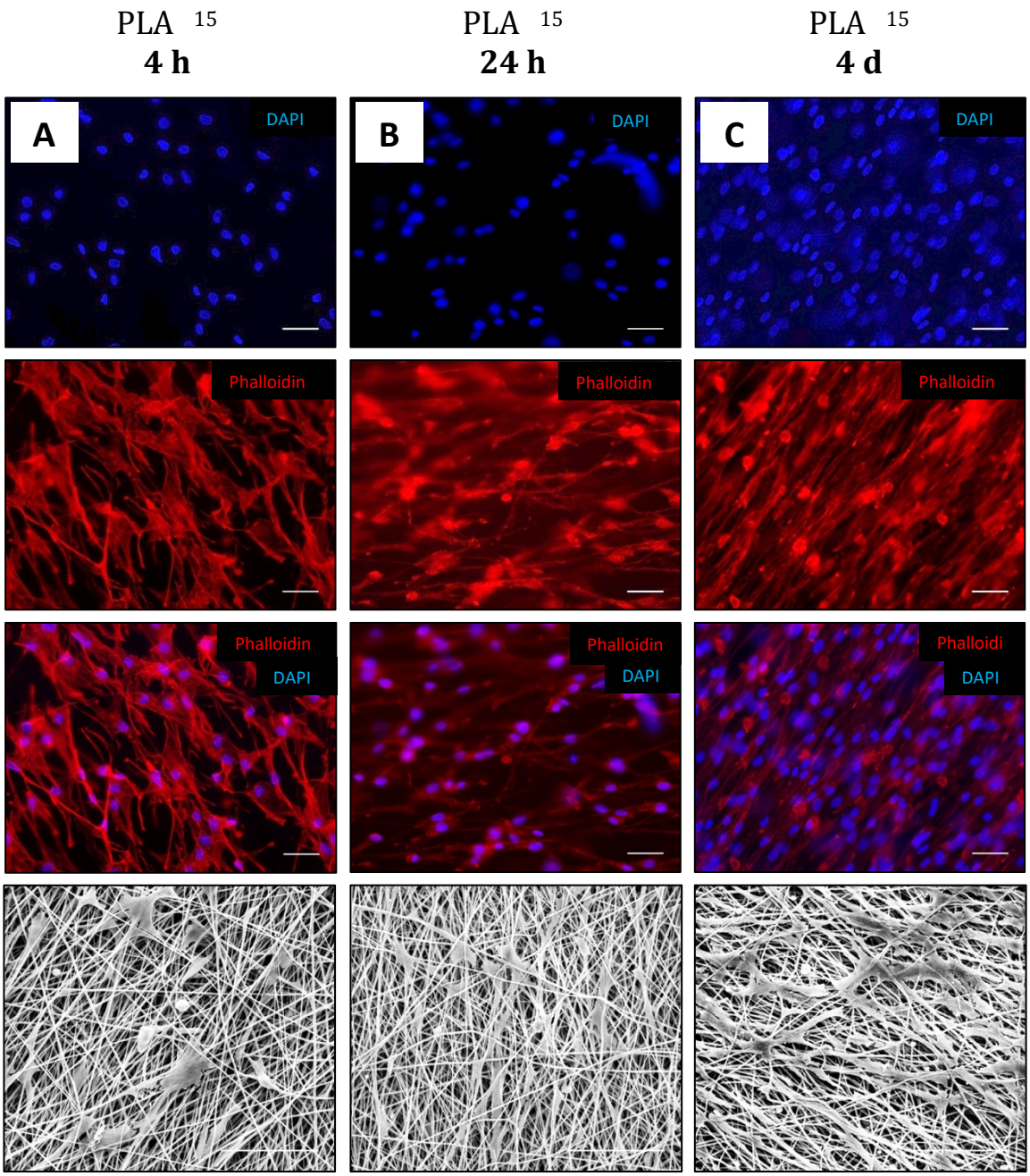

Figure 5.6 - Effect of PLGA[15] fibre diameter on hSVF attachment. hSVFs were seeded onto PLGA[15] scaffolds with randomly orientated fibres at a density of 1x10^5 per 380 μm^2 and cultured for **(A)** 4 h **(B)** 24 h and **(C)** 4 d. Scaffolds were fixed in 4% (w/v) PFA at 24 h, stained then with DAPI and Phalloidin. Representative fluorescent and SEM images are shown. Scale bars represent 100 μm.

5.2.4 PLGA$^{25(a)}$ may select for HUVEC attachment

After identifying that HUVECs and hVSMCs were able to adhere to the PLGA$^{25(a)}$ and PCL$^{11(a)}$ scaffolds, respectively, it was hypothesised that the specific fibre diameters produced by each scaffold could select for specific cell types. Therefore, a heterogeneous solution of 1:1 HUVECs and hVSMCs was seeded onto PLC$^{11(a)}$ and PLGA$^{25(a)}$ scaffolds, and assessed 4 h post seeding for cell attachment. To reduce experimental bias, both endothelial and smooth muscle cell specific culture medias were used.

There were significantly more cells overall on the PLGA scaffolds compared to the PCL scaffolds (Figure 5.7). There were significantly more HUVECS adhered to PLGA scaffolds regardless of media type, compared to hVSMCs (Figure 5.7). There were approximately equal numbers of cells adhering to the PCL$^{11(a)}$ scaffolds regardless of media type (Figure 5.7). HUVECs did not show alignment in any of the conditions (Figure 5.7B-E). In addition to the directly measured observations, hVSMCs cultured under SmGm showed more visible alignment compared to EGM2 media, although this was not quantified (Figure 5.7B and C).

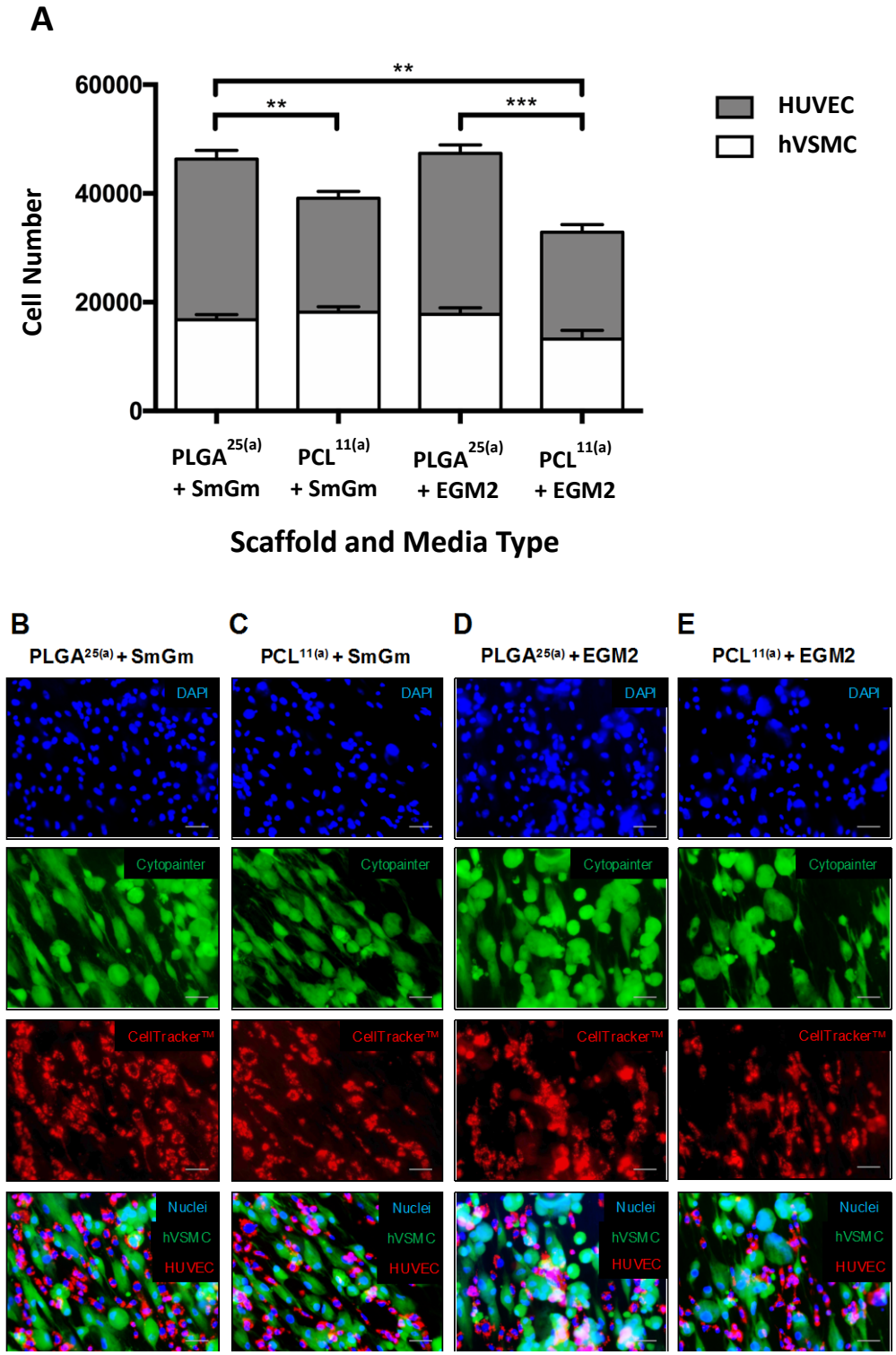

Figure 5.7 – Attachment of a HUVEC and hVSMC co-culture on aligned PLGA^{25} and PCL^{11} scaffolds. HUVECs and hVSMCs were seeded onto both aligned PLGA^{25} and PCL^{11} scaffolds at a density of 1x10^{5} per 380 μm^{2}. HUVECs were stained with CellTracker and hVSMCs were stained with Cytopainter *in vitro,* pre-seeding. Scaffolds were fixed in 4% (w/v) PFA at 24 h, counterstained with DAPI and quantified. **(B – E)** Representative fluorescent images are shown. Data represent the average

results taken from ≥ 36 random microscopic fields per experiment. **(A)** Data are mean ± SEM, n=3. Statistical analysis: two way ANOVA was used in conjunction with a Tukey's *post hoc* test; *$P < 0.05$, **$P < 0.01$, ***$P < 0.001$. Scale bars represent 100 μm.

5.2.5 Porcine blood cells can adhere to each electrospun layer

After testing each individual layer comprising the tri-layered electrospun tube, it was important to identify how an unseeded scaffold might be populated with cells *in vivo* from circulating blood cells. Previously this chapter demonstrated that cells representative of mature vascular cells can be directed toward physiologically representative morphologies using specific electrospun fibre layers; however, extracting and culturing sufficient quantities of mature autologous vascular cells proves challenging, with cells often shown to phenotypically different once cultured *ex vivo* (Yang *et al.*, 2018). Therefore, a suitable seeding method would be needed to help generate autologous mature vascular-like cells that can receive mechanical cues from electrospun fibre to help direct and maintain physiologically relevant morphologies.

It was hypothesised that macrophages from fresh blood could be differentiated into vascular endothelial-like and smooth muscle cell-like cells to produce an autologous tri-layered electrospun vascular graft. As a model for human blood, porcine blood was used due to its accessibility and similarities to human blood. Porcine blood was added to each scaffold layer $PLGA^{25(a)}$ (Layer 1), $PCL^{11(a)}$ (Layer 2) and $PLGA^{13(r)}$ (Layer 3), independently for 24h to assess the ability of cells to adhere to each layer and to determine the suitability of blood for *in vitro* cell seeding of the tri-layered tubes.

Porcine blood cells adhered to all 3 layers (Figure 5.8). Significantly more porcine blood cells adhered to layers 1 and 2 compared to Layer 3 with approximately 7 times more cells adhering to layers 1 and 2 (Figure 5.8). Cells adherent to Layer 2 were distributed in lines (Figure 5.8B).

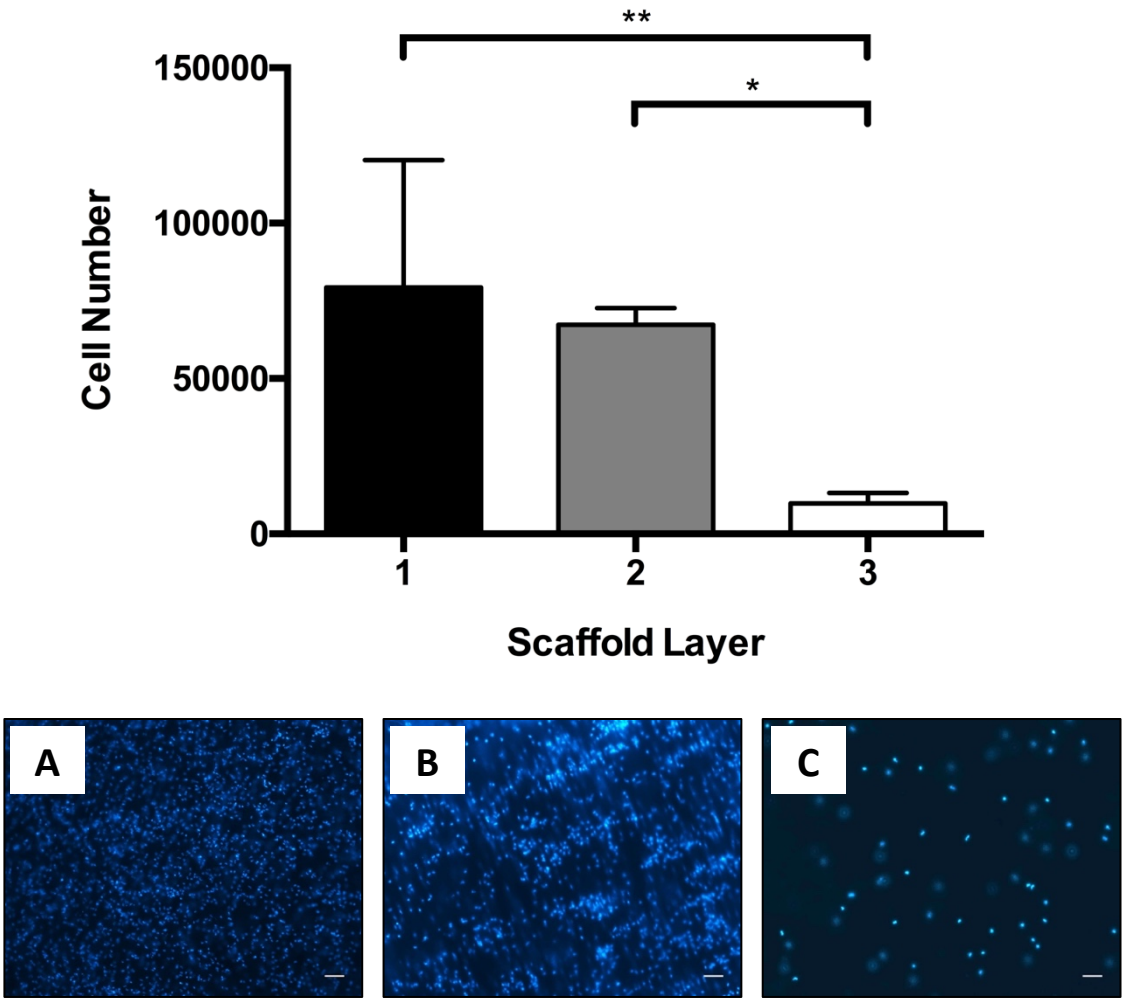

Figure 5.8 - Attachment of porcine blood cells onto separate scaffolds layers. 800 μl of porcine blood was added within 4 h of collection to scaffold tri-layer **(A)** 1, **(B)** 2 and **(C)** 3 held in cell crowns. After 24 h scaffolds were fixed in 4% (w/v) PFA stained with DAPI, and quantified. Data represent the average results taken from ≥ 36 random microscopic fields per experiment. Data are mean ± SEM, n=3. Statistical analysis: ANOVA was used in conjunction with a Tukey's *post hoc* test; **P* < 0.05, ***P* < 0.01. Scale bars represent 100 μm.

5.2.6 Adherent cell population predominantly CD203a positive

Porcine blood contains a heterogeneous population of cells and only adherent cells would have attached to each scaffold layer. It was hypothesised that the majority of adherent cells would be macrophages derived from monocytes. Porcine macrophages widely express CD203a and this protein is not present on monocytes. It was therefore hypothesised that most adherent cells would be monocyte-derived macrophages and would therefore express CD203a.

It was found that the relatively smaller size of porcine blood cells in comparison to HUVECs, hVSMCs and hSVFs meant that cells were observable over a number of planes making it difficult to obtain clear images for antibody staining using a standard epifluorescent microscope. Therefore, confocal laser scanning microscopy was used for the experimental work in this section. Approximately 90% of adherent cells on all 3 layers stained positively for CD203a (Figure 5.9).

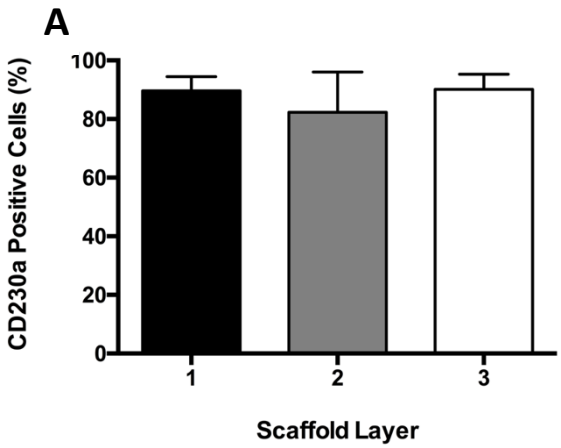
A
CD230a Positive Cells (%)
100
80
60
40
20
0
1
2
3
Scaffold Layer

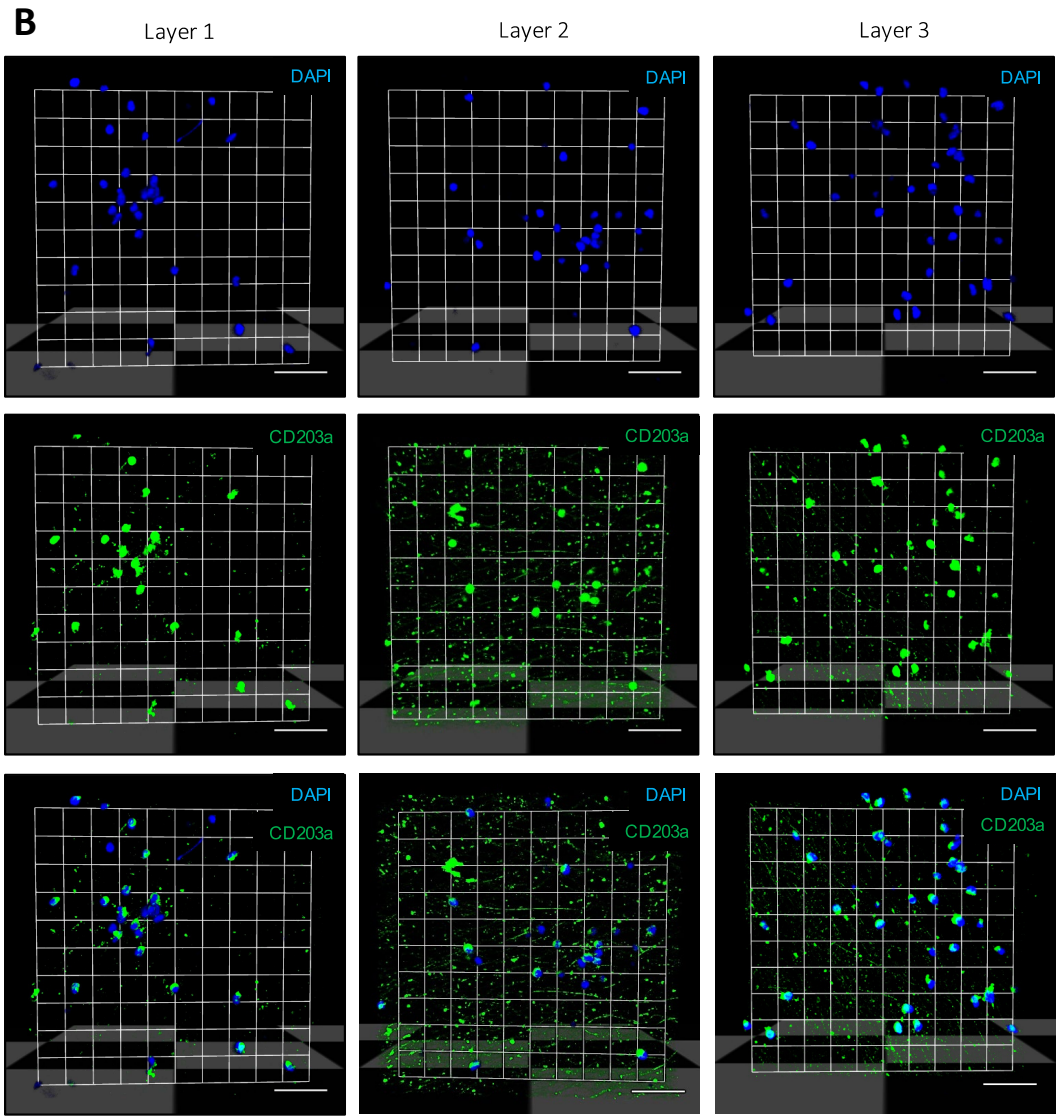
B
Layer 1
Layer 2
Layer 3
DAPI
CD203a
DAPI
CD203a
DAPI
CD203a
DAPI
CD203a
DAPI
CD203a
DAPI
CD203a

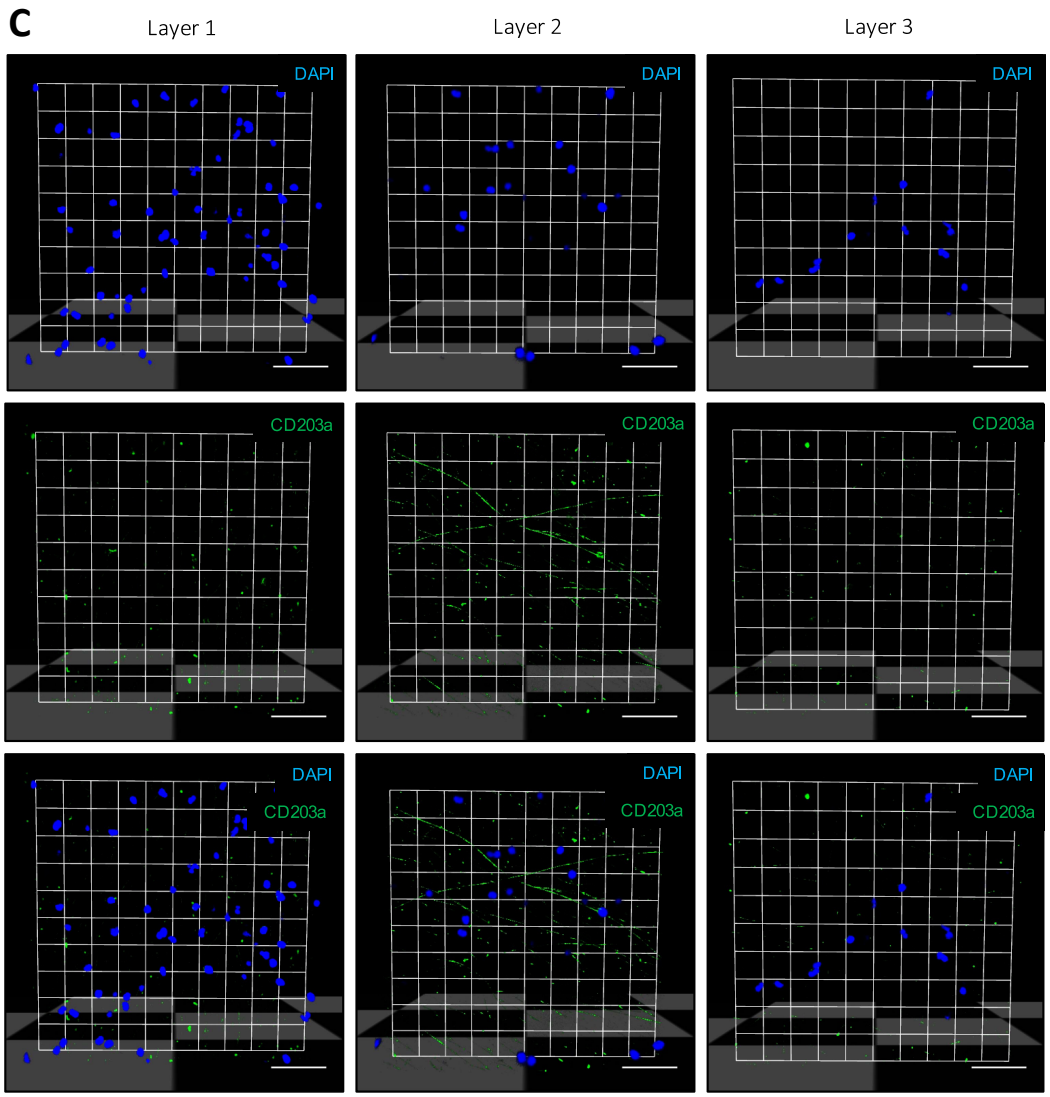

Figure 5.9 - CD203a expression of adherent porcine peripheral blood cells. 800 µl of porcine blood was added within 4 h of collection to each scaffold layer held in cell crowns. After 24 h scaffolds were fixed in 4% (w/v) PFA stained with DAPI and **(B)** CD203a or an **(C)** immunoglobulin control and quantified. Data represent the average results taken from ≥ 36 random microscopic fields per experiment. Data are mean ± SEM, n=3. Statistical analysis: (A) ANOVA was used. Scale bars represent 100 µm.

5.2.7 Thrombin enhances α-SMA expression of adherent blood cells

As porcine blood could adhere to each layer of the scaffold, it was of interest to determine if blood could be used to help generate a tissue engineered vascular graft due to its relative abundance and the lack of laboratory manipulation needed to seed an electrospun structure *in vitro.* Blood contains a number of progenitor cells and macrophages have been shown to transdifferentiate into smooth muscle-like and endothelial-like cells.

By combining the previous data, showing that a tri-layered electrospun tube can be created with distinct layers, that aids the attachment and alignment behaviour of physiologically representative cells, it was hypothesised that adherent monocyte-derived macrophages from porcine blood could be transdifferentiated into endothelial-like cells and smooth muscle cell-like cells on their respective layer, which could help to produce a physiologically similar tissue engineered vascular graft.

Porcine blood was seeded onto Layer 1 and after initial attachment, adherent cells were cultured in endothelial differentiation media with either pleiotrophin or a higher level of VEGF-165. For the derivation of smooth muscle-like cells, porcine blood was seeded onto Layer 2, and after initial attachment adherent cells were cultured in smooth muscle cell differentiation media with either the addition of TGF-β, PDGF-BB or thrombin. Initially, different media were tested and optimised for their ability to increase adherent porcine blood cell expression of α-SMA, before deciding on the final basal control media.

There was no difference in the total number of cells after the differentiation period regardless of the media additives (Figure 5.10A and B). This was true for both smooth muscle cell and endothelial cell differentiations (Figure 5.10A and B). Overall, there were significantly more cells present when cultured in smooth muscle cell medias compared to endothelial cell medias (Figure 5.10C).

Approximately 35% of cells stained positive for eNOS across all endothelial differentiation medias (Figure 5.11A). There was no significant difference in eNOS expression between any of the endothelial differentiation medias (Figure 5.11A).

Approximately 10% of cells stained positive for α-SMA across all smooth muscle cell differentiation medias (Figure 5.11B). Thrombin was the only additive to significantly improve α-SMA expression by approximately 4% compared to control (Figure 5.11B).

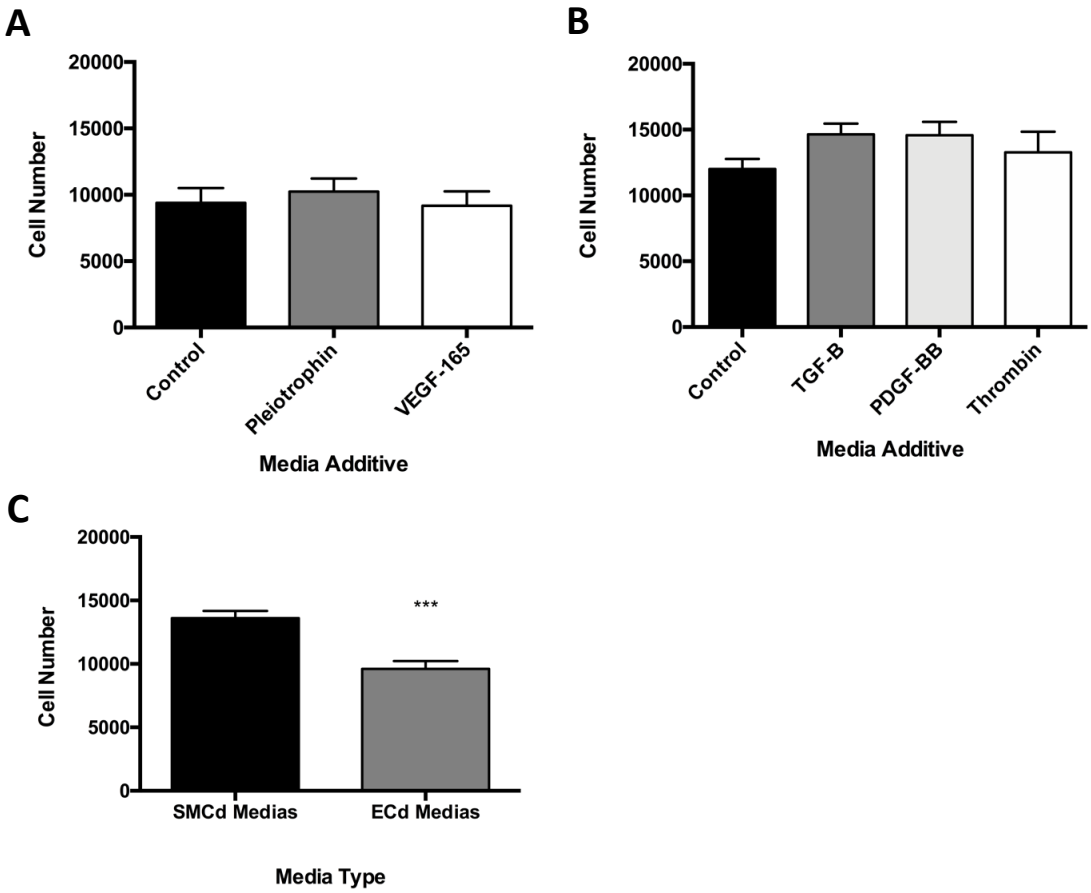

Figure 5.10 - Effect of differentiation media on cell number. 800 μl of porcine blood was added within 4 h of collection to each scaffold layer held in cell crowns. After 24 h scaffolds were washed and **(A)** endothelial differentiation (ECd) or **(B)** smooth muscle cell differentiation (SMCd) or **(C)** control media was added. After 4 d total cell numbers were quantified from DAPI counted images. Data represent the average results taken from ≥ 36 random microscopic fields per experiment. Data are mean ± SEM, n=3. Statistical analysis: **(A - B)** ANOVA was used **(C)** unpaired t-test was used; ***$P < 0.001$.

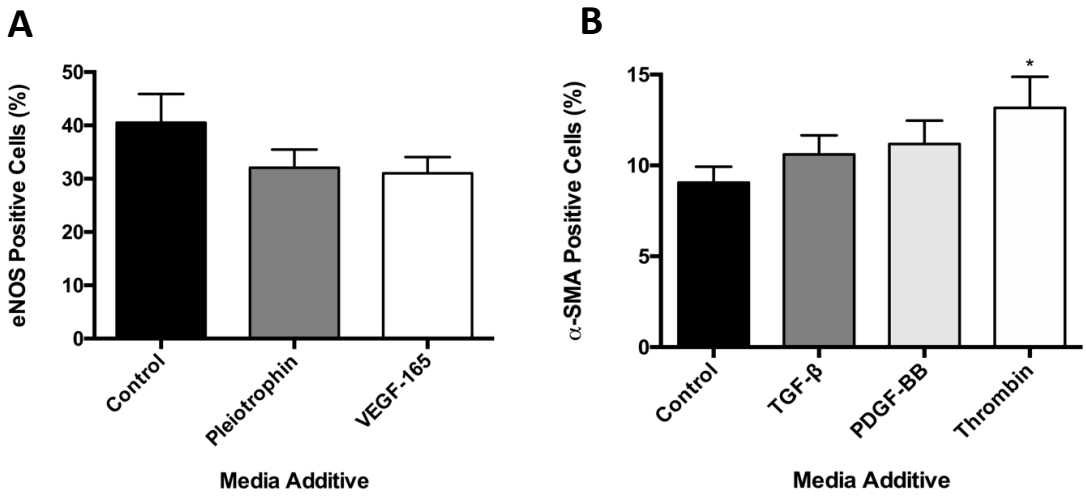

Figure 5.11 – Effect of differentiation media on eNOS and a-SMA expression. 800 μl of porcine blood was added within 4 h of collection to each scaffold layer held in cell crowns. After 24 h scaffolds were washed and **(A)** endothelial differentiation (ECd) or **(B)** smooth muscle cell differentiation (SMCd) media was added. After 4 d total cell numbers were quantified using DAPI and cells were stained for eNOS and α-SMA, respectively for protein expression. Data represent the average results taken from ≥ 36 random microscopic fields per experiment. Data are mean ± SEM, n=3. Statistical analysis: ANOVA was used in conjunction with a Kruskal-Wallis *post hoc* test; **P* < 0.05.

5.3 Discussion

After determining an optimal fibre diameter for HUVECs in Chapter 3 of this thesis, Chapter 4 demonstrated that these cells could be aligned in the direction of blood flow. Endothelial cells are known to display a wide range of shapes, a subject well reviewed by Bentley, Philippides and Ravasz Regan, (2014). In arteries and veins, endothelial cells lining the lumen display a flat cobblestone morphology and cells are orientated in the direction of blood flow (Lee *et al.*, 2008). Blood flow is able to provide a mechanical cue to endothelial cells, which triggers them to align (Poduri *et al.*, 2017). However, it has also been shown that cells can be orientated with the use of aligned electrospun fibres (Liu *et al.*, 2009; Whited and Rylander, 2014a).

These data show that HUVECs, as a model for luminal endothelial can be directed using aligned electrospun PLGA fibres without the need for flow. This alignment was evidence after only 24h, which shows the scaffold substrate provides strong physiological cues guiding cell behaviour during attachment. Cells were not left until confluency as the resulting cell sheet may have detached; however, cells were able to bond together forming monolayer patches across the surface of the scaffolds. This suggests that a single surface monolayer would have been possible, which would be important for any future TEVG lumen. Whited and Rylander, (2014) found that aligned cells that were a result of contact with aligned fibres were more able to resist detachment when subject to flow. This may be due to increased F-actin aiding cell attachment or this could be due to the flatter profile displayed by aligned cells reducing friction between the cells and flow.

The physiologically flat endothelial monolayer is known to help regulate smooth muscle cell behaviour (Lin *et al.*, 2016) and to prevent thrombotic events (Van Hinsbergh, 2012) so it is crucial that we are able to generate TEVGs with a physiologically similar luminal endothelium. Interestingly, it has also been identified that fibre diameter may play a role in the degree of alignment of cells as well as on migration, which could be further assessed in the future (Ahmed *et al.*, 2018). Whited and Rylander, (2014) similarly concluded that smaller fibre diameters enhanced HUVEC alignment on aligned fibres.

VSMC alignment was also highly evident from images stained for actin showing a dramatic different in actin fibre orientation. The alignment of the cells in the direction of the electrospun fibres shows a structure similar to that of a mammalian artery tunica media. Cell-to-cell boundaries were also difficult to detect demonstrating that a VSMC layer can be produced to mimic the vascular Tunic media. This work did not assess the ability of VSMCs to generate multiple layers tissue, which is an important consideration for a vascular media layer as in physiological arteries, this region contains multiple layers of smooth muscle cells.

Fibre alignment from aligned fibre substrates has been attributed to mechanosensing from the cytoskeleton (Discher, Janmey and Wang, 2005), although it has been proposed that the nuclei may also be able to detect changes in substrates independently to the cytoskeleton (McKee *et al.*, 2011). This matches the observations of this thesis whereby the HUVEC and VSMC nuclei were observed to orientate in the direction of the scaffold fibres. It is likely that topological cues leading to enhanced alignment correlate with fundamental changes at the genetic level for genes that regulate the cytoskeleton (Gasiorowski *et al.*, 2010). This is beyond the scope of this work, but would be an area of interest to generate further data elucidating the effect of aligned on cell behaviour. Research such as this could help develop scaffolds that help cells maintain physiologically similar characteristics to their *in vivo* state improving the functionality and patency of future TEVGs.

For randomly aligned fibres it was found that fibre diameter had an effect on cell attachment for HUVECs. To determine if this correlation also extended to fibroblasts two electrospun PLGA scaffolds were fabricated with two fibre diameters. In mammalian arteries, the tunica adventitia consists of collagen and elastic fibres. As these extracellular components cannot be fully replicated *in vitro* it was proposed the host could be used to remodel the adventitial region of the tube to be more physiologically representative of a mammalian artery.

Fibroblasts produce various extracellular matrix components including collagen and elastin, and they are heavily involved in wound healing (Tracy, Minasian and Caterson,

2016). Therefore, it was proposed that a scaffold diameter that enhanced fibroblast attachment could be beneficial during remodelling of a vascular graft. It has been previously shown that 3T3 fibroblasts adhered more successfully to fibres less than 1 μm in diameter (Chen *et al.*, 2007b); however, at this fibre diameter range, pore areas are much smaller than individual fibroblast cells (data shown in Chapter 3; Figure 4.3), which are approximately 10-15 μm. Therefore, fibres with diameters greater than 1 μm were produced to help fabricate scaffolds with large enough pores to help cell infiltration.

These data support the findings by Chen *et al.*, (2007) in that there is a correlation between decreasing fibre diameter and increased fibroblast attachment. Additionally, these data also show that the hSVFs proliferate on both fibre diameters over 4 d, which also supports the conclusions made by Chen *et al.*, (2007). Although the smaller fibre diameter did enhance cell attachment, the larger fibres and resulting larger pore areas showed enhanced cell infiltration. This would need to be further explored to determine the ability of fibroblasts to migrate through scaffolds with larger pore sizes and to understand if this would enhance the production of physiologically relevant extracellular matrix composition.

Further to the ability of scaffold fibre diameter and alignment to help guide cells towards a more physiologically representative morphology, it was of interest to understand whether cells would preferentially adhere to their specific scaffold layer. This would potentially allow for the recruitment of progenitor cells from the blood and surrounding tissue to adhere to the scaffold by being selected for by their preference to a particular fibre diameter and material. It was hypothesised that the smaller PLGA fibre diameter would select for HUVECs out of an even population of HUVECs and hVSMCs. It was also hypothesised that the large PCL fibre scaffolds would select for hVSMCs out of the same population.

HUVECs did adhere more abundantly to the PLGA fibres than hVSMCs, irrespective of media type. However, this may be due to the ability of HUVECs to adhere to the electrospun scaffolds in general when compared to hSMCs, as HUVECs also adhered in similar quantities to the PCL scaffolds. It would be interesting to test further time points

in the future to determine if this trend continued. Furthermore, the co-culture of HUVECs and hVSMCs together may have suppressed the attachment of hVSMCs, although Fillinger *et al.*, (1993) found that endothelial cells actually increased SMC proliferation and that endothelial cells also initially adhered more successfully than SMCs in tissue culture dishes. It is clear that small diameter PLGA fibres of approximately 250 nm enhance initial HUVEC attachment when compared to PCL fibres of approximately 1 μm, whilst hVSMCs adhere in a similar quantity across both scaffolds. Therefore, it can be concluded that HUVECs are selected from a population of both HUVECs and hVSMCs on nano-scaled PLGA fibres, but it is yet to be determine whether this is due to superior attachment capabilities by HUVECs compare to hVSMCs or whether directly related to the fibre diameter. The materials tested in this thesis are limited and this could still be a method in which to select for particular cell types in the future once fibre diameter and material combinations are more broadly tested for their potential select effect on mammalian and human cells. If cells can be selected for by fibre diameter, then this could be used to select for cells in peripheral blood such as endothelial progenitor cells to enhance the ability of a host to generate an autologous luminal epithelium rapidly after implantation. However, this reality remains as speculation until further research is conducted.

The previous work presented in this this thesis shows how mature cell behaviour can be elicited through the use of fibre topography. However, it is difficult to obtain large quantities of cells for populating artificial scaffolds. Therefore, I proposed the use of blood as an autologous cell source that can be used to populate the electrospun tubes for small-diameter vascular graft purposes. Blood contains an abundance of white and red blood cells, which is easily attainable from a small volume of blood. Of primary interest is the large quantity of adherent monocytes that are present in the blood, which would normally adhere to a foreign body inserted *in vivo* such as an artificial scaffold (Anderson, Rodriguez and Chang, 2008). Monocytes have been shown to be able to transdifferentiate into endothelial-like cells (Yan *et al.*, 2017) and it has been proposed that monocytes and macrophages may be able to transdifferentiate into smooth muscle-like cells (Swirski and Nahrendorf, 2014). Therefore, it was hypothesised that macrophages could be transdifferentiated into endothelial and smooth muscle-like cells.

To test this hypothesis, porcine peripheral blood was used due to its accessibility and abundance in comparison to human blood. The porcine peripheral blood was seeded onto each of the separate layers to determine if peripheral blood cells could adhere to the scaffold layers. Adherent blood cells were able to attach to layers 1 and 2 at a similar rate. Contrastingly, far fewer cells were able to adhere to Layer 3. This may have been due to the large fibre diameter resistant adherence or that blood cells migrated through the scaffold via gravity. It is also possible that micro-sized fibres elicit a less active response from immune cells. To determine what quantity of the cells were macrophages, CD203a staining was used, which detects monocyte-derived macrophages (Petersen *et al.*, 2007). This showed that approximately 90% of cells could be considered macrophages demonstrating that monocytes in the blood are activated by the electrospun scaffolds. Although activation could have been initiated by the process of blood collection.

After establishing that porcine blood could be used to derived macrophages that adhere to the electrospun layers, differentiation protocols were used to test whether macrophages could be transdifferentiated to smooth muscle-like and endothelial-like cells. Endothelial differentiated cells showed no difference in the presence of eNOS positive cells after being subjected to differentiation medias containing either Pleiotrophin or a high concentration of VEGF. It is possible that the relatively high presence of eNOS could be attributed to transdifferentiation on the scaffold without the inducement of differentiation media. The lack of distinguishable difference between eNOS positive cells compared to control may be due to the short differentiation period, which could be extended in future work.

These data show that the addition of thrombin was able to significantly increase the number of α-SMA to approximately 14% expression. It is possible that the cells required more time to express α-SMA and that this work could have benefitted from prolonged exposure to differentiation medias. Interestingly, thrombin is not a typical substance used for SMC differentiation but was used in this work due to the emerging believe that the exposure of macrophages to thrombin in luminal thrombi contributes to the increase in smooth muscle cells at these sites. The use of thrombin for smooth muscle cell differentiation was introduced by Martin *et al.*, (2009). For both the differentiation of

macrophages to endothelial-like and smooth muscle-like cells, further investigation into additional markers could also be compared, along with RT-qPCR results that can detect more subtle changes in cell phenotype.

The fibre materials themselves may also exert an effect over cell orientation due to their hydrophobicity and relative stiffness in comparison to mammalian extracellular matrix components. This is especially true for cellular attachment, as it is well observed that components such as fibronectin and collagen enhance cellular attachment through surface protein binding (Xu *et al.*, 2000; Katagiri, Brew and Ingham, 2003).

5.4 Conclusion

This chapter demonstrates that VSMCs and HUVEC are stimulated to orientate with the direction of PCL and PLGA electrospun fibres at a given diameter, respectively. However, further evidence would be required to determine if electrospun fibre diameter alone could be used to select for specific cell populations. Finally, this chapter suggests that it may be feasible to transdifferentiate macrophages into smooth muscle-like cells for a potential autologous cell source for TEVGs.

6

GENERAL DISCUSSION

6.1 Thesis Summary

In this thesis, I set out to explore the feasibility of using electrospinning as a means to develop a physiologically relevant TEVG from note only an academic standpoint, but also from the perspective of clinical translation. Although the development of a TEVG and the field of tissue engineering are of particular focus in clinical medicine today, the role of this thesis was to understand the relatively less well understood effect of electrospun fibre diameters on cellular attachment, with regard to vascular cells.

As one of the main drivers of TEVG failure is occlusion from early thrombus formation, it is prudent to develop TEVGs that do not trigger thrombus formation (Burkel *et al.*, 1981; Eslami *et al.*, 2001). It is well known that luminal endothelial cells help prevent thrombus formation and are likely an essential component to a TEVG (Meinhart, Deutsch and Zilla, 1997; Deutsch *et al.*, 2009). Therefore, the ability to enhance attachment and the support of endothelial cells *in vitro* could help towards developing a TEVG with a functional luminal endothelium, which may in turn reduce the risk of thrombosis *in vivo*. The electrospinning process is the only current manufacturing technique capable of producing fibres in the low nanometre range, which enables the creation of structures more comparable to the mammalian ECM than other available technologies. The literature also contained a small number of studies that suggested electrospun fibre diameter had an effect on cell attachment, though no studies were identified to confirm this for TEVG purposes (Chen *et al.*, 2007b, 2009; Liu *et al.*, 2009). The published studies also had contrasting results, which may have been due to the use of different cells types and electrospun materials. This stimulated the exploration into the effect of electrospun fibre diameter on endothelial cell attachment in Chapter 3.

Chapter 3 was concerned with understanding the effect of fibre diameter on endothelial cell attachment, with the hypothesis that smaller fibre diameters would enhance HUVEC adherence. In order to test this hypothesis, electrospinning methods had to be developed and optimised, which preceded the finding that NaOAc effectively dissolves in HFIP and has a significant effect upon electrospun PLGA fibre diameter. This finding made it possible to produce a variety of fibre diameters for further testing; however, it's

significant to the field may be overshadowed by the environmental and economical related to the use of HFIP. Nevertheless, the ability to drastically reduce and more accurately tailor fibre diameters will assist further research into the effect of fibre diameter of cell-to-scaffold interactions.

Chapter 3 confirmed the hypothesis that HUVECs adhered more successfully to fibre diameters of less than 1 μm. These data suggest that fibre diameter needs to be considered when developing a TEVG using the electrospinning technique as this may have implications for TEVGs being pre-seeded with endothelial cells. The demonstration that fibre diameter can affect cell attachment also has wider implications regarding the host immune response to implanted TEVGs, as the enhanced attachment of immune cells for example may not be desirable. The effect of fibre diameter may also not be limited to enhanced cellular attachment, and further work to understand the role of fibre diameter in cell-to-scaffold interactions in greater depth would be beneficial to this field of research. Elucidation of whether smaller diameter fibres enhance more physiologically relevant endothelial cell populations, such as arterial endothelia, would provide a greater contribution to the current field by helping suggest that there is a clinically translatable benefit to producing a TEVG with fibre diameters that support physiologically representative endothelial cell populations, unlike the limited translational benefit of the results demonstrated in this thesis of enhanced HUVEC attachment. It also remains to be determined whether this effect is observed for other electrospun materials that may be desirable for use in a TEVG.

In Chapter 4, the developmental process of developing a tri-layered electrospun tube was outlined. The specific mechanical environments within each layer of a blood vessel support their respective cell types and help ensure homeostasis. Therefore, this chapter aimed to develop specific layers within a TEVG that may have the potential to enhance the attachment of vascular cells and maintain physiologically relevant morphologies. To create a multi-layered vessel, novel methodologies and custom-built collectors had to be developed, which in turn led to the discovery that fibre alignment, in the experiments conducted within this thesis, was dependent on linear velocity/G-force as opposed to RPM, which is the most commonly used unit found in the literature. Practically, this

subtlety may have limited implications for wider electrospinning work with the development of flat sheets, as large drum rollers are usually employed for their increased surface area. Whereas for work requiring circumferential alignment for small diameter tube applications, the results presented in thesis suggest a specialist high speed motor will be required. However, research requiring circumferential aligned fibre tubes may be limited and the development of TEVGs may gain the most benefit from this knowledge. It is also possible to find some studies referring to linear velocity suggesting this distinction is understood (Qi *et al.*, 2010; Kiselev and Rosell-Llompart, 2012).

A major outcome from Chapter 4 was the development of an optimised collector and electrospinning set up for the generation of axially aligned fibre tubes. Although, air gaps between collectors and the development of axially aligned fibre tubes are not novel in themselves, the optimisation of the adapted collector and methodology presented in this thesis provide a framework for the production of small diameter tubes with highly aligned fibres that could aid future work into the suitability of aligned fibre tubes for TEVGs. It is likely that other materials suitable for electrospinning could also be used in place of PLGA for axially aligned fibre tubes, which could be of interest to future research in the field. However, the main outcome from Chapter 4 was the development of a tri-layered electrospun tube, which has not previously been identified in the current literature. Whether a central layer with limited contact to the external environment would be able to confer any biological benefit to a multi-layered scaffold remains to be determined. It is possible that a central PCL layer could enhance overall TEVG burst strength, providing a clinical benefit, but this suggestion would need to be empirically tested in the future and did not fall under the scope of work presented in this thesis. Chapter 4 has provided proof-of-concept for the development of a tri-layered tubular scaffold designed for TEVG purposes, and future research will be required to understand if there are any clinical benefits to this approach. As the process to develop the tri-layered graft was labour intensive, improved processing methods would also be required for any large-scale commercial development.

Finally, Chapter 5 sought to investigate the ability of each layer to support representative cells types of those found in the layers of a mammalian blood vessel. This resulted in the

confirmation that highly aligned electrospun fibres promote cellular alignment in both HUVECs and VSMCs in static conditions. This suggests that aligned fibres may be more suitable for construction of a TEVG luminal surface as aligned luminal endothelial cells would be more characteristics of those found in a mammalian vessel. The alignment of endothelial cells may also result in a flatter cell layer, thus reducing friction between the luminal wall and blood flow, which could reduce the risk of thrombus formation. However, further research would be required to determine if more physiologically relevant arterial endothelial cells align on highly orientated PLGA fibres and if this results in a more physiologically desirable phenotype, which would likely be required for any clinical benefit to be observed. The finding that VSMCs align on highly orientated fibres also supports the development of an electrospun layer of circumferentially aligned fibres, as this would also move towards developing a structure more physiologically similar to a native blood vessel. A potential clinical benefit from circumferentially aligned VSMCs could be in their ability to potential provide additional strength to the TEVG wall to resist hydrostatic forces from flow. However, to determine if circumferentially aligned VSMCs on a PCL electrospun scaffold confer any clinical benefits, extensive further research would be required.

The outer layer, designed to enhance cellular infiltration into the scaffold, proved to require further research. It is well established that although electrospun scaffolds have high porosity, the size of the pores and the interconnectivity between pores is insufficient for adequate mammalian cell infiltration. Data presented in Chapter 5 is consistent with the literature as there was limited evidence suggested SVFs were able to effectively enter the scaffolds. However, the scope of experimental work into the ability of cells to infiltrate the tri-layered scaffold were limited to basic observations only in this thesis and would require further research. Additionally, Chapter 5 also briefly explored whether endothelial and VSMCs would preferentially attach to their respective scaffold layer, to help preliminarily assess whether the effect of fibre diameter on cell attachment was cell specific. However, the results presented in this thesis suggest that HUVECs adhere more successfully to both PCL and PLGA scaffolds of different fibre sizes, and more successfully adhere to both scaffold types compared to VSMCs. This may be due to HUVECs being able

to grow successfully across a range of surfaces and substrates, which may not be indicative of more physiologically relevant vascular endothelial cells.

Although this thesis assumed any future TEVG would be developed using pre-seeded layers, the clinical application of pre-seeded grafts incorporated with mature vascular cells may not be possible due to the limited growth and availability of vascular cells, and the impact of *ex vivo* culture on cell phenotypes (Tawab *et al.*, 2009; Neumann *et al.*, 2010; Mouriaux *et al.*, 2016; Islam *et al.*, 2017). Therefore, Chapter 5 also briefly explored the use of peripheral blood for cellular seeding due to its relatively high availability and emerging evidence suggesting the possibility of monocyte transdifferentiation into endothelial-like and smooth muscle cell-like cells (Ninomiya *et al.*, 2006; Sharifi *et al.*, 2006; Yan *et al.*, 2017). This idea would require further work to determine the feasibility of this approach and there may be limitations to the number of transdifferentiated cells that can be obtained, as well as any potential adverse effects caused from the culture of peripheral blood cells *ex vivo*. However, the inclusion of this approach was presented in this thesis to help stimulate future research into viable cell sources for TEVGs.

TEVG research is still in its infancy and requires a multidisciplinary approach, which is reflective of the work shown in this thesis. It is crucial to understand how cells interact and are affected by structures and materials at a micro and nano-scale to fully be able to develop bottom-up scaffolds that direct cell behaviour to ensure a positive outcome for implanted TEVGs.

6.2 Conclusion

In summary, the research presented in this thesis used a multidisciplinary approach to explore the feasibility of producing a TEVG for clinical use through the development of a tri-layered electrospun tubular scaffold for further mechanical and cellular testing. This thesis has identified the importance of substrate topography in regard to fibrous scaffolds on cellular attachment and has demonstrated the feasibility of producing a tri-layered electrospun tubular scaffold with topographically distinct layers. The results contained within this thesis help support the use of electrospun scaffolds for further research into

the development of a clinically viable TEVG due to the versatility of the technique to produce more physiologically relevant fibre diameters than other existing technologies to mimic the mammalian ECM, within a multi-layered structure comparable to that of a mammalian artery.

This thesis has also highlighted the challenges involved in the execution of a multidisciplinary project, such as cross-discipline collaboration, a strong academic understanding of all cross-disciplines, and the need to tackle explore experimental questions from a broader perspective than is academically traditional. This thesis highlights the value of conducting multidisciplinary research due to the need for consideration, at each stage, of the feasibility of each project element for potential translation into clinical practice. For example, well perfuming electrospun flat sheet layers at the basic research stage may not be feasibly constructed into a functional 3D TEVG. The development of a clinically successful TEVG will likely require an approach utilising a range of academic disciplines and effective collaboration between such disciplines.

6.2.1 Future Experimental Work

The main focus of the experimental work presented in this thesis was based on the development of electrospun scaffolds for further biological testing. Although the electrospinning outcomes within this thesis were successfully achieved, further work to further understand the cell-to-scaffold interactions between vascular cells and each scaffold layer, and the multi-layered tube would be desirable.

Firstly, although the work presented in Chapter 3 of this thesis demonstrated that HUVECs initially adhered to smaller diameter PLGA fibres, it would be prudent to determine if this trend continued with smaller diameter fibres, and understand the lower limit of average fibres diameter within this electrospinning system. As electrospun fibre diameters have been reported to be as low as 10nm (reference), it is reasonable to postulate that an average fibre diameter below 250nm could be achieved with further experimentation. Whether an electrospun PLGA scaffold with an average diameter of

10nm would have the structural integrity to support cells could also be elucidated during this investigation.

Although cellular attachment is an indicator of scaffold biocompatibility, more extensive data regarding cell phenotype over time course experiments would provide greater detail as to the ability of a scaffold to support phenotypically healthy cells. More appropriate cell models could be used for this work such as arterial endothelial cells and it would be beneficial to understand what changes occur to cellular protein expression in vascular cells that are interacting with the electrospun scaffolds. For example, changes to the expression of arterial endothelial cell-specific proteins may help indicate the suitability of a particular scaffold to support cells with a healthy phenotype, which could affect the patency of a future TEVG.

An additional crucial area for investigation would be the structural properties of a tri-layered tubular scaffold. It is essential that any TEVG could withstand being exposed to the pressure and flow of the coronary arterial environment. Basic strength testing, alongside stress testing within a bioreactor could help determine the suitability of a tri-layered scaffold for translation into the clinic. Furthermore, degradation profiling of the scaffold *in vivo* would also be an important area of scientific enquiry.

Finally, this thesis demonstrated the ability of peripheral blood cells to adhere to each electrospun fibre layer. Future work would be necessary to determine whether monocytes are able to transdifferentiate effectively into endothelial-like and smooth muscle cell-like cells on electrospun scaffolds for use as an autologous cell source. Concomitantly, research into effect of peripheral blood interacting with an electrospun TEVG may also help identify ways to tailor TEVG degradation and remodelling, and reduce the risk of graft failure. This thesis provides support that electrospinning may be a suitable approach for the development of future TEVGs.

7

REFERENCE LIST

Acharya, M., Arumugam, G. K. and Heiden, P. A. (2008) 'Dual electric field induced alignment of electrospun nanofibers', *Macromolecular Materials and Engineering*. doi: 10.1002/mame.200800053.

Adomavičiūtė, E. and Milašius, R. (2007) 'The Influence of Applied Voltage on Poly(vinyl alcohol) (PVA) Nanofibre Diameter', *Fibres & Textiles in Eastern Europe*.

Adomavičiute, E. and Stanys, S. (2011) 'Formation of Electrospun PVA mats on different types of support materials using various kinds of grounded electrodes', *Fibres and Textiles in Eastern Europe*.

Ahmed, M. *et al.* (2018) 'Geometric constraints of endothelial cell migration on electrospun fibres', *Scientific Reports*. doi: 10.1038/s41598-018-24667-7.

Akduman, Ç., Kumabasar, E. P. A. and Çay, A. (2014) *Effect of molecular weight on the morphology of electrospun poly (vinyl alcohol) nanofibers*, *XIII th International Izmir Textile and Apparel Symposium*.

Al-Shammari, B. *et al.* (2011) 'The effect of polymer concentration and temperature on the rheological behavior of metallocene linear low density polyethylene (mLLDPE) solutions', *Journal of King Saud University - Engineering Sciences*. doi: 10.1016/j.jksues.2010.07.001.

Alfaro De Prá, M. A. *et al.* (2017) 'Effect of collector design on the morphological properties of polycaprolactone electrospun fibers', *Materials Letters*. doi: 10.1016/j.matlet.2017.01.102.

Allaire, E. and Clowes, A. W. (1997) 'Endothelial cell injury in cardiovascular surgery: The intimal hyperplastic response', *Annals of Thoracic Surgery*. doi: 10.1016/S0003-4975(96)01045-4.

Anderson, J. M., Rodriguez, A. and Chang, D. T. (2008) 'Foreign body reaction to biomaterials', *Seminars in Immunology*. doi: 10.1016/j.smim.2007.11.004.

Anderson, J. M. and Shive, M. S. (2012) 'Biodegradation and biocompatibility of PLA and PLGA microspheres', *Advanced Drug Delivery Reviews*. doi: 10.1016/j.addr.2012.09.004.

Aniagyei, S. E. *et al.* (2017) 'Evaluation of poly(lactic-co-glycolic acid) and poly(DL-lactide-co-ε-caprolactone) electrospun fibers for the treatment of HSV-2 infection', *Materials Science and Engineering C*. doi: 10.1016/j.msec.2016.11.029.

Arayanarakul, K. *et al.* (2006) 'Effects of poly(ethylene glycol), inorganic salt, sodium dodecyl sulfate, and solvent system on electrospinning of poly(ethylene oxide)', *Macromolecular Materials and Engineering*. doi: 10.1002/mame.200500419.

Ardanaz, N. and Pagano, P. J. (2006) 'Hydrogen peroxide as a paracrine vascular mediator: Regulation and signaling leading to dysfunction', *Experimental Biology and Medicine*. doi: 10.1177/153537020623100302.

Arras, M. M. L. *et al.* (2012) 'Electrospinning of aligned fibers with adjustable orientation using auxiliary electrodes', *Science and Technology of Advanced Materials*, 13(3). doi: 10.1088/1468-6996/13/3/035008.

Artel, A. *et al.* (2011) 'An agent-based model for the investigation of neovascularization within porous scaffolds', *Tissue Engineering - Part A*. doi: 10.1089/ten.tea.2010.0571.

Aviss, K. J., Gough, J. E. and Downes, S. (2010) 'Aligned electrospun polymer fibres for skeletal muscle regeneration', *European Cells and Materials*, 19, pp. 193–204. doi: vol019a19 [pii].

Ayres, C. *et al.* (2006) 'Modulation of anisotropy in electrospun tissue-engineering scaffolds: Analysis of fiber alignment by the fast Fourier transform', *Biomaterials*. doi:

10.1016/j.biomaterials.2006.06.014.

Bacakova, L. *et al.* (2007) 'Adhesion and growth of vascular smooth muscle cells in cultures on bioactive RGD peptide-carrying polylactides', *Journal of Materials Science: Materials in Medicine*, 18, pp. 1317–1323. doi: 10.1007/s10856-006-0074-1.

Bacakova, L. *et al.* (2018) 'The Role of Vascular Smooth Muscle Cells in the Physiology and Pathophysiology of Blood Vessels', in *Muscle Cell and Tissue - Current Status of Research Field*. InTech. doi: 10.5772/intechopen.77115.

Bačáková, L. *et al.* (2004) 'Cell Adhesion on Artificial Materials for Tissue Engineering', *Physiological Research*.

Badami, A. S. *et al.* (2006) 'Effect of fiber diameter on spreading, proliferation, and differentiation of osteoblastic cells on electrospun poly(lactic acid) substrates', *Biomaterials*, 27, pp. 596–606. doi: 10.1016/j.biomaterials.2005.05.084.

Bai, F. *et al.* (2011) 'The effect of pore size on tissue ingrowth and neovascularization in porous bioceramics of controlled architecture in vivo', *Biomedical Materials*. doi: 10.1088/1748-6041/6/1/015007.

Baker, B. M. *et al.* (2009) 'Fabrication and Modeling of Dynamic Multipolymer Nanofibrous Scaffolds', *Journal of Biomechanical Engineering*, 131(10), p. 101012. doi: 10.1115/1.3192140.

Balguid, A. *et al.* (2009) 'Tailoring fiber diameter in electrospun poly(ε-Caprolactone) scaffolds for optimal cellular infiltration in cardiovascular tissue engineering', *Tissue Engineering - Part A*. doi: 10.1089/ten.tea.2007.0294.

Bashur, C. A., Dahlgren, L. A. and Goldstein, A. S. (2006) 'Effect of fiber diameter and orientation on fibroblast morphology and proliferation on electrospun poly(d,l-lactic-co-

glycolic acid) meshes', *Biomaterials*, 27(33), pp. 5681–5688. doi: 10.1016/j.biomaterials.2006.07.005.

Baudequin, T. *et al.* (2017) 'The osteogenic and tenogenic differentiation potential of C3H10T1/2 (mesenchymal stem cell model) cultured on PCL/PLA electrospun scaffolds in the absence of specific differentiation medium', *Materials*, 10(12). doi: 10.3390/ma10121387.

BCcampus (2012) *20.1 Structure and Function of Blood Vessels – Anatomy and Physiology*, *ANATOMY AND PHYSIOLOGY*.

Beachley, V. and Wen, X. (2009) 'Effect of electrospinning parameters on the nanofiber diameter and length', *Materials Science and Engineering C*, 29, pp. 663–668. doi: 10.1016/j.msec.2008.10.037.

Bentley, K., Philippides, A. and Ravasz Regan, E. (2014) 'Do endothelial cells dream of eclectic shape?', *Developmental Cell*. doi: 10.1016/j.devcel.2014.03.019.

Bhattarai, D. P. *et al.* (2018) 'A review on properties of natural and synthetic based electrospun fibrous materials for bone tissue engineering', *Membranes*. doi: 10.3390/membranes8030062.

Bonani, W. *et al.* (2012) 'Biomolecule gradient in micropatterned nanofibrous scaffold for spatiotemporal release', *Langmuir*, 28(38), pp. 13675–13687. doi: 10.1021/la302386u.

Braghirolli, D. I. *et al.* (2014) 'The effect of sterilization methods on electronspun poly(lactide-co-glycolide) and subsequent adhesion efficiency of mesenchymal stem cells', *Journal of Biomedical Materials Research - Part B Applied Biomaterials*. doi: 10.1002/jbm.b.33049.

Bruyneel, A. A. N. and Carr, C. A. (2017) 'Ambiguity in the Presentation of Decellularized

Tissue Composition: The Need for Standardized Approaches', *Artificial Organs*. doi: 10.1111/aor.12838.

Burkel, W. E. *et al.* (1981) 'Sequential studies of healing in endothelial seeded vascular prostheses: Histologic and ultrastructure characteristics of graft incorporation', *Journal of Surgical Research*. doi: 10.1016/0022-4804(81)90165-7.

Burton, T. P., Corcoran, A. and Callanan, A. (2017) 'The effect of electrospun polycaprolactone scaffold morphology on human kidney epithelial cells', *Biomedical Materials*, 13(1), p. 015006. doi: 10.1088/1748-605X/aa8dde.

Butler, H. G., Baker, L. D. and Johnson, J. M. (1977) 'Vascular access for chronic hemodialysis: Polytetrafluoroethylene (PTFE) versus bovine heterograft', *The American Journal of Surgery*. doi: 10.1016/0002-9610(77)90326-9.

Canham, P. B., Finlay, H. M. and Boughner, D. R. (1997) 'Contrasting structure of the saphenous vein and internal mammary artery used as coronary bypass vessels', *Cardiovascular Research*. doi: 10.1016/S0008-6363(97)00056-4.

Carroll, C. P. and Joo, Y. L. (2006) 'Electrospinning of viscoelastic Boger fluids: Modeling and experiments', *Physics of Fluids*. doi: 10.1063/1.2200152.

Casper, C. L. *et al.* (2004) 'Controlling surface morphology of electrospun polystyrene fibers: Effect of humidity and molecular weight in the electrospinning process', *Macromolecules*. doi: 10.1021/ma0351975.

Catto, V. *et al.* (2014) 'Vascular Tissue Engineering: Recent Advances in Small Diameter Blood Vessel Regeneration', *ISRN Vascular Medicine*, 2014, pp. 1–27. doi: 10.1155/2014/923030.

Cengiz, F. and Jirsak, O. (2009) 'The effect of salt on the roller electrospinning of

polyurethane nanofibers', *Fibers and Polymers*. doi: 10.1007/s12221-009-0177-7.

Chemla, E. S. and Morsy, M. (2009) 'Randomized clinical trial comparing decellularized bovine ureter with expanded polytetrafluoroethylene for vascular access', *British Journal of Surgery*. doi: 10.1002/bjs.6434.

Chen, M. *et al.* (2007a) 'Role of fiber diameter in adhesion and proliferation of NIH 3T3 fibroblast on electrospun polycaprolactone scaffolds', *Tissue Engineering*. doi: 10.1089/ten.2006.0205.

Chen, M. *et al.* (2007b) 'Role of Fiber Diameter in Adhesion and Proliferation of NIH 3T3 Fibroblast on Electrospun Polycaprolactone Scaffolds', *Tissue Engineering*, 13(3), pp. 579–587. doi: 10.1089/ten.2006.0205.

Chen, M. *et al.* (2009) 'Role of Electrospun fiber diameter and corresponding specific surface area (SSA) on cell attachment', *Journal of tissue engineering and regenerative medicine*, 3, pp. 269–279. doi: 10.1002/term.163.

Chew, S. Y. *et al.* (2007) 'Aligned protein-polymer composite fibers enhance nerve regeneration: A potential tissue-engineering platform', *Advanced Functional Materials*. doi: 10.1002/adfm.200600441.

Cho, S. W. *et al.* (2005) 'Small-diameter blood vessels engineered with bone marrow-derived cells', *Annals of Surgery*. doi: 10.1097/01.sla.0000154268.12239.ed.

Choi, B. G. *et al.* (2016) 'Impact of cigarette smoking: A 3-Year clinical outcome of vasospastic angina patients', *Korean Circulation Journal*. doi: 10.4070/kcj.2016.46.5.632.

Choi, J. S. *et al.* (2004) 'Effect of organosoluble salts on the nanofibrous structure of electrospun poly(3-hydroxybutyrate-co-3-hydroxyvalerate)', *International Journal of Biological Macromolecules*. doi: 10.1016/j.ijbiomac.2004.06.001.

Choi, J. S. *et al.* (2008) 'The influence of electrospun aligned poly(ε-caprolactone)/collagen nanofiber meshes on the formation of self-aligned skeletal muscle myotubes', *Biomaterials*. doi: 10.1016/j.biomaterials.2008.03.031.

Chou, S. F. and Woodrow, K. A. (2017) 'Relationships between mechanical properties and drug release from electrospun fibers of PCL and PLGA blends', *Journal of the Mechanical Behavior of Biomedical Materials*. doi: 10.1016/j.jmbbm.2016.09.004.

Collins, G. *et al.* (2012) 'Charge generation, charge transport, and residual charge in the electrospinning of polymers: A review of issues and complications', *Journal of Applied Physics*. doi: 10.1063/1.3682464.

Corin, K. A. and Gibson, L. J. (2010) 'Cell contraction forces in scaffolds with varying pore size and cell density', *Biomaterials*. doi: 10.1016/j.biomaterials.2010.01.149.

Cortez Tornello, P. R. *et al.* (2014) 'Structural characterization of electrospun micro/nanofibrous scaffolds by liquid extrusion porosimetry: A comparison with other techniques', *Materials Science and Engineering C*. doi: 10.1016/j.msec.2014.04.065.

Cortez Tornello, P. R. *et al.* (2018) 'Electrospun scaffolds with enlarged pore size: Porosimetry analysis', *Materials Letters*. doi: 10.1016/j.matlet.2018.05.072.

Cuminetti, G. *et al.* (2017) 'Contemporary use of arterial and venous conduits in coronary artery bypass grafting: Anatomical, functional and clinical aspects', *Netherlands Heart Journal*. doi: 10.1007/s12471-016-0919-2.

Cummings, I. *et al.* (2012) 'Tissue-engineered vascular graft remodeling in a growing lamb model: Expression of matrix metalloproteinases', *European Journal of Cardio-thoracic Surgery*. doi: 10.1016/j.ejcts.2011.02.077.

Dai, L., Zhang, Y. and Ou-Yang, Z. C. (2003) 'Elastic theory of single spider silk protein

molecule', in *Thin Solid Films*. doi: 10.1016/S0040-6090(03)00777-6.

Dal-Secco, D. *et al.* (2015) 'A dynamic spectrum of monocytes arising from the in situ reprogramming of CCR2^{+} monocytes at a site of sterile injury', *Journal of Experimental Medicine*. doi: 10.1084/jem.20141539.

Dan Li *et al.* (2003) 'Electrospinning of Polymeric and Ceramic Nanofibers as Uniaxially Aligned Arrays', *Nano Letters*. doi: 10.1021/NL0344256.

Deitzel, J. M. *et al.* (2001) 'The effect of processing variables on the morphology of electrospun nanofibers and textiles', *Polymer*. doi: 10.1016/S0032-3861(00)00250-0.

van Det, R. J. *et al.* (2009) 'Dacron or ePTFE for Femoro-popliteal Above-Knee Bypass Grafting: Short- and Long-term Results of a Multicentre Randomised Trial', *European Journal of Vascular and Endovascular Surgery*. doi: 10.1016/j.ejvs.2008.11.041.

Deutsch, M. *et al.* (2009) 'Long-term experience in autologous in vitro endothelialization of infrainguinal ePTFE grafts', *Journal of Vascular Surgery*. doi: 10.1016/j.jvs.2008.08.101.

Dewey, C. F. *et al.* (1981) 'The dynamic response of vascular endothelial cells to fluid shear stress', *Journal of Biomechanical Engineering*. doi: 10.1115/1.3138276.

Dimitriadis, K. *et al.* (2016) 'Waist circumference compared with other obesity parameters as determinants of coronary artery disease in essential hypertension: A 6-year follow-up study', *Hypertension Research*. doi: 10.1038/hr.2016.8.

Ding, W. *et al.* (2010) 'Manipulated electrospun PVA nanofibers with inexpensive salts', *Macromolecular Materials and Engineering*. doi: 10.1002/mame.201000188.

Discher, D. E., Janmey, P. and Wang, Y. L. (2005) 'Tissue cells feel and respond to the

stiffness of their substrate', *Science*. doi: 10.1126/science.1116995.

Dodge, J. T. *et al.* (1992) 'Lumen diameter of normal human coronary arteries: Influence of age, sex, anatomic variation, and left ventricular hypertrophy or dilation', *Circulation*. doi: 10.1161/01.CIR.86.1.232.

Dohmen, P. M. *et al.* (2014) 'Successful implantation of a decellularized equine pericardial patch into the systemic circulation.', *Medical science monitor basic research*, 20, pp. 1–8. doi: 10.12659/MSMBR.889915.

Doshi, J. and Reneker, D. H. (1995) 'Electrospinning process and applications of electrospun fibers', *Journal of Electrostatics*. doi: 10.1016/0304-3886(95)00041-8.

Druecke, D. *et al.* (2004) 'Neovascularization of poly(ether ester) block-copolymer scaffolds in vivo: Long-term investigations using intravital fluorescent microscopy', *Journal of Biomedical Materials Research - Part A*. doi: 10.1002/jbm.a.20016.

Durand, E. *et al.* (2004) 'In vivo induction of endothelial apoptosis leads to vessel thrombosis and endothelial denudation: A clue to the understanding of the mechanisms of thrombotic plaque erosion', *Circulation*, 109, pp. 2503–2506. doi: 10.1161/01.CIR.0000130172.62481.90.

Eda, G., Liu, J. and Shivkumar, S. (2007) 'Solvent effects on jet evolution during electrospinning of semi-dilute polystyrene solutions', *European Polymer Journal*. doi: 10.1016/j.eurpolymj.2007.01.003.

Eichhorn, Stephen J and Sampson, W. W. (2005) 'Statistical geometry of pores and statistics of porous nanofibrous assemblies.', *Journal of the Royal Society, Interface / the Royal Society*, 2, pp. 309–318. doi: 10.1098/rsif.2005.0039.

Eichhorn, Stephen J. and Sampson, W. W. (2005) 'Statistical geometry of pores and

statistics of porous nanofibrous assemblies', *Journal of the Royal Society Interface*. doi: 10.1098/rsif.2005.0039.

Errico, C. *et al.* (2011) 'Polymeric nanostructured items electrospun on a cylindrical template: a simple procedure for their removal', *Polymer International*, 60(8), pp. 1162–1166. doi: 10.1002/pi.3060.

Eslami, M. H. *et al.* (2001) 'Monocyte adhesion to human vein grafts: A marker for occult intraoperative injury?', *Journal of Vascular Surgery*. doi: 10.1067/mva.2001.118590.

Feng, B. *et al.* (2015) 'Effect of inhomogeneity of the electrospun fibrous scaffolds of gelatin/polycaprolactone hybrid on cell proliferation', *Journal of Biomedical Materials Research - Part A*, 103(2), pp. 431–438. doi: 10.1002/jbm.a.35184.

Filatov, Y., Budyka, A. and Kirichenko, V. (2007) *Electrospinning of micro-and nanofibers : fundamentals and applications in separation and filtration processes*. Begell House. Available at: http://www.begellhouse.com/books/259d705b1b5449e7.html (Accessed: 4 June 2018).

Fillinger, M. F. *et al.* (1993) 'The effect of endothelial cell coculture on smooth muscle cell proliferation.', *Journal of vascular surgery*. Elsevier, 17(6), pp. 1058–67; discussion 1067-8. doi: 10.1016/0741-5214(93)90676-D.

FitzGibbon, G. M. *et al.* (1996) 'Coronary bypass graft fate and patient outcome: Angiographic follow-up of 5,065 grafts related to survival and reoperation in 1,388 patients during 25 years', *Journal of the American College of Cardiology*, 28, pp. 616–626. doi: 10.1016/S0735-1097(96)00206-9.

Fu, W. J. *et al.* (2012) 'New ureteral scaffold constructed with composite poly(L-lactic acid)-collagen and urothelial cells by new centrifugal seeding system', *Journal of Biomedical Materials Research - Part A*. doi: 10.1002/jbm.a.34134.

Fukui, T. *et al.* (2010) 'Graft Selection and One-Year Patency Rates in Patients Undergoing Coronary Artery Bypass Grafting', *Annals of Thoracic Surgery*. doi: 10.1016/j.athoracsur.2010.02.016.

Furchgott, R. F. and Zawadzki, J. V. (1980) 'The obligatory role of endothelial cells in the relaxation of arterial smooth muscle by acetylcholine', *Nature*. doi: 10.1038/288373a0.

Gasiorowski, J. Z. *et al.* (2010) 'Alterations in gene expression of human vascular endothelial cells associated with nanotopographic cues', *Biomaterials*. doi: 10.1016/j.biomaterials.2010.08.026.

Geng, X., Kwon, O. H. and Jang, J. (2005) 'Electrospinning of chitosan dissolved in concentrated acetic acid solution', *Biomaterials*. doi: 10.1016/j.biomaterials.2005.01.066.

Gnavi, S. *et al.* (2015) 'The effect of electrospun gelatin fibers alignment on schwann cell and axon behavior and organization in the perspective of artificial nerve design', *International Journal of Molecular Sciences*, 16(6), pp. 12925–12942. doi: 10.3390/ijms160612925.

Goldman, S. *et al.* (2004) 'Long-term patency of saphenous vein and left internal mammary artery grafts after coronary artery bypass surgery: results from a Department of Veterans Affairs Cooperative Study', *J Am Coll Cardiol*, 44, pp. 2149–2156. doi: 10.1016/j.jacc.2004.08.064.

Grogan, S. P. *et al.* (2014) 'Influence of cartilage extracellular matrix molecules on cell phenotype and neocartilage formation.', *Tissue engineering. Part A*, 20, pp. 264–74. doi: 10.1089/ten.TEA.2012.0618.

Gu, X. *et al.* (2014) 'Electrospinning of poly(butylene-carbonate): Effect of solvents on the properties of the nanofibers film', *International Journal of Electrochemical Science*.

Gupta, B., Revagade, N. and Hilborn, J. (2007) 'Poly(lactic acid) fiber: An overview', *Progress in Polymer Science (Oxford)*. doi: 10.1016/j.progpolymsci.2007.01.005.

Hahn, M. S. *et al.* (2007) 'Physiologic pulsatile flow bioreactor conditioning of poly(ethylene glycol)-based tissue engineered vascular grafts', *Annals of Biomedical Engineering*. doi: 10.1007/s10439-006-9099-3.

Han, D. G. *et al.* (2019) 'Optimization of electrospun poly(caprolactone) fiber diameter for vascular scaffolds to maximize smooth muscle cell infiltration and phenotype modulation', *Polymers*. doi: 10.3390/polym11040643.

Harley, B. A. *et al.* (2007) 'A new technique for calculating individual dermal fibroblast contractile forces generated within collagen-GAG scaffolds', *Biophysical Journal*. doi: 10.1529/biophysj.106.095471.

Harrington, J. K. *et al.* (2011) 'Determining the fate of seeded cells in venous tissue-engineered vascular grafts using serial MRI', *The FASEB Journal*, pp. 4150–4161. doi: 10.1096/fj.11-185140.

He, W. *et al.* (2009) 'Tubular nanofiber scaffolds for tissue engineered small-diameter vascular grafts', *Journal of Biomedical Materials Research - Part A*, 90, pp. 205–216. doi: 10.1002/jbm.a.32081.

Hekmati, A. H. *et al.* (2013) 'Effect of needle length, electrospinning distance, and solution concentration on morphological properties of polyamide-6 electrospun nanowebs', *Textile Research Journal*. doi: 10.1177/0040517512471746.

Helmus, M. N., Gibbons, D. F. and Cebon, D. (2008) 'Biocompatibility: meeting a key functional requirement of next-generation medical devices.', *Toxicologic pathology*, 36, pp. 70–80. doi: 10.1177/0192623307310949.

Henriques, C. *et al.* (2009) 'A systematic study of solution and processing parameters on nanofiber morphology using a new electrospinning apparatus', in *Journal of Nanoscience and Nanotechnology*. doi: 10.1166/jnn.2009.NS27.

Heydarkhan-Hagvall, S. *et al.* (2008) 'Three-dimensional electrospun ECM-based hybrid scaffolds for cardiovascular tissue engineering', *Biomaterials*. doi: 10.1016/j.biomaterials.2008.03.034.

Hibino, N. *et al.* (2015) 'The innate immune system contributes to tissue-engineered vascular graft performance', *FASEB Journal*. doi: 10.1096/fj.14-268334.

Van Hinsbergh, V. W. M. (2012) 'Endothelium - Role in regulation of coagulation and inflammation', *Seminars in Immunopathology*. doi: 10.1007/s00281-011-0285-5.

Hohman, M. M. *et al.* (2001) 'Electrospinning and electrically forced jets. I. Stability theory', *Physics of Fluids*. doi: 10.1063/1.1383791.

Hopkins, R. A. *et al.* (2014) 'Pulmonary arterioplasty with decellularized allogeneic patches', *Annals of Thoracic Surgery*, 97, pp. 1407–1412. doi: 10.1016/j.athoracsur.2013.12.005.

Hotaling, N. A. *et al.* (2015) 'DiameterJ: A validated open source nanofiber diameter measurement tool', *Biomaterials*. doi: 10.1016/j.biomaterials.2015.05.015.

Hu, H. *et al.* (2015) 'Entanglements in marginal solutions: a means of tuning pre-aggregation of conjugated polymers with positive implications for charge transport', *Journal of Materials Chemistry C*. doi: 10.1039/c5tc01425e.

Hu, Y. *et al.* (2004) 'Abundant progenitor cells in the adventitia contribute to atherosclerosis of vein grafts in ApoE-deficient mice', *Journal of Clinical Investigation*. doi: 10.1172/JCI19628.

Humphrey, J. D., Dufresne, E. R. and Schwartz, M. A. (2014) 'Mechanotransduction and extracellular matrix homeostasis', *Nature Reviews Molecular Cell Biology*. doi: 10.1038/nrm3896.

Hurt, A. V. *et al.* (1983) 'Bovine carotid artery heterografts versus polytetrafluoroethylene grafts. A prospective, randomized study', *The American Journal of Surgery*. doi: 10.1016/0002-9610(83)90356-2.

Hussein, K. H. *et al.* (2016) 'Heparin-gelatin mixture improves vascular reconstruction efficiency and hepatic function in bioengineered livers', *Acta Biomaterialia*. doi: 10.1016/j.actbio.2016.04.042.

Hwang, C. M. *et al.* (2009) 'Controlled cellular orientation on PLGA microfibers with defined diameters', *Biomedical Microdevices*. doi: 10.1007/s10544-009-9287-7.

Islam, R. *et al.* (2017) 'Tissue Harvesting Site and Culture Medium Affect Attachment, Growth, and Phenotype of Ex Vivo Expanded Oral Mucosal Epithelial Cells', *Scientific Reports*. doi: 10.1038/s41598-017-00417-z.

Jackson, M. R. *et al.* (2000) 'The consequences of a failed femoropopliteal bypass grafting: Comparison of saphenous vein and PTFE grafts', *Journal of Vascular Surgery*. doi: 10.1067/mva.2000.108634.

Jacot, J. G. and Wong, J. Y. (2008) 'Endothelial injury induces vascular smooth muscle cell proliferation in highly localized regions of a direct contact co-culture system', *Cell Biochemistry and Biophysics*. doi: 10.1007/s12013-008-9023-6.

Jahani, H. *et al.* (2012) 'The effect of aligned and random electrospun fibrous scaffolds on rat mesenchymal stem cell proliferation', *Cell Journal*.

Jalili, R., Hosseini, S. A. and Morshed, M. (2005) 'The effects of operating parameters on

the morphology of electrospun polyacrilonitrile nanofibres', *Iranian Polymer Journal (English Edition)*.

Jana, S. *et al.* (2012) 'Uniaxially aligned nanofibrous cylinders by electrospinning', *ACS Applied Materials and Interfaces*. doi: 10.1021/am301803b.

Jana, S. and Zhang, M. (2013a) 'Fabrication of 3D aligned nanofibrous tubes by direct electrospinning', *Journal of Materials Chemistry B*. Royal Society of Chemistry, 1(20), p. 2575. doi: 10.1039/c3tb20197j.

Jana, S. and Zhang, M. (2013b) 'Fabrication of 3D aligned nanofibrous tubes by direct electrospinning', *Journal of Materials Chemistry B*. doi: 10.1039/c3tb20197j.

Jang, J. *et al.* (2018) 'Biomaterials-based 3D cell printing for next-generation therapeutics and diagnostics', *Biomaterials*. doi: 10.1016/j.biomaterials.2017.11.030.

Jarusuwannapoom, T. *et al.* (2005) 'Effect of solvents on electro-spinnability of polystyrene solutions and morphological appearance of resulting electrospun polystyrene fibers', *European Polymer Journal*. doi: 10.1016/j.eurpolymj.2004.10.010.

Jean-Gilles, R. *et al.* (2010a) 'Novel Modeling Approach to Generate a Polymeric Nanofiber Scaffold for Salivary Gland Cells.', *Journal of nanotechnology in engineering and medicine*, 1(3), p. 31008. doi: 10.1115/1.4001744.

Jean-Gilles, R. *et al.* (2010b) 'Novel Modeling Approach to Generate a Polymeric Nanofiber Scaffold for Salivary Gland Cells.', *Journal of nanotechnology in engineering and medicine*, 1, p. 31008. doi: 10.1115/1.4001744.

Jia, L. *et al.* (2014) 'Guiding the orientation of smooth muscle cells on random and aligned polyurethane/collagen nanofibers', *Journal of Biomaterials Applications*. doi: 10.1177/0885328214529002.

Jose, R. R. *et al.* (2012) 'Seamless, axially aligned, fiber tubes, meshes, microbundles and gradient biomaterial constructs', *Journal of Materials Science: Materials in Medicine*, 23(11), pp. 2679–2695. doi: 10.1007/s10856-012-4739-7.

Jun, Z. *et al.* (2003) 'Poly-L-lactide nanofibers by electrospinning - Influence of solution viscosity and electrical conductivity on fiber diameter and fiber morphology', *E-Polymers*.

Kabirian, F. *et al.* (2018) 'An innovative approach towards 3D-printed scaffolds for the next generation of tissue-engineered vascular grafts', in *Materials Today: Proceedings*. doi: 10.1016/j.matpr.2018.04.167.

Kai, D. *et al.* (2011) 'Guided orientation of cardiomyocytes on electrospun aligned nanofibers for cardiac tissue engineering', *Journal of Biomedical Materials Research - Part B Applied Biomaterials*. doi: 10.1002/jbm.b.31862.

Kastellanos, S. *et al.* (2018) 'Overview of coronary artery variants, aberrations and anomalies', *World Journal of Cardiology*. doi: 10.4330/wjc.v10.i10.127.

Katagiri, Y., Brew, S. A. and Ingham, K. C. (2003) 'All six modules of the gelatin-binding domain of fibronectin are required for full affinity', *Journal of Biological Chemistry*. doi: 10.1074/jbc.M212512200.

Katzman, H. E. *et al.* (2005) 'Multicenter evaluation of the bovine mesenteric vein bioprostheses for hemodialysis access in patients with an earlier failed prosthetic graft', *Journal of the American College of Surgeons*. doi: 10.1016/j.jamcollsurg.2005.03.040.

Kawelke, N. *et al.* (2011) 'Fibronectin protects from excessive liver fibrosis by modulating the availability of and responsiveness of stellate cells to active TGF-β', *PLoS ONE*. doi: 10.1371/journal.pone.0028181.

Kijani, S. *et al.* (2017) 'Intimal hyperplasia induced by vascular intervention causes

lipoprotein retention and accelerated atherosclerosis', *Physiological Reports*. doi: 10.14814/phy2.13334.

Kim, J. E., Kim, S. H. and Jung, Y. (2016) 'Current status of three-dimensional printing inks for soft tissue regeneration', *Tissue Engineering and Regenerative Medicine*. doi: 10.1007/s13770-016-0125-8.

Kim, J. H. *et al.* (2016) 'Dynamic mechanical and nanofibrous topological combinatory cues designed for periodontal ligament engineering', *PLoS ONE*. doi: 10.1371/journal.pone.0149967.

Kim, J. I. *et al.* (2016) 'A Controlled Design of Aligned and Random Nanofibers for 3D Bi-functionalized Nerve Conduits Fabricated via a Novel Electrospinning Set-up', *Scientific Reports*. doi: 10.1038/srep23761.

Kim, S. *et al.* (2015) 'Transparent conductive films of copper nanofiber network fabricated by electrospinning', *Journal of Nanomaterials*. doi: 10.1155/2015/518589.

Kiselev, P. and Rosell-Llompart, J. (2012) 'Highly aligned electrospun nanofibers by elimination of the whipping motion', *Journal of Applied Polymer Science*. doi: 10.1002/app.36519.

Klenke, F. M. *et al.* (2008) 'Impact of pore size on the vascularization and osseointegration of ceramic bone substitutes in vivo', *Journal of Biomedical Materials Research - Part A*. doi: 10.1002/jbm.a.31559.

Koepsell, L. *et al.* (2011) 'Tissue engineering of annulus fibrosus using electrospun fibrous scaffolds with aligned polycaprolactone fibers', *Journal of Biomedical Materials Research - Part A*. doi: 10.1002/jbm.a.33216.

Kolh, P. and Wijns, W. (2011) 'Joint ESC/EACTS guidelines on myocardial

revascularization.', *Journal of cardiovascular medicine (Hagerstown, Md.)*, 12, pp. 264–267. doi: 10.2459/JCM.0b013e328344e647.

Koski, A., Yim, K. and Shivkumar, S. (2004) 'Effect of molecular weight on fibrous PVA produced by electrospinning', *Materials Letters*. doi: 10.1016/S0167-577X(03)00532-9.

Kostakova, E. *et al.* (2014) 'Study of polycaprolactone wet electrospinning process', *Express Polymer Letters*. doi: 10.3144/expresspolymlett.2014.59.

Kovalic, A. J., Beattie, D. K. and Davies, A. H. (2002) 'Outcome of ProCol, a bovine mesenteric vein graft, in infrainguinal reconstruction', *European Journal of Vascular and Endovascular Surgery*. doi: 10.1053/ejvs.2002.1710.

Kuchi, C., Harish, G. S. and Reddy, P. S. (2018) 'Effect of polymer concentration, needle diameter and annealing temperature on TiO2-PVP composite nanofibers synthesized by electrospinning technique', *Ceramics International*. doi: 10.1016/j.ceramint.2017.12.138.

Kulik, A. and Ruel, M. (2011) 'Lipid-lowering therapy and coronary artery bypass graft surgery: What are the benefits?', *Current Opinion in Cardiology*. doi: 10.1097/HCO.0b013e32834b9fb1.

Kurane, A., Simionescu, D. T. and Vyavahare, N. R. (2007) 'In vivo cellular repopulation of tubular elastin scaffolds mediated by basic fibroblast growth factor', *Biomaterials*, 28, pp. 2830–2838. doi: 10.1016/j.biomaterials.2007.02.031.

L'Heureux, N. *et al.* (1998) 'A completely biological tissue-engineered human blood vessel', *FASEB Journal*.

L'Heureux, N. *et al.* (2006) 'Human tissue-engineered blood vessels for adult arterial revascularization.', *Nature medicine*, 12, pp. 361–365. doi: 10.1038/nm1364.

Lawson, C. *et al.* (2016) 'Rapid fabrication of poly(ε-caprolactone) nanofibers using needleless alternating current electrospinning', *Journal of Applied Polymer Science*. doi: 10.1002/app.43232.

Lee, C. K., Kim, S. I. and Kim, S. J. (2005) 'The influence of added ionic salt on nanofiber uniformity for electrospinning of electrolyte polymer', in *Synthetic Metals*. doi: 10.1016/j.synthmet.2005.07.053.

Lee, Y. U. *et al.* (2008) 'Morphologic adaptation of arterial endothelial cells to longitudinal stretch in organ culture', *Journal of Biomechanics*. doi: 10.1016/j.jbiomech.2008.08.016.

Li, G. *et al.* (2000) 'Direct in vivo evidence demonstrating neointimal migration of adventitial fibroblasts after balloon injury of rat carotid arteries', *Circulation*. doi: 10.1161/01.CIR.101.12.1362.

Liao, J., Joyce, E. M. and Sacks, M. S. (2008) 'Effects of decellularization on the mechanical and structural properties of the porcine aortic valve leaflet', *Biomaterials*. doi: 10.1016/j.biomaterials.2007.11.007.

Lin, X. *et al.* (2016) 'Endothelial cells can regulate smooth muscle cells in contractile phenotype through the miR-206/ARF6&NCX1/exosome axis', *PLoS ONE*. doi: 10.1371/journal.pone.0152959.

Liu, C. *et al.* (2015) 'The effect of the fibre orientation of electrospun scaffolds on the matrix production of rabbit annulus fibrosus-derived stem cells', *Bone Research*. doi: 10.1038/boneres.2015.12.

Liu, L., Seyam, A. M. and Oxenham, W. (2013) 'Frictional electrification on polymeric flat surfaces', *Journal of Engineered Fibers and Fabrics*.

Liu, R. *et al.* (2013) 'The in vivo blood compatibility of bio-inspired small diameter

vascular graft: Effect of submicron longitudinally aligned topography', *BMC Cardiovascular Disorders*. doi: 10.1186/1471-2261-13-79.

Liu, Y. *et al.* (2009) 'Effects of fiber orientation and diameter on the behavior of human dermal fibroblasts on electrospun PMMA scaffolds', *Journal of Biomedical Materials Research - Part A*. doi: 10.1002/jbm.a.32165.

Liu, Y. *et al.* (2010) 'Magnetic-field-assisted electrospinning of aligned straight and wavy polymeric nanofibers', *Advanced Materials*. doi: 10.1002/adma.200903870.

Lluri, G. and Aboulhosn, J. (2014) 'Coronary arterial development: A review of normal and congenitally anomalous patterns', *Clinical Cardiology*. doi: 10.1002/clc.22237.

Lobo, A. O. *et al.* (2018) 'Electrospun nanofiber blend with improved mechanical and biological performance', *International Journal of Nanomedicine*. doi: 10.2147/IJN.S175619.

Lofland, G. K. *et al.* (2012) 'Initial pediatric cardiac experience with decellularized allograft patches', *Annals of Thoracic Surgery*, 93, pp. 968–971. doi: 10.1016/j.athoracsur.2011.09.039.

Loop, F. D. *et al.* (1986) 'Influence of the Internal-Mammary-Artery Graft on 10-Year Survival and Other Cardiac Events', *New England Journal of Medicine*. doi: 10.1056/NEJM198601023140101.

Lopes, R. D. *et al.* (2012) 'Relationship between vein graft failure and subsequent clinical outcomes after coronary artery bypass surgery', *Circulation*. doi: 10.1161/CIRCULATIONAHA.111.040311.

López-Guimet, J. *et al.* (2017) 'High-Resolution Morphological Approach to Analyse Elastic Laminae Injuries of the Ascending Aorta in a Murine Model of Marfan Syndrome',

Scientific Reports. doi: 10.1038/s41598-017-01620-8.

Luo, C. J., Stride, E. and Edirisinghe, M. (2012) 'Mapping the influence of solubility and dielectric constant on electrospinning polycaprolactone solutions', *Macromolecules*. doi: 10.1021/ma300656u.

Macossay, J. *et al.* (2007) 'Effect of needle diameter on nanofiber diameter and thermal properties of electrospun poly(methyl methacrylate)', *Polymers for Advanced Technologies*. doi: 10.1002/pat.844.

Madden, R. L. *et al.* (2004) 'Experience with cryopreserved cadaveric femoral vein allografts used for hemodialysis access', *Annals of Vascular Surgery*. doi: 10.1007/s10016-004-0055-0.

Makadia, H. K. and Siegel, S. J. (2011) 'Poly Lactic-co-Glycolic Acid (PLGA) as Biodegradable Controlled Drug Delivery Carrier.', *Polymers*, 3(3), pp. 1377–1397. doi: 10.3390/polym3031377.

Martin, K. *et al.* (2009) 'Thrombin stimulates smooth muscle cell differentiation from peripheral blood mononuclear cells via protease-activated receptor-1, rhoa, and myocardin', *Circulation Research*. doi: 10.1161/CIRCRESAHA.109.199984.

Mathers, C. D. and Loncar, D. (2006) 'Projections of global mortality and burden of disease from 2002 to 2030', *PLoS Medicine*, 3, pp. 2011–2030. doi: 10.1371/journal.pmed.0030442.

McAllister, T. N. *et al.* (2009) 'Effectiveness of haemodialysis access with an autologous tissue-engineered vascular graft: a multicentre cohort study', *The Lancet*. doi: 10.1016/S0140-6736(09)60248-8.

McClure, M. J. *et al.* (2009) 'Electrospinning-aligned and random polydioxanone-

polycaprolactone-silk fibroin-blended scaffolds: Geometry for a vascular matrix', *Biomedical Materials*. doi: 10.1088/1748-6041/4/5/055010.

McKee, C. T. *et al.* (2011) 'Topographic modulation of the orientation and shape of cell nuclei and their influence on the measured elastic modulus of epithelial cells', *Biophysical Journal*. doi: 10.1016/j.bpj.2011.09.042.

Meinhart, J., Deutsch, M. and Zilla, P. (1997) 'Eight years of clinical endothelial cell transplantation: Closing the gap between prosthetic grafts and vein grafts', in *ASAIO Journal*.

Mendis, S., Puska, P. and Norrving, B. (2011) 'Global atlas on cardiovascular disease prevention and control', *World Health Organization*, pp. 2–14.

Michel, J. B., Li, Z. and Lacolley, P. (2012) 'Smooth muscle cells and vascular diseases', *Cardiovascular Research*. doi: 10.1093/cvr/cvs172.

Miguel, M. (2012) 'Immunosuppressive Properties of Mesenchymal Stem Cells: Advances and Applications', *Current Molecular Medicine*. doi: 10.2174/156652412800619950.

Milleret, V. *et al.* (2012a) 'Influence of the fiber diameter and surface roughness of electrospun vascular grafts on blood activation', *Acta Biomaterialia*. doi: 10.1016/j.actbio.2012.07.032.

Milleret, V. *et al.* (2012b) 'Influence of the fiber diameter and surface roughness of electrospun vascular grafts on blood activation', *Acta Biomaterialia*, 8(12), pp. 4349–4356. doi: 10.1016/j.actbio.2012.07.032.

Mohammadian, M. and Haghi, A. K. (2014) 'Systematic parameter study for nano-fiber fabrication via electrospinning process', *Bulgarian Chemical Communications*.

Motamedi, A. S. *et al.* (2017) 'Effect of electrospinning parameters on morphological properties of PVDF nanofibrous scaffolds', *Progress in Biomaterials*. doi: 10.1007/s40204-017-0071-0.

Motwani, J. G. and Topol, E. J. (1998) 'Aortocoronary saphenous vein graft disease: Pathogenesis, predisposition, and prevention', *Circulation*. doi: 10.1161/01.CIR.97.9.916.

Mouriaux, F. *et al.* (2016) 'Effects of Long-term Serial Passaging on the Characteristics and Properties of Cell Lines Derived From Uveal Melanoma Primary Tumors', *Investigative Opthalmology & Visual Science*. doi: 10.1167/iovs.16-19317.

Murphy, C. M. *et al.* (2012) 'Mesenchymal stem cell fate is regulated by the composition and mechanical properties of collagen-glycosaminoglycan scaffolds', *Journal of the Mechanical Behavior of Biomedical Materials*. doi: 10.1016/j.jmbbm.2011.11.009.

Nam, J. *et al.* (2007) 'Improved Cellular Infiltration in Electrospun Fiber via Engineered Porosity', *Tissue Engineering*. doi: 10.1089/ten.2006.0306.

Nar, M. *et al.* (2016) 'Superior plant based carbon fibers from electrospun poly-(caffeyl alcohol) lignin', *Carbon*. doi: 10.1016/j.carbon.2016.02.053.

Narayan, D. and Venkatraman, S. S. (2008) 'Effect of pore size and interpore distance on endothelial cell growth on polymers', *Journal of Biomedical Materials Research - Part A*. doi: 10.1002/jbm.a.31749.

Nerurkar, N. L. *et al.* (2011) 'Dynamic culture enhances stem cell infiltration and modulates extracellular matrix production on aligned electrospun nanofibrous scaffolds', *Acta Biomaterialia*. doi: 10.1016/j.actbio.2010.08.011.

Nestor-Bergmann, A., Goddard, G. and Woolner, S. (2014) 'Force and the spindle: Mechanical cues in mitotic spindle orientation', *Seminars in Cell and Developmental*

Biology. doi: 10.1016/j.semcdb.2014.07.008.

Neumann, E. *et al.* (2010) 'Cell culture and passaging alters gene expression pattern and proliferation rate in rheumatoid arthritis synovial fibroblasts', *Arthritis Research and Therapy*. doi: 10.1186/ar3010.

Nezarati, R. M., Eifert, M. B. and Cosgriff-Hernandez, E. (2013) 'Effects of Humidity and Solution Viscosity on Electrospun Fiber Morphology', *Tissue Engineering Part C: Methods*. doi: 10.1089/ten.tec.2012.0671.

Nguyen, L. B. and Anderson, C. R. (2015) 'Parametric study on the size and alignment of electrospun PLGA nanofibrous matrices', in *2015 41st Annual Northeast Biomedical Engineering Conference (NEBEC)*. IEEE, pp. 1–2. doi: 10.1109/NEBEC.2015.7117078.

Ninomiya, K. *et al.* (2006) 'Transforming growth factor-β signaling enhances transdifferentiation of macrophages into smooth muscle-like cells', *Hypertension Research*. doi: 10.1291/hypres.29.269.

Nivison-Smith, L. and Weiss, A. S. (2012) 'Alignment of human vascular smooth muscle cells on parallel electrospun synthetic elastin fibers', *Journal of Biomedical Materials Research - Part A*. doi: 10.1002/jbm.a.33255.

No, D. Y., Jeong, G. S. and Lee, S. H. (2014) 'Immune-protected xenogeneic bioartificial livers with liver-specific microarchitecture and hydrogel-encapsulated cells', *Biomaterials*. doi: 10.1016/j.biomaterials.2014.07.009.

Noriega, S. E. *et al.* (2012) 'Effect of fiber diameter on the spreading, proliferation and differentiation of chondrocytes on electrospun chitosan matrices', *Cells Tissues Organs*. doi: 10.1159/000325144.

O'Brien, F. J. *et al.* (2005) 'The effect of pore size on cell adhesion in collagen-GAG

scaffolds', *Biomaterials*. doi: 10.1016/j.biomaterials.2004.02.052.

Olausson, M. *et al.* (2012) 'Transplantation of an allogeneic vein bioengineered with autologous stem cells: A proof-of-concept study', *The Lancet*. doi: 10.1016/S0140-6736(12)60633-3.

Otsuka, F. *et al.* (2013) 'Why is the mammary artery so special and what protects it from atherosclerosis?', *Annals of cardiothoracic surgery*. doi: 10.3978/j.issn.2225-319X.2013.07.06.

Owens, C. D. *et al.* (2008) 'Early remodeling of lower extremity vein grafts: Inflammation influences biomechanical adaptation', *Journal of Vascular Surgery*. doi: 10.1016/j.jvs.2008.01.009.

Pappano, A. J. *et al.* (2013) 'Coronary Circulation', *Cardiovascular Physiology*. Content Repository Only!, pp. 223–236. doi: 10.1016/B978-0-323-08697-4.00011-3.

Pashneh-Tala, S., MacNeil, S. and Claeyssens, F. (2016) 'The tissue-engineered vascular graft - Past, present, and future', *Tissue Engineering - Part B: Reviews*. doi: 10.1089/ten.teb.2015.0100.

Pattamaprom, C. *et al.* (2006) 'The influence of solvent properties and functionality on the electrospinnability of polystyrene nanofibers', *Macromolecular Materials and Engineering*. doi: 10.1002/mame.200600135.

Patterson, J. T. *et al.* (2012) 'Tissue-engineered vascular grafts for use in the treatment of congenital heart disease: from the bench to the clinic and back again', *Regen Med*, 7, pp. 409–419. doi: 10.2217/rme.12.12.

Perek, B. *et al.* (2012) 'Histological evaluation of age-related variations in saphenous vein grafts used for coronary artery bypass grafting', *Archives of Medical Science*. doi:

10.5114/aoms.2012.32412.

Perry, R. *et al.* (2013) 'Coronary artery wall thickness of the left anterior descending artery using high resolution transthoracic echocardiography - Normal range of values', *Echocardiography*. doi: 10.1111/echo.12136.

Petersen, C. B. *et al.* (2007) 'Porcine ecto-nucleotide pyrophosphatase/phosphodiesterase 1 (NPP1/CD203a): Cloning, transcription, expression, mapping, and identification of an NPP1/CD203a epitope for swine workshop cluster 9 (SWC9) monoclonal antibodies', *Developmental & Comparative Immunology*, 31(6), pp. 618–631. doi: 10.1016/j.dci.2006.08.012.

Pillai, C. K. S. and Sharma, C. P. (2010) 'Review paper: Absorbable polymeric surgical sutures: Chemistry, production, properties, biodegradability, and performance', *Journal of Biomaterials Applications*. doi: 10.1177/0885328210384890.

Poduri, A. *et al.* (2017) 'Endothelial cells respond to the direction of mechanical stimuli through SMAD signaling to regulate coronary artery size', *Development (Cambridge)*. doi: 10.1242/dev.150904.

Porter, R. S. and Johnson, J. F. (1966) 'The entanglement concept in polymer systems', *Chemical Reviews*. doi: 10.1021/cr60239a001.

Qi, W. *et al.* (2010) 'Influence of collecting velocity on fiber orientation, morphology and tensile properties of electrospun PPESK fabrics', *Journal of Applied Polymer Science*. doi: 10.1002/app.32586.

Qin, X. H. *et al.* (2007) 'Effect of different salts on electrospinning of polyacrylonitrile (PAN) polymer solution', *Journal of Applied Polymer Science*. doi: 10.1002/app.25498.

Quint, C. *et al.* (2011) 'Decellularized tissue-engineered blood vessel as an arterial

conduit.', *Proceedings of the National Academy of Sciences of the United States of America*, 108, pp. 9214–9219. doi: 10.1073/pnas.1019506108.

Quint, C. *et al.* (2012) 'Allogeneic human tissue-engineered blood vessel', *Journal of Vascular Surgery*. doi: 10.1016/j.jvs.2011.07.098.

Rajendran, P. *et al.* (2013) 'The vascular endothelium and human diseases', *International Journal of Biological Sciences*. doi: 10.7150/ijbs.7502.

Ramos, T. *et al.* (2015) 'Schwann cells promote endothelial cell migration', *Cell Adhesion & Migration*. doi: 10.1080/19336918.2015.1103422.

Ramshaw, J. A. M. (2016) 'Biomedical applications of collagens', in *Journal of Biomedical Materials Research - Part B Applied Biomaterials*. doi: 10.1002/jbm.b.33541.

Ratcliffe, A. (2000) 'Tissue engineering of vascular grafts', *Matrix Biology*, 19, pp. 353–357. doi: Doi 10.1016/S0094-1298(03)00069-5.

Rathore, A. *et al.* (2012) 'Development of tissue engineered vascular grafts and application of nanomedicine', *Wiley Interdisciplinary Reviews: Nanomedicine and Nanobiotechnology*, pp. 257–272. doi: 10.1002/wnan.1166.

Ratner, B. and Hoffman, A. (2004) 'Host Reactions to Biomaterials and Their Evaluation Testing Biomaterials', in *Biomaterials Science: An introduction to materials in medicine*.

Regis, S. *et al.* (2014) 'Fibronectin adsorption on functionalized electrospun polycaprolactone scaffolds: Experimental and molecular dynamics studies', *Journal of Biomedical Materials Research - Part A*, 102, pp. 1697–1706. doi: 10.1002/jbm.a.34843.

Reig, J. and Petit, M. (2004) 'Main Trunk of the Left Coronary Artery: Anatomic Study of the Parameters of Clinical Interest', *Clinical Anatomy*. doi: 10.1002/ca.10162.

Rnjak-Kovacina, J. *et al.* (2011) 'Tailoring the porosity and pore size of electrospun synthetic human elastin scaffolds for dermal tissue engineering', *Biomaterials*. doi: 10.1016/j.biomaterials.2011.05.065.

Roeder, R. A., Lantz, G. C. and Geddes, L. A. (2001) 'Mechanical remodeling of small-intestine submucosa small-diameter vascular grafts - A preliminary report', *Biomedical Instrumentation and Technology*.

Rouwkema, J. *et al.* (2009) 'Supply of nutrients to cells in engineered tissues', *Biotechnology and Genetic Engineering Reviews*. doi: 10.5661/bger-26-163.

Rüder, C. *et al.* (2013) 'Influence of fibre diameter and orientation of electrospun copolyetheresterurethanes on smooth muscle and endothelial cell behaviour', *Clinical Hemorheology and Microcirculation*. doi: 10.3233/CH-131787.

Ruusalepp, A., Vaage, J. and Valen, G. (2003) 'A model of neointima formation in the atherosclerotic carotid artery of mice', in *Interactive Cardiovascular and Thoracic Surgery*. doi: 10.1016/S1569-9293(03)00042-2.

Sabry, D., Noh, O. and Samir, M. (2016) 'Comparative evaluation for potential differentiation of endothelial progenitor cells and mesenchymal stem cells into endothelial-like cells', *International Journal of Stem Cells*. doi: 10.15283/ijsc.2016.9.1.44.

Sahay, R., Thavasi, V. and Ramakrishna, S. (2011) 'Design modifications in electrospinning setup for advanced applications', *Journal of Nanomaterials*. doi: 10.1155/2011/317673.

Sakamoto, H. *et al.* (2014) 'Atomic force microscopy visualization of hard segment alignment in stretched polyurethane nanofibers prepared by electrospinning', *Science and Technology of Advanced Materials*. doi: 10.1088/1468-6996/15/1/015008.

Sandusky, G. E., Lantz, G. C. and Badylak, S. F. (1995) 'Healing comparison of small

intestine submucosa and eptfe grafts in the canine carotid artery', *Journal of Surgical Research*. doi: 10.1006/jsre.1995.1064.

Sarkar, S. *et al.* (2007) 'Addressing thrombogenicity in vascular graft construction', *Journal of Biomedical Materials Research - Part B Applied Biomaterials*, pp. 100–108. doi: 10.1002/jbm.b.30710.

Sarzaeem, M. R. *et al.* (2010) 'Scoring system for predicting saphenous vein graft patency: In coronary artery bypass grafting', *Texas Heart Institute Journal*.

Schaner, P. J. *et al.* (2004) 'Decellularized vein as a potential scaffold for vascular tissue engineering', *Journal of Vascular Surgery*. doi: 10.1016/j.jvs.2004.03.033.

Scognamiglio, R. *et al.* (2006) 'Detection of coronary artery disease in asymptomatic patients with type 2 diabetes mellitus', *Journal of the American College of Cardiology*. doi: 10.1016/j.jacc.2005.10.008.

Secasanu, V. P., Giardina, C. K. and Wang, Y. (2009) 'A novel electrospinning target to improve the yield of uniaxially aligned fibers', in *Biotechnology Progress*. doi: 10.1002/btpr.163.

Selcan Gungor-Ozkerim, P. *et al.* (2013) 'Incorporation of growth factor loaded microspheres into polymeric electrospun nanofibers for tissue engineering applications', *Journal of Biomedical Materials Research - Part A*. doi: 10.1002/jbm.a.34857.

Semnani, D. (2016) 'Geometrical characterization of electrospun nanofibers', in *Electrospun Nanofibers*. doi: 10.1016/B978-0-08-100907-9.00007-6.

Shahreen, L. and Chase, G. G. (2015) 'Effects of electrospinning solution properties on formation of beads in Tio2 fibers with PdO particles', *Journal of Engineered Fibers and Fabrics*.

Shang, S. *et al.* (2010) 'The effect of electrospun fibre alignment on the behaviour of rat periodontal ligament cells', *European Cells and Materials*. doi: 10.22203/eCM.v019a18.

Sharifi, B. G. *et al.* (2006) 'Pleiotrophin induces transdifferentiation of monocytes into functional endothelial cells', *Arteriosclerosis, Thrombosis, and Vascular Biology*. doi: 10.1161/01.ATV.0000222017.05085.8e.

Shearer, H. *et al.* (2006) 'Effects of Common Sterilization Methods on the Structure and Properties of Poly(D,L Lactic-Co-Glycolic Acid) Scaffolds', *Tissue Engineering*. doi: 10.1089/ten.2006.12.2717.

Shelton, M. E. *et al.* (1988) 'A comparison of morphologic and angiographic findings in long-term internal mammary artery and saphenous vein bypass grafts', *Journal of the American College of Cardiology*. doi: 10.1016/0735-1097(88)90094-0.

Sheridan, W. S., Duffy, G. P. and Murphy, B. P. (2012) 'Mechanical characterization of a customized decellularized scaffold for vascular tissue engineering', *Journal of the Mechanical Behavior of Biomedical Materials*. doi: 10.1016/j.jmbbm.2011.12.003.

Shi, Y. *et al.* (1996) 'Adventitial remodeling after coronary arterial injury', *Circulation*. doi: 10.1161/01.CIR.93.2.340.

Shukla, N. and Jeremy, J. Y. (2012) 'Pathophysiology of saphenous vein graft failure: A brief overview of interventions', *Current Opinion in Pharmacology*. doi: 10.1016/j.coph.2012.01.001.

Simper, D. *et al.* (2002) 'Smooth muscle progenitor cells in human blood', *Circulation*. doi: 10.1161/01.CIR.0000031525.61826.A8.

Smith, I. O. *et al.* (2009) 'Nanostructured polymer scaffolds for tissue engineering and regenerative medicine', *Wiley Interdiscip Rev Nanomed Nanobiotechnol*, 1, pp. 226–236.

doi: 10.1002/wnan.26.

Soffer, L. *et al.* (2008) 'Silk-based electrospun tubular scaffolds for tissue-engineered vascular grafts', *Journal of Biomaterials Science, Polymer Edition*. doi: 10.1163/156856208784089607.

Soletti, L. *et al.* (2006) 'A seeding device for tissue engineered tubular structures', *Biomaterials*. doi: 10.1016/j.biomaterials.2006.04.042.

Song, S. J. *et al.* (2018) 'Aligned laminin core-polydioxanone/collagen shell fiber matrices effective for neuritogenesis', *Scientific Reports*. doi: 10.1038/s41598-018-23958-3.

Sowers, J. R., Epstein, M. and Frohlich, E. D. (2001) 'Diabetes, hypertension, and cardiovascular disease an update', *Hypertension*. doi: 10.1161/01.HYP.37.4.1053.

Stegemann, J. P., Hong, H. and Nerem, R. M. (2005) 'Mechanical, biochemical, and extracellular matrix effects on vascular smooth muscle cell phenotype.', *Journal of applied physiology (Bethesda, Md.: 1985)*, 98, pp. 2321–2327. doi: 10.1152/japplphysiol.01114.2004.

Swirski, F. K. and Nahrendorf, M. (2014) 'Do vascular smooth muscle cells differentiate to macrophages in atherosclerotic lesions?', *Circulation Research*. doi: 10.1161/CIRCRESAHA.114.304925.

Takagi, H. *et al.* (2010) 'A contemporary meta-analysis of Dacron versus polytetrafluoroethylene grafts for femoropopliteal bypass grafting', *Journal of Vascular Surgery*. doi: 10.1016/j.jvs.2010.02.010.

Tatoulis, J., Buxton, B. F. and Fuller, J. A. (2011) 'The right internal thoracic artery: The forgotten conduit5,766 patients and 991 angiograms', *Annals of Thoracic Surgery*. doi: 10.1016/j.athoracsur.2011.03.099.

Tawab, A. *et al.* (2009) 'Effect of ex vivo culture duration on phenotype and cytokine production by mature dendritic cells derived from peripheral blood monocytes', *Transfusion*. doi: 10.1111/j.1537-2995.2008.02020.x.

Taylor, G. (1964) 'Disintegration of Water Drops in an Electric Field', *Proceedings of the Royal Society A: Mathematical, Physical and Engineering Sciences*. doi: 10.1098/rspa.1964.0151.

Taylor, G. (1969) 'Electrically Driven Jets', *Proceedings of the Royal Society A: Mathematical, Physical and Engineering Sciences*. doi: 10.1098/rspa.1969.0205.

Teas, J. P. (1968) 'Graphic analysis of resin solubilities', *Journal of Paint Technology*.

Thevenot, P. *et al.* (2008) 'Method to Analyze Three-Dimensional Cell Distribution and Infiltration in Degradable Scaffolds', *Tissue Engineering Part C: Methods*. doi: 10.1089/ten.tec.2008.0221.

Tillman, B. W. *et al.* (2012) 'Bioengineered vascular access maintains structural integrity in response to arteriovenous flow and repeated needle puncture', *Journal of Vascular Surgery*. doi: 10.1016/j.jvs.2012.02.030.

Tondon, A. and Kaunas, R. (2014) 'The direction of stretch-induced cell and stress fiber orientation depends on collagen matrix stress', *PLoS ONE*. doi: 10.1371/journal.pone.0089592.

Tosun, Z. and Mcfetridge, P. S. (2013) 'Improved recellularization of ex vivo vascular scaffolds using directed transport gradients to modulate ECM remodeling', *Biotechnology and Bioengineering*. doi: 10.1002/bit.24934.

Tracy, L. E., Minasian, R. A. and Caterson, E. J. (2016) 'Extracellular Matrix and Dermal Fibroblast Function in the Healing Wound', *Advances in Wound Care*. doi:

10.1089/wound.2014.0561.

Trindade, A. C. *et al.* (2013) 'First curl, then wrinkle', *Macromolecular Rapid Communications*. doi: 10.1002/marc.201300436.

Tseng, Y. Y. *et al.* (2013) 'Biodegradable drug-eluting poly[lactic-co-glycol acid] nanofibers for the sustainable delivery of vancomycin to brain tissue: In vitro and in vivo studies', *ACS Chemical Neuroscience*, 4(9), pp. 1314–1321. doi: 10.1021/cn400108q.

de Valence, S. *et al.* (2012) 'Long term performance of polycaprolactone vascular grafts in a rat abdominal aorta replacement model', *Biomaterials*, 33(1), pp. 38–47. doi: 10.1016/j.biomaterials.2011.09.024.

Valentin, J. E. *et al.* (2006) 'Extracellular matrix bioscaffolds for orthopaedic applications: A comparative histologic study', *Journal of Bone and Joint Surgery - Series A*. doi: 10.2106/JBJS.E.01008.

Venugopal, J. *et al.* (2005) 'In vitro study of smooth muscle cells on polycaprolactone and collagen nanofibrous matrices', *Cell Biology International*. doi: 10.1016/j.cellbi.2005.03.026.

Vollrath, F. and Knight, D. P. (2001) 'Liquid crystalline spinning of spider silk', *Nature*. doi: 10.1038/35069000.

Waller, B. F. *et al.* (1992) 'Anatomy, histology, and pathology of coronary arteries: A review relevant to new interventional and imaging techniques—Part II', *Clinical Cardiology*. doi: 10.1002/clc.4960150712.

Walser, J. and Ferguson, S. J. (2016) 'Oriented nanofibrous membranes for tissue engineering applications: Electrospinning with secondary field control', *Journal of the Mechanical Behavior of Biomedical Materials*. doi: 10.1016/j.jmbbm.2015.06.027.

Wang, D. *et al.* (2017) 'Roles of Cells from the Arterial Vessel Wall in Atherosclerosis', *Mediators of Inflammation*. doi: 10.1155/2017/8135934.

Wang, H. B. *et al.* (2009) 'Creation of highly aligned electrospun poly-L-lactic acid fibers for nerve regeneration applications', *Journal of Neural Engineering*. doi: 10.1088/1741-2560/6/1/016001.

Wang, H. Di *et al.* (2010) 'Adventitial fibroblasts in vascular structure and function: The role of oxidative stress and beyond', *Canadian Journal of Physiology and Pharmacology*. doi: 10.1139/Y10-015.

Wang, Y. *et al.* (2014) 'Electrospun tubular scaffold with circumferentially aligned nanofibers for regulating smooth muscle cell growth', *ACS Applied Materials and Interfaces*. doi: 10.1021/am405556x.

Wang, Yuzhen *et al.* (2016) 'Biomimetic fibroblast-loaded artificial dermis with "sandwich" structure and designed gradient pore sizes promotes wound healing by favoring granulation tissue formation and wound re-epithelialization', *Acta Biomaterialia*. doi: 10.1016/j.actbio.2015.11.035.

Wang, Yi *et al.* (2016) 'High shear stress induces atherosclerotic vulnerable plaque formation through angiogenesis', *Regenerative Biomaterials*. doi: 10.1093/rb/rbw021.

Wannatong, L., Sirivat, A. and Supaphol, P. (2004) 'Effects of solvents on electrospun polymeric fibers: Preliminary study on polystyrene', *Polymer International*. doi: 10.1002/pi.1599.

Whited, B. M. and Rylander, M. N. (2014a) 'The influence of electrospun scaffold topography on endothelial cell morphology, alignment, and adhesion in response to fluid flow', *Biotechnology and Bioengineering*. doi: 10.1002/bit.24995.

Whited, B. M. and Rylander, M. N. (2014b) 'The influence of electrospun scaffold topography on endothelial cell morphology, alignment, and adhesion in response to fluid flow', *Biotechnology and Bioengineering*. doi: 10.1002/bit.24995.

WHO, W. H. O. (2011) *Global status report on noncommunicable diseases 2010*, *Description of the Global Burden of NCDs Their Risk Factors and Determinants Geneva World Health Organization*. Available at: http://www.who.int/nmh/publications/ncd_report2010/en/.

Wise, J. K. *et al.* (2009) 'Chondrogenic differentiation of human mesenchymal stem cells on oriented nanofibrous scaffolds: Engineering the superficial zone of articular cartilage', *Tissue Engineering - Part A*. doi: 10.1089/ten.tea.2008.0109.

Wu, J. and Hong, Y. (2016) 'Enhancing cell infiltration of electrospun fibrous scaffolds in tissue regeneration', *Bioactive Materials*. doi: 10.1016/j.bioactmat.2016.07.001.

Wu, Z. *et al.* (2018) 'Effect of Electrospun Fibrous Scaffolds with Different Fiber Orientations on the Alignment of Microvessel-Like Structures', *Journal of Medical and Biological Engineering*. doi: 10.1007/s40846-017-0284-7.

Wystrychowski, W. *et al.* (2014) 'First human use of an allogeneic tissue-engineered vascular graft for hemodialysis access', *Journal of Vascular Surgery*. doi: 10.1016/j.jvs.2013.08.018.

Xiao, X. *et al.* (2015) 'The promotion of angiogenesis induced by three-dimensional porous beta-tricalcium phosphate scaffold with different interconnection sizes via activation of PI3K/Akt pathways', *Scientific Reports*. doi: 10.1038/srep09409.

Xie, J. *et al.* (2010) '"Aligned-to-random" nanofiber scaffolds for mimicking the structure of the tendon-to-bone insertion site', *Nanoscale*. doi: 10.1039/c0nr00192a.

Xin, X., Hussain, M. and Mao, J. J. (2007) 'Continuing differentiation of human mesenchymal stem cells and induced chondrogenic and osteogenic lineages in electrospun PLGA nanofiber scaffold', *Biomaterials*, 28(2), pp. 316–325. doi: 10.1016/j.biomaterials.2006.08.042.

Xu, C. *et al.* (2004) 'Electrospun Nanofiber Fabrication as Synthetic Extracellular Matrix and Its Potential for Vascular Tissue Engineering', *Tissue Engineering*. doi: 10.1089/ten.2004.10.1160.

Xu, Y. *et al.* (2000) 'Multiple binding sites in collagen type I for the integrins alpha1beta1 and alpha2beta1.', *The Journal of biological chemistry*. doi: 10.1074/jbc.M007668200.

Xu, Y. *et al.* (2017) 'Effect of different solvent systems on PHBV/PEO electrospun fibers', *RSC Advances*. doi: 10.1039/c6ra26783a.

Yalcinkaya, F., Yalcinkaya, B. and Jirsak, O. (2015) 'Influence of salts on electrospinning of aqueous and nonaqueous polymer solutions', *Journal of Nanomaterials*. doi: 10.1155/2015/134251.

Yan, D. *et al.* (2011) 'Macrophages overexpressing VEGF, transdifferentiate into endothelial-like cells in vitro and in vivo', *Biotechnology Letters*. doi: 10.1007/s10529-011-0645-1.

Yan, D. *et al.* (2017) 'Vascular endothelial growth factor modified macrophages transdifferentiate into endothelial-like cells and decrease foam cell formation', *Bioscience Reports*. doi: 10.1042/BSR20170002.

Yan, J. *et al.* (2012) 'Effect of fiber alignment in electrospun scaffolds on keratocytes and corneal epithelial cells behavior', *Journal of Biomedical Materials Research Part A*, 100A(2), pp. 527–535. doi: 10.1002/jbm.a.33301.

Yang, H. *et al.* (2006) 'Fine ceramic lattices prepared by extrusion freeforming', *Journal of Biomedical Materials Research - Part B Applied Biomaterials*. doi: 10.1002/jbm.b.30520.

Yang, Y.-H. K. *et al.* (2018) 'Changes in phenotype and differentiation potential of human mesenchymal stem cells aging in vitro', *Stem Cell Research & Therapy*. BioMed Central, 9(1), p. 131. doi: 10.1186/s13287-018-0876-3.

Yarin, A. L., Koombhongse, S. and Reneker, D. H. (2001) 'Taylor cone and jetting from liquid droplets in electrospinning of nanofibers', *Journal of Applied Physics*. doi: 10.1063/1.1408260.

Yau, J. W., Teoh, H. and Verma, S. (2015) 'Endothelial cell control of thrombosis', *BMC Cardiovascular Disorders*. doi: 10.1186/s12872-015-0124-z.

Yazdani, S. K. *et al.* (2009) 'Smooth muscle cell seeding of decellularized scaffolds: the importance of bioreactor preconditioning to development of a more native architecture for tissue-engineered blood vessels.', *Tissue engineering. Part A*, 15, pp. 827–840. doi: 10.1089/ten.tea.2008.0092.

You, Young Lee, Seung Jin Min, Byung M. Park, W. H. (2006) 'Effect of solution properties on nanofibrous structure of electrospun poly(lactic-co-glycolic acid)', *Journal of Applied Polymer Science*, 99, pp. 1214–1221. doi: 10.1002/app.22602.

Yu, L. *et al.* (2017) 'High throughput preparation of aligned nanofibers using an improved bubble-electrospinning', *Polymers*. doi: 10.3390/polym9120658.

Zeltinger, J. *et al.* (2001) 'Effect of Pore Size and Void Fraction on Cellular Adhesion, Proliferation, and Matrix Deposition', *Tissue Engineering*. doi: 10.1089/107632701753213183.

Zhan, J. and Lan, P. (2012) 'The Review on Electrospun Gelatin Fiber Scaffold', *Journal of*

Research Updates in Polymer Science, 1, pp. 59–71. doi: 10.6000/1929-5995.2012.01.02.1.

Zhang, B. *et al.* (2017) 'Solvent-free electrospinning: Opportunities and challenges', *Polymer Chemistry*. doi: 10.1039/c6py01898j.

Zhang, C. *et al.* (2015) 'In situ growth induction of the corneal stroma cells using uniaxially aligned composite fibrous scaffolds', *RSC Advances*. doi: 10.1039/c4ra16609d.

Zhang, F., Zuo, B. Q. and Bai, L. (2009) 'Study on the structure of SF fiber mats electrospun with HFIP and FA and cells behavior', *Journal of Materials Science*. doi: 10.1007/s10853-009-3800-5.

Zhang, Y. Z. *et al.* (2005) 'Characterization of the surface biocompatibility of the electrospun PCL-Collagen nanofibers using fibroblasts', *Biomacromolecules*, 6, pp. 2583–2589. doi: 10.1021/bm050314k.

Zheng, M. H. *et al.* (2005) 'Porcine small intestine submucosa (SIS) is not an acellular collagenous matrix and contains porcine DNA: Possible implications in human implantation', *Journal of Biomedical Materials Research - Part B Applied Biomaterials*. doi: 10.1002/jbm.b.30170.

Zhou, C., Jin, S. and Willing, R. (2016) 'Simulation of extracellular matrix remodeling by fibroblast cells in soft three-dimensional bioresorbable scaffolds', *Biomechanics and Modeling in Mechanobiology*. doi: 10.1007/s10237-016-0791-4.

Zhou, Q. *et al.* (2015) 'Engineering aligned electrospun PLLA microfibers with nano-porous surface nanotopography for modulating the responses of vascular smooth muscle cells', *Journal of Materials Chemistry B*. doi: 10.1039/c5tb00051c.

Zhu, P. *et al.* (2016) 'Fabrication of three-dimensional nanofibrous macrostructures by

electrospinning', *Citation: AIP Advances*, 6, p. 55304. doi: 10.1063/1.4948797.

Zong, X. *et al.* (2002) 'Structure and process relationship of electrospun bioabsorbable nanofiber membranes', *Polymer*. doi: 10.1016/S0032-3861(02)00275-6.

8

APPENDIX 1 – RAW DATA